OPERATIONAL MODAL ANALYSIS OF AN EXISTING LARGE TRUSS BRIDGE AND PASSIVE VIBRATION CONTROL USING UPDATED MODEL

Thesis Submitted in Partial Fulfilment of the Requirements for the Degree of

DOCTOR OF PHILOSOPHY

By

NIRMALENDU DEBNATH

DEPARTMENT OF CIVIL ENGINEERING

INDIAN INSTITUTE OF TECHNOLOGY GUWAHATI

GUWAHATI-781039, INDIA

MAY 2014

To the loving memory

of

my parents

CANDIDATE'S DECLARATION

I hereby declare that the work presented in the thesis entitled "Operational Modal Analysis of an Existing Large Truss Bridge and Passive Vibration Control using Updated Model" in fulfilment of the requirement for the award of the degree of Doctor of Philosophy in an authentic record of my own work carried out in Department of Civil Engineering of the Institute. The work has been carried out under active guidance of Prof. A. Dutta and Prof. S.K. Deb.

The content presented in this thesis has not been submitted by me for the award of any other degree of this or any other Institute.

Nirmalendu Debnath

This is to clarify that the above statement made by the candidate is correct to the best of our knowledge.

Dr. Anjan Dutta
Professor
Department of Civil Engineering
Indian Institute of Technology Guwahati
Guwahati-781039
India

Dr. Sajal Kanti Deb
Professor
Department of Civil Engineering
Indian Institute of Technology Guwahati
Guwahati-781039
India

ACKNOWLEDGEMENT

This thesis is the outcome of analytical and experimental studies carried out in the department of civil engineering at Indian Institute of Technology (IIT) Guwahti, India. At the outset, I would like to express my sincere gratitude to my supervisors, Prof. Anjan Dutta and Prof. Sajal Kanti Deb for initiating an interesting and innovative research topic and for their personal commitment, unconditional support, valuable advices and continuous guidance. I appreciate the opportunities I got to develop myself in an evolving area of Structural Engineering.

The experimental study in this thesis is associated with field experiments. This would not have been possible without the support of technical staff of the department of Civil Engineering, IIT Guwahati. I express my gratitude to Dr. Arun Chandra Borsaikia and Mr. Biswajit Debnath for their earnest effort during experimentation, data acquisition and post processing.

I would like to thank the members of my doctoral committee, Prof. Sudip Talukdar (chairman), Prof. Sashindra K. Kakoty and Dr. Arunasis Chakraborty for their remarks and valuable suggestions during the entire course of my research.

I acknowledge the assistance of the student colleagues, Mr. Gajula Rajkumar, Mr. Battina Narendra Babu and Mr. Dachepally Pradeep Kumar involved with this study in various ways.

Last but not the least, I would like to thank my loving parents for their moral support.

Nirmalendu Debnath

TABLE OF CONTENTS

ABSTRACT

The present study is associated with both the analytical and experimental aspects of structural health monitoring (SHM) as well as structural control. A very important existing large truss bridge structure, named as Saraighat Bridge which is situated in northeast region of India is considered as a sample structure. It is a large rail-cum-road double-deck multi-span steel truss bridge with length of 1.3 km over the mighty river Brahmaputra in Assam. The Saraighat Bridge is in service for more than fifty years as a lifeline structure for the north-east India. Further, the bridge is situated in the highest seismic zone of India. In view of this, adoption of such a large bridge structure for the present study may be considered as quite meaningful. Although various aspects of this study are associated with the Saraighat Bridge structure, works/developments related to the analytical aspect of this study are in fact general in nature. The health monitoring aspect of the present study is limited to the identification of modal parameters. These identified modal parameters would be useful as benchmark for comparison during the next phase of modal identification. Identification of modal parameters is carried out using the principles of operational modal analysis (OMA) or output-only system identification. The identified modal parameters are used for updating of finite element model of the bridge. Further studies have been carried out on design of passive vibration control system for Saraighat Bridge using updated FE model.

It is usually known that OMA requires appropriate placing of sensors for effective modal identification. In the present study, a modal approach is considered for sensor placement evaluation in view of its various flexible features compared to other major techniques like effective independence (EI) and modal kinetic energy (MKE). In this approach, modal participation at individual degree of freedom (DOF) is evaluated separately for the target modes and subsequently suitable locations are identified using these

participation profiles. Modal contribution in output energy (MCOE) is proposed as modal measure to evaluate modal participation and same has been applied in this modal approach framework for sensor placement evaluation. MCOE is evaluated using observability grammian for any types of response measurement (displacement, velocity or acceleration), while a system is released from any initial condition. In order to understand the efficiency of this proposed technique, MCOE is compared with existing modal measures (H2 norm, H∞ norm and modal Hankel singular value or MHSV) as well as with other techniques like EI and MKE. Analytical similarity is found for participation of a mode with EI method. Further, the sample bridge structure is considered for comparative study using acceleration measurement. In this comparison, MCOE technique is found to be in very good agreement with EI method as expected, while good agreement is observed with MHSV as well as various system-norms and reasonable agreement with MKE method. The proposed modal measure (MCOE) is associated with simple physical understanding providing a good level of confidence for applying it as a modal measure. MCOE considers only output with solely employing observability grammian while other modal measures employ both the observability and controllability grammians. Therefore, MCOE, comparing to system norms based other modal measures, appears as more suitable for sensor placement in operational modal analysis (OMA) where input is unknown. Finally, planning for suitable locations of accelerometers are carried out for the sample bridge targeting major modes and taking into account availability of limited numbers of accelerometers.

OMA is carried out for the Saraighat Bridge using ambient acceleration responses to identify modal parameters like natural frequencies, mode shapes and damping ratios. Effects of measurement noise are likely to influence the identified parameters. Moreover, deviations of real ambient vibration from theoretical assumption of white-noise induced vibration are also likely to influence the accuracy of identification techniques. Two approaches are

considered for better acceptability of identified modal parameters against above mentioned constraints. These are: (a) employing multiple techniques both in time and frequency domain for comparison of identified modal parameters from different techniques and (b) identifying modal parameters in terms of central tendency and dispersion based on multiple data sets. The modal parameters are identified using three important techniques like: (a) Natural excitation technique with eigensystem realization algorithm (NExT-ERA) (b) Stochastic subspace identification (SSI) (data driven) (c) Frequency spatial domain decomposition (FSDD). Moreover, stabilization diagrams are employed to identify suitable sizes of Hankel matrices for both the NExT-ERA and SSI techniques. Finally, central tendencies obtained employing multiple techniques is compared to realize the acceptance of identified modal parameters. The OMA exercise for the Saraighat Bridge has been able to identify its major horizontal, vertical and torsional modes. Central tendencies of mode shapes (representing the plane along rail-level deck) identified using three techniques are found to be in good agreement. Similarly, central tendencies of natural frequencies identified using three techniques are found to be in good agreement as well. Moreover, the 95% confidence bounds for the natural frequencies are observed to be in narrow range. Higher variations, however, are observed for the central tendencies of damping ratios identified using these three techniques.

The FE model of the Saraighat Bridge is updated using the experimental frequencies and mode shapes. In this present study, direct updating techniques are used considering their better performance in terms of exact reproduction of the experimentally identified modal parameters. The direct method is considered since the sole purpose of updating in this study is the design of an efficient passive control system. Two popular techniques, with the ability of exact reproduction of experimental natural frequencies and mode shapes, employed for updating model in this exercise are: (a) Berman and Nagy updating technique and (b) matrix

mixing updating technique. A commonly used structural analysis software package SAP 2000 is used for modelling the bridge structure. SAP2000 provides mass and stiffness matrices of the modelled structure, which are needed for model updating. Eight measured mode shapes at rail-deck level having 28 DOFs have been expanded to 854 DOFs matching the size of analytical matrices. These expanded measured mode shapes associated to this complicated bridge structure have demonstrated good agreement with their analytical counterparts. Both the updating techniques have determined updated mass and stiffness matrices while exactly reproducing the measured natural frequencies and mode shapes (in expanded form). The updated mode shapes along the rail-deck level are in excellent agreement with those identified experimentally.

In the final phase, an analytical design of passive vibration control system for the Saraighat Bridge is carried out using updated FE model. The Saraighat Bridge, with the superstructure made of steel and having a span of 118.72 m, experiences considerable vibration. The tuned mass damper (TMD), one of the oldest and widely used passive vibration control devices, is considered for this vibration control study. Multiple TMD (MTMD) system, which is widely accepted to perform better than the single unit based TMD system is finally considered. A strategy using modal frequency response function (FRF) is proposed based on the traditional mode-wise control approach. Further, an approach for simultaneous control of horizontal and vertical modes is proposed in this study. Prominent modes both in horizontal (transverse) and vertical directions are simultaneously targeted in the design considerations of TMD system by assigning equal weightage to both the directions. Therefore, the designed TMD system is supposed to perform effectively against vehicle type loading as well as wind type loading, in contrary to the traditional design where either transverse modes or the vertical modes are usually taken into account. Prominent modes of the Saraighat Bridges as 1st horizontal, 1st vertical, 2nd horizontal, 2nd vertical and

1st torsional modes are simultaneously targeted in the design of MTMD system based on the proposed strategy. The MTMD systems are designed with an assigned mass of 1% of the total superstructure mass and this has been found quite effective to reduce the peak frequency responses. In the proposed strategy, equal weightages have been provided for both transverse and vertical modes. The designed MTMD system has also demonstrated good control performance in both transverse and vertical directions against different types of loadings.

LIST OF TABLES

LIST OF FIGURES

Symbols	Meaning
$[A]$	State space system matrix
$[A_i]$	State space system matrix associated to i^{th} mode
$[B]$	State space input matrix
$[B_i]$	State space input matrix associated to i^{th} mode
$[C]$	State space output matrix
$[C_i]$	State space output matrix associated to i^{th} mode
$[D]$	Damping matrix
Δt	Sampling time
$[E]$	State space direct feed through matrix
$[E_i]$	State space direct feed through matrix associated to i^{th} mode
$[G(\omega)]$	Frequency response function (FRF) matrix
$\|\|G\|\|_2$	H_2 norm of a system with FRF matrix as $[G(\omega)]$
$\|\|G\|\|_\infty$	H_∞ norm of a system with FRF matrix as $[G(\omega)]$
$\left[h(.)\right]$	Markov parameters
$[I]$	Identity matrix
$[K]$	Stiffness matrix
$[K_A]$	Analytical stiffness matrix
$[K_U]$	Updated stiffness matrix
$\left[\Lambda_E\right]$	Diagonal matrix with measured natural frequencies in eigen-value format
$[M]$	Mass matrix
$[M_A]$	Analytical mass matrix
$[M_U]$	Updated mass matrix

ω	Circular natural frequency
$[\Omega]$	Circular natural frequency matrix diagonally containing the circular natural frequencies
$[O]$	Projection matrix as used in SSI
$[\Phi]$	Mode shape matrix
$[\Phi_E]$	Experimentally identified mode shape matrix
$\{\Phi_i\}$	Mode shape vector associated to i^{th} mode
$[\Sigma]$	Matrix having non-negative real singular values obtained in singular value decomposition in the form of $[U][\Sigma][V]^T$
$\{u\}$	Input force vector
$[U]$	Unitary matrix obtained in the singular value decomposition in the form of $[U][\Sigma][V]^T$
$[V]$	Unitary matrix obtained in the singular value decomposition in the form of $[U][\Sigma][V]^T$
$[W_c]$	Controllability grammian
$[W_o]$	Observability grammian
$\{\ddot{x}\}$	Acceleration vector
$\{\dot{x}\}$	Velocity vector
$\{x\}$	Displacement vector
ξ	Damping ratio
$[\Xi]$	Damping ratio matrix diagonally containing the damping ratios
$[Y]$	Block Hankel matrix as used in SSI

Abbreviations	Meaning
AR	Auto regressive
ARMA	Auto regressive moving average
CMIF	Complex mode indication function
CVA	Canonical variant algorithm
DOF	Degree of freedom
DVA	Dynamic vibration absorber
EI	Effective independence
EMA	Experimental modal analysis
ERA	Eigensystem realization algorithm
FDD	Frequency domain decomposition
FE	Finite element
FIM	Fisher information matrix
FRF	Frequency response function
FSDD	Frequency-spatial domain decomposition
HSV	Hankel singular value
IRF	Impulse response function
ITD	Ibrahim time-domain
LSCE	Least-squares complex exponential
LTI	Linear time invariant
MAC	Modal assurance criteria
MCOE	Modal contribution in output energy
MDOF	Multi degree of freedom
MHSV	Modal Hankel singular value
MIMO	Multi input multi output
MISO	Multi input single output
MKE	Modal kinetic energy
MLE	Maximum likelihood estimator
MPC	Modal phase collinearity
MTMD	Multiple tuned mass damper
N4SID	Numerical algorithms for subspace state space system identification
NDE	Non-destructive evaluation

NExT	Natural excitation technique
OMA	Operational modal analysis
PC	Principal component
POC	Pseudo orthogonality check
PP	Peak-picking
PRCE	Polyreference least-squares complex exponential
PSD	Power spectral density
RC	Reinforced concrete
SDOF	Single degree of freedom
SEREP	System equivalent reduction expansion process
SHM	Structural health monitoring
SIMO	Single input multi output
SISO	Single input single output
SSI	Stochastic subspace identification
SVD	Singular value decomposition
TF	Transfer function
TMD	Tuned mass damper
UPC	Unweighted principal component

Chapter 1

INTRODUCTION

1.1. PREAMBLE

Scopes of engineering activities for civil structures are not limited to only design and construction. There exist ample scopes for many other related engineering activities like structural health monitoring and structural control during the lifespan of structures. Health monitoring aspect, associated to the present study can be considered as non-continuous health monitoring approach where responses are not continuously monitored. Multiple approaches are emerging in the area of non-continuous methods of health monitoring for civil structures, e.g. wave-propagation based health monitoring, vibration based health monitoring etc. The modal parameter based health monitoring which is associated with the vibration based health monitoring, is found to be one of the immensely interesting domains to the researchers. In this approach, modal parameters identified before and after the occurrences of damages in any structure are taken into account for health diagnosis. Such evaluation of modal parameters of the structural system is associated to the discipline commonly known as system identification. It may be mentioned that efficient system identification requires appropriate sensor-placement, which is another area of research associated to the domain of structural health monitoring. The identified modal parameters, in addition to possible health diagnosis are also useful for updating/adjusting initial finite element (FE) model to a more accurate FE model for extraction of modal parameters having close agreement with the measured modal parameters. Further, structural control, another area of research associated with the structural lifespan management, is an active area of research. An updated FE model is usually utilized for efficient design of controllers for any structural system.

1.2. STRUCTURAL HEALTH MONITORING

Structural health monitoring (Balageas 2006) can be defined as an engineering arrangement aiming to provide a diagnosis of the state of the constituent materials, as well as state of the different parts and the whole structure at every moment during the life of a structure. The time-dimension of monitoring further helps in supervising dynamic-responses as well as in prognosis (e.g. evolution of damage). Structural health monitoring (SHM) may be considered as innovative and improved methodology compared to traditional non-destructive evaluation (NDE). SHM encompasses wide domain including selection and placement of sensors, use of smart materials, data collection and transmission, computations etc.

1.2.1. Motivation for SHM

Major motivations for application of SHM are as follows:

(a) To allow an optimal use of the structure with minimized downtime.

(b) To avoid any catastrophic failures.

(c) To make possible the replacement of traditional scheduled and periodic maintenance inspection with performance or condition based maintenance (usually long term).

(d) To reduce labour and human errors by minimizing the human involvement. Thus SHM can improve the safety and reliability.

(e) To have better handling of the typical difficulties of monitoring associated with hidden-defects.

1.2.2. SHM and biomimetics

It may be noticed that, the research on SHM is influenced by biomimetics (or bio inspiration) to some extent. Many similarities exist between the SHM activities and the medical activities.

One such similarity is presented in Table 1.1 based on the work of Gandhi and Thompson (1992).

Table 1.1. Similarity-parallelism between SHM and medical activities (Gandhi and Thompson 1992)

Phase of life	Man	Structures
Birth	Birth monitoring	Process monitoring
Sound life	Health check-up	Health and usage monitoring
Illness and death	Clinical monitoring	Health (damage) monitoring

1.2.3. Arrangement of SHM

A typical organization of SHM system is presented in Fig. 1.1 based on the works of Balageas (2006). In Fig. 1.1, two basic sub-systems can be found: (i) one corresponds to the structural integrity monitoring function and (ii) another corresponds to the usage monitoring function. Mixing the information of the integrity monitoring sub-system with that of the usage monitoring sub-system based on the knowledge of damage mechanics as well as behaviour laws makes it possible to determine the prognosis (residual life) and the health management of the structure (organization of maintenance, repair operations etc.). At the end, the basic components of the SHM-arrangements are as follows.

(a) Sensors

(b) Data acquisition systems

(c) Data transfer and storage mechanism

(d) Data management system

(e) Data interpretation and diagnosis arrangement

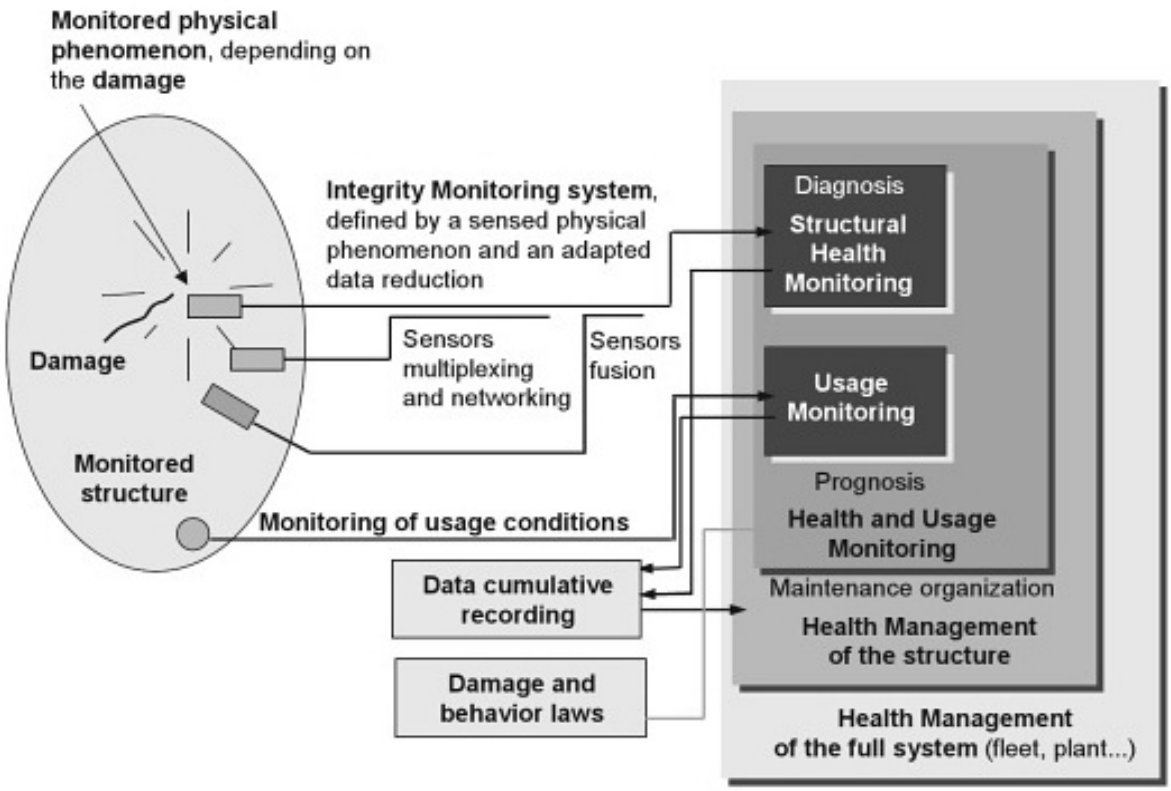

Fig. 1.1. Principle and organization of a SHM system (courtesy of Balageas 2006)

1.2.4. Non-continuous health monitoring

Health monitoring may be viewed as of continuous and non-continuous form based on the nature of monitoring. In regard to non-continuous health monitoring strategy, multiple approaches are observed in the field of SHM like wave propagation based health monitoring, vibration based health monitoring etc. The vibration based SHM adopts various strategies e.g. monitoring of dynamic-responses, prognosis, the inverse problem etc. The inverse problem takes into account the identified dynamic characteristics to diagnose damages. The present study is associated to this type of health monitoring approach.

1.3. SYSTEM IDENTIFICATION

At first, it may be mentioned that a system is an entity that processes a set of signals (inputs) to yield another set of signals (outputs). A system may be classified as continuous-time

system and discrete-time system as shown in Fig 1.2(a). Another classification of system, based on number of input and output channels, is frequently considered as: (i) single input single output (SISO), (ii) single input multi output (SIMO), (iii) multi input single output (MISO) and (iv) multi input multi output (MIMO). A MIMO system is shown in Fig 1.2(b). System identification (Ljung 1999) is generally defined as the process of constructing mathematical-models based on the experimental data. The techniques of system identification are applicable in many domains of engineering including structural engineering. System identification serves many useful objectives in structural engineering domain like: (i) updating or refinement of FE models, (ii) SHM or condition assessment, (iii) efficient design of control system and (iv) possible diagnosis of unpredicted/unusual behaviour. System identification is inter-disciplinary in nature and presently there exists a vast literature in the domain of system identification. Some of the commonly used system identification techniques are mentioned in the next sub-section.

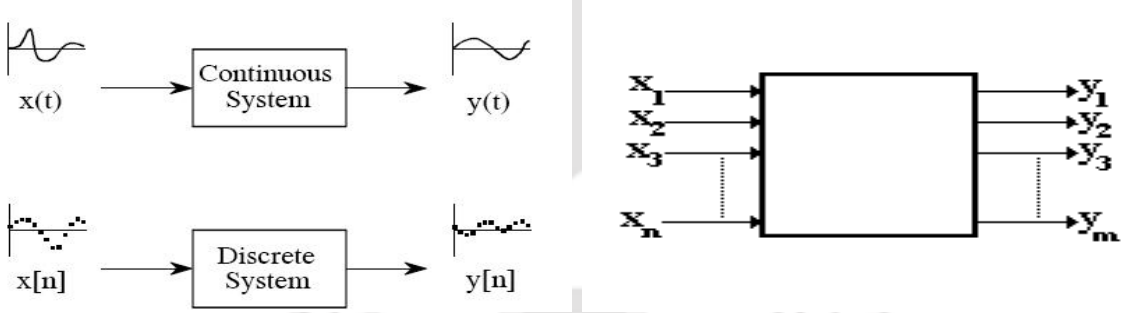

(a) (b)

Fig. 1.2. Schematic diagram representing (a) continuous and discrete system and (b) an MIMO system

1.3.1. Parametric and non-parametric system identification

The system identification techniques are primarily classified into two classes: (a) parametric technique and (b) non-parametric technique. The parametric system identification techniques

first choose the model structure and subsequently estimate the model parameters based on the best fit with measured data. On the other hand, the non-parametric system identification techniques do not (explicitly) employ the model structure and determine the system from either transfer functions (also, frequency response functions) or the impulse response functions. It may be mentioned that a linear time-invariant model can be described by its transfer functions or by the corresponding impulse response functions. Impulse response model and the frequency response model are considered as in Eq. (1.1) and Eq. (1.2) respectively.

$$y(t) = \int_0^t h(t-\tau)u(\tau)\mathrm{d}\tau \tag{1.1}$$

$$Y(j\omega) = H(j\omega)U(j\omega) \tag{1.2}$$

where, $h(t)$ represents impulse response function and $H(j\omega)$ represents frequency response function. $U(j\omega)$ and $u(t)$ are the frequency and time domain counterparts of input, while $Y(j\omega)$ and $y(t)$ are such counterparts of the output.

1.3.2. Major groups of system identification techniques

Presently, there exist many system identification techniques in literature considering the overall domain of applications. Some of these major system identification techniques are mentioned as follows:

(a) Least squares based techniques:

- Ordinary least squares
- Weighted least squares
- Recursive least squares
- Kalman filter etc.

(b) Maximum likelihood estimator (MLE) and Bayesian Estimation.

(c) Minimal realization theory based technique:

- Eigensystem realization algorithm (ERA) etc.

(d) Subspace based techniques:

- Numerical algorithms for subspace state space system identification (N4SID).
- Stochastic subspace identification (SSI) etc.

(e) Signal-processing based techniques

1.3.3. *System identification of large Structural systems*

In case of the system identification of structural systems, the excitation-force is considered as the input, while the generated response (displacement, velocity or acceleration) is taken as output. The excitation force is usually provided in the form of periodic, transient or random excitations. System identification exercises associated with civil, aerospace or mechanical structures generally evaluates the system parameters in terms of modal parameters. Such exercises are also regarded as experimental modal analysis (EMA). However, traditional EMA faces various limitations while applying for the large structural systems like:

(a) Artificial excitation, a requirement for the traditional EMA, becomes very difficult in the field test associated with large structures.

(b) Traditional EMA is normally conducted in the laboratory environment creating appropriate loading condition. Creating such environment is usually a difficult task for large structures.

(c) Component, instead of complete system, is often tested in the lab environment, and boundary condition is required to be reasonably simulated. Simulation of boundary condition for large structure is quite challenging.

In case of large structure, modal analysis is carried out rather using only the output response data recorded in the operational condition. Such modal analysis is referred as operational modal analysis (OMA) or output-only modal analysis or output-only system-identification. Presently, multiples techniques are available to perform OMA having good success record. All the techniques primarily consider that the responses in operational condition are generated based on white-noise excitation.

1.4. FINITE ELEMENT MODEL UPDATING

Finite element model updating is the process to update/adjust any initial finite element model to an updated model having modal parameters with closer agreement with the experimentally identified modal parameters. The updating techniques are primarily classified as direct updating techniques and iterative updating techniques. A chart is presented in Fig. 1.3 representing different major techniques related to finite element model updating. Finally,

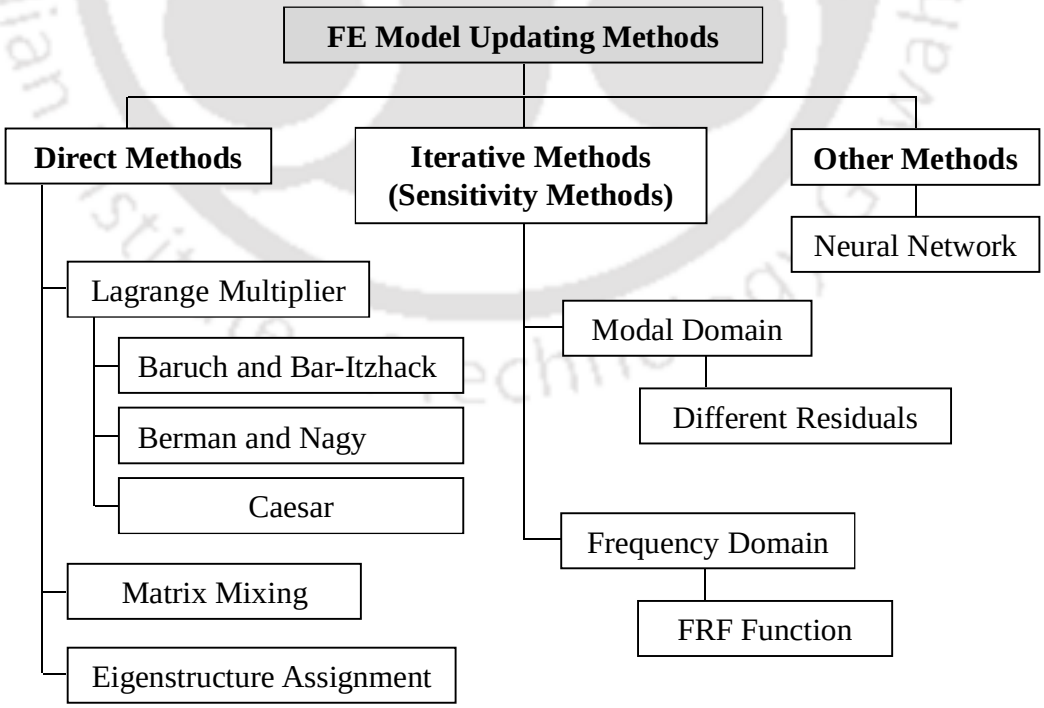

Fig.1.3. Major techniques associated to finite element model updating

applications of model updating in the civil engineering structures are summarised as follows:

(a) Structural parameter identification

(b) Structural damage identification

(c) Structural health monitoring

(d) Structural response prediction

(e) Efficient design of vibration controller.

1.5. PASSIVE VIBRATION CONTROL

Structural vibration control is an interesting area of research applicable to wide domain of civil, aerospace or mechanical engineering. Structural vibration control usually classified as:

(a) Passive control, which is performed solely with structural modification without any requirement of external energy.

(b) Active control, which is performed applying external energy in the form of control force.

(c) Semi-active control, which is performed by developing control forces in the form of changing the mechanical properties of devices at a very lesser requirement of external energy.

The present study considers the passive vibration control of bridge structure. The major passive vibration control devices are as follows:

(a) Tuned mass damper

(b) Metallic yield damper

(c) Friction devices

(d) Tuned liquid column damper

(e) Base isolation devices etc.

1.6. OBJECTIVE OF THE PRESENT STUDY

The present work is related to both analytical and experimental study , which is associated to structural health monitoring (non-continuous) as well as structural life span management. An existing important large truss bridge is considered as the sample structure in the present study. The major objectives of the present study are considered as follows:

(a) System identification evaluating the modal parameters of the bridge structure is a significant objective of this study. However, damage detection has not been considered as a feasible objective in view of the availability of bridge response data over a short period of time.

(b) This study considers the sensor-placement study as an important objective, since efficient system identification requires suitable placement of sensor.

(c) An accurate finite element model of the bridge with closer match of dynamic characteristics with those of the measured characteristics is considered as a goal.

(d) Design of passive vibration control system for the bridge is considered as the final objective of the present study. The controller design is intended to be carried out using the updated FE model.

1.7. OVERVIEW OF THE THESIS

This dissertation is an effort in both analytical and experimental aspects taking into account a very important existing large bridge as the sample structure. The studies reported in this thesis for fulfilling the objectives are presented in eight chapters. An introductory note on various domains associated to this thesis work is concisely presented in Chapter 1.

Chapter 2 presents a literature review covering various domains involved in the present study. A reasonably detailed literature review is carried out in five sections as (i) placement of sensors in operation modal analysis, (ii) experimentation: ambient vibration

data acquisition, (iii) identification of modal parameters, (iv) updating of FE model (direct updating) and (v) design of passive control device (tuned mass damper). Finally, scopes of the present study are identified in the light of the literature survey.

In Chapter 3, description of the sample truss bridge structure is presented in details along with the finite element modelling issues as implemented in SAP2000. The steps for extraction of mass and stiffness matrices for the bridge structure are also mentioned.

In Chapter 4, a detailed study is carried out regarding placement of sensor in operational modal analysis. A placement technique is proposed in this chapter, which is referred as modal contribution in output energy (MCOE). Details of this proposed technique, supportive analytical developments along with comparative study with other major existing techniques are presented in this chapter. Finally, suitable placement of sensor for the sample bridge structure is identified considering the limitations of availability of sensors.

Chapter 5 presents exercises on identification of modal parameters using the recorded ambient vibration response in terms of acceleration. Multiple techniques are applied for modal identification and the identified modal parameters are further statistically represented to have good level of confidence on the identified modal parameters.

In Chapter 6, direct updating of an initial finite element model of the sample bridge structure is carried out. Updated model is intended for efficient design of passive vibration control device. Two direct updating techniques are implemented to evaluate updated model having modal parameters (natural frequencies and mode shapes) with exact match to the corresponding measured parameters.

In Chapter 7, a study is carried out regarding analytical design of passive control device for the sample bridge in terms of tuned mass damper system. A strategy using modal frequency response function and further an approach for simultaneous control of horizontal as well as vertical modes are proposed. It also presents the time history simulations under

different types of loading for the demonstration of control performance of the designed passive control devices.

Chapter 8 presents the general conclusions of works carried out in the previous chapters along with the possible scopes for future works.

Chapter 2

LITERATURE REVIEW

2.1. INTRODUCTION

The present study is associated with both the analytical and experimental aspects of structural health monitoring as well as structural control. A very important existing large truss bridge, named as Saraighat Bridge which is situated in northeast region of India, is considered as sample bridge structure for this study. A photographic view of the Saraighat Bridge is shown in Fig. 2.1. It is a large rail-cum-road double-deck multi-span steel truss bridge with length of 1.3 km over the mighty river Brahmaputra in Assam. This bridge is situated in the highest seismic zone of India and hence, consideration of such a large bridge structure for the present study would be useful. Although various aspects of this study are associated with the Saraighat Bridge structure, works/developments related to the analytical aspect of this study are indeed general in nature.

Fig. 2.1. A photographic view of the Saraighat Bridge

Structural health monitoring (SHM) and structural control are the areas of engineering associated with the lifespan management of structures. Identification of modal parameters is commonly carried out as the primary phase of modal parameter based health monitoring

approach (vibration based non-continuous health monitoring). Modal parameters, which are important representative of dynamic characteristics for any structural system, exhibit good sensitivity to any changes in structural condition. In the identification of modal parameters of large structures, experimental modal analysis (EMA) becomes a difficult due to difficulties of large setup requirements of the EMA. Hence, operational modal analysis (OMA) or output-only system identification is generally performed for modal parameter identification of large structures. OMA can be performed efficiently if placement of sensor is carried out appropriately. Placement of sensor is an important area of research in the domain of structural health monitoring. The present study takes into account in details the placement of sensor in OMA of large structural system. Once the modal parameters are identified successfully, a baseline model is formed for the next phase of modal identification leading to damage-detection (based on the changes in modal parameters). Extent of health monitoring in the present study is limited to modal identification only as field data has been collected over a relatively small period of time. However, the identified modal parameters would be useful as benchmark for comparison during the next phase of modal identification. The present study is also focused towards finite element (FE) model updating and passive structural control. Direct model updating techniques with the ability of exact replication of measured natural frequencies and mode shapes in the updated FE model are adopted. The sole purpose of updating here is the effective design of passive control device. Finally, design of passive control device (tuned mass damper) is considered for the Saraighat Bridge with the objective of better serviceability and longer fatigue life.

2.2. LITERATURE REVIEW

The work plans of this study, as referred in introduction, may be subdivided broadly into five parts as: (i) placement of sensors in operation modal analysis, (ii) experimentation: ambient

vibration data acquisition, (iii) identification of modal parameters, (iv) updating of FE model (direct updating) and (v) design of passive control device (tuned mass damper). Accordingly, the literature survey is also classified in five parts.

2.2.1. Placement of sensors in operation modal analysis

Any arbitrary sensor placement may not provide good modal information like modal frequency and modal damping for a set of target modes. Thus, there exists a great deal of interest to identify the sensor locations for extraction of better modal information for target single or multiple modes in OMA. Limitation of availability of sensors, which is a common issue for large structural systems, attracts more interests in this regard. Observability (Chen 1984) measure was considered by many authors for identification of better sensor locations. Waldraff et al. (1998) considered maximization of minimum singular value of the observability grammian for sensor placement problem. Wilson and Guhe (2005) considered the minimization of condition number of the observability grammian. Similar work was implemented in structural system based on maximization of minimum eigen-value of observability grammian by Reynier and Abou-Kandil (1999). Hac and Liu (1993) considered the correlation between output-energy and observability grammian in the problem of control of flexible structure. Udwadia (1994) and Kirkegaard and Brincker (1994) evaluated sensor placement considering better information about identifying parameters based on the information and entropy theory. In these methods, the optimal sensor configuration is taken as the one that maximizes various norms (determinant or trace) of the Fisher information matrix (FIM) or its variants. In another approach based on information theory, Yuen et al. (2001) and Papadimitriou (2004) selected optimal sensor configuration as the one that minimizes the information entropy which gives a direct measure of the uncertainty in the estimate of system parameters. Kammer (1990) developed an iterative technique (effective-

independence) to find sensor location based on determinant of FIM. Yao et al. (1992) employed GA (genetic algorithm) using determinant of FIM. In these works of Kammer (1990) and Yao et al. (1992), modal responses were considered as parameters of estimation with best possible information and FIM was found as function of only target mode shape vector matrix. A modal approach framework was presented for placement of actuator / sensor for the flexible structures by Gawronski and Lim (1996); Gawronski (1997); Gawronski (2004). This modal approach framework evaluates modal participation at individual degree of freedom (DOF). Modal participation is evaluated separately for the target modes and subsequently sensor locations are identified using these participation profiles. System norms (H_2, H_∞, Hankel) associated to a mode of system were considered in the problem of active control by Gawronski (2004). Placement issues were analysed in almost-balanced coordinate (Gawronski 1997) as well as balanced coordinate (Gawronski and Lim 1996). Heo et al. (1997) proposed kinetic energy optimization technique (EOT) for sensor placement evaluation. Basic derivation of EOT has similarity with that of effective independence method. Papadopoulos and Garcia (1998) presented two methods for structural sensor placement. The first method selects the most linearly independent impulse responses at all candidate sensor locations and the second method iteratively removes sensors with lesser information contribution to FIM using principal component analysis. Pickrel (1999) presented sensor location methodology in test engineer's perspective with an example of a transport aeroplane. Cherng (2003) presented an approach based on the analytical formulation of singular value decomposition for a candidate-blocked Hankel matrix using signal subspace correlation techniques. Li et al. (2004) presented an easy to implement sensor placement technique for structural vibration measurement based on uniform design theory.

Meo and Zumpano (2005) carried out a comparative study among three groups of techniques as effective independence based techniques, kinetic energy based techniques and

variance method. They considered the Nottingham suspension bridge for comparisons and showed that effective independence based techniques perform better. Li et al. (2008) discussed an extension of MinMAC algorithm and carried out a comparative study with other techniques considering a bridge structure. It may be mentioned that works of Meo and Zumpano (2005); Li et al. (2008), regarding other techniques e.g. effective independence driving-point residue (EFI-DPR), eigenvalue vector product (EVP), non-optimal drive point (NODP), mode shape summation plot (MSSP), QR decomposition (QRD) as well as space domain sampling, are useful. Li et al. (2007) studied inherent relationship between two important sensor placement methods, modal kinetic energy (MKE) and effective independence (EI). Liu et al. (2008) attempted to overcome the difficulties of the GA and proposed the decimal two-dimension array coding method instead of binary coding method. Li et al. (2009) presented a simple and fast computational algorithm for evaluation of Effective Independence (EI) technique for sensor location identification based on QR decomposition. Stephan (2012) presented an approach for identifying the most relevant sensor placement locations based on two criteria: observability of mode shapes and information shared by sensors. A novel approach was introduced for optimal sensor and/or actuator placement for structural health monitoring (SHM) applications in a Bayesian framework (Flynn and Todd 2010). Starting from a general formulation of Bayes risk Flynn and Todd derived a global optimality criterion within a detection theory framework. Nestorovic and Trajkov (2013) considered the problem of optimal actuator and sensor placement for active large flexible structures. A placement optimization method was proposed based on balanced reduced models to overcome disadvantages arising from challenging numerical procedures related with high order structural models. It may be mentioned that many times sensor placement is carried out with reduced model retaining selected DOF as master nodes. A static reduction proposed by Guyan (1965) and System

equivalent reduction expansion process (SEREP) proposed by O'Callahan et al. (1989) are commonly considered for reduced model retaining only master nodes. Bonisoli et al. (2009) presented a master node selection criteria by means of applying SEREP approach with modal-geometrical selection criterion (MoGeSeC) methodology. Meo and Zumpano (2005) presented an example of master node selection for a bridge structure. Finally, a sensor placement methodology developed in the present work and same is proposed to be used in operational modal analysis (OMA) (Debnath et al. 2012). In this sensor placement methodology, modal contribution in output energy (MCOE) was proposed as a modal measure to evaluate modal participation. MCOE is evaluated using observability grammian for any types of response measurement (displacement, velocity or acceleration), when a system is released from any initial condition.

Major techniques for sensor placement as found in literature are: EI technique, kinetic energy approach based MKE technique and modal approach based technique. The modal approach provides more flexibility in the selection of sensor-location as compared to the other techniques. However, the existing modal measures (Hankel, H_∞ and H_2 norms) used by the modal approach require the knowledge of input-locations where excitations are provided. It is indeed difficult to precisely identify the input-locations in case of output-only system identification or OMA. In view of this, existing modal measures don't appear to be quite suitable for sensor placement in OMA based on the modal approach methodology. Therefore, there is a scope for further exploration of a new modal measure which is more suitable in OMA.

2.2.2. Ambient vibration data acquisition

Many practical applications of OMA have been published in literature. The experimental issues, namely the ambient response type, data sampling rate along with filtering operations

are presented here including information on bridge-type. At the end of this section, sensor placement details are discussed with particular ref. to five major bridge structures. Tsing Ma bridge, Hong Kong was investigated for modal parameters using OMA (Qin et al. 2001). With 1377m main span it is the longest suspension bridge in the world carrying both road and rail traffic. Ambient vibration data in the form of acceleration response were recorded. Data were recorded at the sampling rate of 50 Hz and finally anti-aliasing was performed with a cut-off frequency as 20 Hz. OMA was carried out for the North Grand Island (NGI) Bridge, a cantilever truss bridge in USA, by Shama et al. (2001). This bridge consists of 19 spans having total length of 1227 meters. Acceleration responses were measured at the sampling rate of 100 Hz. Later an anti-aliasing filtering was performed at the sampling rate of 50 Hz. Cumberland River Bridge in USA, a three span continuous plate-girder bridge with length of 509 m, was investigated with output-only system identification by Ren et al. (2004). Acceleration responses were recorded for the system identification. Sampling rate for data acquisition was considered at 1000 Hz which was much higher than the required rate of 10 Hz. The recorded data later re-sampled at 25 Hz thus covering frequency of interest till 12.5 Hz. Output-only system identification using wireless sensor network is gaining popularity as an attractive strategy due to the ease of deployment and data acquisition. An investigation was carried out for validation of such wireless sensor network based OMA. The Geumdang Bridge in Korea, a concrete box girder bridge, was considered for such investigation by Lynch et al. (2006). Acceleration responses were recorded at 200 Hz using both the traditional wired as well as wireless system. Later data were filtered for frequencies higher than 25 Hz. The data acquired in the both the wireless as well as wired manner were found to be in good agreement. Alfred Zampa Memorial Bridge, San Francisco, USA, a long-span suspension bridge, was considered for dynamic testing and OMA by Conte et al. (2008); He et al. (2009). Ambient responses were recorded in the form of acceleration histories at a

sampling rate of 200 Hz. The Nyquist frequency (100 Hz) was much higher than the frequency of interest (4 Hz). Data was filtered in two steps as (a) below 1 Hz and (b) 1–4 Hz for separately performing analysis for lower and higher frequency modes. Gi-Lu Bridge, a long-span cable-stayed bridge in Taiwan, was studied for output-only system identification by Weng et al. (2008). Ambient velocity responses were recorded using sampling rate of 100 Hz. A FRP composite pedestrian truss bridge was investigated using OMA in the laboratory of Swiss Federal Institute of Technology by Bai and Keller (2008). The ambient excitation was provided by random walking across the bridge by three persons. Acceleration responses were considered. Data acquisition was carried out using a sampling rate of 600 Hz and later data was re-sampled at 60 Hz. Hakucho Suspension Bridge, Japan was considered for OMA by Siringoringo and Fujino (2008). Data acquisition was carried out in the form of acceleration histories at a sampling rate of 100 Hz. Wireless sensor-network based OMA was performed for the Golden Gate Bridge which is long-span suspension bridge in San Francisco, USA by Pakzad and Fenves (2009). Acceleration response was considered and data were recorded at a sampling rate of 50 Hz. Later data were filtered for the frequencies more than 5 Hz. Eynel Highway Bridge, an arch type steel highway bridges in Turkey, was investigated by Altunişik et al. (2011a) using ambient acceleration response data. Altunişik et al. (2011b) performed OMA using acceleration response for the Gülburnu Highway Bridge which is a post-tensioned segmental concrete highway bridge situated in Turkey. A cable-stayed bridge over the river Oglio in Italy was investigated using OMA considering measured acceleration response by Benedettini and Gentile (2011). Data were recorded at sampling rate of 400 Hz and later down-sampled to 40 Hz. A stress-ribbon footbridge, situated in the Faculty of Engineering of University of Porto, was considered for OMA using acceleration response (Hu et al. 2012) where data were recorded at 100 Hz. Shi et al. (2012) studied the modal parameters based on OMA for the Shanghai World Financial Center. Acceleration

responses were recorded at the sampling rate of 20 Hz. Long-time monitoring of Tamar Bridge, a long-span suspension bridge in Southwest England, carried out by Cross et al. (2013) based on OMA. Acceleration responses were measured at a sampling rate of 64 Hz. Moreover, variations of the modal frequencies were presented with respect to temperature, traffic loading and wind speed. Finally, various interesting approaches e.g. Magalhães et al. (2009); Ubertini et al. (2013) for automated OMA are reported in literature. Results are identified based on multiple data-sets. Magalhães et al. (2009) used hierarchical clustering based automation, while Ubertini et al. (2013) used non-hierarchical clustering based automation.

Finally, sensors arrangements are discussed with particular references to five major cases of output-only system-identification. Firstly, instrumentation arrangement adopted in the OMA of Tsing Ma Bridge (Qin et al. 2001) is shown in Fig. 2.2. A total of 96 locations and a total of 170 DOF were considered for response measurements. Vertical, transverse & longitudinal responses have been measured (with lesser numbers of longitudinal measurements). Due to the limitations in availability of sensors, all the DOF have been covered with groups of 13 DOF. In each group, 3 DOF ware considered as the reference channels (one in each of vertical, longitudinal and transversal directions respectively). Locations of sensors (accelerometers) and the measured coordinates are shown in Fig. 2.2.

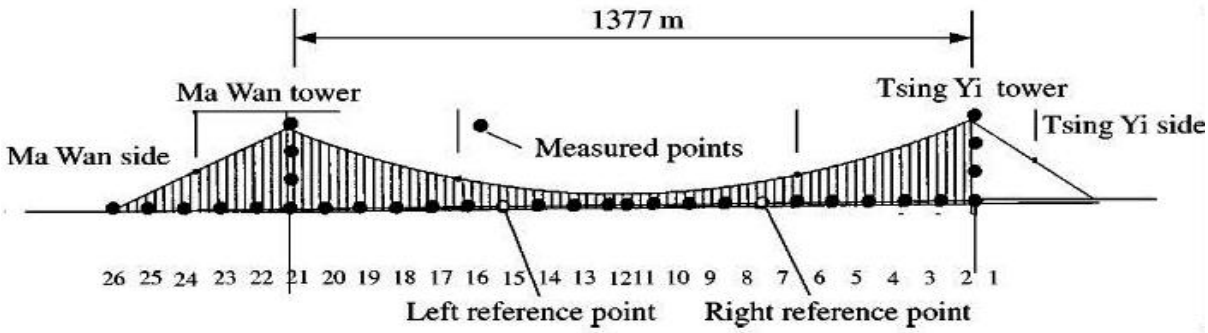

(a)

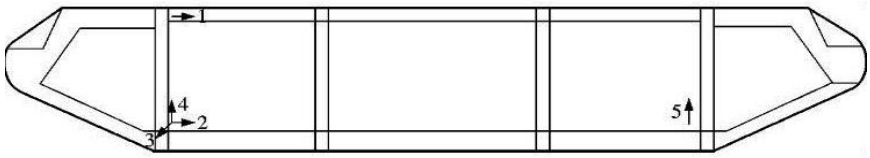

(b)

Fig. 2.2. (a) Measurement locations along Tsing Ma bridge (b) Layout of sensors on each measurement section (courtesy of Qin et al. 2001)

Secondly, instrumentation arrangement considered for OMA of NGI Bridge (Shama et al. 2001) is shown in Fig. 2.3. Ten numbers of data-channels were used for response measurement at a time to cover all the measurement channels based on different data-acquisition sessions. Out of these ten channels five channels were kept stationary as reference at reference section marked as "R", while the rest five channels were taken along each of the section marked as 1 to 13.

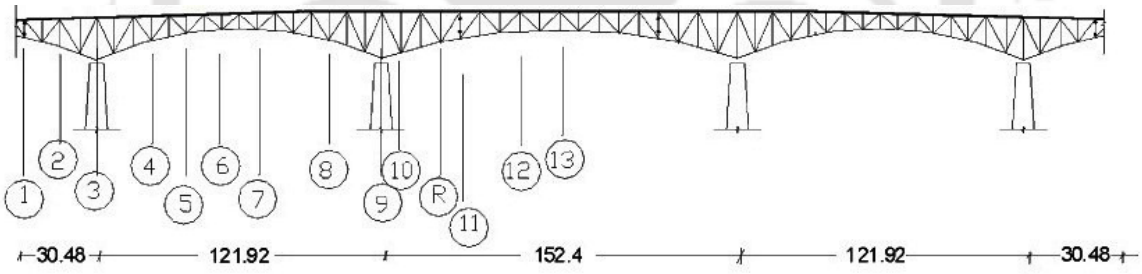

(a) Measurement Stations Along the NGI Bridge

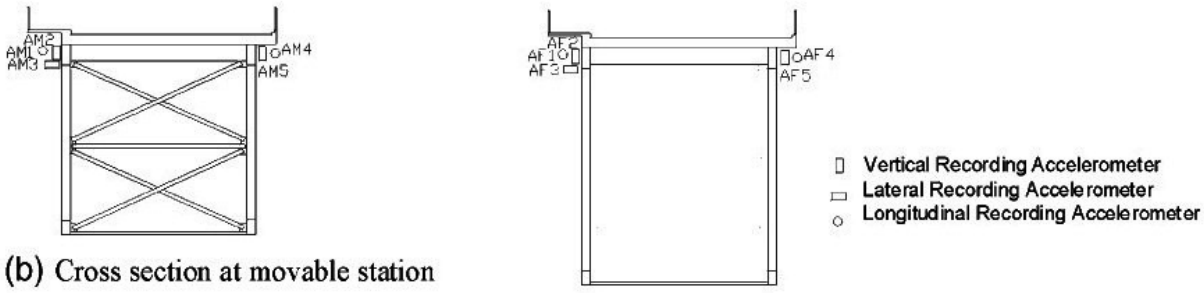

(b) Cross section at movable station

(c) Cross section at Reference station

Fig. 2.3. Measurement stations along the NGI Bridge (courtesy of Shama et al. 2001)

Thirdly, instrumentation arrangement employed in the OMA of Gi-Lu cable-stayed bridge (Weng et al. 2008) is shown in Fig. 2.4. Instrumentation of the Gi-Lu cable-stayed bridge was carried out with low-cost and easy-to-deploy wireless sensors. Three types of tests were carried out. Test-1: 10 wireless sensor (velocity meter) pairs were installed along the bridge deck to record its vertical vibration. Test 2: Similarly 10 pairs were installed to record the transverse vibrations. Test 3: 12 wireless sensor (velocity meter) pairs were installed on one side of the bridge to simultaneously record the cables and deck vibrations (vertical and transverse).

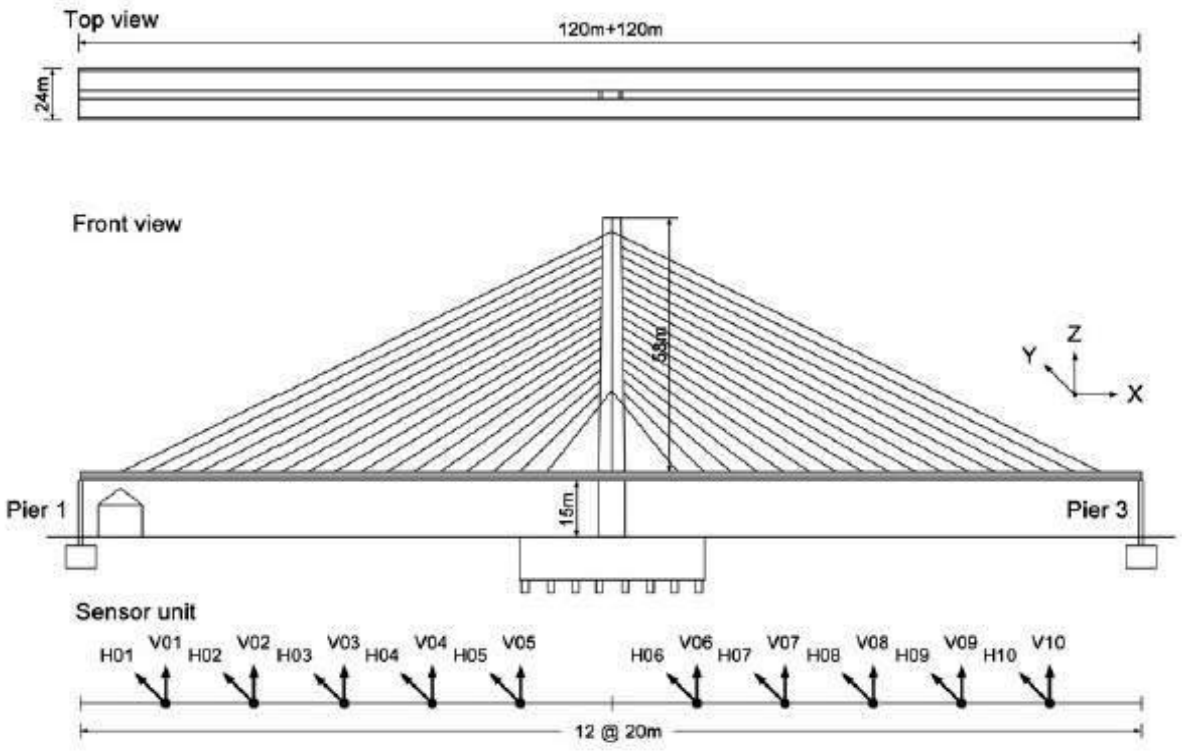

(a)

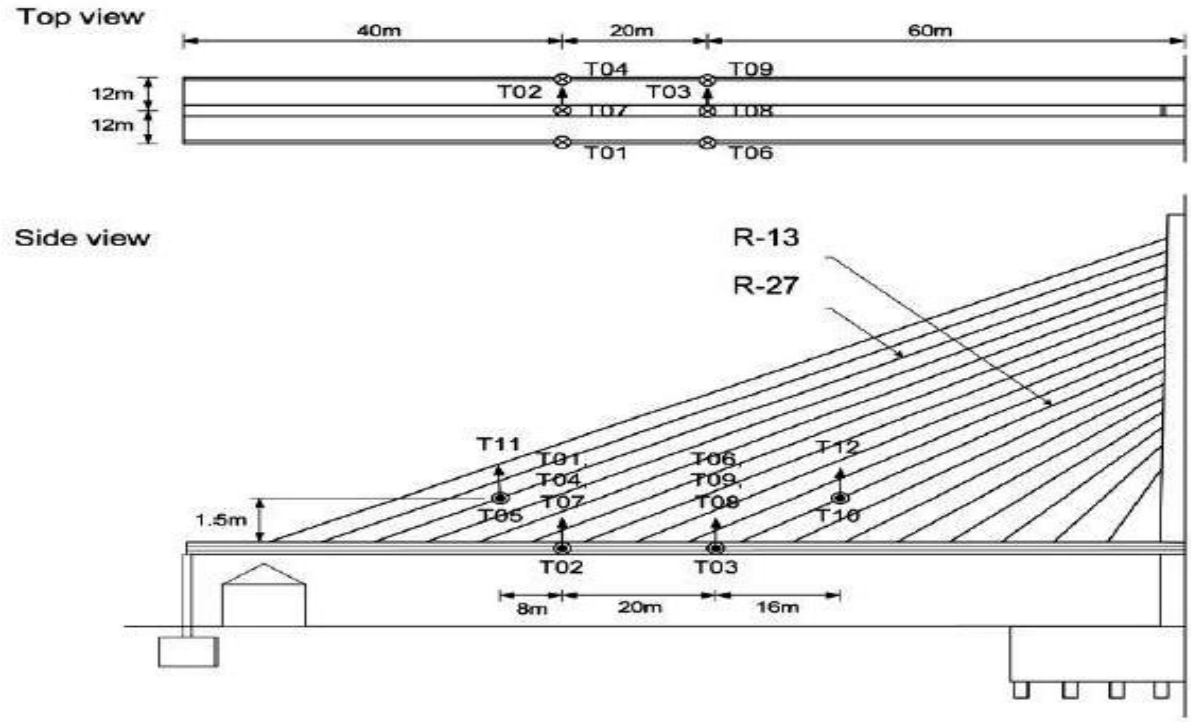

(b)

Fig. 2.4. Measurement locations considered for (a) test 1 and 2 (b) test 3 during the data acquisition of the Gi-Lu cable-stayed bridge (courtesy of Weng et al. 2008)

Fourthly, instrumentation arrangement utilized in the OMA of Alfred Zampa Memorial Bridge (He et al. 2009) is shown in Fig. 2.5. The vibration responses of the bridge were measured using 34 uniaxial accelerometers and 10 triaxial accelerometers. Along the west side of the bridge deck, 14 stations were considered for measuring responses along all three directions, while 11 stations were taken into account along the east side of the bridge deck measuring responses along the vertical and horizontal directions. Thus, total 64 channels of acceleration responses were recorded where 25 channels were recorded along each of the vertical and horizontal directions while 14 channels were recorded along longitudinal direction.

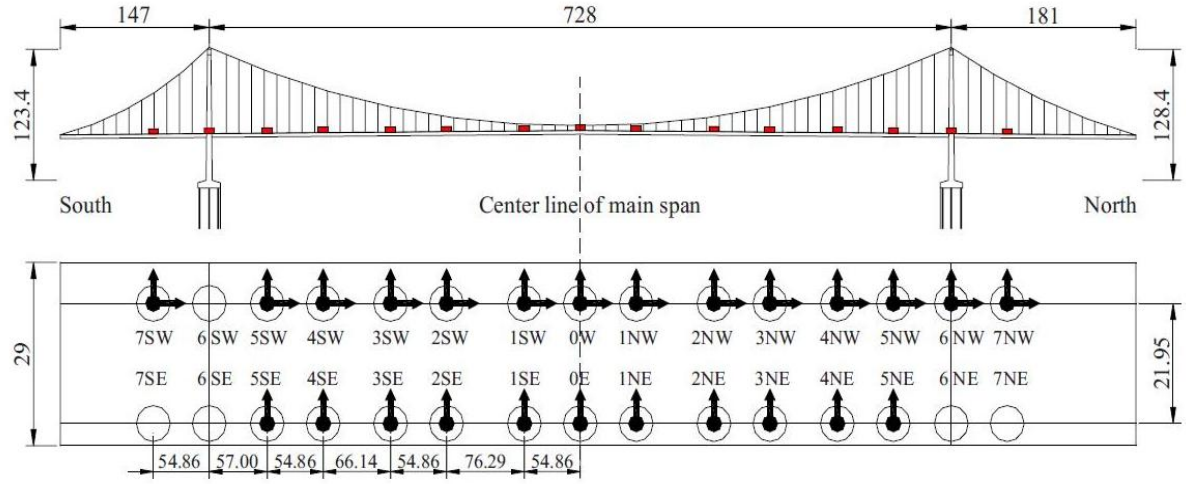

Fig. 2.5. Instrumentation (accelerometers) layout used in data acquisition for Alfred Zampa Memorial Bridge (courtesy of He et al. 2009)

Finally, instrumentation arrangement used in the OMA of Golden Gate Bridge (Pakzad and Fenves 2009) is shown in Fig. 2.6. Wireless sensor network based instrumentation was employed in the Golden Gate Bridge. The main span of the bridge is covered with 56 nodes/locations measuring responses along the vertical and horizontal (transverse) directions.

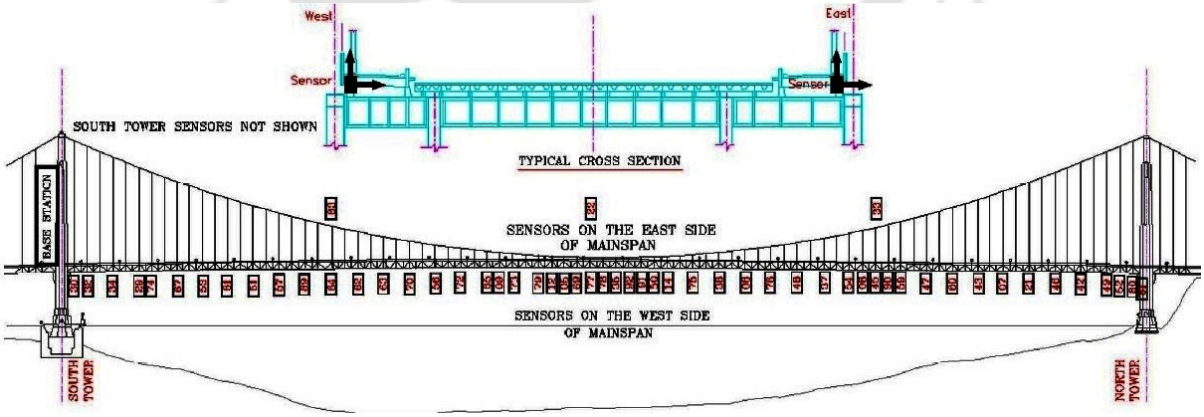

Fig. 2.6. Instrumentation plan for 56 acceleration sensor nodes on main span of Golden Gate Bridge (courtesy of Pakzad and Fenves 2009)

2.2.3. Identification of modal parameters

Structural system identification (Alvin et al. 2003) helps to construct nearly accurate numerical model of a structural system based on the knowledge of physical input and output. Commonly modal model (Ewins 2000a) is considered for identification using OMA. Techniques associated to OMA are classified as time domain technique, frequency domain technique and time-frequency domain technique. Time domain techniques as well frequency domain techniques are being used successfully for quite a long time while time-frequency techniques are not yet observed to be used so frequently. Time-frequency techniques are not considered in the present study. Literature survey here is limited with time and frequency domain techniques only.

Natural excitation technique (NExT) (James et al. 1995) is considered as major development in OMA in time domain. It established that the correlation function (CF) between two ambient vibration response measurements has the same analytical form as the impulse response function (IRF). This helps to apply the major non-parametric (Ljung 1999) system identification techniques using CF instead of IRF in OMA. Eigensystem realization algorithm (ERA) (Juang and Pappa 1985; Juang and Pappa 1986), one such popular non-parametric technique, identifies state space matrices in multi-input multi output (MIMO) framework using IRF as well as CF. ERA was developed based on minimum realization theory (Ho and Kalman 1966) of system engineering. Least-squares complex exponential (LSCE) algorithm (Maia et al. 1998) and polyreference least-squares complex exponential (PRCE) method (Vold et al. 1982) are two techniques which apply least-square for modal parameter identification. LSCE is single input multi output (SIMO) based technique and PRCE is considered as the MIMO extension of LSCE. Ibrahim time-domain (ITD) technique (Ibrahim and Milkulcik 1976; Ibrahim and Milkulcik 1977) is another SIMO technique which identifies the modal parameters using the free decay responses. Free decay responses can be

estimated from the ambient vibration responses using the random decrement technique (RDT) (Ibrahim 1977) and this makes possible for the techniques like ITD to identify the modal parameters using ambient vibration data. The data-driven stochastic subspace identification (SSI-DATA) technique (Van Overschee and De Moor 1996) identifies the structural system in the form of state space matrices directly from the ambient response data. Some of the important inherent steps / measures of SSI-DATA are orthogonal or oblique projection, estimation of Kalman states, least-square, singular value decomposition (SVD) etc. Finally the modal parameters are obtained using the identified state space model. Covariance-driven stochastic subspace identification (SSI-COR) technique (Peeters and De Roeck 1999) is another technique based on the framework of SSI. The block Toeplitz matrix is decomposed using SVD to obtain the observability matrix and the stochastic controllability matrix. Subsequently the modal parameters are obtained. Further, auto regressive (AR) as well as auto regressive moving average (ARMA) based identification techniques have been implemented (Pandit 1991; Huang 2001; Pakzad and Fenves 2009; Loh and Wu 1996; He and De Roeck 1997; Kirkegaard el al. 1996) for modal parameter identification using ambient responses. It may be mentioned that Smail et al. (1999a; 1999b) proposed a new approach for modal analysis using the autoregressive moving average (ARMA) model and further presented the effect of model order and sampling frequency in modal analysis using ARMA model. Pakzad and Fenves (2009) identified the modal parameters in terms of central tendency and dispersion for better acceptability of the identified modal parameters. In many cases, it becomes difficult to measure from all the degrees of freedom (DOFs) in a single attempt while carrying out the ambient testing of large structures. All these DOFs are considered in multiple set-ups with overlapping reference sensors. A novel approach based on SSI named as SSI-ref (Peeters and De Roeck 1999; Peeters and De Roeck 2008) is developed to consider the multiple set-ups in the identification stage itself.

The simplest method in frequency domain is the peak-picking (PP) method (Bishop and Gladwell 1963). It provides reasonably good results under the assumption that the modes are well separated and the damping is lower. To avoid such limitations, frequency domain decomposition (FDD) method (Brincker et al. 2001) was presented based on the SVD of the power spectral density (PSD) matrix at every discrete frequency. First singular vector becomes an estimate of mode shape associated to a modal frequency and nearby PSD function helps to identify natural frequency and damping ratio. FDD method is further improved as frequency-spatial domain decomposition (FSDD) method (Zhang et al. 2005; Zhang et al. 2010) considering similarity establishment with the well-accepted complex mode indicator function (CMIF) method (Shih et al. 1988). FSDD identifies natural frequency and damping ratio using curve fitting with enhanced PSD. Enhanced PSD may be viewed as similar entity as enhanced FRF which was proposed by Shih et al. (1988). A frequency domain based maximum likelihood (ML) identification technique (Hermans et al. 1998) was proposed to extract the modal parameters from output-only response data. Rational fraction orthogonal polynomial (RFOP) method (Richardson and Formenti 1985; Richardson 1986) was presented to obtain the modal parameters using the output-only data, where frequency response function (FRF) is expressed in rational fraction form (orthogonal Forsythe polynomials) instead of partial fraction form. Further, a different version of ERA, in frequency domain, was presented by Juang and Suzuki (1988) along with demonstration of its good performance. Polyreference least-squares complex frequency (PolyMAX) technique was proposed by Peeters et al. (2004). In the first phase a stabilization diagram is constructed and frequencies along with damping ratios are evaluated. Secondly, the mode shapes, associated to the stable poles, are estimated using the least-squares frequency-domain (LSFD) method. In the recent time, output-only system identification in the framework of Bayesian statistics is observed to be carried out in the works of Yuen (2003); Au S-K (2012a, 2012b);

Au S-K et al. (2013). Finally, various OMA applications along with the employed OMA techniques are presented in Table 2.1 helping to understand popularity of various OMA techniques.

Table 2.1. Various OMA applications along with the employed OMA techniques

SL no.	Investigated structure (reference)	Employed techniques
1	Tsing Ma bridge (Qin et al. 2001)	An improved version of ERA (FERA)
2	North Grand Island Bridge (Shama et al. 2001)	Peak picking
3	Cumberland River Bridge (Ren et al. 2004)	Peak picking, SSI
4	FRP composite pedestrian truss bridge (Bai and Keller 2008)	Peak picking, SSI
5	Hakucho Suspension Bridge (Siringoringo and Fujino 2008)	ITD, NExT-ERA
6	Gi-Lu Bridge (Weng el at 2008)	SSI, FDD
7	Alfred Zampa Memorial Bridge (He et al. 2009)	NExT-ERA, SSI, EFDD
8	Concrete arch bridge, over the Douro River, North Portugal (Magalhães et al. 2009)	SSI
9	Golden Gate Bridge (Pakzad and Fenves 2009)	Autoregressive with moving average models (ARMA) based identification
10	Eynel Highway Bridge, an arch type steel highway bridges, located in Turkey (Altunişik et al. 2011a)	EFDD, SSI
11	Gülburnu Highway Bridge, a post-tensioned segmental concrete highway bridge, situated in Turkey (Altunişik et al. 2011b)	EFDD, SSI

12	A cable-stayed bridge over the river Oglio in Italy (Benedettini and Gentile 2011)	EFDD, SSI
13	A stress-ribbon footbridge situated in the Faculty of Engineering of University of Porto (Hu et al. 2012)	SSI
14	Shanghai World Financial Center (Shi et al. 2012)	PP, RDT, Hilbert-Huang transform
15	Tamar Bridge - a long-span suspension in Southwest England (Cross et al. 2013)	SSI
16	The San Michele Bridge and A13 highway overpass in Bologna (Ubertini et al. 2013)	FDD, SSI

Although many case studies are observed in the literature for various existing bridges as well as building structures, no large and complex bridge structure like the Saraighat Bridge is found to be investigated for modal parameters. Various strategies are found in literature for efficient modal identification against various unfavourable conditions, which are usually involved in OMA exercises. There are (a) implementation of multiple techniques, usually, both in time and frequency domains (b) identification of modal parameters in statistical way (central tendency, dispersion, confidence interval). Combined effort based on these major approaches is likely to have better acceptance of the identified modal parameters. Further, detailed study is not reported in the literature to find out the suitable size of Hankel Matrix, which is an important factor for efficient modal identification.

2.2.4. Updating of FE model

Finite element (FE) model updating is one of the most demanding applications associated to modal analysis/testing. FE model updating usually refines, corrects i.e. updates an initial

numerical FE model to an improved numerical model using the measured response of the corresponding real structural-system. Thus the improved numerical model becomes capable of simulating the corresponding real structural-system more accurately. The existing updating techniques can be broadly classified into three classes as: (i) direct updating techniques (ii) iterative techniques and (iii) frequency response based techniques. Present work deals with the direct model updating. Hence, literature review is kept here confined within the scope of direct updating only. FE model updating is quite a vast domain. However, an extensive review of literature on various types of updating techniques are presented by Mottershead and Friswell (1993); Friswell and Mottershead (1995); Ewins (2000b) etc.

An important as well as very popular branch of direct updating techniques is Lagrange multiplier based technique for direct updating. Optimization is carried out with the objective of minimal changes in the system matrices subjected to constraints, namely, modal orthogonality conditions in terms of mass and stiffness matrices; maintaining the symmetry of system matrices. All these Lagrange multiplier based techniques consider three quantities: measured modal data (natural frequencies and mode shapes), analytical mass matrix and analytical stiffness matrix. Baruch and Bar-Itzhack (1978); Baruch (1978) performed direct updating using Lagrange multiplier considering exact mass matrix. Baruch (1982, 1984) described these methods as reference basis methods because one of the quantities out of measured modal data, analytical mass matrix and analytical stiffness matrix is assumed to be exact or the reference, while the remaining two quantities are updated. The measured eigenvectors are primarily corrected so that they become orthogonal with respected to the analytical mass matrix and the updated stiffness matrix. Therefore, the experimental mode shapes are not reproduced exactly. In a similar framework, as adopted by Baruch (1984), Berman and Nagy (1983) used the measured data as the reference and both the analytical mass and stiffness matrices in separate attempts. The measured modal data is exactly

reproduced by the updated matrices. The Berman and Nagy technique is presented with additional details in Section 6.2.1. Caesar (1986) further suggested a range of methods in a similar framework based on this Lagrange multiplier method where analytical mass and stiffness matrices are updated in separate attempts. Wei (1989; 1990a; 1990b) proposed an alternative way of updating where both the mass and stiffness matrices updated simultaneously using the measured eigenvector matrix as the reference. Constraints are considered as mass orthogonality and symmetry of the updated matrices. Usually the stiffness matrix elements are far larger than the mass matrix elements, hence this technique is considered to be biased providing higher weight to stiffness matrix.

The direct updating techniques have limitations with respect to the updated mass and stiffness matrices because of lesser physical significance due to non-compliance of the connectivity of nodes. Moreover the updated matrices are fully populated while ideally the system matrices contain non-zero elements in band-format along the leading diagonal. An attempt was carried out to update the only non-zero elements of the stiffness matrix based on the Lagrange multiplier method (Kabe 1985). Kabe's approch is able to preserve the sparsity pattern of the original stiffness matrix, however, large volume of computation is required in this approach. In another attempt to maintain the connectivity, Smith and Beattie (1991) considered quasi-Newton methods for updating of the stiffness matrix preserving the structural connectivity. However, the complicacy of interpretation of results is not much reduced since the higher frequency modes, which are usually not measured, contribute most to the stiffness matrix. Based on the Kabe’s (1985) study on maintaining connectivity, further attempt in this direction were observed in works carried out by Kammer (1988); Halevi and Bucher (2003). Kammer's presented a reformulation of Kabe's method to achieve more numrical stability and to provide more flexibility in defining weights in objective function. However, computational cost was not improved.

Another type of popular direct updating technique is mentioned here as matrix mixing technique. This technique has the ability for exact reproduction of the measured modal frequencies and measured mode shapes. It utilizes the property of exact reconstruction of the mass and stiffness matrices using all the modal frequencies and mass normalized mode shapes with all DOF. Measurements of responses are carried out generally at limited numbers of coordinates. Moreover the numbers of identified modes are quite fewer than the numbers of analytical DOF. Such incompleteness in estimation of modal parameters gives raises various problems in estimating of mass and stiffness matrices. To overcome such difficulty, Thoren (1972) limited the number of DOF to equal the number of modes to maintain the modal matrix as square. Further, Ross (1971) added arbitrary linear independent vectors to the modal matrix to make it square as well as invertible. Further, Luk (1987) applied pseudo inversion to deal with the rectangular modal matrix. Matrix mixing technique (Caesar 1987; Link et al. 1987) is usually considered as a development over the methods of Ross (1971) and Thoren (1972). The matrix mixing technique is presented in chapter 6 with further details.

Another class of direct FE model updating techniques has been emerged from control theory is known as eigen-structure assignment method. This method updates the system matrices (usually stiffness and damping matrices) to assign the measured eigenvalues and eigenvectors (natural frequencies, damping ratios and mode shapes). If the eigenvalues alone are assigned then this method may be regarded as well known pole placement technique. In an early study, Srinathkumar (1978) presented some guidelines to determine numbers of eigenvalues and eigenvectors elements may be assigned based on the concept of controllability and observability. The updated stiffness and damping matrices may not be necessarily symmetric. Minas and Inman (1988; 1990) carried out an attempt based on optimization procedure to maintain these matrices as symmetric. Overcoming this symmetry issue, Zimmerman and Windengren (1990) produced symmetric updated stiffness and

damping matrices directly by solving a Riccati type matrix equation. Early discussions on maintaining symmetry in the eigen-structure assignment problem can be found in the work of Andry et al. (1983).

Apart from various classes of direct updating techniques mentioned above, there have been some other relevant developments as well. Bucher and Braun (1993) presented a theoretical development showing in details how the necessary mass and stiffness modifications can be computed using modal test data only, even when the measured data are incomplete. Baruch and Bar-Itzhack (1998) presented a technique to force the measured modes for satisfying the theoretical condition of weighted orthogonality in an optimal way with the objective of minimum differences among the measured and corrected modes. Such corrected shapes can be further utilized in appropriate direct updating exercises. Friswell et al. (1998) extended the reference basis methods to update the damping matrix. The mass matrix was considered as correct and damping along with stiffness matrices were updated simultaneously. In a similar attempt, Kuo et al. (2006) presented finite element model updating problem which incorporated the measured modal data into the analytical finite element model with updating the damping and stiffness matrices. Kenigsbuch and Halevi (1998) presented the reference basis approach of direct updating in a general framework in terms of solving constrained optimization problem. Datta et al. (2000, 2002) presented the partial eigenstructure assignment problem. It was demonstrated that with the appropriate choice of gain and input influence matrices, certain eigenpairs of a vibrating system may be assigned while the other eigenpairs remain unchanged. Carvalho et al. (2007) presented computationally convenient a new method for finite element matrix updating problem in an undamped model with the capability of preventing the appearance of spurious modes. Jacquelin et al. (2012) presented a direct updating technique based on a probabilistic approach where the natural frequencies and the eigenvectors of the system are measured and

assumed to be uncertain. Mao and Dai (2012) presented a new direct method for the finite element model updating technique which can preserve both no spill-over and positive semi-definiteness of the mass and stiffness matrices. Yuan (2013) recently presented a direct updating technique based on updating the analytical stiffness matrix. Updated matrix is attempted to retain many desired matrix properties satisfying the dynamic equation, symmetry, positive semi-definiteness and physical connectivity.

Although various updating techniques are available, the direct model updating is considered for the sample bridge. The sole aim of updating in the present study being efficient design of controller, direct updating is considered for their advantages like exact matching of the updated frequencies and mode shapes with the corresponding experimental frequencies and mode shapes. Moreover, applications of direct updating for large structural systems are not much observed in literature. Therefore it is a matter of great interest as well as challenge to consider this large bridge structure for direct FE model updating.

2.2.5. Design of passive control device

Amongst passive vibration control systems, the tuned mass damper (TMD) is considered as the oldest passive vibration control devices in existence. TMD system, when connected with a single degree of freedom (SDOF) primary system, is also observed to be referred as dynamic vibration absorber (DVA). One of primary reporting of the TMD/DVA problem is observed in the works of Ormondroyd and Den Hartog (1928). In an early attempt, Den Hartog (1956) solved the DVA problem considering the SDOF primary system is excited with sinusoidal varying force. The early research/application on TMD system was usually focused more towards structural vibration control under the wind excitations. Wiesner (1979) extended Den Hartog's (1956) study for similar SDOF primary system considering the wind-excitation as white noise. Investigation of performances of TMD systems under seismic

loading (base-excitation) also became an area of interest. Sladek and Klingner (1983) investigated the performance of TMD system under seismic excitations considering the primary system as an SDOF system. A performance study of TMD system, coupled with SDOF primary system, with uncertain parameters was carried out by Jensen et al. (1992). Uncertain parameters were modelled as time-independent random variables in that study. It was demonstrated that uncertainties in the system parameters may have significant effect on the TMD efficiency, especially for the lightly damped systems. In an introductory work regarding multiple TMD (MTMD) system, Xu and Igusa (1992) considered a main structure supporting a large number of substructures having closely spaced natural frequencies. Effects of the substructures on the response of the main structure were characterized considering the base-excitation type as well as the non base-excitation type of loading. A comparative study between single TMD (STMD) system and MTMD system, both coupled with SDOF primary system, was carried out to asses their effectiveness and robustness by Yamaguchi and Harnpornchai (1993). A numerical searching procedure for finding out the optimal parameters of single TMD system coupled with SDOF primary system was presented by Tsai and Lin (1993). Fujino and Abé (1993) presented various formulas based on perturbation solutions for designing the STMD system coupled with SDOF primary system. These formulas were recommended for mass ratios less than 0.02 to achieve accuracy. Abé and Fujino (1994) further presented various formulas for designing the MTMD system coupled with SDOF primary system using perturbation solutions. It was demonstrated that MTMD system is more robust than the STMD system although efficiency is similar. Igusa and Xu (1994) further extended their work based on asymptotic theories (Dowell and Kubota 1985) and mean value theory (Skudrzyk 1968). Jangid (1995) studied the performance of MTMD system considering the excitation as stationary random process and MTMD system was found more efficient than the STMD system. Abé and Igusa (1995) studied the characteristics

of TMD systems for response control of structures with closely spaced natural frequencies. This study was based on perturbation theory considering both the lumped-mass and distributed mass structures idea. Papadimitriou et al. (1997) presented a probabilistic optimal design methodology modelling time-invariant uncertain structural parameters as random variables with prescribed probability distribution. Consideration of structural uncertainties is found to improve considerably the robustness of TMD designs. Sadek et al. (1997) presented a comprehensive study regarding performance of optimally designed TMD system under the seismic loading. It is shown that significant reduction in the response of tall buildings can be achieved under seismic excitations. Jangid and Datta (1997) investigated the dynamic response behaviour of a simple torsionally coupled system with MTMD system. Excitation was modelled as stationary random process in this study. Hadi and Arfiadi (1998) studied designs of TMD systems for MDOF system taking into account all the modes instead of contemporary approach of targeting single mode. The H_2 norm of the transfer function was considered as the objective function and optimization was carried out using the genetic algorithm (GA). Rana and Soong (1998) explained the correspondence of designing MTMD system for a particular mode of MDOF structural system with designing of MTMD system for a SDOF structure. Therefore, design of TMD system for MDOF structural system has become simplified based on this mode-wise TMD design approach. Li (2002) presented design of MTMD system subjected to base-excitation type loading along with a comprehensive discussion on various possible models of MTMD systems.

Design of TMD/DVA is also observed to be carried out based on H_∞ optimization i.e. minimization of H_∞ norm. Nishihara and Asami (2002) developed exact optimal solution with minimization of the maximum amplitude magnification factor in the form of H_∞ norm of an SDOF primary system using DVA. Asami et al. (2002) proposed a series solution for analytical evaluation of the H_∞ norm for an SDOF primary system using DVA as the control

device. Numerical evaluation of H_∞ norm for the design of vibration absorber was carried out by Randall et al. (1981), Thompson (1981), Soom and Lee (1983). The first application of minimization of H_∞ norm for the design of vibration absorber was reported by Ormondroyd and Den Hartog (1928). Cheung and Wong (2011) proposed an alternative procedure for the H_∞ optimization of the DVA problem. A new set of optimum tuning frequency and damping of the absorber is derived resulting in lower maximum amplitude of responses than those reported in the literature. Ozer and Royston (2005) extended the classical Den Hartog approach of fixed points to multi-degree-of-freedom (MDOF) undamped primary systems. Similarly, Dayou (2006) extended the fixed point concept for response control of the continuous structure with well separated natural frequencies.

The present study focuses on OMA of truss bridge structure and passive vibration control using TMD system based on updated model. In view of this, literature survey regarding the applications of TMD systems is confined associated to bridge structures only. Das and Dey (1992) investigated the performance of TMD system for numerically simulated multi-modal bridge structure subjected to random process-excitation. TMD system for a particular mode was design based on the guidelines of Den Hartog (1956). Application of TMD systems for bridge structures are usually observed for suppressing wind and vehicle/traffic induced vibrations. In cases of wind-induced vibration, three kinds of vibration mechanisms are observed namely, buffeting, flutter and vortex-induced vibration. TMD systems are observed to be effective to control all types of wind-induced vibrations. Gu and Xiang (1992) developed a mathematical model, based on the buffeting analysis method proposed by Scanlan and Gade (1977), for design of TMD system to suppress the buffeting response of long-span bridges. Gu et al. (1994) presented formulas providing optimal solutions for the parameters of TMD system for suppressing the wind-induced vertical buffeting response of long span bridges. Lin et al. (2000) presented a TMD device which

simultaneously reduces the vertical and torsional buffeting responses of long-span bridges. Gu et al. (2001) presented a study on buffeting induced vibration control of the Yangpu Bridge using MTMD system. Chang et al. (2003) presented an idea for control of the dual-mode buffeting response in suspension bridges under service conditions using two TMD systems. The bridge was assumed to vibrate in two vertical modes. Xing et al. (2013) suggested the use of counterweight as the mass of TMD system in case of long-span bridges. Thus the extra dead-loading from the mass of TMD system can be avoided.

Pourzeynali and Datta (2002) studied the control of flutter condition of suspension bridges using a combined vertical and torsional tuned mass damper (TMD) system. The effectiveness of the TMD system is investigated through a parametric study. Chen and Kareem (2003) investigated the efficiency of MTMD system for flutter control of bridge structures and demonstrated that TMD systems are more effective against soft-type flutter than hard-type flutter. Kwon and Park (2004) presented design methodologies of TMD system to control the bridge flutter considering uncertainties of aerodynamic data in order to enhance the robustness of TMD devices against frequency drift caused by wind-bridge interaction. An irregular MTMD (IMTMD) device was proposed having unequal frequency interval and different damping ratio of each individual TMD-unit. IMTMD was found to be more effective in flutter-response control compared to STMD and conventional MTMD system. Chen and Cai (2004) presented an alternative design approach for TMD systems for suppression of the modal coupling effect (flutter) among modes under strong wind.

Larsena et al. (1995) presented design aspects of TMD systems for control of vortex-induced vibrations of the Great Belt East Bridge approach spans. The bridge structure was tested with wind tunnel tests and it was confirmed that approach bridge structures were prone to vortex-shedding excitation at wind speeds encountered regularly at the bridge site. Larose et al. (1995) carried out a full-bridge aero-elastic model study of a multi-span approach

bridge to examine the vortex-shedding oscillations for the vertical bending modes. The model TMD systems were installed in the bridge model to observe the performance of the control devices. Fujino and Yoshida (2002) developed MTMD system specifically to control first and second vertical flexural modes of the Trans-Tokyo Bay Highway Crossing Bridge. Designed MTMD systems were installed in the bridge and a significant improvement in performance was reported. Patil et al. (2011) presented the mitigation of vortex-induced vibrations control for long-span bridges as a multi-objective optimization problem. The objective of mitigation of vortex-induced vibrations can be achieved by either retrofitting cross-sectional shapes or adding TMD devices.

Kwon et al. (1998) carried out a study for vibration control of bridges under moving loads using a TMD device where the TMD device was tuned to the first dominant vertical mode. Moving loads, in terms of TGV high-speed trains, were modelled as 2 degree of freedom (DOF) systems. Jo et al. (2001) investigated the performance of TMD system for a three-span steel box bridge. The TMD device installed on the steel box bridge was not so effective in reducing the maximum deflection however same is found to reduce efficiently the free vibrations. Wang et al. (2003) investigated the applicability of TMD system to suppress train-induced vibration on bridges while modelling the railway bridge as an Euler-Bernouli beam. Yau and Yang (2004a) studied the vibration reduction of cable-stayed bridges subjected to the passage of high-speed trains considering multiple dominant vertical modes. STMD system was designed for each of the target modes. The overall design was carried out by enforcing the resonant peaks of target modes to be equal. Further, Yau and Yang (2004b) achieved vibration reduction of continuous truss bridges subjected to moving train loads adopting a similar principle. However, a wide-band MTMD system was considered as passive control device in this work. Lin et al. (2005) studied the applicability of MTMD systems to suppress train-induced vibration on bridges modelling a railway bridge as an

Euler-Bernoulli beam. The proposed MTMD system was observed to be more effective and reliable than STMD system. Li et al. (2005) investigated the performance of MTMD system for vibration mitigation of railway bridges under high-speed trains. Luu et al. (2012) proposed the design of TMD systems based on H_2 optimization to suppress multi-resonant dynamic structural response of high-speed railway bridges. It was suggested that the parameters of TMD systems were optimized simultaneously for different modes contributing significantly to attenuate the multi-resonant peaks in order to make the TMD systems more effective and robust. Chen and Wu (2008) carried out an interesting study to design TMD system targeting both the vehicle and wind induced vibrations simultaneously contrary to the conventional approach of considering either vehicle or wind induced vibration. An integrated analytical model was proposed for a long-span bridge in that study. Finally, it may be mentioned that TMD system are also observed to be implemented for pedestrian or foot-bridges (Brownjohn and Pavic 2007; Caetano et al. 2010a; Caetano et al. 2010b; Li et al. 2010).

From the literature survey, very limited works are observed for design of TMD systems considering generalized loading with simultaneous consideration of vertical, horizontal as well as torsional modes. The design of TMD system for bridge structures are carried out usually considering either wind loading or vehicle loading. Therefore, there are scopes for further research in the design of tuned mass damper systems for bridge structures, which are capable of suppressing the modal frequency responses from horizontal, transverse as well as torsional modes. Such design is expected to provide effective design of TMD systems suppressing vibration under general loading conditions e.g. wind-induced vibration, vehicle-induced vibration etc.

2.3. SCOPE OF THE PRESENT STUDY

On the basis of literature survey, scopes of the present study on OMA of large truss bridge structure and passive vibration control using TMD system based on updated model are identified as follows:

Three major strategies for optimal sensor placement are observed in literature as: (a) effective independence (EI) method (b) kinetic energy approach based modal kinetic energy (MKE) method and (c) a modal approach using various system norms (Hankel, H_∞ and H_2) applied to mode. EI and MKE methods are observed to be popular techniques in sensor placement evaluation. On the other hand the modal approach using various norms, primarily from the works of Gawronski (2004), appears appealing from the following points: (a) it provides options for consideration of different types of response measurement and (b) it uses a modal approach framework where modal participation of each of the target modes at individual DOF are first evaluated and subsequently the locations of sensors are identified for target modes using those participation profiles in a flexible as well as insightful manner. It may be interesting to carry out study regarding the optimal sensor placement for the Saraighat Bridge based on this modal approach framework. The existing modal measures (e.g. Hankel, H_∞ and H_2 norms), used by the modal approach methodology, require the knowledge of input-locations where excitations are provided. Therefore, the existing modal measures don't seem to be much appropriate for sensor placement in output-only system identification or OMA, since precise identification of input-locations is not easy. Further effort may be made in favour of any new modal measure having no dependency on the knowledge of input-locations and thus enabling this attractive modal approach framework more suitable for sensor placement in case of output only system identification or OMA. It is moreover desirable to have simple physical understanding associated with such a new modal measure to ensure higher confidence in sensor placement.

From the literature survey regarding instrumentation and ambient vibration measurements, some of key features may be noticed as: (a) Measurement of acceleration response is a usual practice. (b) Data was recorded at quite higher sampling rate in spite of actual requirement of lower sampling rate considering frequency range of interest of structures. (c) Sensors are primarily placed at the deck level of bridges providing priority on measuring data along the vertical and horizontal (transverse) directions. All such observations are taken into account during the data acquisition phase of this present study.

There is no investigation for output-only system identification for large truss bridge structure like the Saraighat Bridge is found in literature. Hence there exists a great deal of interest for modal identification of the Saraighat Bridge structure. Applying multiple techniques is usually considered for better acceptability of the identified modal parameters against various unfavourable conditions. Three most commonly are used techniques selected based on the literature review are: NExT-ERA, SSI and FDD. OMA of the Saraighat Bridge is proposed using these three techniques for better acceptability in identification of modal parameters. Further, for even better acceptability of modal identification, modal parameters are observed to be represented in terms of cental tendency and dispersion (Pakzad and Fenves 2009). Such statistical representation is intended to be considered in addition to applying multiple techniques for superior acceptability in modal identification of the Saraighat Bridge. Moreover, suitable size of the Hankel matrix, which is an important factor for efficient modal identification can be further investigated for better estimation of the modal parameters.

Many direct updating techniques are likely to be applicable for the Saraighat Bridge based on the literature survey. The present requirement of model updating is solely for design of more accurate passive control device. In view of the above, those direct updating techniques may be preferred which exactly replicate the measured modal frequencies and mode shapes in the updated finite element model. Two such important direct updating

techniques are observed in literature as: Lagrange multiplier based technique (Berman and Nagy 1983) and matrix mixing technique (Caser 1987; Link et al. 1987). It may be mentioned that although many other techniques are developed later, in many cases those techniques are not capable of exactly replicate the measured data in the updated model and further applications of those techniques are observed to be very limited. The analytical mass and stiffness matrices of the Saraighat Bridge are planned to be updated using these two above mentioned techniques. Any study towards further development of any updating methodology is not considered in the scope of present work. However, applications of direct updating for large structural systems are not much observed in literature and therefore it is a matter of interest to undertake a direct updating exercise for this large bridge structure.

From the literature survey, it is observed that the design of TMD system for bridge structures are carried out usually considering either wind loading or vehicle loading. To control wind-induced and vehicle-induced vibrations, different types of modes are to be targeted. Very limited works are observed for design considering generalized loading with simultaneous consideration of vertical, horizontal as well as torsional modes. Simultaneous design-considerations of dominant horizontal and vertical modes are indeed quite challenging. Thus, it is apparent that there are scopes for further research in the design of tuned mass damper systems for bridge structures, which are capable of suppressing the modal frequency responses from horizontal, transverse as well as torsional modes. Such design may lead to effective design of passive control devices suppressing wind-induced, vehicle-induced vibrations as well as vibrations from other excitation-sources.

Chapter 3

DESCRIPTION OF SAMPLE BRIDGE

3.1. INTRODUCTION

The major motives behind consideration of the Saraighat Bridge as the sample bridge structure in this present study are: (a) its importance as a life-line structure for the North-East India (b) its existence in the highest seismic zone of India (c) its age of service over more than 50 years. Thus, there exists great deal of interest in monitoring the health of this large bridge structure situated over the mighty river Brahmaputra. A concise descriptions regarding the salient structural details of elements, sectional properties etc. are presented in this chapter. Further, mass and stiffness matrices are required in the present study associated with passive vibration control using updated FE model. Therefore, finite element modelling is carried out for the same Bridge. SAP2000 (Non Linear V14.2.2), a commonly used structural analysis software is used for modelling the bridge structure.

3.2. DESCRIPTION OF THE SAMPLE BRIDGE

The Saraighat Bridge is comprised of 10 main spans and 2 approach spans. All the spans are simply supported. Length of each main span and approach span are 118.72 meters and 31.4 meters respectively. While the superstructure of the bridge is made of steel, the substructure and the foundation parts are made of reinforced concrete (RC). A photographic view of the bridge, showing a few main spans and some part of substructure/foundation system may be seen in Fig. 3.1. The finite element model of the bridge using SAP2000 and comprising of one main-span and the connected approach-span is shown in Fig. 3.2.

Fig. 3.1. A photographic view of the Saraighat Bridge

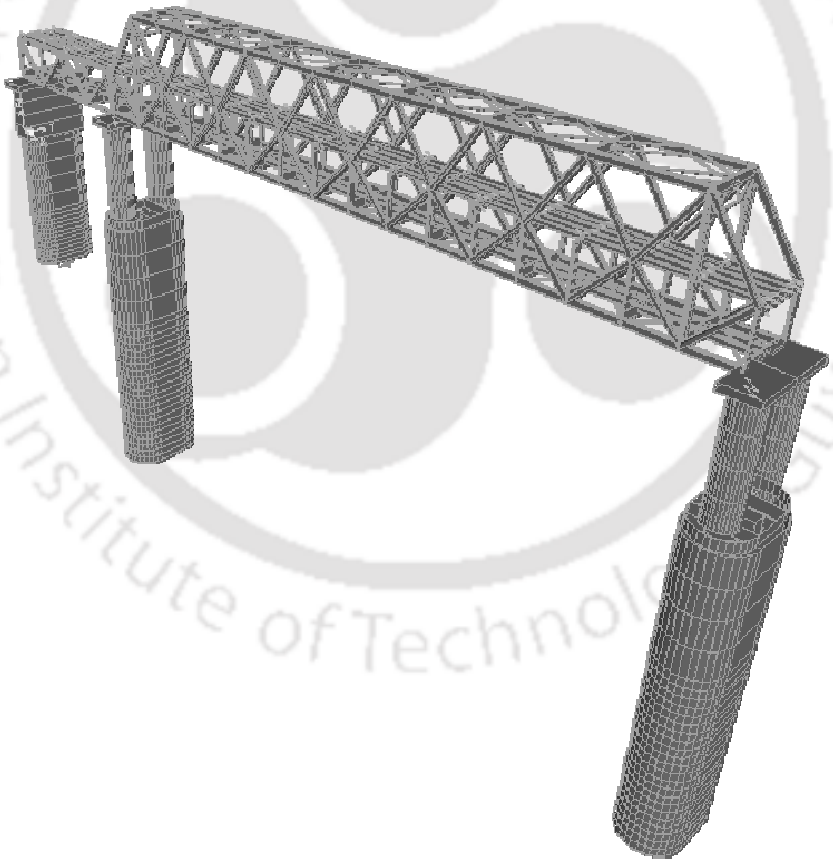

Fig. 3.2. Finite element model of Saraighat Bridge for one main-span and the connected approach-span

3.2.1. FE model of the Saraighat Bridge

The present study is primarily associated with system identification based on the dynamic response of the bridge. Therefore, portion of bridge showing significant dynamic response is considered for the finite element modelling. The following considerations are made in the selection of adopted FE model of the Saraighat Bridge:

(a) The RC substructure/foundation is significantly stiffer than the superstructure, which is made of steel. Therefore, contribution of substructure in the ambient vibration response of the superstructure is insignificant. In view of this, the superstructure can be modelled assuming restraints at the bearing level and thus neglecting the interaction of substructure/foundation.

(b) The approach span is not taken into account as the main span is considerably larger than the approach span.

(c) All the main spans are simply supported. Moreover, geometrical as well as sectional properties of the bridge elements in each span are similar and hence, one main span is considered for modal identification as well as for dynamic analysis.

Hence, a single main-span is adopted as the FE model for this study. The simply-supported end conditions are simulated using rocker-bearings at one side and roller-bearings at another. This bearing-action is modelled with typical restraints: (a) rocker-bearings are modelled with restraining all the three translational displacement-DOFs (b) roller-bearings are modelled by restraining two displacement-DOFs except the longitudinal DOF. A skeletal view (based on SAP2000 model) is shown in Fig. 3.3. The dimensions of this FE model are presented in Fig. 3.4.

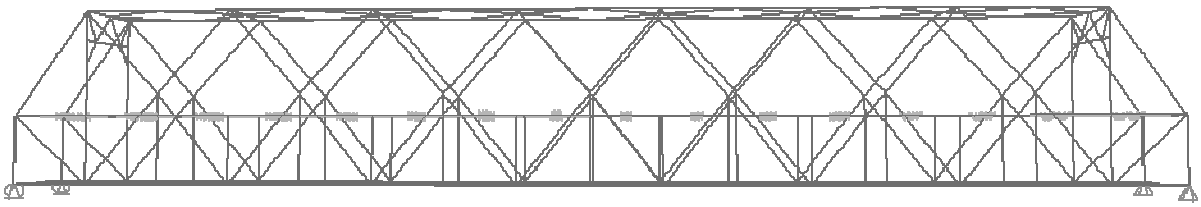

Fig. 3.3. FE model of the Saraighat Bridge (modelled using SAP2000 model)

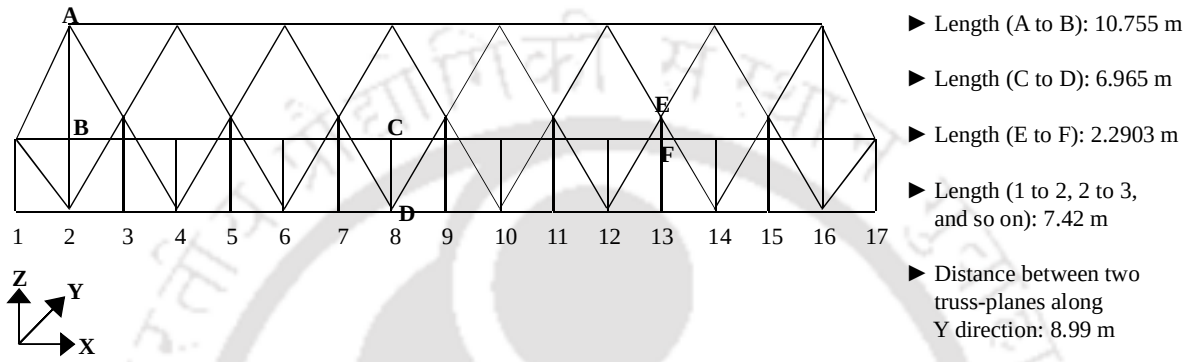

Fig. 3.4. Dimensions of the FE model of Saraighat Bridge

3.2.2. Details of structural members

Various members of the adopted FE model of Saraighat Bridge are shown in Fig. 3.5. These members are shown in side view (along Y axis) and in plan at three different levels as (i) rail level (ii) road level and (iii) top level as well as in a portal frame along A and B (as in Fig. 3.4). In Fig. 3.5, if a node position in any truss with least Y coordinate is denoted as P, then the corresponding (with same X and Z coordinates) point in another truss is denoted as P′. Sectional properties like cross-sectional area, area moments of inertia (denoted as I_1 and I_2) and torsion constant of all the members are presented in Table 3.1. Further, the thickness of slab at road-level deck is 0.175 m.

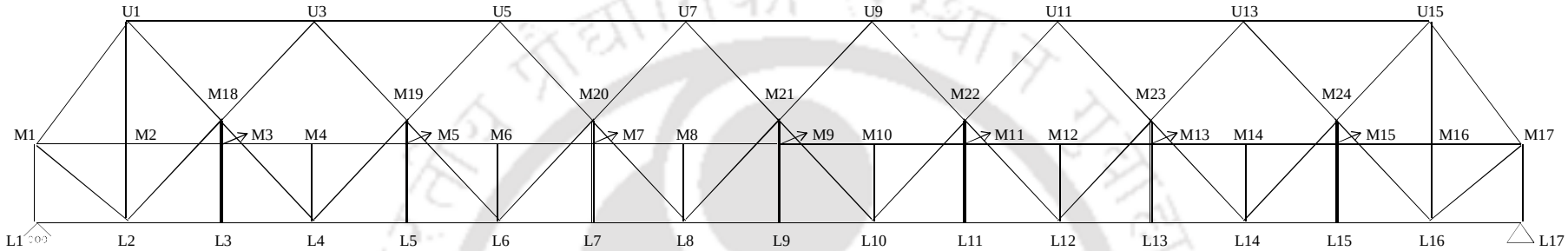

(a)

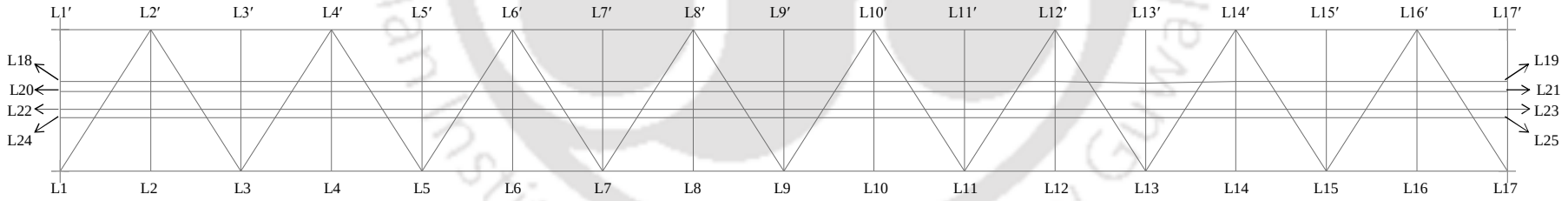

(b)

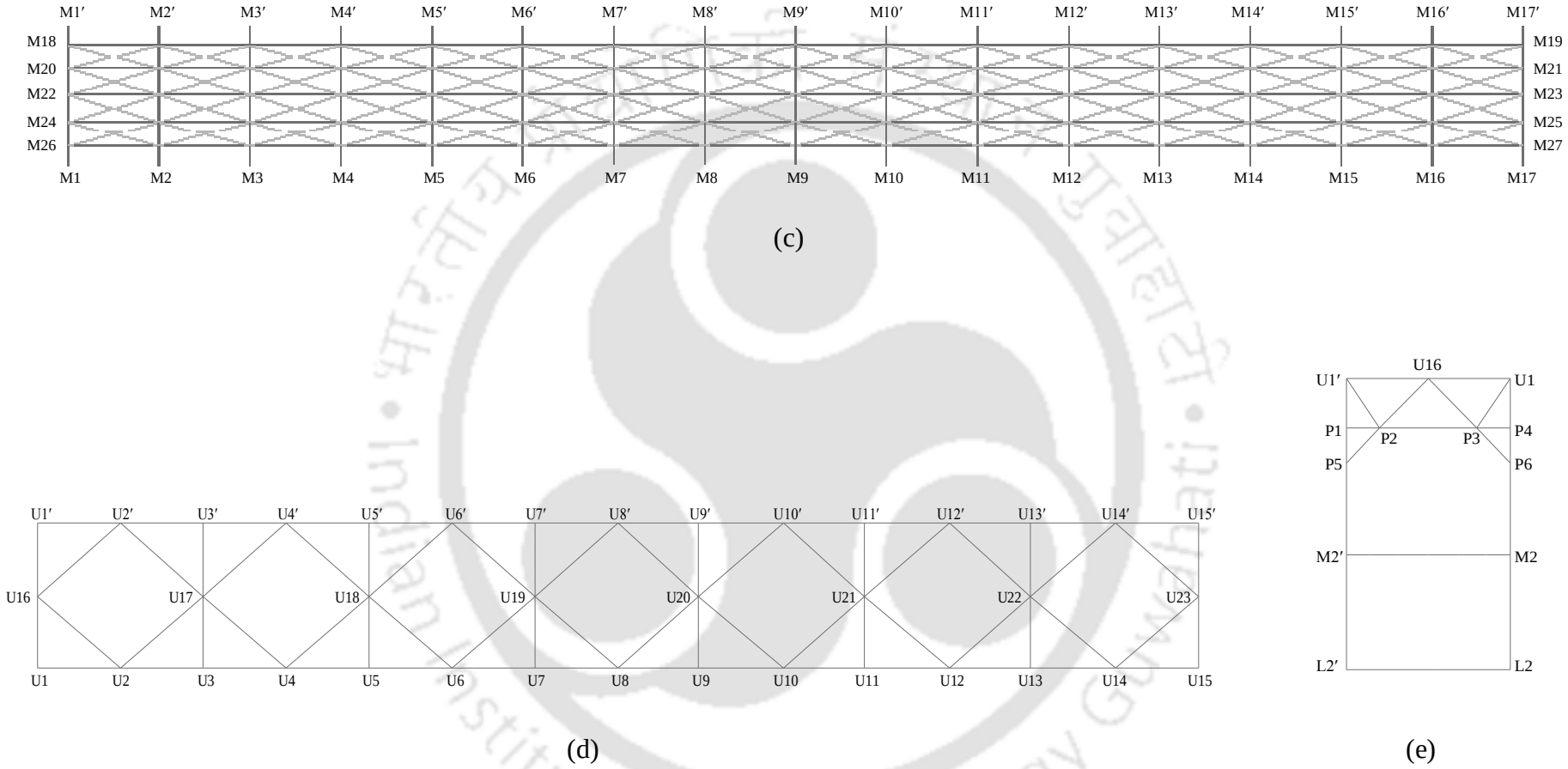

Fig. 3.5. Members of FE model of Saraighat Bridge in (a) side view (along Y axis) (b) plan at rail level (c) plan at road level (d) plan at top level and (e) portal frame along A and B (as in Fig. 3.4)

Table 3.1. Sectional properties of various members of the bridge

SL no.	Names of members (identifier)	Cross-sectional area (m^2)	Torsion constant (m^4)	Area moments of inertia (m^4)	
				I_1	I_2
1	Bottom Chord (L1L17, L1′L17′)	6.79E–02	2.31E–05	6.93E–03	5.68E–03
2	Rail Level - Cross Girder (L1L1′, L2L2′ … L17L17′)	3.06E–02	4.22E–06	1.24E–02	1.21E–04
3	Rail Level - Stringer (L18L19, L20L21, L22L23, L24L25)	1.80 E–02	1.94E–06	1.82E–03	6.01E–05
4	Bottom Lateral Bracing (L1L2′, L2′L3, L3L4′, L4′L5, L5L6′, L6′L7, L7L8′, L8′L9, L9L10′, L10′L11, L11L12′, L12′L13, L13L14′, L14′L15, L15L16′, L16′L17)	1.13E–03	1.36E–09	9.61E–06	4.67E–06
5	Road Level - Stringer (M18M19, M20M21, M22M23, M24M25, M26M27)	1.15E–02	7.66E–07	5.70E–04	2.76E–05
6	Road Level - Cross Girder (M1M1′, M2M2′ … M17M17′)	1.88E–02	1.62E–06	3.58E–03	3.10E–05
7	Top Cord (U1U15, U1′U15′)	4.46E–02	6.19E–06	5.02E–03	3.59E–03
8	Top Lateral Bracing (U2U16, U2U17, U2'U16, U2'U17, U4U17, U4U18, U4'U17, U4'U18, U6U18, U6U19, U6'U18, U6'U19, U8U19, U8U20, U8'U19, U8'U20, U10U20, U10U21, U10'U20, U10'U21, U12U21, U12U22, U12'U21, U12'U22, U14U22, U14U23, U14'U22, U14'U23)	1.06E–02	9.77E–07	1.93E–03	6.51E–05
9	Portal Strut (U1U1′, U15U15′)	1.46E–02	9.40E–07	1.83E–03	1.03E–05

10	Strut (U3U3′, U5U5′ … U13U13′)	5.42E–03	1.60E–07	1.17E–03	6.88E–06
11	Vertical (M1L1) [NB: Similar types of members for another truss as well]	5.54E–02	1.16E–05	2.76E–03	3.92E–03
12	Vertical (M17L17) [NB: Similar types of members for another truss as well]	6.97E–02	1.54E–05	3.61E–03	4.80E–03
13	Vertical (U1L2, U15L16) [NB: Similar types of members for another truss as well]	2.79E–02	3.94E–06	2.34E–04	2.10E–03
14	Vertical (M18L3, M19L5, M20L7, M21L9, M22L11, M23L13, M24L15) [NB: Similar types of members for another truss as well]	2.30E–02	2.82E–06	1.43E–03	8.98E–05
15	Vertical (M4L4, M6L6, M8L8, M10L10, M12L12, M14L14) [NB: Similar types of members for another truss as well]	2.10E–02	3.36E–06	1.59E–03	1.19E–04
16	Diagonal (U1M1, U1M18, U3M18, U3M19, U5M19, U5M20, U7M20, U7M21, U9M21, U9M22, U11M22, U11M23, U13M23, U13M24, U15M24, U15M17) [NB: Similar types of members for another truss as well]	2.38E–02	2.57E–06	7.11E–04	1.94E–03
17	Diagonal (L2M1, L2M18, L4M18, L4M19,	2.12E–02	1.82E–06	6.34E–04	1.73E–03

	L6M19, L6M20, L8M20, L8M21, L10M21, L10M22, L12M22, L12M23, L14M23, L14M24, L16M24, L16M17) [NB: Similar types of members for another truss as well]				
18	Portal Bracing (P2P5, P2U16, P3U16, P3P6) [NB: Similar types of members for another portal frame as well]	5.88E–03	6.99E–07	1.28E–05	1.60E–05
19	Portal Bracing (P1P2, P2P3, P3P4, P2U16, P3U16) [NB: Similar types of members for another portal frame as well]	3.36E–03	3.72E–07	2.32E–06	3.38E–06

3.3. MODELLING OF THE SAMPLE BRIDGE

The members of the truss bridge structure are modelled using 3D frame elements and 3D truss elements. Additional structural modelling issues like modelling of deck-slab, modelling of joints associated with frame members having non-coincident centre-lines/neutral-axis have also been discussed. Another important aspect of modelling is the modelling of mass. The modelling is elaborated with reasonable details in the following sub-sections. Finally, it may be mentioned that the non-structural elements are modelled as dead load.

3.3.1. Frame and truss members

Each of the side trusses comprises of Bottom Chord, Top Chord, Vertical and Diagonal members. Both the trusses are connected through various members namely, “Rail Level - Cross Girder”, “Road Level - Cross Girder”, “Portal Strut” / “Strut”, “Bottom Lateral Bracing”, “Top Lateral Bracing”, etc. Some of the major joints are shown in Figs. 3.6–3.8. A

joint along the rail level plane connecting members like “Vertical”, “Bottom Chord”, “Diagonal” and “Rail Level - Cross Girder” is shown in Fig. 3.6. Further, a joint along the road level plane connecting members as “Vertical” and “Road Level - Cross Girder” is shown in Fig. 3.7. Finally, a joint along the top level is displayed in Fig. 3.8. Finally, the structural members modelled as 3D frame elements are identified as follows:

(a) Rail Level - Cross Girder

(b) Rail Level - Stringer

(c) Road Level - Cross Girder

(d) Road Level - Stringer

(e) Strut

(f) Portal Strut

(g) Vertical

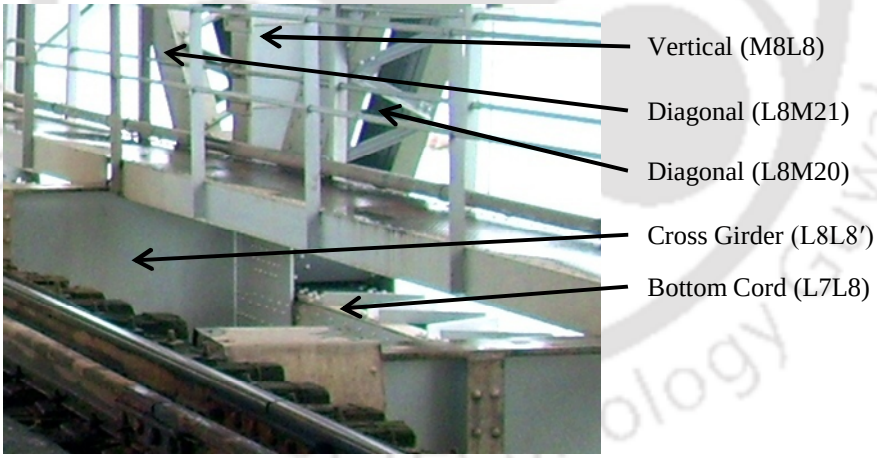

Fig. 3.6. View of a joint along the rail level

On the other hand, the structural members, modelled as 3D truss elements, are termed as follows:

(a) Bottom Chord

(b) Top Cord

(c) Diagonal

(d) Bottom Lateral Bracing

(e) Top Lateral Bracing

(f) Portal Bracing

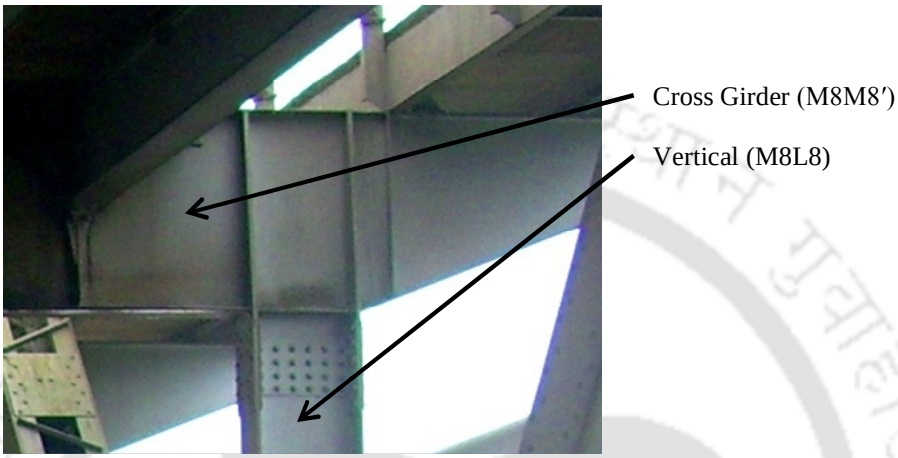

Fig. 3.7. View of a joint along the road level

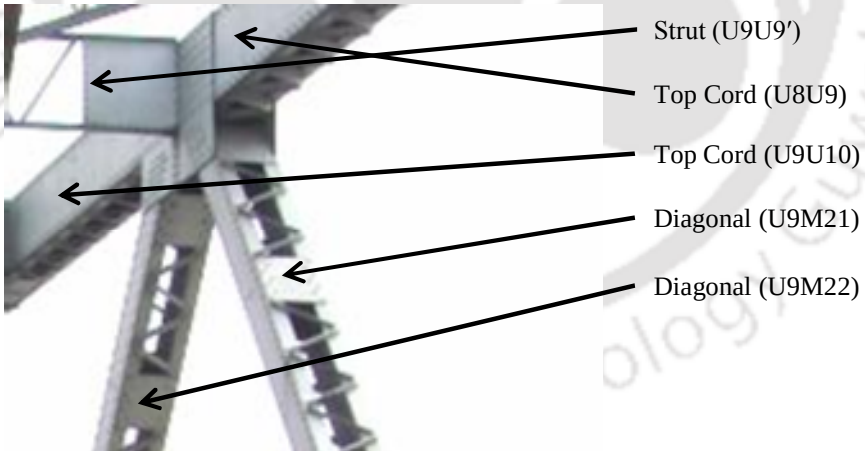

Fig. 3.8. View of a joint along the top level

The modelling of the bridge is done with a combination of truss and frame elements as appropriate to simulate the behaviour of the bridge. The local coordinate orientation for a

beam element is shown in Fig. 3.9. The default local coordinate system as considered in SAP2000 is briefly mentioned here. Local 1 axis is along the length of frame element with positive direction from first node to second node. The default orientation of local 2 and 3 axes is determined by the relationship between the local 1 axis and the global +Z or +3 axis. The local 1-2 plane is taken to be vertical, i.e. parallel to the global Z or 3 axis. The exceptional case while the frame element is parallel to global Z axis, the local 2 axis is taken to be globally horizontal along global +X or +1 direction. Now the local 1 and 2 axes are set, suppose in form of unit vectors v_1 and v_2 respectively. The unit vector of local 3 axis can be computed with the cross product as $v_3 = v_1 \times v_2$. The direction cosines of local axes unit vectors v_1, v_2 and v_3 can be referred as (l_1, m_1, n_1), (l_2, m_2, n_2) and (l_3, m_3, n_3) respectively. The transformation matrix [T] to compute the global stiffness matrix is considered as

$$[T] = \begin{bmatrix} R & 0 & 0 & 0 \\ 0 & R & 0 & 0 \\ 0 & 0 & R & 0 \\ 0 & 0 & 0 & R \end{bmatrix} \tag{3.1}$$

where, matrix [R] is represented as

$$[R] = \begin{bmatrix} l_1 & m_1 & n_1 \\ l_2 & m_2 & n_2 \\ l_3 & m_3 & n_3 \end{bmatrix} \tag{3.2}$$

The global stiffness matrix [K_{fg}] of frame element based on the global DOF is computed as

$$\left[K_{fg}\right] = [T]^{\mathrm{T}} \left[K_f\right][T] \tag{3.3}$$

Where, $\left[K_f\right]$ is the local stiffness matrix of a frame element.

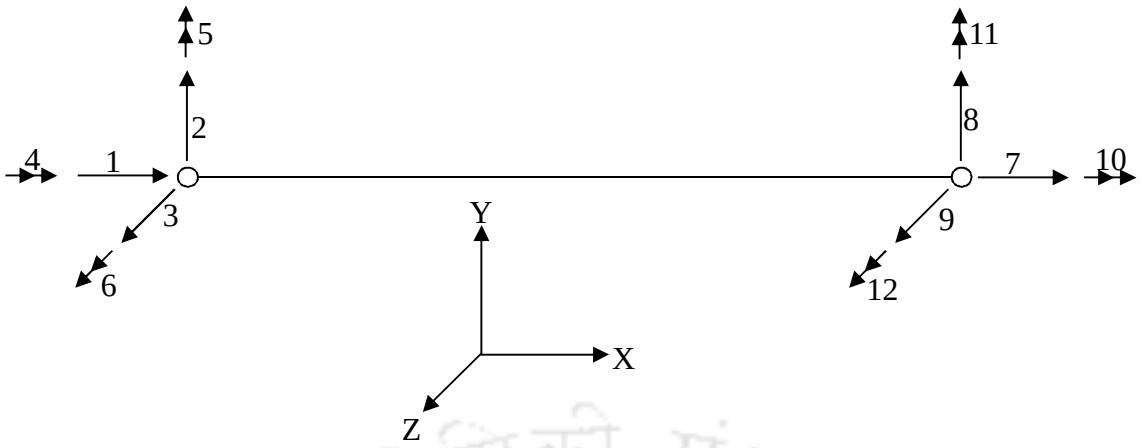

Fig. 3.9. DOF assigned at two joints of a frame elements in local coordinate

3.3.2. Other structural modelling issues

An important aspect of the structural modelling of the bridge is the modelling of the road-level deck-slab. The deck-slab is placed over cross-girders and stringers at roadway level without monolithic bonding. Such a non-monolithic type of bonding may be modelled with in-plane high (finite) stiffness. Diaphragm modelling associated with infinite in-plane stiffness may not be considered appropriate in this case. The in-plane high stiffness action can be considered using inplane diagonal bracings with higher stiffness taking into account the mass of deck-slab in appropriate way. This approach is followed in the modelling of the deck-slab as shown in Fig. 3.5(c) where the diagonal bracings are shown representing deck-slab. The diagonal-bracings are modelled using link element (CSI 2010). The link-element is a two noded element with user defined stiffness properties. First, link-elements evaluate relative deformations (between two joints) corresponding to 6 DOFs and subsequently use a (6×6) force-deformation relation matrix to relate force and deformation. In the present study, link elements are used with uncoupled behaviour having diagonal force-deformation relation matrix with possible 6 non-zero stiffness coefficients. In the modelling, only axial force-deformation relation with only 1 non-zero stiffness coefficient (k_a) is considered. Link

elements with zero mass having only stiffness property are considered. In this regard, the mass of the deck-slab is assigned as dead-load distributed over the DOFs along road-level plane. The total mass for the deck-slab for one main-span is 4000 kN. Finally, the work remains to find a suitable value of k_a based on agreement with experimental findings and this exercise is carried in Chapter 6 in Section 6.3.1. It may be mentioned that the value of k_a is observed to have significant effect on the major natural frequencies of this bridge structure.

In case of modelling of frame-joints, it is observed that centre-lines/neutral-axes of the associated frame members don't coincide in some situations. In such conditions, rigid-links are usually incorporated in modelling. A rigid link creates a new joint known as master joint and the kinematics of the intersection points are governed by the kinematics of the new master joint. This also reduces the size of dynamic system matrices (mass, stiffness and damping). Initially, in the modelling of joints connecting members having non-coincident centre-lines/neutral-axes, rigid-links were incorporated. However, it is observed that modelling without using rigid-links doesn't make any significant difference (e.g. in terms of modal parameters) compared that using rigid-links. In view of this, modelling is finally considered without using rigid-links for avoiding modelling complexity. This simplification in modelling doesn't have any adverse effect since the final studies (design of passive control system) are intended to be carried out based on direct-updated FE model.

3.3.3. Modelling of joint mass

In a dynamic analysis, the mass of the structure is used to compute inertial forces. Normally, the mass is obtained from the elements using the mass density of the material and the volume of the element. SAP2000 automatically produces lumped (uncoupled) masses at the joints. The element mass values are equal for each of the three translational degrees of freedom. No mass moments of inertia are assigned for the rotational degrees of freedom. In many cases,

such lumping approach is observed to be adequate for modal or time-history analyses. Further, joint-masses from the non-structural elements (e.g. deck slab, rail tracks, sleepers etc) are assigned equally along three translational DOFs in a manner similar to element mass.

3.4. DYNAMIC ANALYSIS

The present study requires mainly eigen analysis and time history analysis. However, contributions of mass along the rotational DOF are neglected in the modelling of mass matrices. Further, it is observed in the literature that various lumped mass models are considered for simulation of dynamic characteristics of the actual structure. Hence, usually there exist large numbers of DOFs with zero mass assigned and static condensation is generally adopted for reduction in the computational time for the dynamic analysis. The equation of motion for a dynamic system excluding damping is written in partitioned form as

$$\begin{bmatrix} [M_{tt}] & [0] \\ [0] & [0] \end{bmatrix} \begin{Bmatrix} \{\ddot{u}_t\} \\ \{\ddot{u}_0\} \end{Bmatrix} + \begin{bmatrix} [K_{tt}] & [K_{t0}] \\ [K_{0t}] & [K_{00}] \end{bmatrix} \begin{Bmatrix} \{u_t\} \\ \{u_0\} \end{Bmatrix} = \begin{Bmatrix} \{P_t(t)\} \\ \{0\} \end{Bmatrix} \tag{3.4}$$

where, u_0 denotes the DOF with zero mass and u_t the DOF with mass. The Eq. (3.4) can be written in two separate equations as

$$[M_{tt}]\{\ddot{u}_t\} + [K_{tt}]\{u_t\} + [K_{t0}]\{u_0\} = \{P_t(t)\} \tag{3.5a}$$

$$[K_{0t}]\{u_t\} + [K_{00}]\{u_0\} = \{0\} \tag{3.5b}$$

With the help of Eq. (3.5b), Eq. (3.5a) can be expressed with only those DOFs associated with mass as

$$[M_{tt}]\{\ddot{u}_t\} + [\hat{K}_{tt}]\{u_t\} = \{P_t(t)\} \tag{3.6}$$

where, $[M_{tt}]$ is the condensed stiffness matrix expressed as

$$[\hat{K}_{tt}] = [K_{tt}] - [K_{0t}]^{\mathrm{T}}[K_{00}]^{-1}[K_{0t}] \tag{3.7}$$

3.5. EVALUATION OF MASS AND STIFFNESS MATRICES

The present study deals with direct FE model updating and subsequently passive vibration control design using the updated FE model. Therefore, the mass and stiffness matrices are required for the exercises. SAP2000 provides the mass and stiffness matrices for any structure, which is modelled using the software. Mass and stiffness matrices can be obtained in the following steps:

(a) Open the window titled “Analysis Options” (click “Analyze” > click “Set Analysis Options…”).

(b) Open the window titled “Equation Solver Options” (click “Solver Options”).

(c) Select “Analysis Case Name” as “MODAL”.

After attempting the above steps, while analysis is run with “MODAL” case selected, the mass and stiffness matrices are obtained in text file format.

3.6. CONCLUDING REMARKS

The sample bridge is modelled by considering a single main span with suitable restraints. A concise description of various members of this bridge is presented. The FE modelling of the bridge is done using SAP2000 (Non Linear V14.2.2) considering appropriate elements. The mass and stiffness matrices of the simulated bridge are obtained for subsequent use in direct FE model updating and passive vibration control based on the updated FE model.

Chapter 4

PLACEMENT OF SENSORS IN OPERATIONAL MODAL ANALYSIS

4.1. INTRODUCTION

Output-only system identification or operational modal analysis (OMA) is gaining popularity for evaluation of modal parameters for structural systems, specially, for large structural systems under operational environment. Specifically, the difficulty in applicability of the precise artificial excitation has led to greater application of OMA. Regarding OMA, a great interest is usually observed for the selection of suitable sensor locations intended for better modal information of the target modes. The present work plans to analyse and explore the sensor location identification in order to achieve better modal participation for single or multiple modes in OMA. In the present study, a modal approach framework, as considered by Gawronski (2004), is followed for sensor placement evaluation in operational modal analysis (OMA) where modal participation at individual degree of freedom (DOF) is evaluated separately for the target modes. Subsequently locations are identified using these participation profiles. In this study, modal contribution in output energy (MCOE) is proposed as modal measure to evaluate modal participation and same has been applied in this modal approach framework for sensor placement evaluation. MCOE is evaluated using observability grammian for any types of response measurement (displacement, velocity or acceleration), when a system is released from any initial condition. Further, existing modal measures e.g. modal Hankel singular value (MHSV) and system norms (H_2, H_∞ and Hankel) are explained in the perspective of OMA. To understand the efficiency of this proposed technique, MCOE is compared in terms of modal participation with existing modal measures as well as with other techniques like effective independence (EI) and modal kinetic energy (MKE). Finally,

the Saraighat Bridge structure is considered for comparative study based on modal participation of individual target modes with acceleration measurement. Moreover, planning for suitable sensor locations are carried out for detailed OMA exercise of Saraighat Bridge.

4.2. SYSTEM FORMULATION

The equation of motion for n DOF dynamic system with mass matrix $[M]$, damping matrix $[D]$, stiffness matrix $[K]$ and input force vector $\{u\}$ is represented as

$$[M]\{\ddot{x}\} + [D]\{\dot{x}\} + [K]\{x\} = \{u\} \tag{4.1}$$

4.2.1. Modal coordinate

Considering proportional damping, Eq. (4.1) is converted in modal coordinate as follows using the transformation $\{x\} = [\Phi]\{q\}$, with $[\Phi]$ being the mode shape matrix.

$$[M_m]\{\ddot{q}\} + [D_m]\{\dot{q}\} + [K_m]\{q\} = [\Phi]^{\mathrm{T}}\{u\} \tag{4.2}$$

$$\{\ddot{q}\} + 2[\Xi][\Omega]\{\dot{q}\} + [\Omega]^2\{q\} = [B_m]\{u\} \tag{4.3}$$

where,

$[\Xi] = \mathrm{diag}(\xi_1, \xi_2 \ldots \xi_n)$

$[\Omega] = \mathrm{diag}(\omega_1, \omega_2 \ldots \omega_n)$

$2[\Xi][\Omega] = [M_m]^{-1}[D_m] = \mathrm{diag}(2\xi_1\omega_1, 2\xi_2\omega_2 \ldots 2\xi_n\omega_n)$

$[\Omega]^2 = [M_m]^{-1}[K_m] = \mathrm{diag}(\omega_1^2, \omega_2^2 \ldots \omega_n^2)$

$[B_m] = [M_m]^{-1}[\Phi]^{\mathrm{T}}$

The i^{th} row of $[B_m]$ is mentioned as $\{B_{mi}\}^{\mathrm{T}}$. The output vector $\{y\}$ is represented in modal coordinates as in Eq. (4.4) referring the modal velocity state vector $\{\dot{q}\}$ as $\{v\}$.

$$\{y\} = [C_q]\{q\} + [C_v]\{v\} + [E]\{u\} \tag{4.4}$$

Matrices $[C_q]$ and $[C_v]$ are column-wise represented as

$[C_q] = [\{C_{q1}\} \quad \dots \quad \{C_{qi}\} \quad \dots \quad \{C_{qn}\}]$

$[C_v] = [\{C_{v1}\} \quad \dots \quad \{C_{vi}\} \quad \dots \quad \{C_{vn}\}]$

Matrices, $[C_q]$, $[C_v]$ and $[E]$ for different types of response measurements become,

$[C_q] = [\Phi]$, $[C_v] = 0$, $[E] = 0$ (Displacement measurement)

$[C_q] = 0$, $[C_v] = [\Phi]$, $[E] = 0$ (Velocity measurement)

$[C_q] = -[\Phi][M_m]^{-1}[K_m]$, $[C_v] = -[\Phi][M_m]^{-1}[D_m]$, $[E] = [\Phi][M_m]^{-1}[\Phi]^{\mathrm{T}}$ (Acceleration measurement)

Eqs. (4.3) and (4.4) are represented in state space form (with all input and output) as in Eqs. (4.6a) and (4.6b) based on the state vector as in Eq. (4.5).

$$\{z\}=\{q_1 \; \dot{q}_1 \; q_2 \; \dot{q}_2 \dots q_n \; \dot{q}_n\}^{\mathrm{T}} \tag{4.5}$$

$$\{\dot{z}\} = [A]\{z\} + [B]\{u\} \tag{4.6a}$$

$$\{y\} = [C]\{z\} + [E]\{u\} \tag{4.6b}$$

where,

$$[A] = \begin{bmatrix} [A_1] & 0 & 0 & 0 \\ 0 & [A_2] & 0 & 0 \\ 0 & 0 & .. & 0 \\ 0 & 0 & 0 & [A_n] \end{bmatrix} \text{ and } [A_i] = \begin{bmatrix} 0 & 1 \\ -\omega_i^2 & -2\xi_i\omega_i \end{bmatrix}$$

$$[B] = \begin{bmatrix} [B_1] \\ [B_2] \\ \dots \\ [B_n] \end{bmatrix} \text{ and } [B_i] = \begin{bmatrix} 0 \\ \{B_{mi}\}^{\mathrm{T}} \end{bmatrix}$$

$[C] = [[C_1] \quad [C_2] \quad \dots \quad [C_n]]$ and $[C_i] = [\{C_{qi}\} \quad \{C_{vi}\}]$

4.2.2. Modal components of system

System input-output behaviour is generally described with transfer function (TF) or frequency response function (FRF) in Laplace and Fourier domain respectively. Input-output behaviour of system is influenced with all the modes. A second order system can be decomposed into modal components where each modal component describes the system

input-output behaviour associated with that single mode. Next, FRF is derived based on standard modal analysis technique (Ewins 2000a, Maia and Silva 1998) in modal coordinate with any type of response measurement. Subsequently, modal FRF corresponding to a modal component is also obtained. It is assumed that there exists an displacement vector, $\{x\} = \{\bar{x}\}\exp(j\omega t)$ (where, $j = \sqrt{-1}$) while an LTI system is subjected to an input vector, $\{u\} = \{\bar{u}\}\exp(j\omega t)$. It can be shown that modal displacement takes the form as $\{q\} = \{\bar{q}\}\exp(j\omega t)$ for the displacement vector, $\{x\} = \{\bar{x}\}\exp(j\omega t)$. In Eq. (4.3), putting $\{u\} = \{\bar{u}\}\exp(j\omega t)$ and $\{q\} = \{\bar{q}\}\exp(j\omega t)$ the following relation can be found

$$\left(-\omega^2[I] + 2j\omega[\Xi][\Omega] + [\Omega]^2\right)\{\bar{q}\}\exp(j\omega t) = [B_m]\{\bar{u}\}\exp(j\omega t) \tag{4.7}$$

$[I]$ is used to represent the identity matrix. For modal displacement $\{q\} = \{\bar{q}\}\exp(j\omega t)$, modal velocity becomes $\{v\} = \{\dot{q}\} = j\omega\{\bar{q}\}\exp(j\omega t)$, hence modal velocity gets the form as $\{v\} = \{\bar{v}\}\exp(j\omega t)$, where $\{\bar{v}\} = j\omega\{\bar{q}\}$. Now multiplying Eq. (4.7) both sides with $j\omega$ it can be written as

$$\left(-\omega^2[I] + 2j\omega[\Xi][\Omega] + [\Omega]^2\right)\{\bar{v}\}\exp(j\omega t) = j\omega[B_m]\{\bar{u}\}\exp(j\omega t) \tag{4.8}$$

In Eq. (4.4), $\{u\} = \{\bar{u}\}\exp(j\omega t)$, $\{q\} = \{\bar{q}\}\exp(j\omega t)$, $\{v\} = \{\bar{v}\}\exp(j\omega t)$ and hence, output $\{y\}$ also takes the form, $\{y\} = \{\bar{y}\}\exp(j\omega t)$. So it can be written as

$$\{\bar{y}\}\exp(j\omega t) = [C_q]\{\bar{q}\}\exp(j\omega t) + [C_v]\{\bar{v}\}\exp(j\omega t) + [E]\{\bar{u}\}\exp(j\omega t) \tag{4.9}$$

Using Eqs. (4.7) and (4.8) in Eq. (4.9),

$$\{\bar{y}\}\exp(j\omega t) = \left\{\left([C_q] + j\omega[C_v]\right)\left(-\omega^2[I] + 2j\omega[\Xi][\Omega] + [\Omega]^2\right)^{-1}[B_m] + [E]\right\}\{\bar{u}\}\exp(j\omega t)$$

Hence, the general FRF matrix of the structural system for any type of response (displacement, velocity or acceleration) measurement is obtained as

$$[G(\omega)] = \left([C_q] + j\omega[C_v]\right)\left(-\omega^2[I] + 2j\omega[\Xi][\Omega] + [\Omega]^2\right)^{-1}[B_m] + [E] \tag{4.10}$$

In the LTI system theory, FRF also directly evaluated from state-space matrices as

$$[G(\omega)] = [C](j\omega[I] - [A])^{-1}[B] + [E] \tag{4.11}$$

Since, matrices $[\Xi]$ and $[\Omega]$ are diagonal, Eq. (4.10) can be written as the summation of modal components as

$$[G(\omega)] = \sum_{i=1}^{n} \frac{\left(\{C_{qi}\} + j\omega\{C_{vi}\}\right)\{B_{mi}\}^{\mathrm{T}}}{\omega_i^2 - \omega^2 + 2j\xi_i\omega_i\omega} + [E] = \sum_{i=1}^{n}[G_i(\omega)] + [E] \tag{4.12}$$

Here, $[G_i(\omega)]$ can be exactly referred as modal FRF for displacement and velocity measurement since $[E] = 0$ for these responses measurement. In case of acceleration measurement $[E] \neq 0$ and moreover modal components of $[E]$ are not available. Therefore, $G_i(\omega)$ can be referred as modal FRF only in approximate sense for acceleration measurement. It can be now shown that modal component in state space, ($[A_i]$, $[B_i]$, $[C_i]$) (as in Eqs. (4.6a) and (4.6b)) creates similar modal FRF as in Eq. (4.12). Hence, the following relation is obtained as

$$[C_i](j\omega[I] - [A_i])^{-1}[B_i] = \frac{\left(\{C_{qi}\} + j\omega\{C_{vi}\}\right)\{B_{mi}\}^{\mathrm{T}}}{\omega_i^2 - \omega^2 + 2j\xi_i\omega_i\omega} = [G_i(\omega)] \tag{4.13}$$

All these FRF equations in Fourier domain can be converted in Laplace domain with replacing $j\omega$ with s, where s is the parameter of standard Laplace transform, $\mathrm{F}(s) = \int_0^\infty \mathrm{f}(t)\exp(-st)dt$ with $\mathrm{f}(t)$ and $\mathrm{F}(s)$ as the pair in time and Laplace domain respectively.

4.3. MISO MODELLING OF STRUCTURAL SYSTEM

In operational environment a structural system commonly is subjected to live load (e.g. traffic load), wind load etc. A structural system in such environment is expected to be excited at all the DOF or input locations to some extent. Output in form of response is observed along all the DOF as well. Hence, in operational environment a structural system behaves as multi input multi output (MIMO) system. Performance of each output DOF is considered individually. Hence, consideration of an output DOF and all the available input DOF forms

the structural system as MISO system. Relation between MIMO and MISO models of a system is straight forward. Conventionally, FRF of MIMO system is arranged as matrix where rows represent the output locations and columns represent the input locations. FRF of MISO model is the appropriate row of FRF of MIMO model of a structural system. Similarly, FRF of MISO model associated with a mode is the appropriate row of modal FRF matrix (as in Eq. (4.13)) associated with that mode. FRF of MISO model, associated with all the modes, can be directly evaluated corresponding to k^{th} output as

$$\{G_k(\omega)\}^T = \left(\{C_{qk}\}^T + j\omega\{C_{vk}\}^T\right)(-\omega^2[I] + 2j\omega[\Xi][\Omega] + [\Omega]^2)^{-1}[B_m] + \{E_k\}^T$$

$$\{C_k\}^T(j\omega[I] - [A])^{-1}[B] + \{E_k\}^T \qquad (4.14)$$

where, each of the k^{th} row of $[C_q]$, $[C_v]$, $[C]$, $[E]$, $[G(\omega)]$, $[G(s)]$ is referred as $\{C_{qk}\}^T$, $\{C_{vk}\}^T$, $\{C_k\}^T$, $\{E_k\}^T$, $\{G_k(\omega)\}^T$, $\{G_k(s)\}^T$ respectively.

FRF of MISO model, associated with i^{th} mode, can be directly evaluated corresponding to k^{th} output as

$$\{G_{ik}(\omega)\}^T = \{C_{ik}\}^T\left(j\omega[I] - [A_i]\right)^{-1}[B_i] = \frac{\left(C_{qik} + j\omega C_{vik}\right)\{B_{mi}\}^T}{\omega_i^2 - \omega^2 + 2j\xi_i\omega_i\omega} \qquad (4.15)$$

where, each of the k^{th} row of $\{C_{qi}\}$, $\{C_{vi}\}$, $[C_i]$, $[G_i(\omega)]$, $[G_i(s)]$ is referred as C_{qik}, C_{vik}, $\{C_{ik}\}^T$, $\{G_{ik}(\omega)\}^T$, $\{G_{ik}(s)\}^T$ respectively.

4.4. MODAL MEASURES

The adopted modal approach utilizes the modal participations of individual target modes for sensor location identification. Evaluation of modal participation using different existing modal measures in the perspective of OMA and based on different existing techniques along with the proposed modal measure is presented in the following sub-sections.

4.4.1. Modal Hankel singular value

Applicability of modal Hankel singular value (MHSV) as a modal measure and computational issues are presented here.

(a) Hankel Singular value (HSV):

Controllability and observability grammians for LTI system at time *t* are defined as

$$[W_c(t)] = \int_0^t \exp([A]\tau)[B][B]^{\mathrm{T}} \exp([A]^{\mathrm{T}}\tau)d\tau \tag{4.16a}$$

$$[W_o(t)] = \int_0^t \exp([A]^{\mathrm{T}}\tau)[C]^{\mathrm{T}}[C]\exp([A]\tau)d\tau \tag{4.16b}$$

In case of stable system, grammian matrices $[W_c(t)]$ and $[W_o(t)]$ converge to constant matrices $[W_c]$ and $[W_o]$ with increasing time. All the eigen values of state space matrix $[A]$ are having negative real parts for a stable system. Matrices $[W_c]$ and $[W_o]$ are related to state space matrices with Lyapunov equations as

$$[A][W_c] + [W_c][A]^{\mathrm{T}} + [B][B]^{\mathrm{T}} = 0 \tag{4.17a}$$

$$[A]^{\mathrm{T}}[W_o] + [W_o][A] + [C]^{\mathrm{T}}[C] = 0 \tag{4.17b}$$

The square root of eigen values of product of grammian matrices are defined as Hankel singular values (also known as “second order modes”) (Moore 1981). Thus, HSV can be represented as

$$\sigma_i = \sqrt{\lambda_i([W_c][W_o])} \tag{4.18}$$

where, $\lambda_i(.)$ represents the eigen value.

(b) Modal Hankel Singular value (MHSV):

HSV can be computed for modal component as well as for the complete system. Modal controllability and observability grammians can be computed with Lyapunov Eqs. (4.17a) and (4.17b) based on the modal component in state space ($[A_i]$, $[B_i]$, $[C_i]$). Exact MHSV pair

then can be computed from those modal grammians. There is no closed form relation available for system HSV (with all modes available) and MHSV. However, inspection shows that when damping is low, MHSV pair becomes close to the modal pair subset of system HSV set.

(c) Applicability of MHSV as modal measure:

Moore (1981) showed the model reduction (balanced truncation) based on retaining stronger HSV fairly retains the system signature in the form of impulse response function (IRF). For second order system, similar IRF and FRF are observed between balanced truncation based reduced system and modal truncation based reduced model, if modes with stronger HSV are retained in modal truncation. Obinata and Anderson (2001) may be referred for further details regarding model reduction techniques. Hence, MHSV represents importance of a mode in second order system in form of contribution in system IR signature. It may be mentioned that direct feed through matrix [E] is either zero or non-zero, modal truncation as well as balanced truncation is valid and MHSV similarly represents the importance of a mode. MHSV based modal importance evaluation can be considered as computationally ideal if MHSV pairs can be arranged as $\sigma_{11} \geq \sigma_{12} \geq \ldots \geq \sigma_{i1} \geq \sigma_{i2} \geq \ldots \geq \sigma_{n1} \geq \sigma_{n2}$ where, σ_{i1} and σ_{i2} represent the MHSV pair of i^{th} mode and modes may appear in any arbitrary order of frequency. This trend is approximately observed for second order systems. Here MHSV is considered as the modal measure since a mode with higher MHSV contributes higher in system behaviour i.e. input-output signature.

(d) MHSV computation:

Exact computation of MHSV is mentioned in 4.4.1(b). Next, approximate evaluation of MHSV is presented. For second order system with small damping, controllability and

observability grammians are observed to be diagonally dominant in modal coordinate (Gawronski 2004). MHSV can be computed with good accuracy with diagonal dominant grammians. A state space form in modal coordinate which makes the grammians as diagonally dominant is expressed in form of state vector as

$$\{z\} = \begin{bmatrix} \omega_1 q_1 & \omega_2 q_2 & \cdots & \dot{q}_1 & \dot{q}_2 & \cdots \end{bmatrix}^{\mathrm{T}} \tag{4.19}$$

For such state representation the full input-output system matrices become

$$[A] = \begin{bmatrix} [0] & [\Omega] \\ -[\Omega] & -2[\Xi][\Omega] \end{bmatrix}, [B] = \begin{bmatrix} [0] \\ [B_m] \end{bmatrix}, [C] = \begin{bmatrix} [C_q][\Omega]^{-1} & [C_v] \end{bmatrix}$$

where, $[0]$ are matrix of zeros. The diagonally dominant grammians in modal coordinate (as in Eq. (4.19)) are observed in the following form considering any type of response (displacement, velocity or acceleration) measurement.

$$[W_c] \cong \begin{bmatrix} [w_{cU}] & [0] \\ [0] & [w_{cL}] \end{bmatrix} \tag{4.20a}$$

$$[W_o] \cong \begin{bmatrix} [w_{oU}] & [0] \\ [0] & [w_{oL}] \end{bmatrix} \tag{4.20b}$$

where, $[w_{cU}]$, $[w_{cL}]$, $[w_{oU}]$ and $[w_{oL}]$ are diagonally dominant sub-matrices as

$[w_{cU}] \cong \text{diag}(w_{cU1} \ldots w_{cUi} \ldots w_{cUn})$

$[w_{cL}] \cong \text{diag}(w_{cL1} \ldots w_{cLi} \ldots w_{cLn})$

$[w_{oU}] \cong \text{diag}(w_{oU1} \ldots w_{oUi} \ldots w_{oUn})$

$[w_{oL}] \cong \text{diag}(w_{oL1} \ldots w_{oLi} \ldots w_{oLn})$

Approximate HSV σ_i for i^{th} mode can be computed with any of the Eq. (4.21a) or (4.21b), while grammians are computed in modal coordinate as in Eq. (4.19).

$$\sigma_i \cong \sqrt{w_{cUi} w_{oUi}} \tag{4.21a}$$

$$\sigma_i \cong \sqrt{w_{cLi} w_{oLi}} \tag{4.21b}$$

System HSV set is computed using Eq. (4.18) and it is difficult to track HSV pair for a mode from that system HSV set. Hence, MHSV is to be computed corresponding to a mode

separately. Here two comparisons are made to understand the level of accuracy in the MHSV computation.

Comparison 1: comparison between the system HSV (generally computed in descending order) and sorted MHSV pairs of all modes in descending order.

Comparison 2: comparison between the average of MHSV (or, exact MHSV) pair and approximate MHSV of the modes.

Though comparison 1 explains well, still mode wise comparison is not considered. Mode wise comparison is carried out in comparison 2 with the help of approximate MHSV.

(e) MHSV for MISO model:

MISO model helps in evaluation of modal presence along an output DOF. Similarly MISO model helps in the computation of this modal measure (MHSV) to indicate modal presence of a mode along an output DOF. MHSV is computed based on MISO modal model. MHSV of i^{th} mode for MISO model with k^{th} output is computed with modal component in state space as ($[A_i]$, $[B_i]$, $\{C_{ik}\}^T$). Approximate computation of MHSV for MISO model is also possible, since diagonal dominancy of grammians is also observed in case of MISO model of system. However smaller damping demand is observed for MISO model than MIMO model of the system for diagonal dominancy of observability grammian. Controllability grammian is similar in both the cases of MIMO and MISO model.

4.4.2. Norms

Various system norms (H_2, H_∞, Hankel) associated with a mode are also considered as modal measures to observe the behaviour of a system from a wide rage of modal measures. System norms are computed for modal component of system based on MISO model helping the

evaluation of modal presence along output DOF. Brief notes for these system norms are mentioned here.

(a) H_2 Norm:

For a single-input single-output (SISO) system with FRF $G(\omega)$, H_2 norm is defined as

$$\| G \|_2 = \left(\frac{1}{2\pi} \int_{-\infty}^{\infty} | G(j\omega) |^2 \, d\omega \right)^{1/2} \tag{4.22a}$$

And, for MIMO system with FRF matrix $[G(\omega)]$, H_2 norm is defined as

$$\| G \|_2 = \left(\sum_{kl} \| G_{kl}(j\omega) \|_2^2 \right)^{1/2} = \left(\frac{1}{2\pi} \int_{-\infty}^{\infty} \sum_{kl} | G_{kl}(j\omega) |^2 \, d\omega \right)^{1/2} \tag{4.22b}$$

According to Parseval's theorem, $\|G\|_2$ is equal to the corresponding time-domain norm of impulse response function matrix $[H(t)]$. Hence H_2 norm in time domain is represented as

$$\| G \|_2 = \| H \|_2 = \left(\int_{-\infty}^{\infty} \sum_{kl} H_{kl}(t)^2 \, dt \right)^{1/2} \tag{4.23a}$$

For stable system H_2 norm can also be represented as

$$\|G\|_2 = \|H\|_2 = \text{trace}([C][W_c][C]^{\mathrm{T}}) \tag{4.23b}$$

Solution of the Eq. (4.17a) provides the controllability matrix $[W_c]$. For a system with non-zero direct feed through matrix $[E]$, H_2 norm is infinite theoretically.

(b) H_∞ Norm:

H_∞ norm is a measure of the largest factor by which any sinusoid is magnified by the system. H_∞ norm is defined as

for SISO case,

$$\|G\|_\infty = \max_{\omega} |G(\omega)| \tag{4.24}$$

and for MIMO case,

$$\|G\|_{\infty} = \sup_{\omega} \bar{\sigma}(G(\omega)) \tag{4.25}$$

where, $\bar{\sigma}(G(\omega))$ is the largest singular value of FRF matrix $G(\omega)$. H_{∞} norm associated to a mode can be computed based on the modal frequency function matrix (Eq. (4.12)). Direct feed through matrix [E] is considered in the computation of H_{∞} norm. In case of non-zero [E], exact computation of H_{∞} norm for mode is not possible as the modal components of [E] are not available.

(c) Hankel Norm:

Hankel norm of a mode is the largest of the MHSV pair. In second order system HSV pair is found to be closely valued. Hence Hankel norm is approximately equal to MHSV which is considered here as the average of HSV pair. Hankel norm is not thus evaluated separately.

(d) Relation between H_{∞} and Hankel norm for a mode:

There exists an approximate relation (Gawronski 2004) between H_{∞} norm and Hankel norm for a mode of a second order system, while direct feed through matrix [E] = 0 or neglected and damping is low. The relation states that H_{∞} norm is approximately twice the Hankel norm i.e. approximately twice the MHSV.

4.4.3. Effective independence (EI) method

EI method (Kammer 1990) is a popular technique applied for the sensor placement evaluation. EI method maximises the determinant of FIM. With the full mode shape matrix FIM is considered as

$$[F] = [\Phi]^{T}[\Phi] \tag{4.26}$$

FIM can be represented for single target mode (i^{th} mode) along any subset of full DOF as

$$f = \{\psi_i\}^T\{\psi_i\} \tag{4.27}$$

where, $\{\psi_i\}$ is subset of full mode shape vector $\{\phi_i\}$ of i^{th} mode and retains the elements of $\{\phi_i\}$ corresponding to the considering DOF. It may be mentioned that FIM becomes a scalar for a single target mode consideration. Determinant of FIM as in Eq. (4.27) is considered as a modal measure to evaluate the modal participation of a target mode along those output DOF (retained in$\{\psi_i\}$) in form of information content. Further Eq. (4.27) can also be used for evaluation of FIM for a target mode along a single output DOF and hence participation of a mode along each DOF can be evaluated.

4.4.4. Kinetic energy based approach

Kinetic energy based approaches are another class of popular techniques for sensor placement evaluation. EOT (Heo et al. 1997) maximizes any suitable measure based on kinetic energy matrix. Kinetic energy matrix is obtained as follows

$$[KE] = [\Phi]^T[M][\Phi] \tag{4.28}$$

The kinetic energy matrix evaluated corresponding to a single target mode and a single DOF is known as modal kinetic energy (MKE). MKE is computed for sensor location selection and commonly known as MKE method. MKE for i^{th} DOF and k^{th} mode is referred as

$$KE_{ik} = \Phi_{ik}\sum_{r=1}^{n} M_{ir}\Phi_{rk} \tag{4.29}$$

where, Φ_{ik} is the i^{th} element of k^{th} mode shape vector, M_{ir} is the i^{th} row and r^{th} column of mass matrix $[M]$ and Φ_{rk} is the r^{th} element of the k^{th} mode shape vector. MKE is considered as a modal measure to evaluate the modal participation of a target mode along each of the DOF in form of kinetic energy intensity.

4.4.5. Modal contribution in output energy

According to the literature related to system theory, when a system is excited by releasing from any initial state, the total output energy can be related with observability grammian and initial state. Considering the observability grammian in a particular modal coordinate, modal contribution in output energy (MCOE) is evaluated when a system is released from any initial condition. Evaluation of MCOE and its application in identification of sensor locations are presented next.

(a) Output energy with initial state release:

Observability grammian relates the initial state and output energy while the system is released from that initial state. The output vector $\{y_\tau\}$ at time instant τ is expressed as $\{y_\tau\} = [C]\exp([A]\tau)\{z_0\}$, while the system is released form an initial state $\{z_0\}$. The output energy (Chen 1984) is commonly computed as Euclidean norm of output vector $\{y_\tau\}$ as

$$\int_0^\infty \| y_\tau \|_2^2 \, d\tau = \int_0^\infty \{y_\tau\}^{\mathrm{T}}\{y_\tau\} d\tau = \{z_0\}^{\mathrm{T}} \left(\int_0^\infty \exp([A]^{\mathrm{T}}\tau)[C]^{\mathrm{T}}[C]\exp([A]\tau) d\tau \right) \{z_0\}$$

$$= \{z_0\}^{\mathrm{T}} [W_o] \{z_0\} \qquad (4.30)$$

(b) Contribution of a state in output energy:

Contribution of a state in output energy can be estimated if the observability grammian is diagonal. The observability grammian $[W_o]$ depends on the coordinate basis of state space. In any appropriate coordinate basis where the observability grammian is diagonal, the Eq. (4.30) can be written as

$$\{z_0\}^{\mathrm{T}} [W_o] \{z_0\} = w_{d1} z_{01}^2 + w_{d2} z_{02}^2 + \ldots + w_{dN} z_{0N}^2 \qquad (4.31)$$

where, $\{z_0\} = [z_{01}\ z_{02}\ \ldots\ z_{0N}]^T$ and $[W_o] = \text{diag}(w_{d1}\ w_{d2}\ \ldots\ w_{dN})$. Hence, contribution of any state in output-energy is well correlated with diagonal values of observability grammian.

(c) Contribution of a modal state in output energy:

In modal coordinate, observability grammian becomes diagonally dominant (Gawronski 2004). Hence, contribution of a modal state in output energy can be approximately evaluated with the Eq. (4.31). A modal coordinate which makes observability grammian diagonally dominant is mentioned in Eq. (4.19). Another states in modal coordinate is observed to makes the grammians as diagonally dominant as

$$\{z\} = \begin{bmatrix} q_1 & q_2 & \ldots & \dot{q}_1 & \dot{q}_2 & \ldots \end{bmatrix}^T \tag{4.32}$$

The corresponding state space matrices become

$$[A] = \begin{bmatrix} [0] & [I] \\ -[\Omega]^2 & -2[\Xi][\Omega] \end{bmatrix},\ [B] = \begin{bmatrix} [0] \\ [B_m] \end{bmatrix},\ [C] = \begin{bmatrix} [C_q] & [C_v] \end{bmatrix}$$

Diagonal dominancy in the observability grammian is observed with only low damping, hence neglecting the off-diagonal terms of observability grammian is not always possible. An attempt is made here to understand the effect of off-diagonal terms in contribution of a modal state in output energy. If $[W_o]$ is considered as non-diagonal general matrix, the output-energy expression with initial modal state vector $\{z_0\}$ can be expressed as

$$\{z_0\}^T[W_o]\{z_0\} = \{z_{01} \quad z_{02} \quad \ldots \quad z_{0N}\} \begin{bmatrix} w_{11} & w_{12} & \ldots & w_{1N} \\ w_{21} & w_{22} & \ldots & w_{2N} \\ \ldots & \ldots & \ldots & \ldots \\ w_{N1} & w_{N2} & \ldots & w_{NN} \end{bmatrix} \begin{Bmatrix} z_{01} \\ z_{02} \\ \ldots \\ z_{0N} \end{Bmatrix}$$

$$= w_{11}z_{01}^2 + w_{12}z_{01}z_{02} + \ldots + w_{1N}z_{01}z_{0N}$$

$$+ w_{21}z_{02}z_{01} + w_{22}z_{02}^2 + \ldots + w_{2N}z_{02}z_{0N}$$

$$\ldots\ \ldots\ \ldots\ \ldots\ \ldots\ \ldots\ \ldots\ \ldots\ \ldots$$

$$+ w_{N1}z_{0N}z_{01} + w_{N2}z_{0N}z_{01} + \ldots + w_{NN}z_{0N}^2$$

It is observed form the above expression that off-diagonal terms contribute in energy for coupled modal states, while only the diagonal terms of grammian contributes in energy with pure uncoupled modal states. Hence only diagonal terms of observability grammian are of interest in terms of uncoupled pure contribution of different modes in output energy.

(d) Contribution of a modal state to output energy associated with an output DOF:

In the present study, each output DOF is considered individually to observe the modal presence for a mode along each output DOF. The k^{th} output (DOF) associated output energy can be computed considering the k^{th} row of state space matrix [C] and using the Eq. (4.30). Further, k^{th} output (DOF) related observability grammian can be computed considering the k^{th} row of state space matrix [C] and solving the Lyapunov Eq. (4.17b). Now, contribution of a modal state to an output (DOF) associated output energy can be estimated based on that output (DOF) related observability grammian. Diagonal dominancy of observability grammian is the motivation for correlation between output energy and modal state, moreover diagonal dominancy is preferred as well. However, it is demonstrated that lack of good diagonal dominancy of observability grammian is not an obstacle. Anyway, single output based observability grammian shows higher diagonal dominancy with lower damping.

(e) Modal contribution in output energy (MCOE) as modal measure:

A closed form solution of the observability grammian based on modal states as in Eq. (4.5) is presented in the Appendix-A for displacement, velocity and acceleration measurement. Addition of uncoupled contributions of modal displacement and modal velocity states for a mode is considered as the contribution of that mode. For any type of response measurement, it is observed that contribution of a mode in output energy is proportional to $\{\psi_i\}^T\{\psi_i\}$, where $\{\psi_i\}$ represents the i^{th} mode shape vector containing the elements corresponding to the

chosen set of output DOF. The participation of a mode with this proposed technique appears to be similar to modal participation based on EI method as mentioned in the Eq. (4.27). MCOE is proposed as a modal measure which appears simple with simple physical understanding and same is considered for the evaluation of modal participation.

4.4.6. Sensor placement evaluation for multiple target modes

Using the adopted modal approach framework (Gawronski 2004), a technique for sensor placement evaluation is proposed where modal participation is evaluated for the target modes individually along individual DOF based on MCOE and subsequently locations are identified for target modes using these participation profiles. A placement matrix as in Eq. (4.33) with *m* numbers of target modes and *o* numbers of candidate output locations is considered useful to put the modal participation profiles of target modes.

$$\Sigma = \begin{bmatrix} \sigma_{11} & \sigma_{12} & \cdots & \sigma_{1o} \\ \sigma_{21} & \sigma_{22} & \cdots & \sigma_{2o} \\ \vdots & \vdots & \ddots & \vdots \\ \sigma_{m1} & \sigma_{m2} & \cdots & \sigma_{mo} \end{bmatrix} \tag{4.33}$$

where, k^{th} row and i^{th} column represents the modal participation of k^{th} mode along i^{th} DOF. The basic steps for sensor location identification are considered as below.

(i) The numbers of sensors are selected for each of the target modes first and sensors are placed at DOF-locations with higher modal participation. Here a mode can be given priority by assigning higher number of sensors.

(ii) There are some DOF-locations which are common to multiple modes. Hence the required number of sensor is reduced from the number assessed in the previous step.

(iii) There exist some groups of DOF-locations with similar modal participation profile for the target modes. Sensors placed at the locations of such a group provide similar information and hence placing a single sensor at a suitable location out of those locations serve the

purpose. Similarity of modal participation profile between two DOF-locations e.g. i^{th} and r^{th} DOF is evaluated using a correlation index as

$$\rho_{ir} = \frac{\{g_i\}^T \{g_r\}}{\| g_i \|_2 \| g_r \|_2} \tag{4.34}$$

where, $\{g_i\}$and $\{g_r\}$ are the i^{th} and r^{th} columns of placement matrix and $\|.\|_2$ represents Euclidean norm. This correlation analysis further reduces the required number of sensors depending on the margin of correlation index. Thus, it may be mentioned that such approach is insightful and also provides many options for applying judgements in placement of sensors. Moreover, there exists heuristic scope for applying weights to the elements of the placement matrix. Details of this strategy are presented in Gawronski (2004). However, it may be mentioned that sensor placement targeting a single mode is straightforward and placing of sensors along the DOF with higher modal participation is considered sufficient.

4.5. ISSUES WITH ACCELERATION MEASUREMENT

With acceleration measurement, the direct feed through matrix [E] is non-zero, which creates some complications in the computation of modal H_2 norm and H_∞ norm. These complications and possible remedies are mentioned here.

4.5.1. H_2 Norm

H_2 norm is evaluated using the impulse response function (IRF) of a system. With the presence of direct feed through matrix [E], IRF becomes theoretically infinite at time $\tau = 0$, since there exists delta function associated with [E]. Here, theoretically infinite value refers to undefined impulse response (e.g. for acceleration) at time $\tau = 0$. Ignoring this discontinuity is not uncommon. Here, this discontinuity is ignored considering [E] = 0 for computing H_2 norm and it is expected that signature of impulse response is almost retained (except during impulse at time $\tau = 0$). Further, direct feed through matrix [E] is diagonal for lumped mass

system and this represents zero effect of direct feed through matrix except the collocated input and output DOF. Thus assumption of neglecting [*E*] for H_2 norm computation can be considered acceptable.

4.5.2. H_∞ Norm

H_∞ norm evaluation considers the direct feed through matrix [*E*]. H_∞ norm associated to a mode is computed with a modal TF or modal FRF component from the Eq. (4.12), but modal components of [*E*] are not available. While the effect of [*E*] is negligible, H_∞ norm for a mode can be approximately computed. To analyse the effect of [*E*], H_∞ norm for modes are computed in the following two ways.

[a] Computing H_∞ norm for a mode without considering [*E*] i.e. [*E*] = 0.

[b] Computing H_∞ norm for a mode considering [*E*] equally for each mode.

A good agreement between these two ways of computed modal H_∞ norm can establish that the direct feed through matrix [*E*] be neglected. If [*E*] is negligible then H_∞ norm for a mode can be computed approximately. Further, with negligible effect of [*E*], the relation between modal H_∞ norm and MHSV (as mentioned in 4.4.2 (d)) makes it possible to approximately compute modal H_∞ norm from MHSV.

4.5.3. An alternative approach

It may be mentioned that there is an alternative approach to compute acceleration based norm. Thus comparative observations evaluating the significance of [*E*] can be avoided. An approximate relation provided by Gawronski (2004) facilitates the evaluation of acceleration based modal norm using the velocity based modal norm. This relation states that acceleration based modal norm for say k^{th} mode is approximately equals to the product of velocity based modal norm for k^{th} mode and circular frequency of k^{th} mode. It may be mentioned that the

proposed MCOE technique is not affected by the presence of [*E*] i.e. MCOE technique doesn't face difficulty in numerical computation with acceleration measurement.

4.6. VALIDATION WITH BEAM PROBLEM

For validation of sensor placement strategy, beam problem is commonly found to be considered. Sensor locations for this classical problem are well accepted. Thus, a simply supported beam of span 6 m having I-section of overall depth 0.3 m is considered. The beam is discretized considering the expected sensor locations of first five modes as in Table 4.1. Forty elements are chosen so that peak modal participations for the first five modes at the expected sensor locations can be captured with good accuracy. Two DOF (transverse and rotation) are considered at each node. Total number of DOF after applying boundary conditions becomes 80. Mass and stiffness proportional damping is considered with the assumption of monotonic increment of damping ratio with natural frequency (Cheng 2000) and damping ratio corresponding to the fundamental frequency is considered as 1%. Here the sensor locations for individual modes are evaluated considering higher modal measure value. Modal measures (y-axis) along different output DOF (x-axis) are displayed for only first three modes for better visibility.

Table 4.1. Expected sensor location for first 5 modes of beam

	Mode1 (1 sensor)	**Mode 2 (2 sensors)**	**Mode 3 (3 sensors)**	**Mode 4 (4 sensors)**	**Mode5 (5 sensors)**
Sensor location (Beam length: L)	0.500L	0.250L	0.167L	0.125L	0.100L
		0.750L	0.500L	0.375L	0.300L
			0.833L	0.625L	0.500L
				0.875L	0.700L
					0.900L

First, the comparisons associated to MHSV computation (as mentioned under 4.4.1 (d)) are considered based on MIMO model. These comparisons are shown in Fig. 4.1. Acceleration measurement is considered for these comparisons, since the MHSV of higher modes attain higher values to be better visible in case of acceleration measurement. Fig. 4.1(a) shows that sorted (descending) MHSV computed separately for all the modes are in good agreement with HSV of the structural (beam) system. Further, mode-wise comparison for MHSV with approximate MHSV shows good similarity in Fig. 4.1(b). Hence, these comparisons demonstrate an acceptable level of accuracy in MHSV computation for the beam problem. Next, the profile of MHSV along the output locations (transverse DOF) is shown in Fig. 4.2 for any type of response measurement. MHSV profiles for first three modes are showing higher participation of modes at the expected sensor locations as mentioned in Table 4.1 with any type of response measurement.

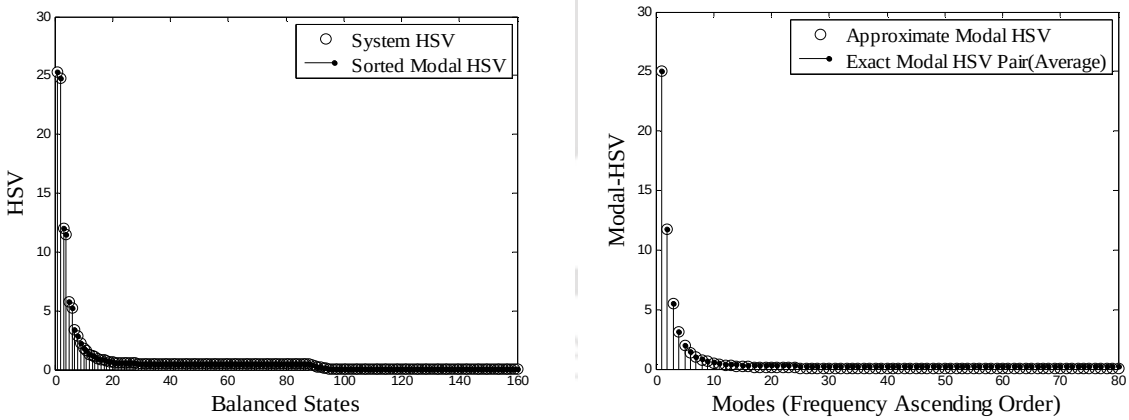

(a) (b)

Fig. 4.1. (a) Comparison of system HSV (sorted) and MHSV of all modes (sorted) (b) comparison of average of MHSV pair and approximate MHSV

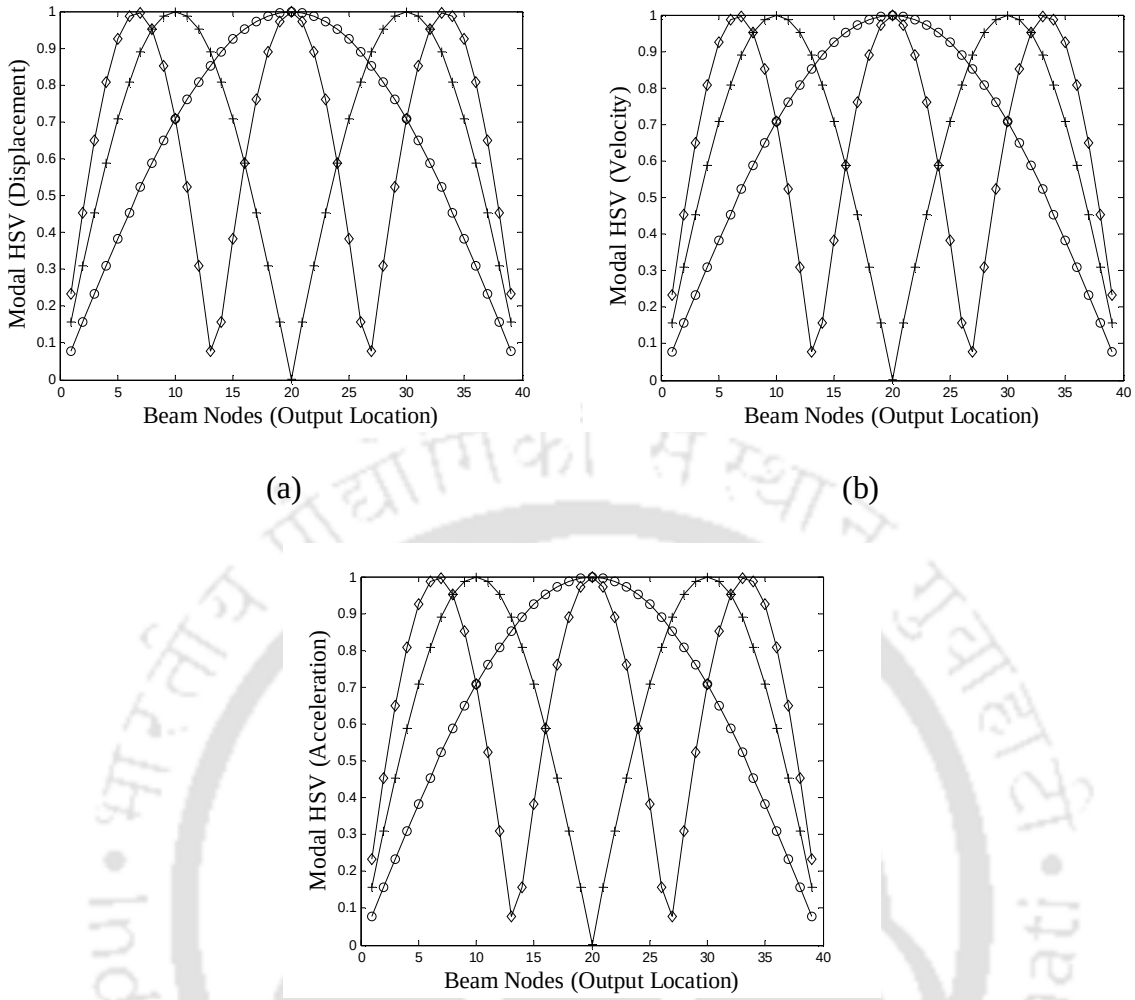

Fig. 4.2. MHSV profile for first three modes (1st mode: circle, 2nd mode: plus, 3rd mode: diamond) along the output locations with (a) displacement (b) velocity and (c) acceleration measurement

Diagonal elements of diagonally dominant observability grammian represent the uncoupled modal contribution of modal states to output energy. Grammian becomes diagonally dominant in modal coordinate based on various modal states and such diagonal dominancy is preferred. For better visibility of diagonal dominancy, profile of the grammian is shown in the Fig. 4.3 based on the modal states as

$$\{z\} = \{\omega_1 q_1 \;\; \dot{q}_1 \;\; \omega_2 q_2 \;\; \dot{q}_2 \;\; \ldots \; \omega_n q_n \;\; \dot{q}_n\}^{\mathrm{T}} \tag{4.35}$$

The grammian is computed based on MIMO model using acceleration measurement. From Fig. 4.3 it is observed that the observability grammian is diagonally dominant and hence uncoupled contribution of modes in the output energy is dominant. It is preferable to use MCOE as a modal measure, since MCOE considers the uncoupled contribution of mode in the output energy.

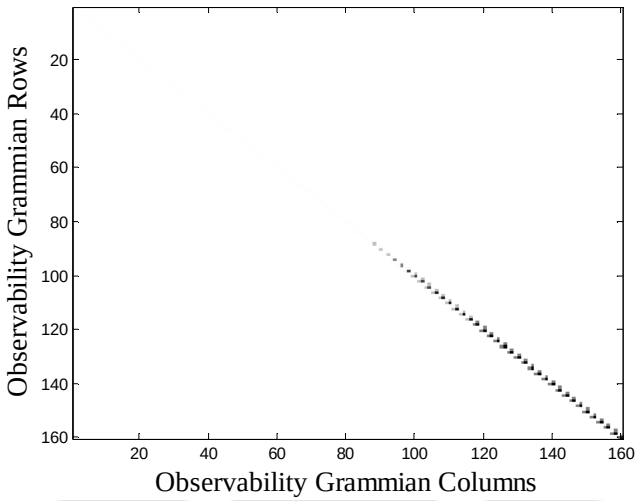

Fig. 4.3. Profile of observability grammian matrices (160×160) based on modal states as in Eq. (4.35)

Contribution of a mode in output energy is considered as modal measure for that mode. Contribution or share of first three modes in individual output (transverse DOF) associated output energy is shown in Fig. 4.4 (normalized equally for all three modes). Fig. 4.4 shows that first three modes are showing higher participation in the form of higher contributions to output energy at the expected sensor locations for any type of response measurement.

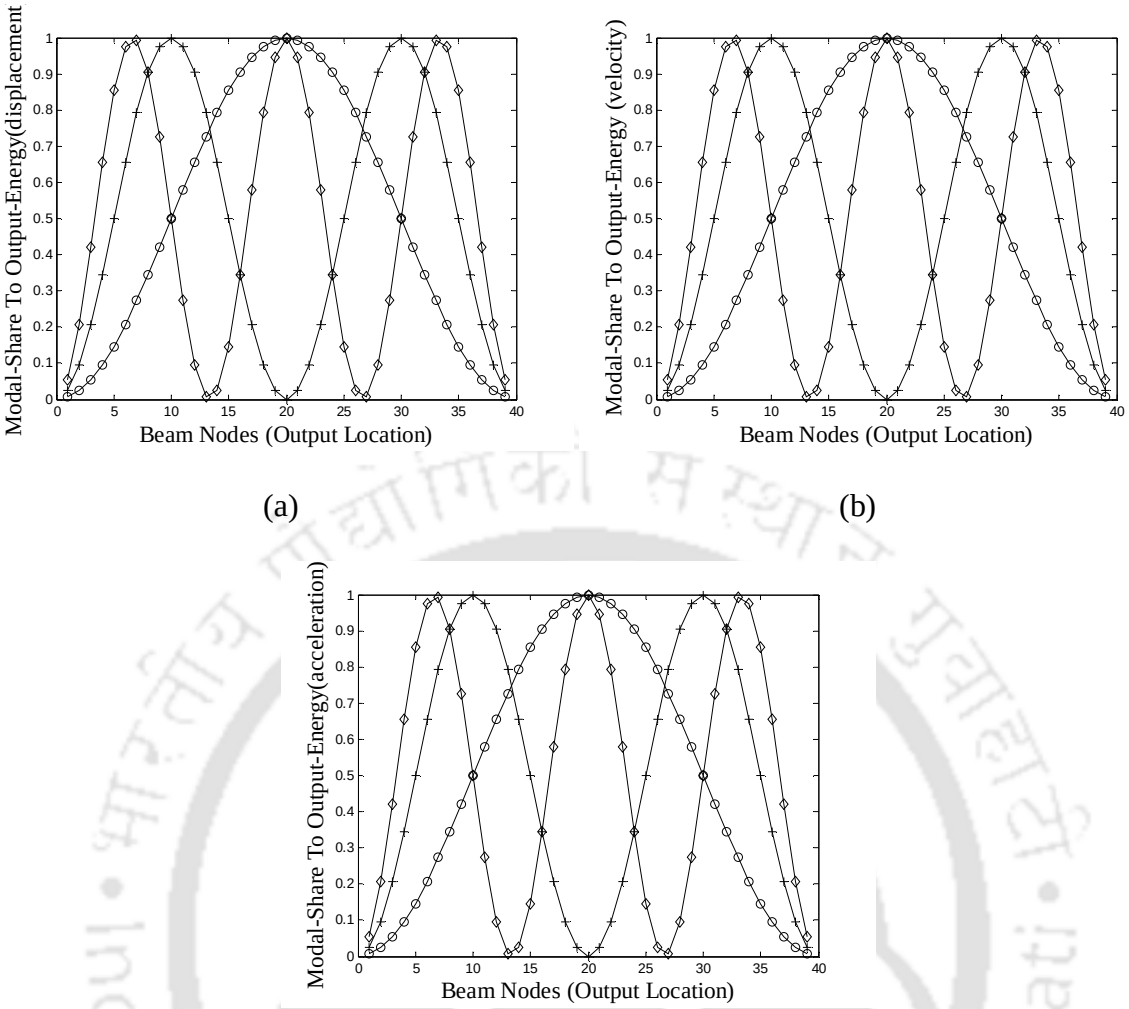

Fig. 4.4. Contribution of first three modes in individual output locations (transverse DOF) associated output energy (normalized to 1) for (a) displacement (b) velocity and (c) acceleration measurement

Next, H_2 norm associated with first three modes along individual output locations (transverse DOF) are shown in Fig. 4.5 considering any type of response measurement. It is evident from Fig. 4.5 that first three modes are showing higher participation in the form of higher magnitude of norm at the expected sensor locations for any type of response measurement.

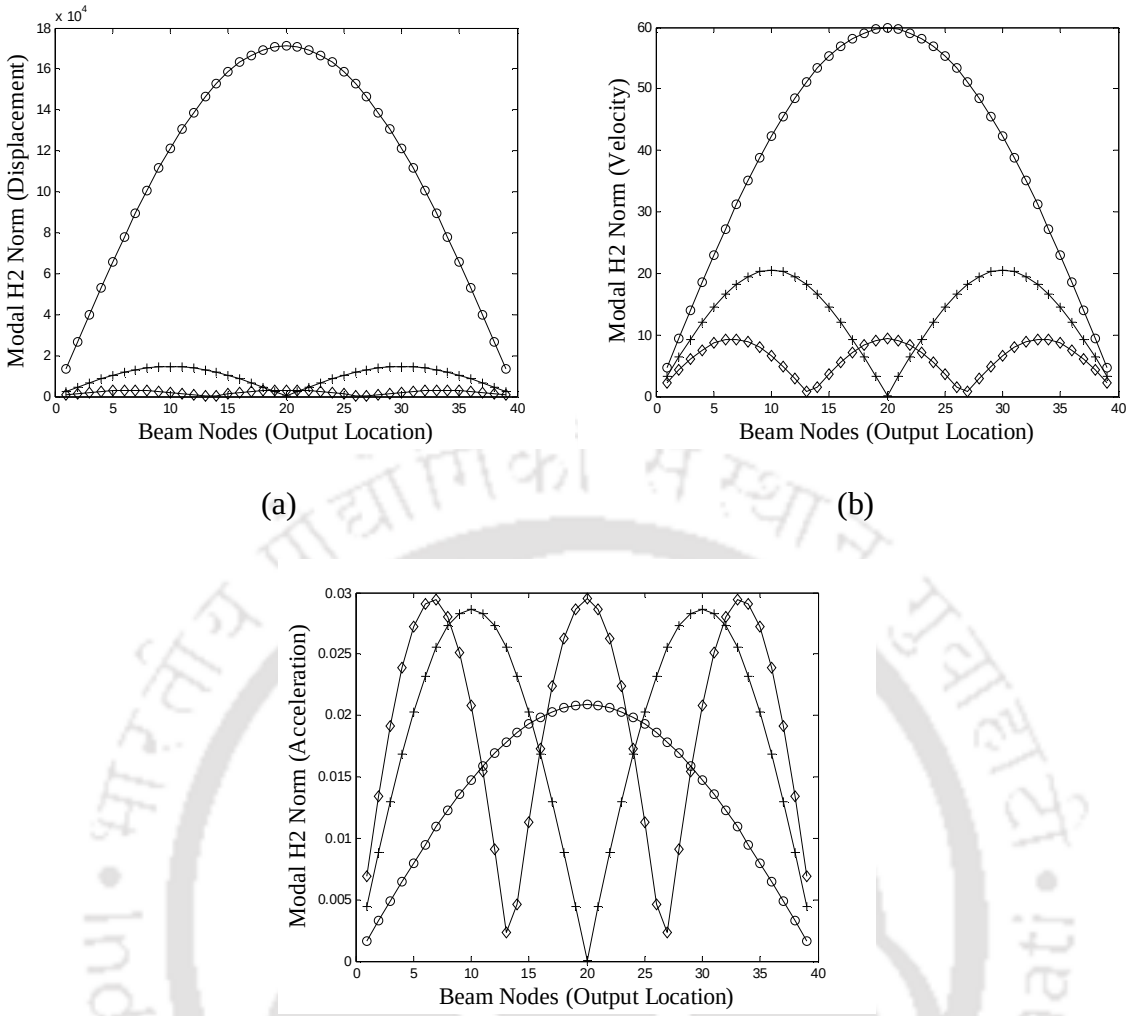

Fig. 4.5. H_2 Norm associated with first three modes along the output locations for (a) displacement (b) velocity and (c) acceleration measurement

Considering the relation (as mentioned under 4.4.2 (d)) between modal H_∞ norm and MHSV for displacement and velocity measurement with $[E] = 0$, H_∞ norm for a mode is proportional (twice) to the corresponding MHSV. Hence profiles of H_∞ norm and MHSV for a mode are similar along output locations. This helps to avoid H_∞ norm computation for displacement and velocity measurement. For acceleration measurement, effect of $[E]$ is evaluated considering the comparisons (as mentioned in Section 4.5.2) based on MIMO model. This comparison is shown in the Fig. 4.6(a). Effect of direct feed through matrix $[E]$

appears quite negligible from Fig. 4.6(a), since consideration of [*E*] for a mode does not make any considerable difference. Hence, modal H_∞ norm can be considered as twice of MHSV and this is apparent from Fig. 4.6(b). Hence modal participation profile based on modal H_∞ norm can be considered as similar to MHSV based modal participation profile for acceleration measurement as well.

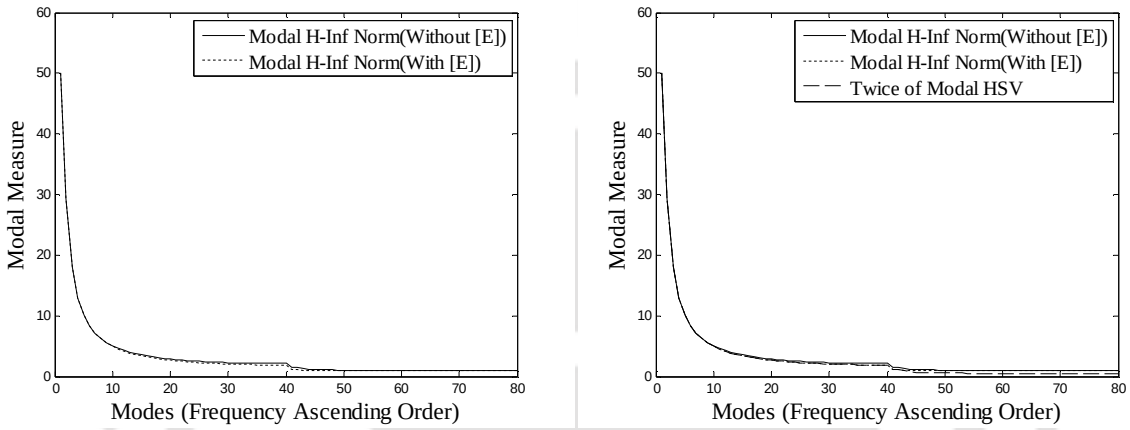

(a) (b)

Fig. 4.6. Comparison of (a) H_∞ Norm without [*E*] and with [*E*] (b) H_∞ Norm without [*E*], H_∞ Norm with [*E*] and twice of MHSV

Considering clarity of representation, only three modes are displayed for modal participation profile in Figs. 4.2, 4.4 and 4.5. Modal participation profiles evaluated for higher modes are also observed to show higher participation at the expected sensor locations. Modal participation based on EI method is not presented, since it is understood from the Eq. (4.27) that modal participation profiles exactly agree with the expected sensor locations. Further, MKE method agrees with EI method in form of modal participation profiles as the beam is considered with uniform mass distribution (Li et al. 2007) and hence modal participation for this beam problem based on MKE method is also avoided.

4.7. SENSOR PLACEMENT FOR SARAIGHAT BRIDGE

The study on sensor placement for the Saraighat Bridge is carried out in three parts: (a) comparative observations among various modal measures based on this large bridge structure; (b) a typical exercise on sensor placement using MCOE based on the modal approach framework; (c) finding suitable locations using limited numbers of sensors while targeting only the major modes of the bridge. These segments are presented in the following sub-sections.

4.7.1. Comparative observations on various modal measures

One main span along with one approach span is considered for FE modelling to carry out these comparative observations. Thus, a relatively larger structural model is considered to validate the proposed modal measure, MCOE. FE model of superstructure of the bridge for the selected spans is shown in Fig. 4.7. Masses of this structure are lumped in total 94 locations which are possible sensor locations. Inertia corresponding to rotational DOF is considered as zero. The number of DOF of the condensed second order system matrices is obtained as 282. Mass and stiffness proportional damping is considered with the assumption of monotonic increment of damping ratio with natural frequency (Cheng 2000). Damping ratio corresponding to the fundamental frequency is considered as 1%. Fundamental frequency is found from the FE model as 1.02 Hz with mode shape dominant along transverse direction. State space modal model is then constructed with mass, stiffness and damping matrices to carry out necessary computations. Here only acceleration measurement type is considered for computation of various modal measures, since computations for other response (displacement or velocity) measurement are comparatively easier than acceleration measurement.

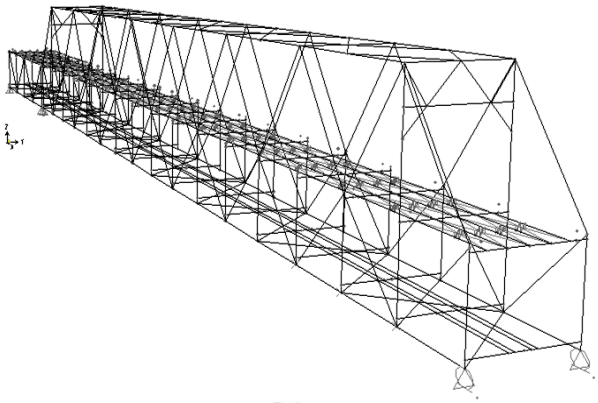

Fig. 4.7. FE model of one main span along with approach span

First, a comparative study, as mentioned in Section 4.4.1 (d), is made for computation of MHSV based on MIMO model. Such comparisons are shown in Fig. 4.8. Sorted (descending order) MHSV computed separately for all the modes are observed to be in good agreement with HSV of the structural (bridge) system in Fig. 4.8(a). Further based on mode-wise comparison, MHSV show good agreement with the approximate MHSV in Fig. 4.8(b). These comparisons demonstrate an acceptable level of accuracy in MHSV computation for the bridge structure.

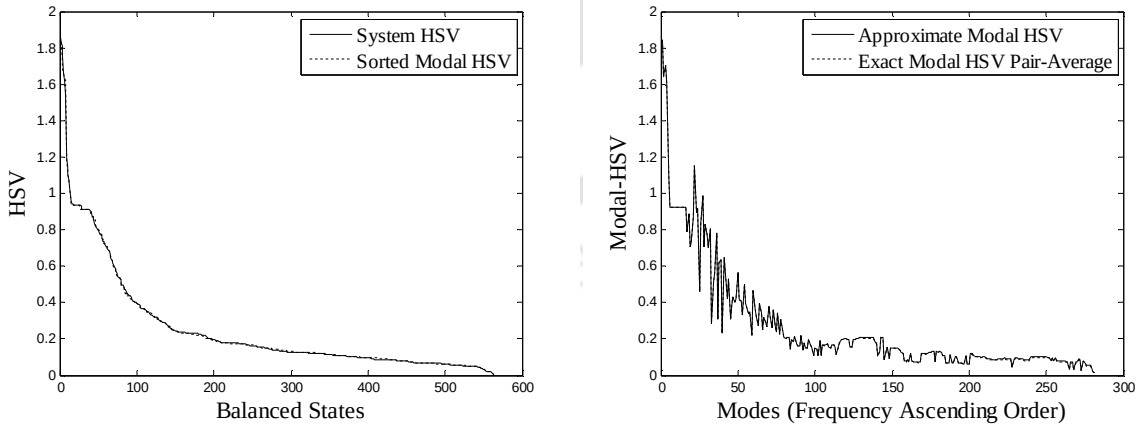

(a) (b)

Fig. 4.8. (a) Comparison of system HSV (sorted) and MHSV of all modes (sorted) (b) comparison of average of MHSV pair and approximate MHSV

Diagonal dominancy of the observability grammian is preferred for the application of MCOE as modal measure. Profile of the observability grammian matrix based on MIMO model and corresponding to the modal states as per Eq. (4.35) is shown in Fig. 4.9. From Fig. 4.9, it is observed that the observability grammian is diagonally dominant. Hence the preferred criterion is met for use of MCOE as modal measure for this large bridge structure.

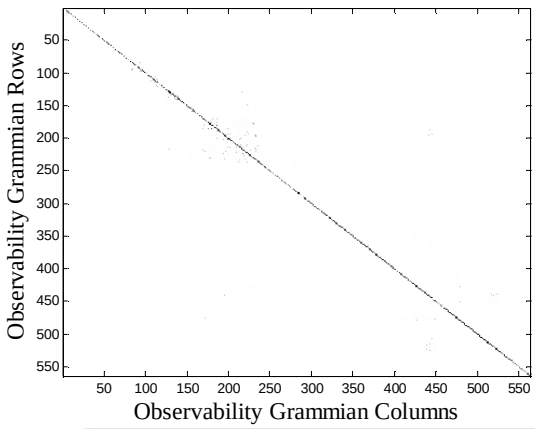

Fig. 4.9. Profile of observability grammian matrices (564×564) based on modal states as in Eq. (4.35)

As acceleration measurement is considered here, direct feed through matrix [*E*] is non zero. Effect of [*E*] is evaluated here based on the comparative approach as mentioned in Section 4.5.2. For insignificant effect of [*E*], modal H_∞ norm computation is possible from known MHSV (twice of MHSV). Such comparisons, with and without considering [*E*], are shown in the Fig. 4.10(a) where quite negligible effect of [*E*] is observed. Modal H_∞ norm now can be considered as twice of MHSV and this is apparent from Fig. 4.10(b). Hence, it can be considered that modal participation profiles based on modal H_∞ norm and MHSV are similar and this allows to avoid the computation of H_∞ norm for this bridge structure.

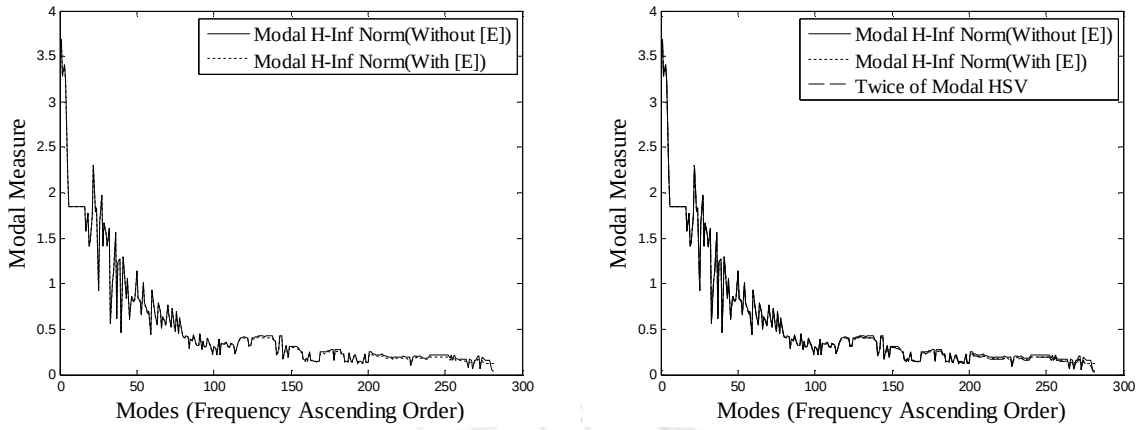

(a) (b)

Fig. 4.10. Comparison of (a) H_∞ Norm without [*E*] and with [*E*] (b) H_∞ Norm without [*E*], H_∞ Norm with [*E*] and twice of MHSV

Strong modes of this bridge system are identified as the modes with strong MHSV. It is observed from Fig. 4.8(a) that consideration of 100 balanced states (i.e. 50 modes) may be a good choice. Using the FE model, a preliminary idea regrading the frequency range of the selected stronger modes is made and is observed to be approximately 10 Hz for 50 stronger modes for the bridge. Next, the comparisons are carried out among the profiles of modal participation based on MHSV, H_2 norm, MCOE, EI method and MKE method. First 5 strong modes based on strong MHSV (1, 3, 2, 4, 22) and 50^{th} mode are chosen to display the profile of modal participation along each DOF in Fig. 4.11. From Fig. 4.11, it is observed that MCOE shows (i) very good agreement with EI method as expected (ii) good agreement with norm based modal measures specially, for the higher modal participating locations which are actually of our interest and (iii) reasonable agreement with MKE method for the higher modal participating locations. The comparison among the proposed and existing techniques in the form of identified sensor locations is not really feasible since, there exists many options for judgement e.g. assignment of different numbers of sensors to different individual target

modes, identification of redundant correlated locations with similar modal participation for target modes, heuristic treatment to placement matrix containing modal participation profiles of target modes etc. Thus, even with the physical difficulty of carrying out comparison in terms of sensor locations, this technique can be viewed as attractive due its flexible and insightful approach for sensor location identification for multiple target modes.

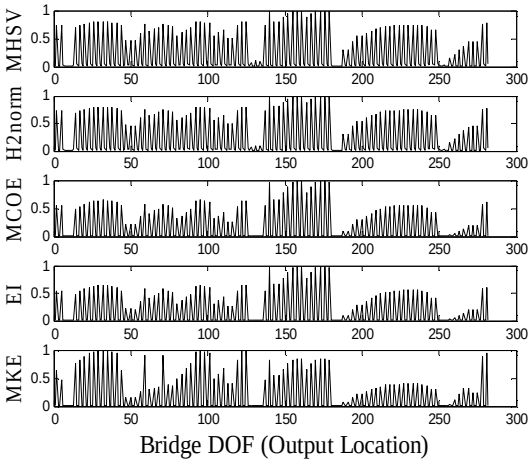

(a)

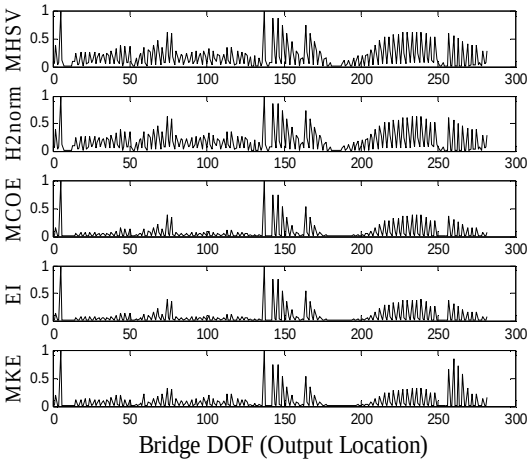

(b)

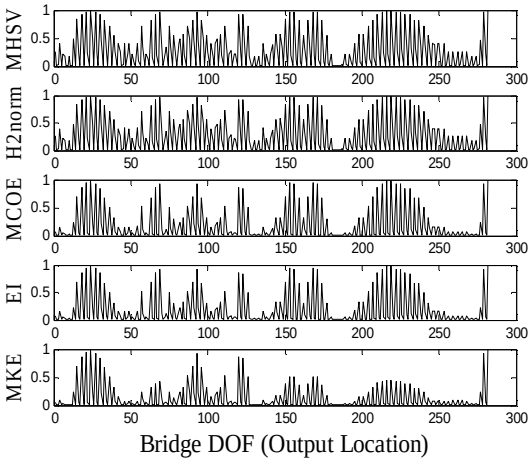

(c)

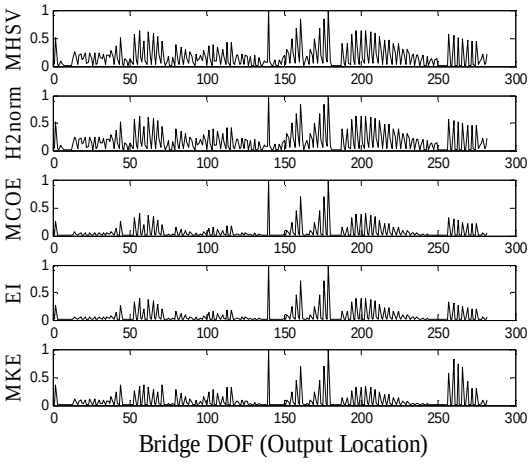

(d)

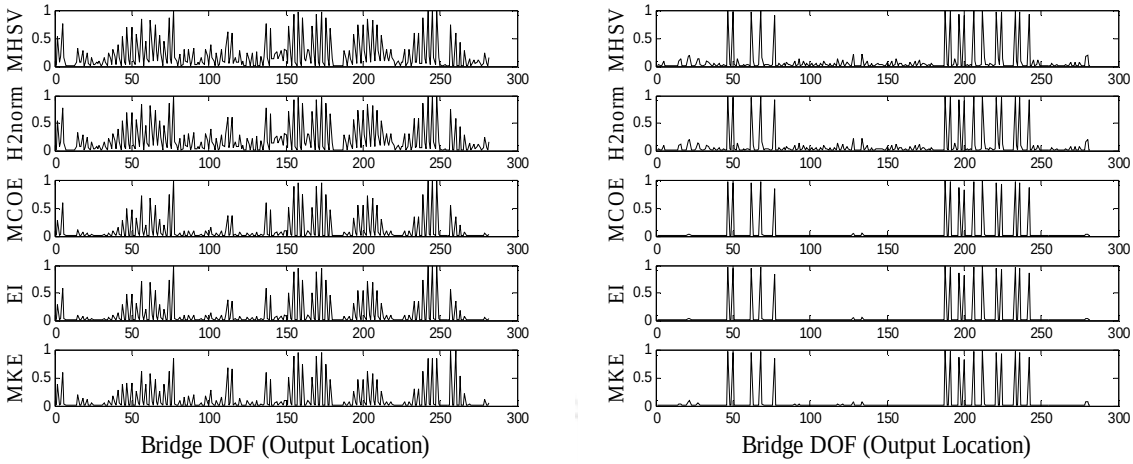

(e) (f)

Fig. 4.11. Profile of modal participation based on various techniques for (a) 1st (b) 3rd (c) 2nd (d) 4th (e) 22nd and (f) 50th mode

4.7.2. Sensor placement using the proposed methodology

Sensor locations are identified for fifty numbers of target modes which are selected based on stronger MHSV. Sensor locations are identified based on modal participation profiles for each of the target modes and participation profiles are evaluated using MCOE. Total 100 numbers of locations are identified for placing uni-axial accelerometers in three directions (longitudinal, transverse and vertical). Locations of these 100 uni-axial accelerometers are shown in Fig. 4.12. It is clearly observed from Fig. 4.12 that

(a) Locations of sensors are suitable at the road-level for longitudinal measurement.

(b) For transverse direction, suitable locations of sensors are primarily along the rail-level. However, few modes out of the considered fifty modes might have high deformations at the top level leading to identification of some sensor locations at that level.

(c) For vertical direction, any of the rail-level, road-level or top-level may be considered suitable for sensor location.

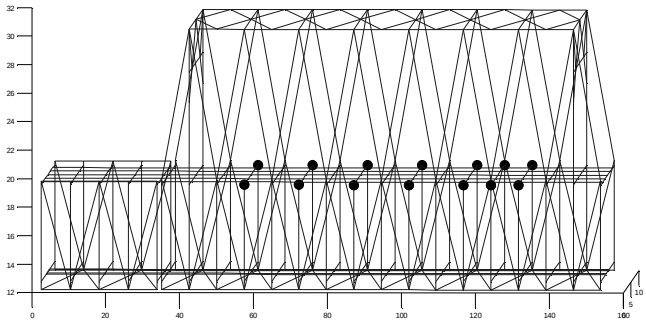

(a)

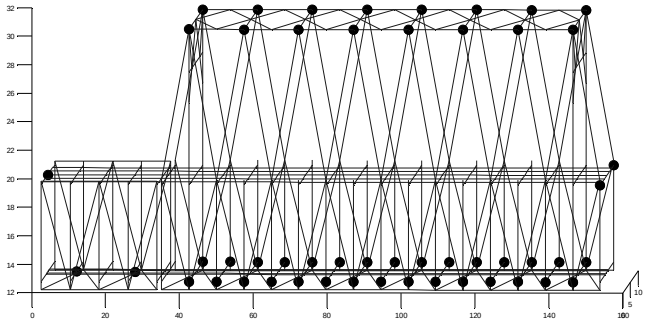

(b)

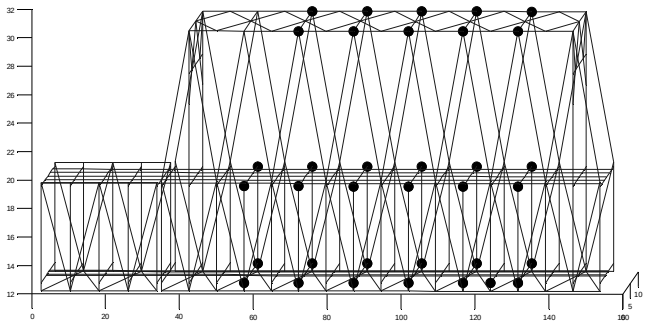

(c)

Fig. 4.12. Locations of total 100 uni-axial accelerometers in (a) longitudinal (b) transverse and (c) vertical directions

4.7.3. Sensor placement for Saraighat Bridge targeting few major modes

The sensor placement exercise carried out in the last sub-section can be considered as a general approach for general types of structures. In many cases in structural engineering, only first few modes are of major interest. In the case of bridge under study, only first few major modes are targeted for identification based on experimentally observed data. Further, it is usually observed that deck-level of a bridge is given importance in instrumentation as it is easier to interpret the observed mode shape for horizontal, vertical and torsional behaviour of the bridge structure. Further, the evaluation of locations for the placement of sensors requires a judicious combination of analysis based on the proposed methodology as well as the general understanding of the deformation pattern of the bridge.

Effective independence (EI) technique (Kammer 1990), system norm based modal-measures as H_2, H_∞, Hankel norms (Gawronski 2004), modal measure in terms of modal contribution in output energy (MCOE) advocate for higher presence of a mode along DOF-locations having higher modal deformation. DOF-locations associated with higher modal deformations for a mode: (a) provide better information for that mode according to the EI methodology; (b) contribute higher in the output energy associated that mode, while a structural system is excited by releasing from any initial state. First three modes, each in transverse direction (1^{st} transverse, 2^{nd} transverse and 3^{rd} transverse modes) and vertical direction (1^{st} vertical, 2^{nd} vertical and 3^{rd} vertical modes), are considered for evaluating the locations with higher modal deformations. These mode shapes, computed using SAP2000 (V14.2.2) based on the adopted FE model of Saraighat Bridge are shown in Figs. 4.13 and 4.14 for horizontal (transverse) and vertical direction respectively. Figs. 4.13–4.14 show higher deformation along the rail-level plane associated to these prominent horizontal and vertical modes. Hence, the rail-level plane is considered as suitable locations for identification of these prominent modes where better presence of those modes is most likely.

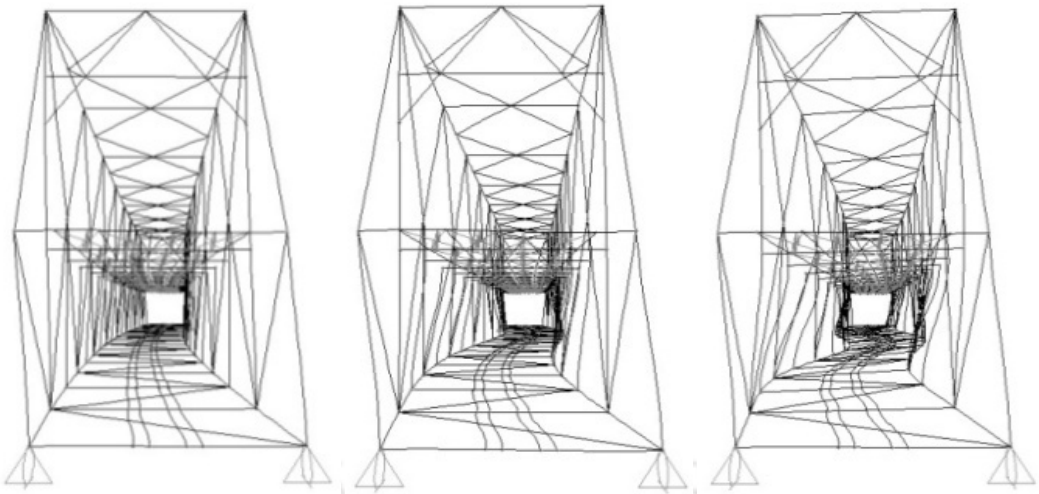

(a) (b) (c)

Fig. 4.13. Numerical mode shapes (a) 1st transverse (b) 2nd transverse and (c) 3rd transverse

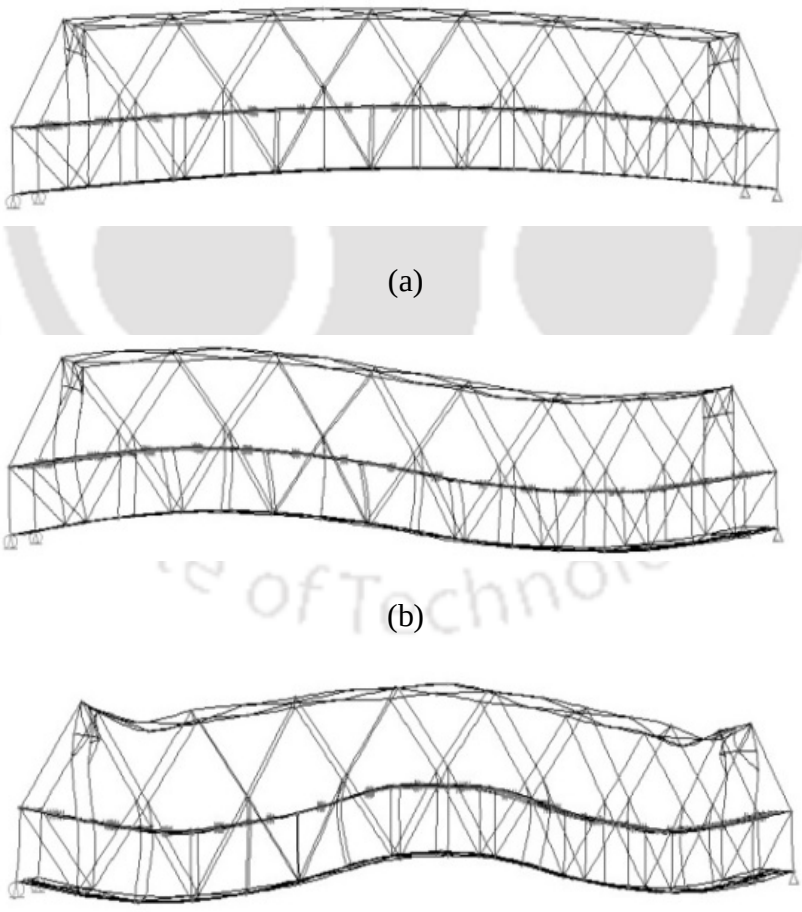

(a)

(b)

(c)

Fig. 4.14. Numerical mode shapes (a) 1st vertical (b) 2nd vertical and (c) 3rd vertical

The locations of accelerometers and measurement directions are considered as shown in Fig. 4.15. The rationale behind the selection of locations of sensors and their chosen directions are explained here in details.

(A) From the numerical mode shapes, it is observed that transverse (along Y) modal deformations for any two locations with similar X, Z coordinates (e.g. 9L and 9R as in Fig. 4.15) become nearly equal. In view of this observation, respective locations of 3R, 5R… 15R and 3L, 5L… 15L are assumed to have same modal deformations in transverse (Y) direction and transverse measurements are taken only along left side of the deck. A probable reason for such behaviour may be due to presence of the strong rail-level cross girders (Fig. 4.16).

(B) The considered span is simply supported and hence five locations are considered as sufficient to extract better modal information as well as to capture the peaks associated to first three modes as [l/6, l/4, l/2, 3l/4, 5l/6], where l denotes length of the simply supported span. The location l/6 lies between two nodes 3 and 4, while the location 5l/6 lies between two nodes 14 and 15 (Fig. 4.15). The instrumentation of the Saraighat Bridge is planned to be carried out using sensors at 14 locations along both sides of the rail-level deck for both transverse and vertical directions (Fig. 4.15). The locations are arrived at using the numerical mode shapes and analysis based on the proposed methodology. In this exercise, first two steps, as mentioned in Section 4.4.6, are followed while the third step is avoided to keep the locations along both sides of the rail-level deck. Further in this exercise, number of sensors (n_S) for individual modes are assigned for fulfilling the minimum requirement based on the assumption of simply-supported behaviour e.g. (a) for 1st mode $n_S \geq 2$ (b) for 2nd mode $n_S \geq 4$ (c) for 3rd mode $n_S \geq 6$. Suitable sensor arrangements for transverse and vertical directions having 14 locations in each direction, are evaluated as shown in Fig. 4.17. It can be observed from Fig. 4.17 that the sensor locations along the transverse direction reasonably follow the

pattern [*l*/6, *l*/4, *l*/2, 3*l*/4, 5*l*/6] in the form of nodes [4, 5, 9, 13, 14] (as per Fig. 4.15). Similarly, sensor locations along the vertical direction also reasonably follow that pattern in the form of nodes [3, 5, 9, 13, 14 or 15] (as per Fig. 4.15). Extra four locations can be suitably adjusted for capturing a smooth shape of modal displacement. Thus, with minor adjustments of appropriate locations as observed in Fig. 4.17 and based on the observation from 4.7.3(A), the measurement locations, measurement directions and types of accelerometers considered for the actual field study are decided as shown in Fig. 4.15. Total 15 uniaxial accelerometers and 4 triaxial accelerometers are used, thus measuring data along 27 channels. Measurements at the location 10L (along Y and Z) are employed as reference channels which are useful for application of NExT. The longitudinal measurements are usually not given much importance since longitudinal deformations are quite insignificant. However, with the availability of the tri-axial sensors, the acceleration data along the longitudinal directions are also recorded.

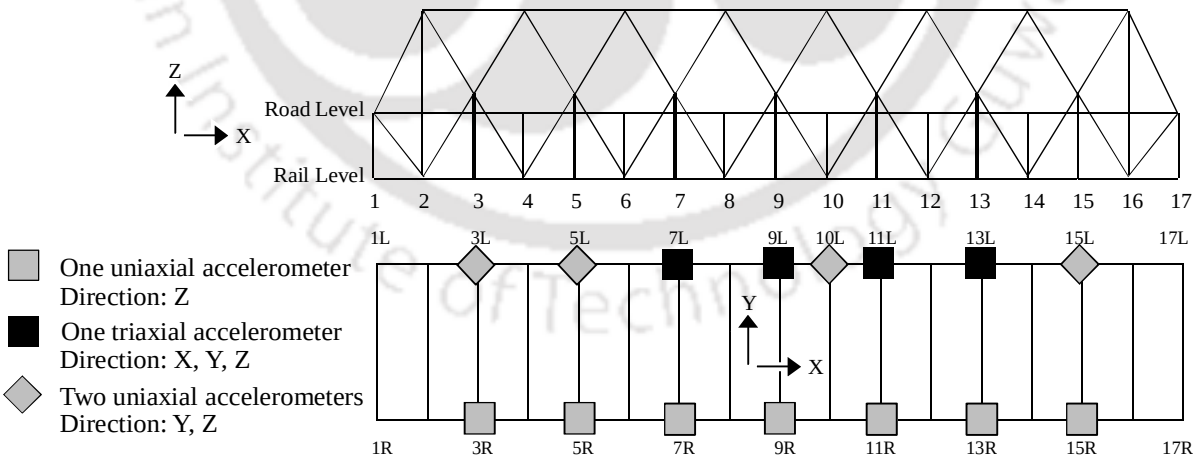

Fig. 4.15. Details of locations of accelerometers and measurement directions (letters "L" and "R" indicate left and right respectively while facing along positive direction of X)

Fig. 4.16. View of rail-level cross-girders

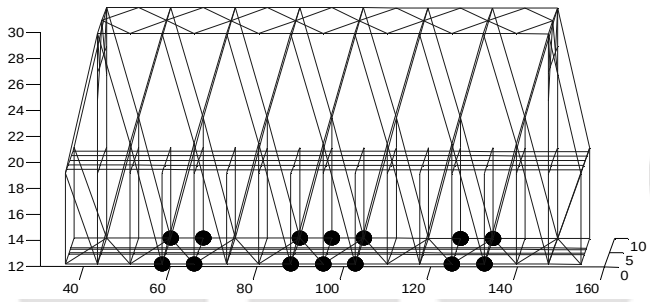

(a)

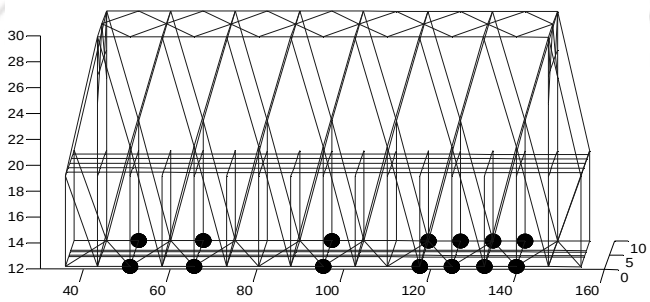

(b)

Fig. 4.17. Appropriate sensor locations along (a) transverse and (b) vertical direction

4.8. CONCLUDING REMARKS

Three major strategies for optimal sensor placement are observed in literature as: EI method, MKE method and modal approach using various system norms (e.g. Hankel, H_∞ and H_2). In comparison with two popular techniques, viz. EI and MKE, the modal approach using various norms appears appealing in view of the following points: (a) it provides options for consideration of different types of response measurement and (b) it uses a modal approach framework where modal participation of each of the target modes at individual DOF are first evaluated and subsequently the locations of sensors are identified for target modes using those participation profiles in a flexible as well as easier insightful manner. The modal approach employs various system norms in terms of modal measures to estimate the modal participations. Although the existing modal measures are well established, those modal measures require the knowledge of input-locations where excitations are provided. In case of output-only system identification or OMA, it is indeed difficult to precisely identify the input-locations. In view of this, existing modal measures don't appear to be quite suitable for sensor placement in OMA based on the modal approach methodology. The proposed modal measure (MCOE) estimates the modal participation considering only the output in terms of employing solely the observability grammian and also associated with simple physical understanding ensuring higher confidence in sensor placement. MCOE thus establishes itself as a suitable modal measure for sensor placement in OMA based on the modal approach. Comparisons with other methods are carried out based on participation of a mode. It has been established that the proposed technique is analytically similar to EI method in form of modal participation. Further, comparisons are carried out using an existing large truss bridge structure with acceleration measurement. In this comparison, MCOE technique demonstrates very good agreement with EI method as expected, good agreement with MHSV as well as system norms and reasonable agreement with MKE method. In short it is concluded that MCOE technique based on the modal approach framework may be viewed as an effective methodology for sensor placement in OMA.

Chapter 5

SYSTEM IDENTIFICATION: A STATISTICAL APPROACH

5.1. INTRODUCTION

System identification is carried out for the evaluation of modal parameters such as natural frequencies, damping ratios and mode shapes based on measured ambient vibration responses of the structure. Output-only system identification i.e. operation modal analysis (OMA) is considered for the identification of the modal parameters of the Saraighat Bridge. Effects of measurement noise are likely to influence the identified parameters. Moreover, deviations of real ambient vibration from theoretical assumption of white-noise induced vibration are also likely to influence the accuracy of identification techniques. Two approaches are considered for enhanced precision against such unfavourable condition as well as theoretical limitation. These are: (a) employing multiple techniques both in time and frequency domain for comparison of identified modal parameters from different techniques and (b) identifying modal parameters in terms of central tendency and dispersion based on multiple data sets. Central tendency of a modal parameter ensures higher acceptance and the dispersion measure helps further to assess the confidence bounds. Finally central tendencies obtained employing multiple techniques are compared to realize the acceptance of identified modal parameters.

5.2. SENSOR AND DATA ACQUISITION SYSTEM

Data are recorded using uniaxial and triaxial force balance accelerometers (Model: EpiSensor ES-U2 and EpiSensor ES-T; make: Kinemetrics Inc., USA). These accelerometers can be used in a variety of applications for measuring accelerations up to ±4g. ES-U2 and ES-T can detect any structural motion that may vibrate in frequency range of DC to 200 Hz. These accelerometers have the facility of amplification and conditioning of measured data.

Therefore, there is no requirement for any external electronics other than a data acquisition system. On the other hand, a 48 channel dynamic data acquisition system (model: MGCplus; make: HBM GmbH, Germany) is used in data-recording. Maximum sampling rate for data-acquisition by MGCplus are 2400, 4800 and 9600 Hz associated with different sets of channels. Data acquisition is performed with a sampling rate of 100 Hz and with resolution of 20 bit. Additionally a notebook computer is used for controlling the data acquisition system and storing the measured data. Two photographs of sensors and the data acquisition system during the time of data recording are shown in Figs. 5.1 and 5.2 respectively.

Fig. 5.1. Sensors for data acquisition: (a) EpiSensor ES-U2 and (b) EpiSensor ES-T

Fig. 5.2. Data acquisition system (MGCplus) along with notebook computer

5.3. APPLIED IDENTIFICATION TECHNIQUES

The modal parameters are identified using three important techniques: NExT-ERA, SSI (data driven) and FSDD. NExT estimates the impulse response function directly from the ambient vibration data, which is based on sound theoretical background. On the other hand, ERA estimates the modal parameters using the impulse response sequence based on the principle of minimal realization theory. Secondly, the system theory, statistics, optimization theory and (numerical) linear algebra culminate in the evolution of 'subspace' techniques which enables to obtain state sequence directly from input-output data or only output data (ambient). The subspace-methods don't require an explicit model parametrization. Moreover, subspace algorithms have the advantages of being elegant and computationally efficient. SSI as a sub-sect of subspace-methods using only output data (ambient), provide all these advantage in identification of modal parameters. Finally, FSDD, established based on a reasonable theoretical background, doesn't require any data-fitting as well as parametrization. FSDD also has various advantages over classical pick-picking method which is usually considered as an important methodology. These three techniques are also found to be used frequently for modal identification from ambient vibration data. The major highlights of these techniques are presented in the following sub-sections. Both of the techniques, ERA and SSI identify the state space matrices in discrete time domain and modal parameters are finally evaluated using those identified state space matrices. The state space equations in discrete time domain, considered in this present study, are as follows.

$$\{s(k+1)\} = [A]\{s(k)\} + [B]\{u(k)\} \tag{5.1a}$$

$$\{y(k)\} = [C]\{s(k)\} + [E]\{u(k)\} \tag{5.1b}$$

where, [*A*], [*B*], [*C*], [*E*] represents the discrete time state space matrices, {*s*} represents the states, *k* is integer to represent discrete time as $t=k(\Delta t)$ with Δt being sampling time, {*u*} and

{y} represent the input and output respectively. Estimation of [A] and [C] are sufficient for identification of modal parameters.

5.3.1. Natural excitation technique with eigensystem realization algorithm (NExT-ERA)

It is a two-step identification where NExT is applied to estimate the impulse responses from ambient data in the first phase. Subsequently, ERA is employed to identify the state space matrices in discrete time domain from the estimated impulse responses. The displacement vector associated to the equation of motion as $\{x(t)\}$ at time t is related to the modal coordinate as $\{q(t)\}$ in the form of the following equation.

$$\{x(t)\} = [\Phi]\{q(t)\} = \sum_{r=1}^{n} \{\Phi_r\} q_r(t) \tag{5.2}$$

where, n, $[\Phi]$ and $\{\Phi_r\}$ represent the number of DOF, modal matrix and r^{th} mode shape vector respectively. With consideration of proportional damping the r^{th} modal coordinate can be expressed as follows.

$$\ddot{q}_r(t) + 2\xi_r\omega_r\dot{q}_r(t) + \omega_r^2 q_r(t) = \frac{1}{m_r}\{\Phi_r\}^T \{u(t)\} \tag{5.3}$$

where, m_r represents the r^{th} modal mass. Solution of the Eq. (5.3) can be carried out using the Duhamel integral. Solution can be found out for the displacement vector, $\{x(t)\}$, based on the assumption of zero initial condition in the following form.

$$\{x(t)\} = \sum_{r=1}^{n} \{\Phi_r\} \int_{-\infty}^{\tau} \{\Phi_r\}^T \{u(\tau)\} g_r(t-\tau)\mathrm{d}\tau \tag{5.4}$$

where, $g_r(t) = \frac{1}{m_r\bar{\omega}_r}\exp(-\xi_r\omega_r t)\sin(\bar{\omega}_r t)$ and $\bar{\omega}_r = \omega_r(1-\xi_r^2)^{1/2}$ is the r^{th} damped modal frequency. Eq. (5.4) can be transformed for a single output, $x_{ik}(t)$ and a single input force, $u_k(t)$ at a location k in the following form.

$$x_{ik}(t) = \sum_{r=1}^{n} \frac{\Phi_{ir}\Phi_{kr}}{m_r \bar{\omega}_r} \exp(-\xi_r \omega_r t) \sin(\bar{\omega}_r t) \tag{5.5}$$

where, Φ_{ir} is the i^{th} component of the r^{th} mode shape vector $\{\Phi_r\}$. The next step is to form the cross-correlation function of two responses, x_{ik} and x_{jk}, due to a white-noise input at a particular location k. The cross-correlation function $R_{ijk}(T)$ is defined as the expected value of the product of two responses evaluated at a time separation of T as follows.

$$R_{ijk}(T) = \mathrm{E}[x_{ik}(t+T)x_{jk}(t)] \tag{5.6}$$

Based on the assumption of white-noise, the cross-correlation function due to all the input can be found out by summing up contributions from all the input locations as

$$R_{ij}(T) = \sum_{r=1}^{n} \frac{\Phi_{ir}\bar{A}_{jr}}{m_r \bar{\omega}_r} \exp(-\xi_r \omega_r T) \sin(\bar{\omega}_r T + \theta_r) \tag{5.7}$$

It can observed from the Eq. (5.7) that the cross-correlation function is expressed as a single sine function with a new phase angle (θ_r) and a new constant multiplier ($\bar{A}_{jr}$). Hence, the cross-correlation function is a sum of decaying sinusoids of the same form as the impulse response function of the original system as expressed in the Eq. (5.5). Based on this observation, it is well understood that the impulse response functions can be estimated from the ambient vibration data.

In the next step, Markov parameters blocks are formed using the estimated impulse responses to construct finally the Hankel matrix. Subsequently, ERA uses the Hankel matrix to identify the modal parameters. The Markov parameters can be written as

$$\left[h(k)\right] = \left[C\right]\left[A\right]^{k-1}\left[B\right] \tag{5.8}$$

Considering the number of input and output as n_1 and n_2 respectively, the size of a Markov parameters becomes $n_2 \times n_1$. Now, the Hankel matrix is represented as

$$\left[H\left(k-1\right)\right]=\begin{bmatrix}\left[h(k)\right] & \left[h(k+1)\right] & \cdots & \left[h(k+j)\right]\\ \left[h(k+1)\right] & \left[h(k+2)\right] & \cdots & \left[h(k+j+1)\right]\\ \vdots & \vdots & \ddots & \vdots\\ \left[h(k+i)\right] & \left[h(k+i+1)\right] & \cdots & \left[h(k+i+j)\right]\end{bmatrix} \tag{5.9}$$

where, i=1, 2, ….. r_1–1 and j=1, 2, …. s_1–1, with r_1 and s_1 as integers. Now the size of the Hankel matrix becomes as ($n_2r\times n_1s$). Hankel matrix for k = 1 i.e. [H(0)] is decomposed using SVD as

$$\left[H\left(0\right)\right]=\left[U\right]\left[\Sigma\right]\left[V\right]^T \tag{5.10}$$

where, the sizes of [U], $\left[\Sigma\right]$ and [V]^T are ($n_2r\times$ n_2r), ($n_2r\times n_1s$) and ($n_1s\times$ n_1s) respectively. It is considered that [H(0)] has 2N non-zero singular values (i.e. rank=2N) equivalent to the order of state space system. Therefore, expression for [H(0)] can be rewritten as

$$\left[H\left(0\right)\right]\approx\left[U_{2N}\right]\left[\Sigma_{2N}\right]\left[V_{2N}\right]^T \tag{5.11}$$

where, the sizes of $\left[U_{2N}\right]$, $\left[\Sigma_{2N}\right]$ and $\left[V_{2N}\right]^T$ are ($n_2r\times$ 2N), (2N×2N) and (2N×n_1s) respectively. The estimate of the discrete time state-space are obtained as follows

$$\left[A\right]=\left[\Sigma_{2N}\right]^{-1/2}\left[U_{2N}\right]^T\left[H(1)\right]\left[V_{2N}\right]\left[\Sigma_{2N}\right]^{-1/2} \tag{5.12a}$$

$$\left[B\right]=\left[\Sigma_{2N}\right]^{1/2}\left[V_{2N}\right]^T\left[E_2\right] \tag{5.12b}$$

$$\left[C\right]=\left[E_1\right]^T\left[H(1)\right]\left[U_{2N}\right]\left[\Sigma_{2N}\right]^{1/2} \tag{5.12c}$$

$\left[E_1\right]^T$ and $\left[E_2\right]$ as appeared in the above equations, are defined as follows,

$$\left[E_1\right]^T=\begin{bmatrix}\left[I\right] & \left[0\right] & \cdots & \left[0\right]\end{bmatrix} \tag{5.13a}$$

where, each sub-matrices (identity and zero matrices) is of the size ($n_2\times n_2$).

$$\left[E_2\right]=\begin{bmatrix}\left[I\right]\\ \left[0\right]\\ \vdots\\ \left[0\right]\end{bmatrix} \tag{5.13b}$$

where, each sub-matrices (identity and zero matrices) is of the size ($n_1 \times n_1$).

5.3.2. Stochastic subspace identification (SSI)

Next, SSI-DATA method is considered for evaluation of the modal parameters. The summary of this identification technique are mentioned below. The output block Hankel matrix (consisting of $2i$ rows and j columns of output block sub-matrices) is represented in two forms as in Eqs. (5.14a) and (5.14b).

$$\left[Y_{0|2i-1}\right] \triangleq \left(\begin{array}{cccc} \{y_0\} & \{y_1\} & \cdots & \{y_{j-1}\} \\ \cdots & \cdots & \cdots & \cdots \\ \{y_{i-2}\} & \{y_{i-1}\} & \cdots & \{y_{i+j-3}\} \\ \{y_{i-1}\} & \{y_i\} & \cdots & \{y_{i+j-2}\} \\ \hline \{y_i\} & \{y_{i+1}\} & \cdots & \{y_{i+j-1}\} \\ \{y_{i+1}\} & \{y_{i+2}\} & \cdots & \{y_{i+j}\} \\ \cdots & \cdots & \cdots & \cdots \\ \{y_{2i-1}\} & \{y_{2i}\} & \cdots & \{y_{2i+j-2}\} \end{array}\right) \triangleq \left(\frac{\left[Y_{0|i-1}\right]}{\left[Y_{i|2i-1}\right]}\right) \triangleq \left(\frac{\left[Y_1\right]}{\left[Y_2\right]}\right) \tag{5.14a}$$

$$\left[Y_{0|2i-1}\right] \triangleq \left(\begin{array}{cccc} \{y_0\} & \{y_1\} & \cdots & \{y_{j-1}\} \\ \cdots & \cdots & \cdots & \cdots \\ \{y_{i-2}\} & \{y_{i-1}\} & \cdots & \{y_{i+j-3}\} \\ \{y_{i-1}\} & \{y_i\} & \cdots & \{y_{i+j-2}\} \\ \{y_i\} & \{y_{i+1}\} & \cdots & \{y_{i+j-1}\} \\ \hline \{y_{i+1}\} & \{y_{i+2}\} & \cdots & \{y_{i+j}\} \\ \cdots & \cdots & \cdots & \cdots \\ \{y_{2i-1}\} & \{y_{2i}\} & \cdots & \{y_{2i+j-2}\} \end{array}\right) \triangleq \left(\frac{\left[Y_{0|i}\right]}{\left[Y_{i+1|2i-1}\right]}\right) \triangleq \left(\frac{\left[Y_1^+\right]}{\left[Y_2^-\right]}\right) \tag{5.14b}$$

One of the key steps in SSI-DATA is projection. The projections are computed as in Eqs. (5.15a) and (5.15b).

$$[O_i] \triangleq [Y_2] / [Y_1] \tag{5.15a}$$

$$[O_{i-1}] \triangleq \left[Y_2^-\right] / \left[Y_1^+\right] \tag{5.15b}$$

Three different choices of algorithms are implemented in SSI-DATA based on three choices of weighting matrices for projection matrix: (a) unweighted principal component (UPC) algorithm, (b) principal component (PC) algorithm and (c) canonical variant algorithm (CVA) (Van Overschee and De Moor 1996). Weighting matrices ($[W_1]$ and $[W_2]$) are incorporated with projection matrix to form the weighted projection like $[W_1][O_i][W_2]$. SVD is applied next for the weighted projection as in Eq. (5.16).

$$[W_1][O_i][W_2] = [U][\Sigma][V]^T \tag{5.16}$$

The order is determined by inspecting $[\Sigma]$. It is here assumed that the order is 2*N*. Using the significant part of the decomposed matrices as in Eq. (5.16), the extended observability matrix now is expressed as in Eq. (5.17).

$$[\Gamma_i] = [W_1]^{-1}[U_{2N}][\Sigma_{2N}]^{1/2} \tag{5.17}$$

$[\Gamma_{i-1}]$ is found out with stripping the last *l* (number of outputs) rows from $[\Gamma_i]$. Evaluation of the Kalman filter state sequences is carried out using the Eqs. (5.18a) and (5.18b). Here the symbol "†" represents the Moore-Penrose pseudo-inverse of a matrix.

$$\left[\hat{X}_i\right] = [\Gamma_i]^{\dagger}[O_i] \tag{5.18a}$$

$$\left[\hat{X}_{i+1}\right] = [\Gamma_{i-1}]^{\dagger}[O_{i-1}] \tag{5.18b}$$

The least-squares solution is carried out using the Eq. (5.19) finally to compute an asymptotically unbiased estimate of [*A*] and [*C*].

$$\begin{bmatrix}[A]\\[C]\end{bmatrix}=\begin{bmatrix}\left[\hat{X}_{i+1}\right]\\\left[Y_{i|i}\right]\end{bmatrix}.\left[\hat{X}_i\right]^{\dagger} \tag{5.19}$$

5.3.3. Frequency spatial domain decomposition (FSDD)

Frequency domain decomposition is theoretically established based on the following formula relating the output PSD, $\left[G_{yy}(\omega)\right]$ and stochastic input PSD, $\left[G_{xx}(\omega)\right]$.

$$\left[G_{yy}(\omega)\right]=[G(\omega)]\left[G_{xx}(\omega)\right][G(\omega)]^{H} \tag{5.20}$$

where, $[G(\omega)]$ represents the FRF matrix. The input is considered as white noise and hence the stochastic input PSD, $\left[G_{xx}(\omega)\right]$ becomes a constant matrix. This helps in the evolution of FSDD technique. It can be shown that while frequency reaches close to the m^{th} modal frequency as ω_m, the output PSD can be approximated as follows.

$$\left[\underset{\omega\to\omega_m}{G_{yy}(i\omega_m)}\right]^{T}\approx\alpha_m\{\Phi_m\}\{\Phi_m\}^{H} \tag{5.21}$$

where, $\{\Phi_m\}$ represents the m^{th} mode shape and α_m is a constant associated to that mode. The above equation is derived taking all the measurement-locations as reference and thus the output PSD becomes as a square matrix. The key step in FSDD is the singular value decomposition of the estimated output PSD as shown below.

$$\left[\hat{G}_{yy}(i\omega)\right]=[U(\omega)][\Sigma(\omega)][V(\omega)]^{H} \tag{5.22}$$

It may be mentioned that all the measurements are considered as reference and hence $[U(\omega)]$ becomes similar as $[V(\omega)]$. While the frequency approaches a modal frequency ω_m, the PSD matrix approximates a matrix of rank one. This observation enables the following relation.

$$\left[\underset{\omega\to\omega_m}{\hat{G}_{yy}(i\omega_m)}\right]\approx\Sigma_1(\omega_m)\{U_1(\omega_m)\}\{U_1(\omega_m)\}^{H} \tag{5.23}$$

where, $\Sigma_1(\omega_m)$ and $\{U_1(\omega_m)\}$ are the first singular value and first singular vector at the frequency ω_m. While the first singular value reaches maximum within the narrow modal frequency range for the m^{th} mode, the corresponding singular vector $\{U_1(\omega_m)\}$ becomes an estimate of the m^{th} mode shape. It may be mentioned that the rank of the output PSD is expected to be nearly equal for multiple repeated modes for repeated modal frequencies. Thus the singular values acts as the complex mode indication function (CMIF) (Shih et al. 1988). After the estimation of mode shape, FSDD use enhanced PSD to evaluate natural frequency and damping ratio. Enhanced PSD in the vicinity of the m^{th} mode is evaluated as

$$\underset{\omega\to\omega_m}{e\hat{G}_{yy}}(i\omega) = \{U_1(\omega_m)\}^H \left[\hat{G}_{yy}(i\omega)\right]\{U_1(\omega_m)\} \tag{5.24}$$

The enhanced PSD is a scalar function of frequency and can be approximated as an SDOF system in the narrow frequency range around a modal frequency. An SDOF curve fitter can be utilized in the vicinity of a modal frequency for identification of natural frequency and damping ratio of that mode. It may be mentioned that in the case when all the measurements are not considered as reference, similar approach is applicable with FSDD.

5.4. IDENTIFICATION OF MODAL PARAMETERS

Identification of modal parameters has been carried out using 55 different data-sets. Each data-set comprises of ambient vibration time history of duration 250 seconds. Ambient data, originally recorded with a sampling rate of 100 Hz, processed at 50 Hz using a Butterworth filter of 5^{th} order for anti-aliasing. It may be mentioned that entire duration of data, either in terms of full Markov sequence or full output data series, is applied by each of the employed techniques while using different data-sets. Therefore analysis is carried out without allowing any loss of information. Details of the modal parameter identification are presented in the following sub-sections.

5.4.1. Identification using NExT-ERA

Ambient data captured with both of the reference channels are used while employing NExT-ERA for modal identification. Such multiple-reference based NExT-ERA is also termed as MNExT-ERA (He et al. 2006) and expected to improve the performance of modal parameters identification. Impulse response is estimated in the form of the inverse Fourier transform of the cross power spectral density function. In the computation of cross power spectral density function, Hanning windows with 50% overlap is used in order to reduce the effects of spectral leakage. Finally, a suitable model-order as well as a suitable size of Hankel matrix is required to be found out for good performance of ERA. In this regard, Hankel matrices are formed with various ratios of row-numbers and column-numbers. Ratios are considered in a reasonably wide range from 0.1 to 10 and chosen as nearly {0.1, 0.3, 0.5, 1, 5, 10}. Ratios are chosen with higher density in lower part of the range 0.1–10, since better performances are observed in lower part of the range. It may be mentioned that an arbitrarily selected single data-set amongst the recorded data-sets (total 55 numbers) is considered for this analysis towards selection of suitable size of Hankel matrix. Other data-sets are assumed to perform in similar manners.

At first, an observation is made on the profile of singular values of the Hankel matrix to have an idea/suggestion regarding the system order. Singular values of Hankel matrices are evaluated based on three different ratios of row-numbers and column-numbers as {0.1, 5, 10} covering a wide spectrum. Profiles of first 200 stronger singular values associated to these ratios are shown in the Fig. 5.3. Singular values are normalized to unity for even-handed observation for three different ratios of row-numbers and column-numbers. It is observed from Fig. 5.3 that demand of system order is indeed on lower side in the range of model orders up to 200. A reasonably conservative choice for system order is made as 100 for the subsequent analysis using NExT-ERA.

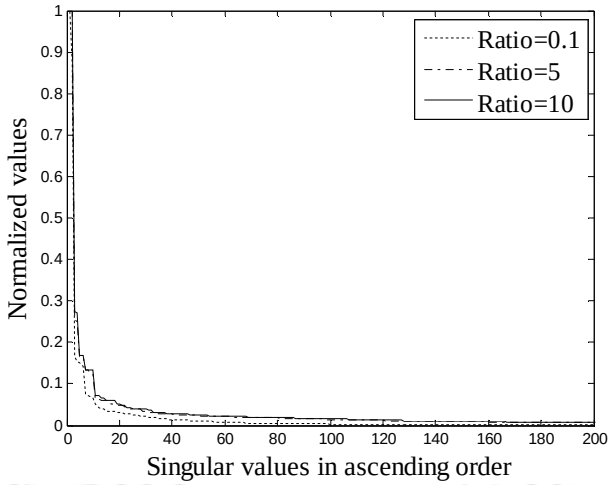

Fig. 5.3. Singular values (normalized to unity) of Hankel matrices associated to different ratios of the number of rows and the number of columns

Six different sizes of Hankel matrix based on those six ratios of row-numbers and column-numbers are considered to find out the suitable size of Hankel matrix for good performance of ERA. Performance of ERA is examined here with the help of stabilization diagram. A stabilization diagram displays the poles of a system at different model orders and differentiates physical poles from numerical poles. Physical poles occur at the same frequency at increasing model orders forming a vertical column of poles and hence show the trend of stabilization. Stabilization diagrams are commonly used to observe the presence of any mode. Superior stabilization provides higher confidence in ascertaining presence of any mode. Therefore, the stabilization diagram can be utilized for examining the suitable size of the Hankel matrix to have good performance in identification of modal parameters while employing ERA. The frequency is plotted along the abscissa while the model order is plotted along the ordinate in a stabilization diagram. Model order is considered in a reasonable range from 100 to 140. This range can be considered fairly sufficient since the lower-bound is selected in terms of a higher model order. A commonly used stabilization criteria are also considered here as: 1% for frequency, 5% for damping, and 2.5% for mode shape. Additional

measures such as damping margin and modal phase collinearity (MPC) (Juang and Pappa 1985) are considered to avoid further the presence of numerical poles obtaining clearer stabilization. Both these measures can be considered appropriate based on the assumption of lower damping existing in the Saraighat Bridge. Damping margin is taken as 15% to avoid a pole having damping ratio more than 15%. On the other hand a pole having MPC less than 0.75, a value chosen based on the commonly considerations of MPC, are avoided. In this exercise, full Markov parameter sequences are used for all the cases associated to different sizes of Hankel matrices. The stabilization diagrams are shown in the Figs. 5.4(a–f). Meaning of the symbols used are: 'f' as pole with stable frequency, 'd' as pole with stable frequency as well as damping, 'v' as pole with stable frequency as well as mode shape, 's' as pole with stable frequency as well as mode shape and damping and '+' as new pole. Symbols are plotted aligning at left horizontally and at centre vertically. The background curve is considered as the first singular values of PSD matrices. The ratio of row-number and column-number as 0.5 is finally selected based on the observations on all the stabilization diagrams as shown in Figs. 5.4(a–f).

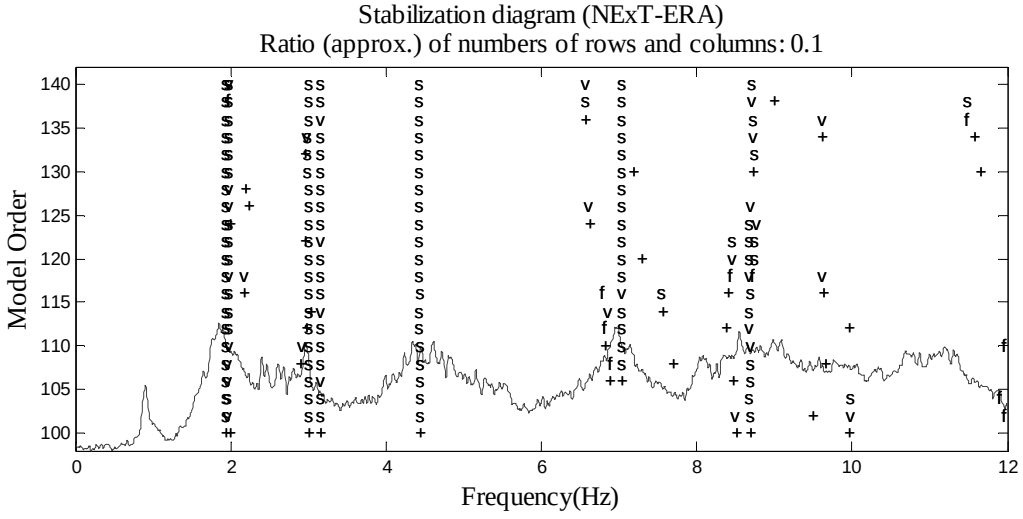

(a)

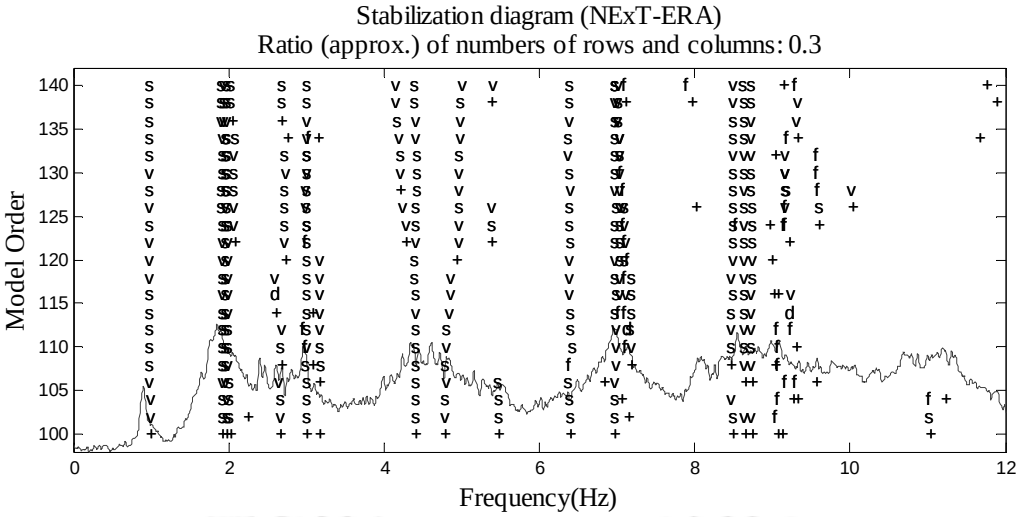

(b)

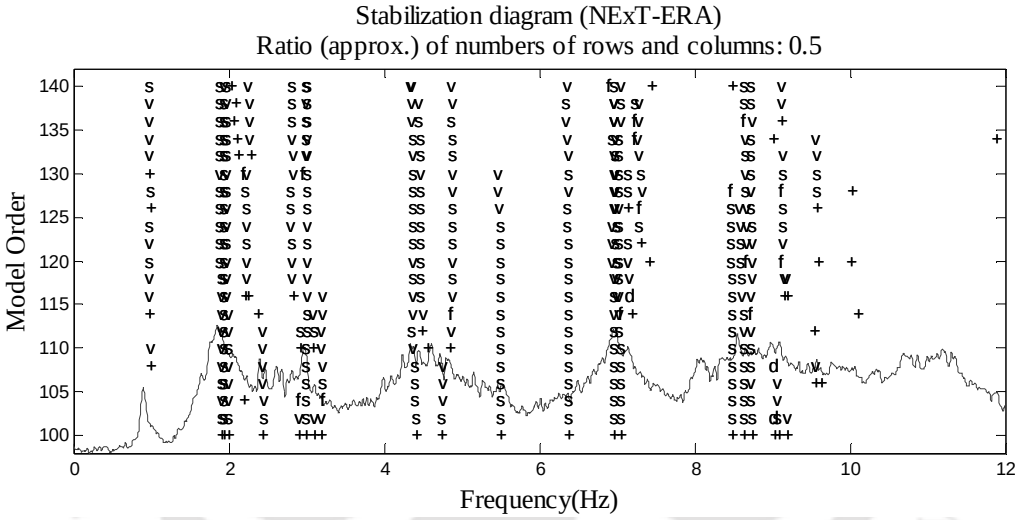

(c)

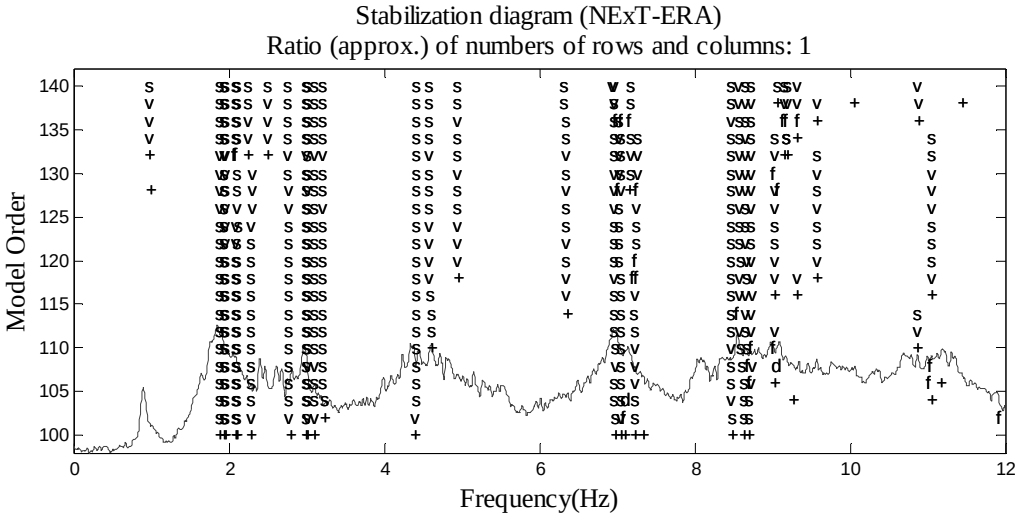

(d)

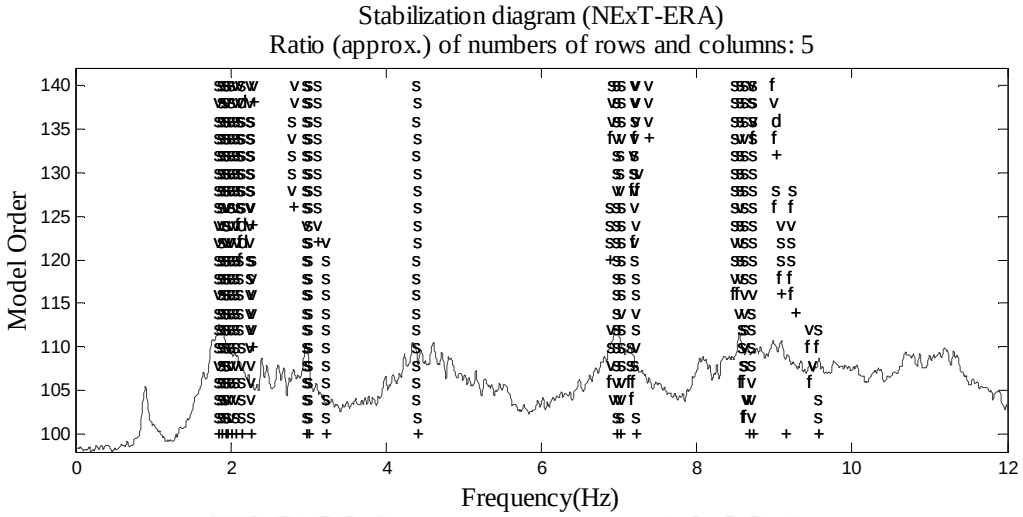

(e)

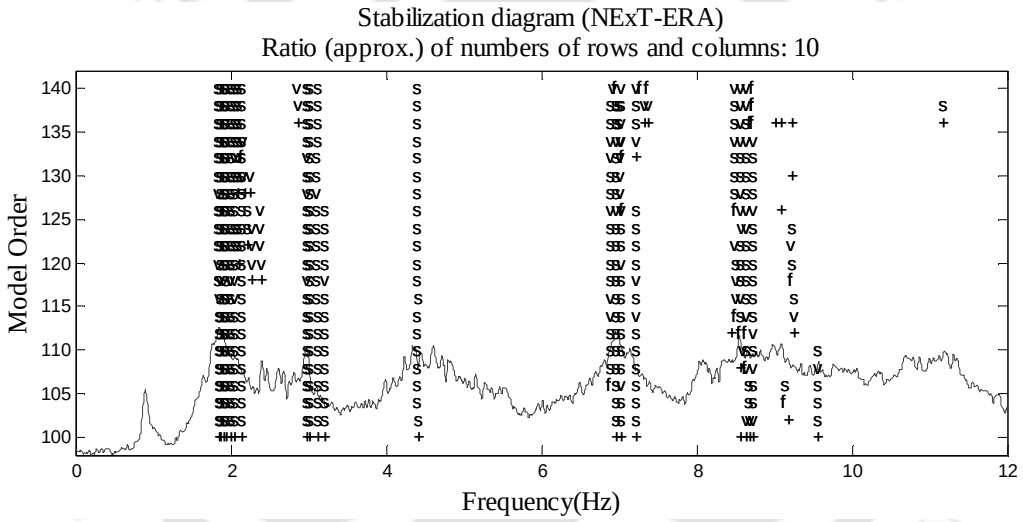

(f)

Fig. 5.4. Stabilization diagram based on NExT-ERA for six different ratios of row-numbers and column-numbers of Hankel matrix

5.4.2. Identification using SSI

In the identification of modal parameters using SSI, size of the output block Hankel matrix is commonly considered to be an important parameter affecting the performance in modal identification. Number of block-rows (i) is generally varied to construct Hankel matrices with different sizes. Six possible cases of numbers of block-rows are considered here as {10, 25,

50, 75, 100, 125} covering from lower number to a reasonably large number of block-rows. In all the cases, all data points are considered to construct the Hankel matrices. Denoting the number of total data points and number of columns as n_y and $j_{\max}$ respectively, j_{max} can be expressed as $j_{\max} = n_y - 2i + 1$ while considering all the data points. Consideration of all the data points with column-number as j_{max} is commonly observed to perform well compared to any other cases with column-number as $j < j_{max}$. It may be mentioned that an arbitrarily selected single data-set out of all the recorded data-sets (total 55 numbers) is considered in place of all the data-sets for this analysis for selection of suitable size of Hankel matrix.

First, an observation is made on the profile of singular values of the weighted projection matrix as in Eq. (5.16) to have an idea regarding the system order. The UPC algorithm is considered in this regard. Profiles of first 200 stronger singular values associated to the numbers of block rows are shown in the Fig. 5.5. Singular values are normalized to unity for even-handed observation among different numbers of block rows. Comparatively higher demand of system order than ERA is observed from the Fig. 5.5. A choice for system order is made as 100 for the subsequent analysis using SSI. Hence, a reasonable number of modes are expected to be identified as 50.

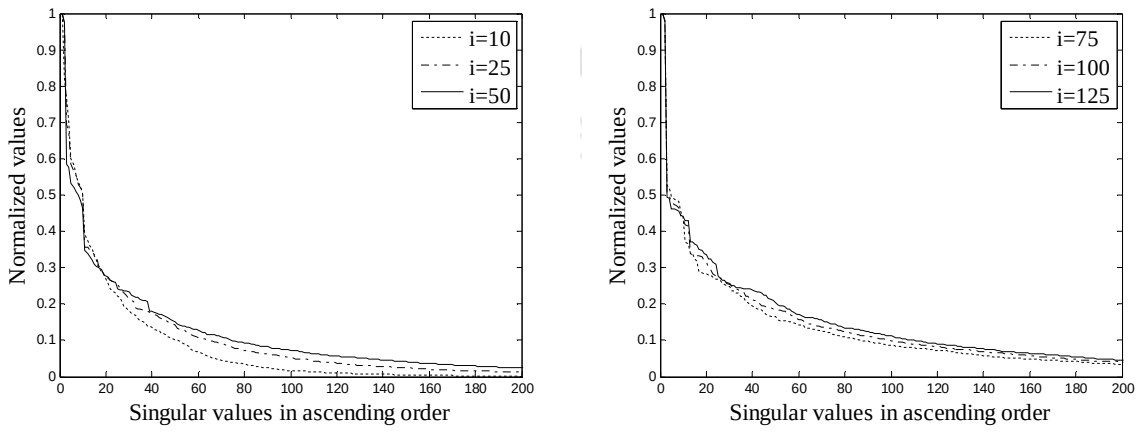

Fig. 5.5. Singular values (normalized to unity) of output block Hankel matrices associated to different number of block rows

The stabilization diagram is employed here to understand the performance of SSI associated to six different numbers of block rows as mentioned in preceding section. Three stabilization diagrams are constructed for each number of block rows using three different algorithms (UPC, PC and CVA). Total 18 numbers of stabilization diagrams are constructed and these are shown in Figs. 5.6(a–r). In the stabilization diagram, model orders are considered from 100 to 140 with lower-bound being fairly high. Meanings of the symbols used in these diagrams are similar to those used in stabilization diagram for NExT-ERA. Damping margin of 15% and MPC margin of 0.75 are also considered here as in the case of NExT-ERA. It is observed from Figs. 5.6(a–r) that good performance is demonstrated while number of block rows is considered as 50 associated with CVA as well as PC algorithms and 75 associated with CVA algorithm. Finally the number of block rows as 50 associated to PC algorithm is chosen for efficient performance in modal identification.

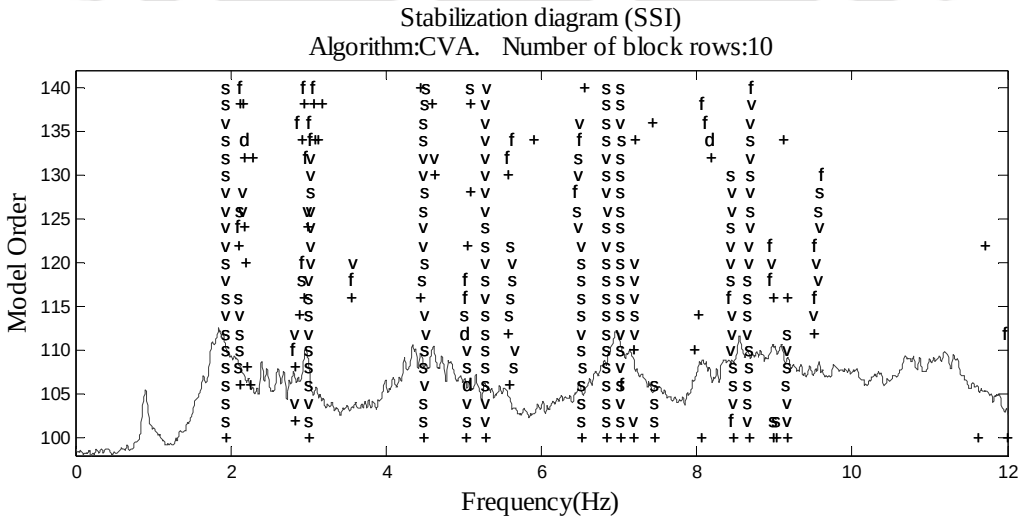

(a)

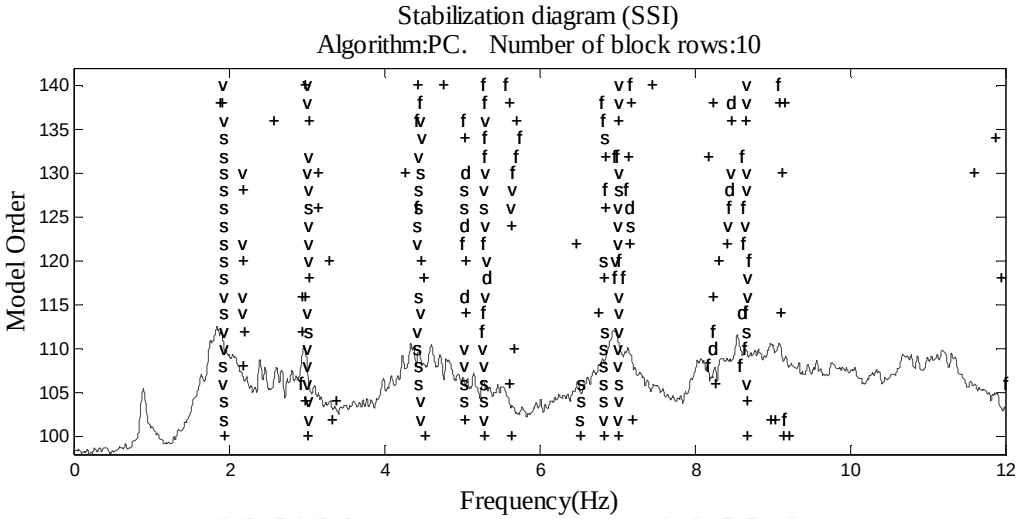

(b)

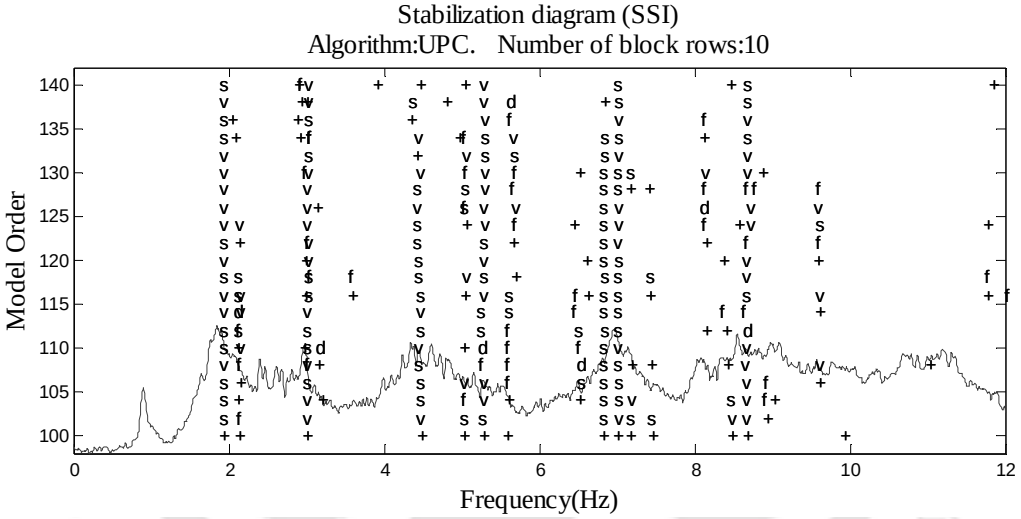

(c)

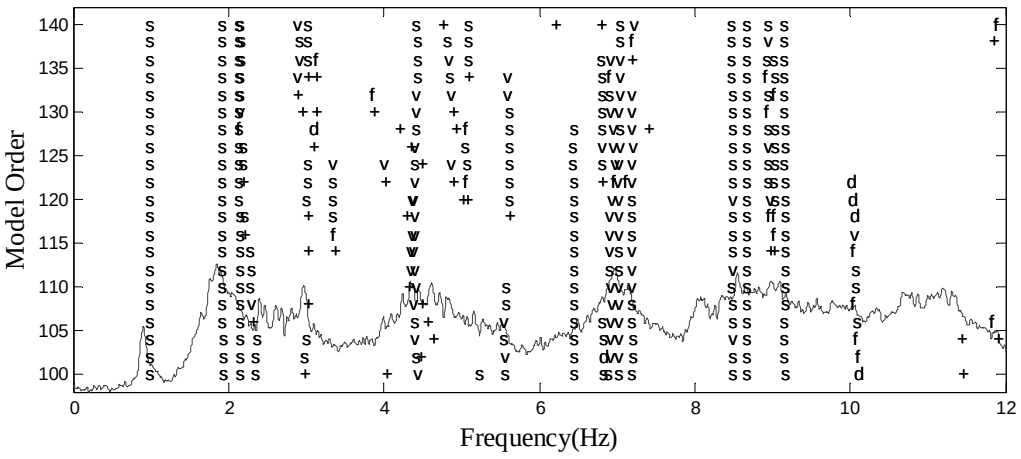

(d)

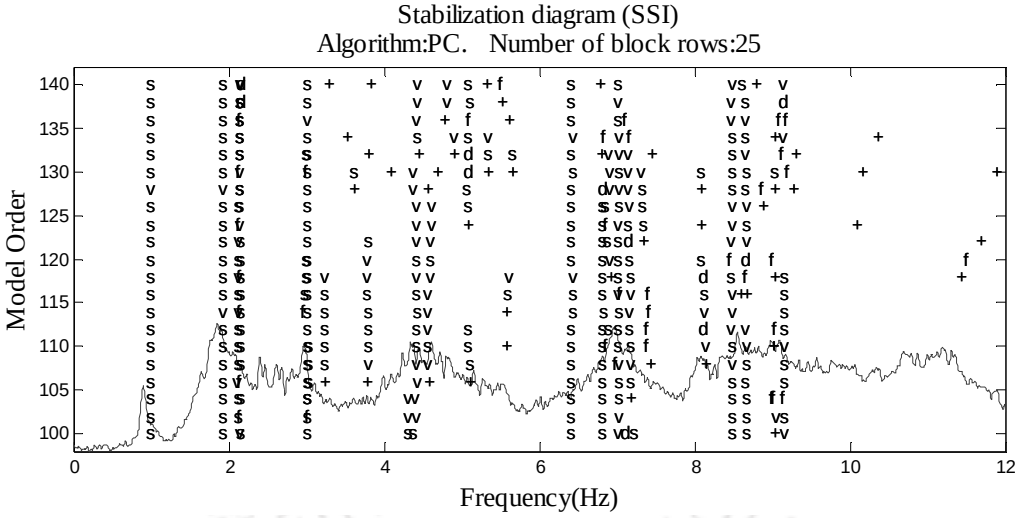

(e)

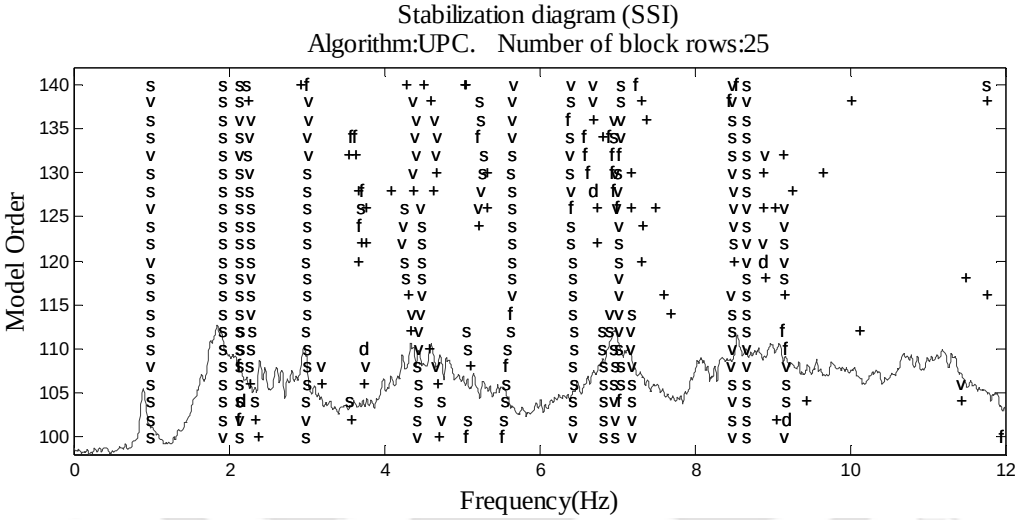

(f)

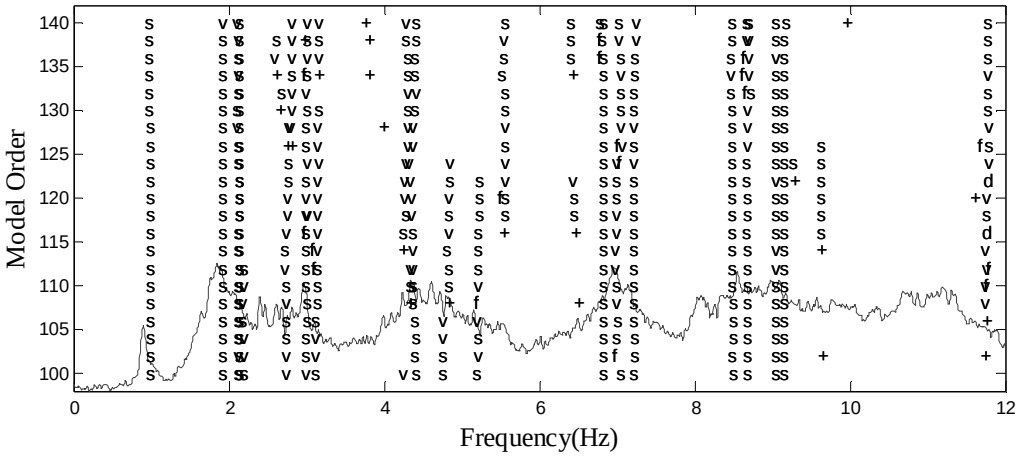

(g)

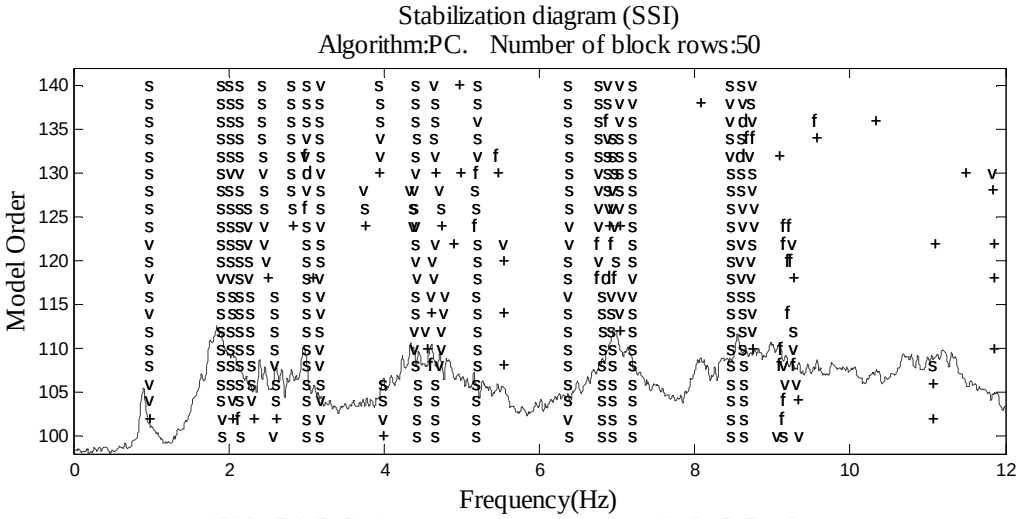

(h)

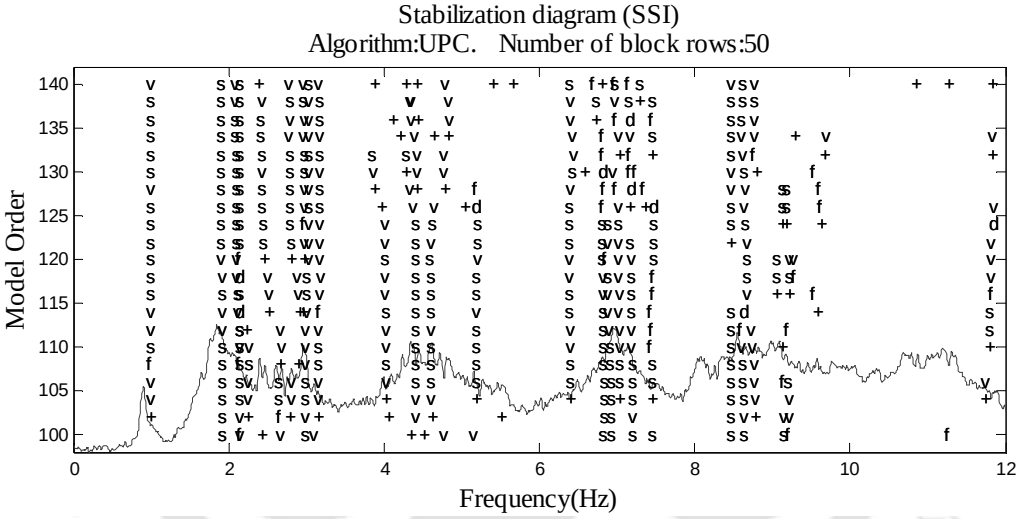

(i)

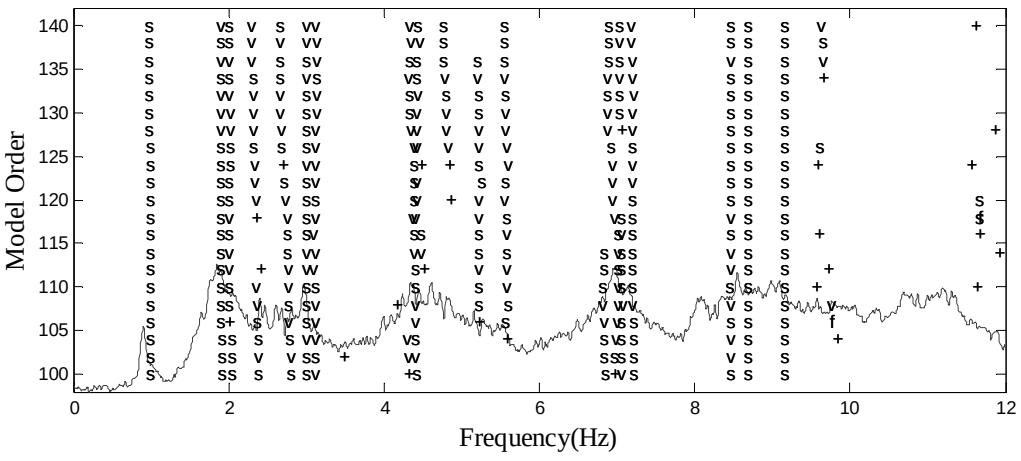

(j)

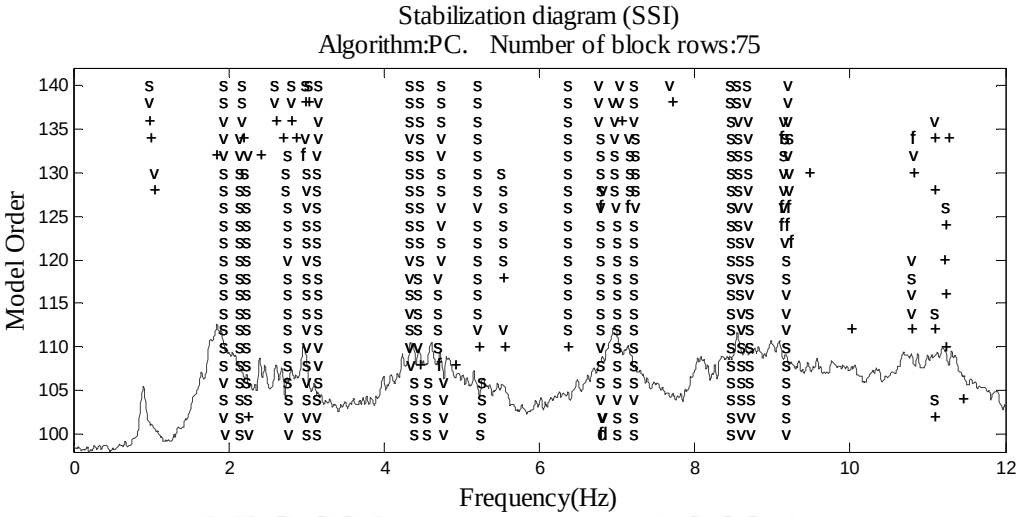

(k)

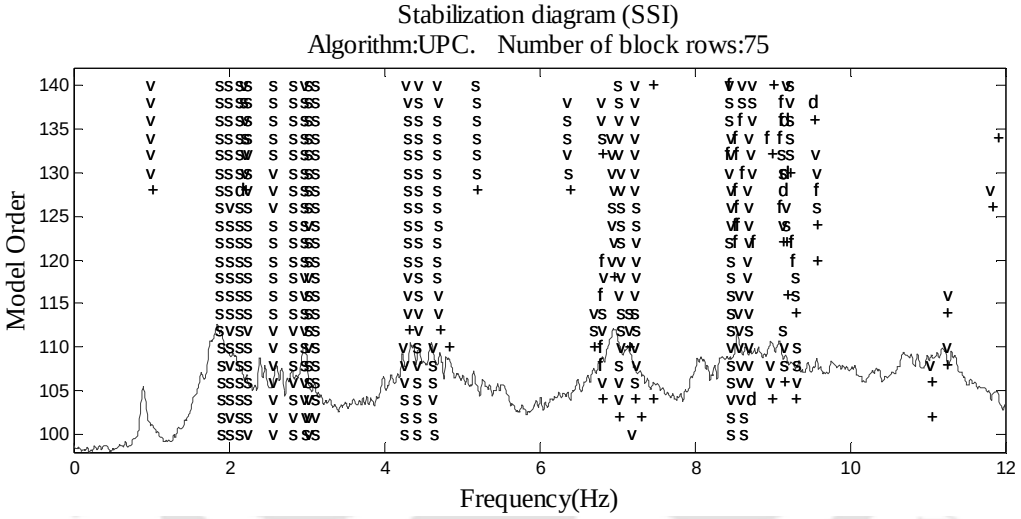

(l)

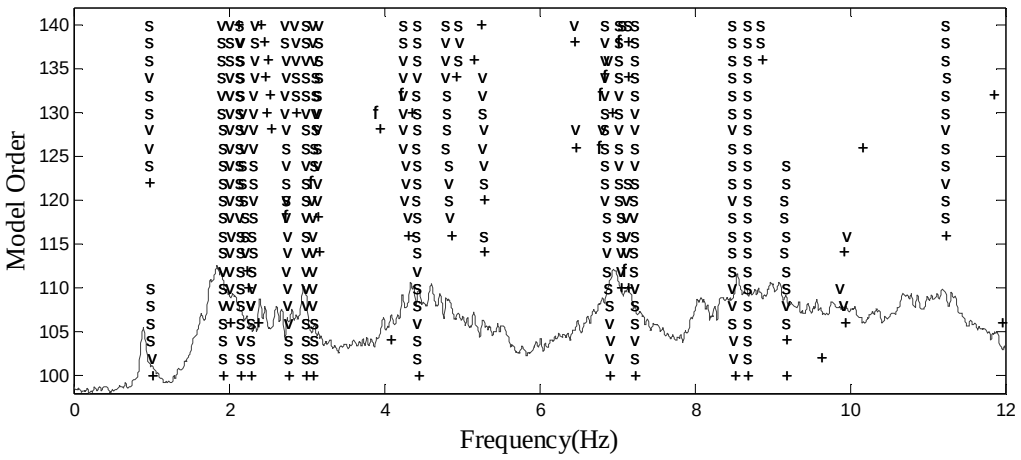

(m)

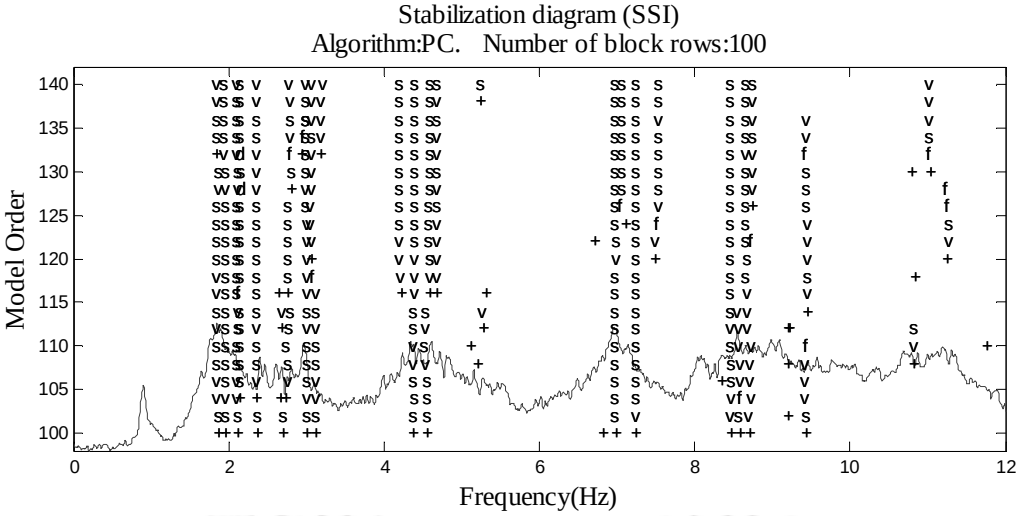

(n)

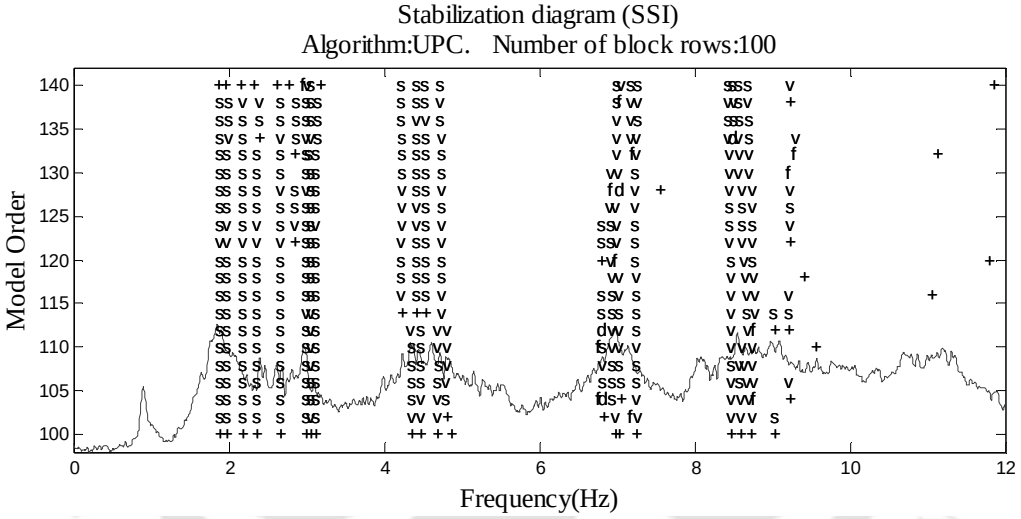

(o)

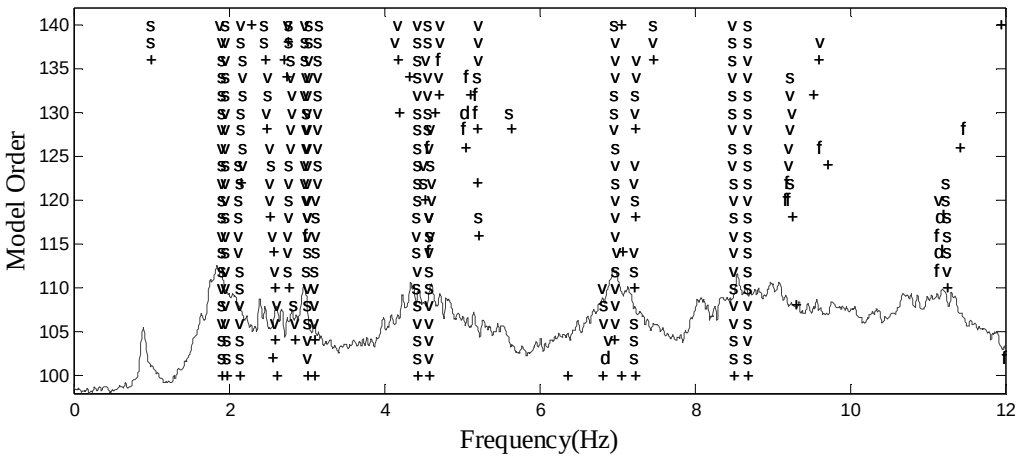

(p)

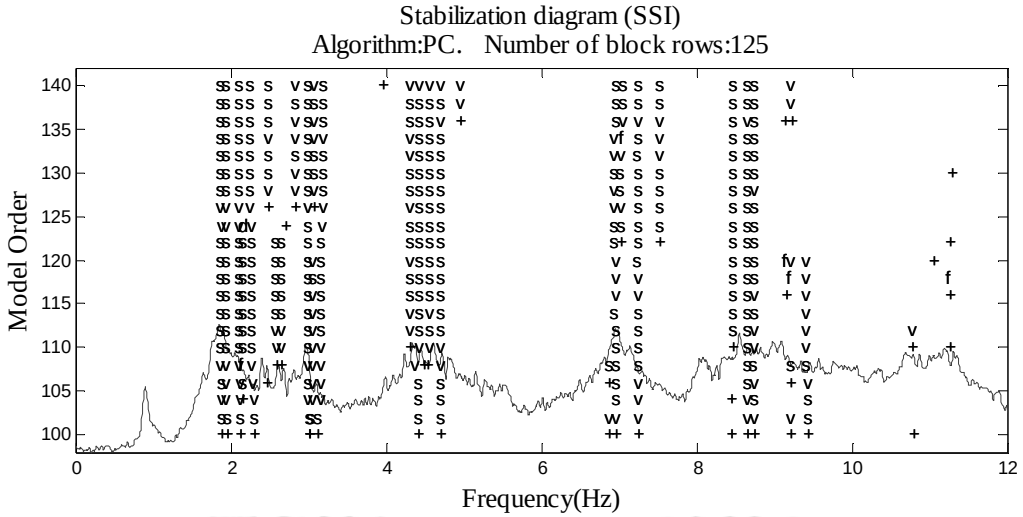

(q)

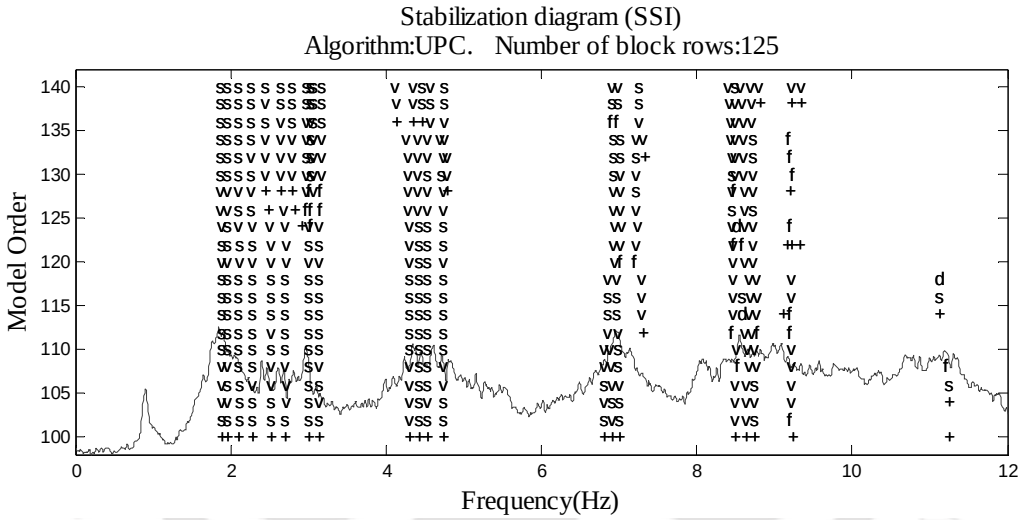

(r)

Fig. 5.6. Stabilization diagram based on SSI using three different algorithms for six different numbers of block rows of Hankel matrix

5.4.3. Identification using FSDD

Singular values obtained from the PSD matrices at discrete frequencies are plotted with respect to frequencies and observed for peaks which indicate presence of possible modes. The first, second and third singular values for the data-sets are plotted in the Fig. 5.7. Singular values based on different data-sets are scaled in similar lower and higher bounds to have

even-handed observation. In the computation of auto or cross power spectral density functions to find out the PSD matrix, Hanning windows with 50% overlap is used in order to reduce the effects of spectral leakage. Possibility of a mode around a frequency is confirmed using the singular vectors, since singular vectors show higher modal assurance criteria (MAC) around a modal frequency. Finally enhanced PSD around a modal frequency are used to evaluate the natural frequency and damping ratio for that mode. A peak in the singular plot usually indicates the presence of a mode, though it may not be very evident always. In the present work, identified frequencies using NExT-ERA as well as SSI are also considered along with the frequencies corresponding to the peaks as shown in Fig. 5.7 as possible modal

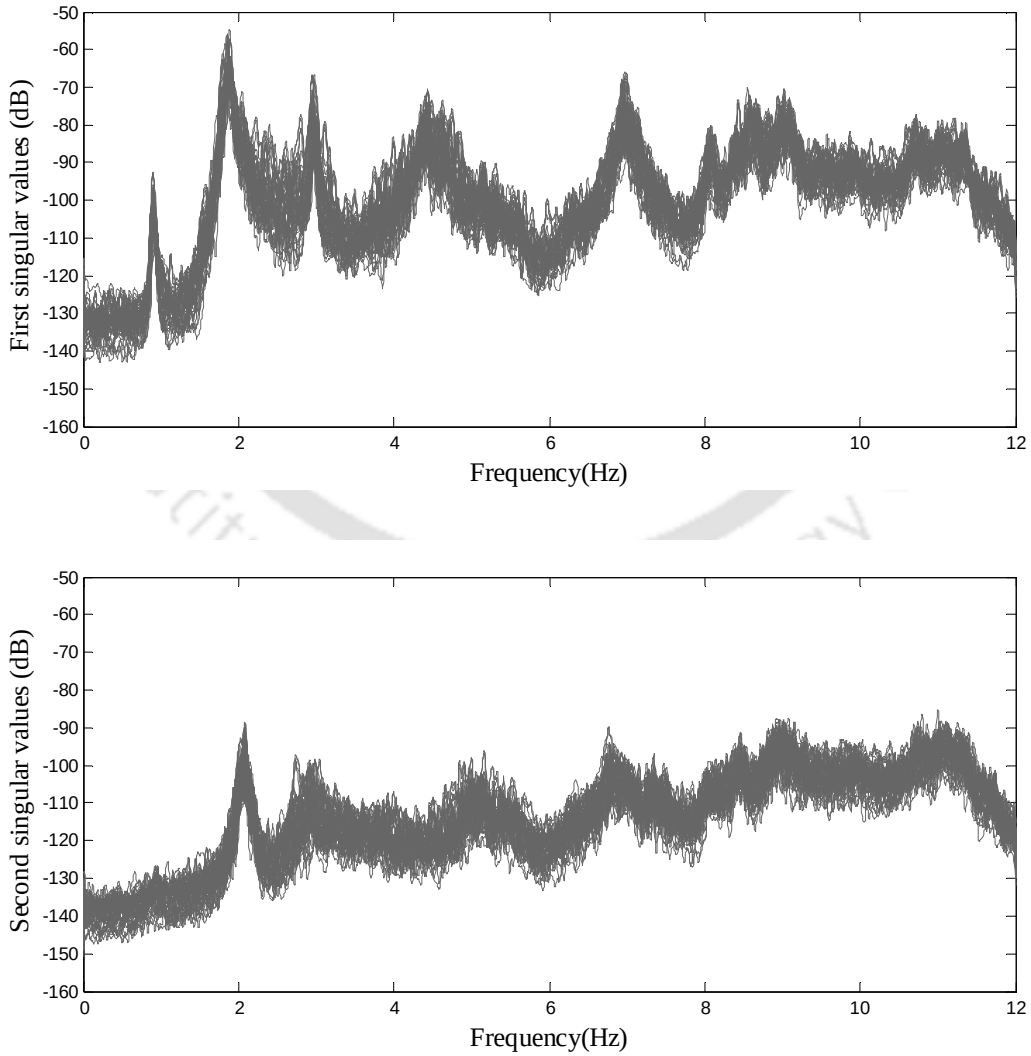

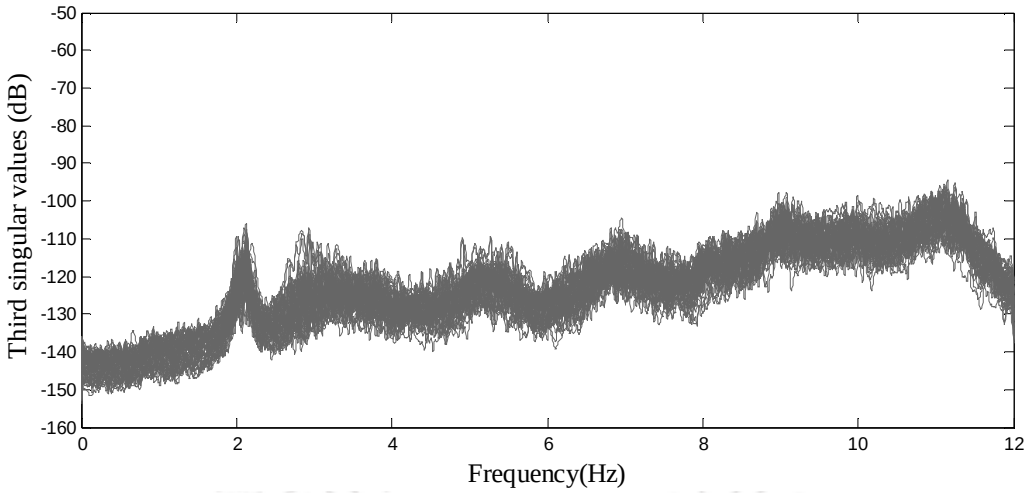

Fig. 5.7. First, second and third singular values computed from all the data-sets

frequencies. Subsequently, MAC is examined for identifying the final modal frequencies and in the next step modal parameters are evaluated associated to those modal frequencies.

5.5. IDENTIFIED MODAL PARAMETERS: CENTRAL TENDENCY AND DISPERSION

Modal identification is carried out based on the total 55 different data-sets. The natural frequencies and damping ratios identified from all the data-sets are represented in terms of mean frequencies and mean damping ratios along with their standard deviations and 95% confidence limits. The mode shapes are represented as the mean of those shapes identified from different data-sets.

5.5.1. Natural frequency

Central tendency, dispersion and confidence bounds for the identified natural frequencies using NExT-ERA, SSI and FSDD are presented in Table 5.1. It can be observed from Table 5.1 that mean-values for a modal frequency identified using three different techniques are fairly close to each other. Moreover, all three techniques identify modal frequencies with

lesser standard deviations along with narrow margin of 95% confidence bounds. Therefore, natural frequencies for different modes have been identified with good level of confidence.

Table 5.1. Mean, standard deviation and 95% confidence bounds of the identified natural frequencies

Mode No. (Mode type)	Identification Technique	Mean	Standard deviation	95% Confidence bounds	
				Lower	Upper
1 (H1)	NExT-ERA	0.9101	0.0189	0.9057	0.9145
	SSI	0.9119	0.0094	0.9098	0.9140
	FSDD	0.9061	0.0146	0.9021	0.9100
2 (V1)	NExT-ERA	1.8795	0.0549	1.8731	1.8859
	SSI	1.8624	0.0529	1.8547	1.8701
	FSDD	1.8609	0.0341	1.8517	1.8701
3 (H2)	NExT-ERA	2.1090	0.0005	2.1082	2.1099
	SSI	2.1550	0.0492	2.1320	2.1780
	FSDD	2.1586	0.0757	2.1381	2.1791
4 (T1)	NExT-ERA	2.9593	0.0204	2.9552	2.9633
	SSI	2.9626	0.0157	2.9595	2.9656
	FSDD	2.9628	0.0201	2.9574	2.9682
5 (V2)	NExT-ERA	4.4150	0.0535	4.4061	4.4239
	SSI	4.3976	0.0601	4.3878	4.4073
	FSDD	4.4068	0.0489	4.3936	4.4200
6 (T2)	NExT-ERA	5.1164	0.0013	5.1142	5.1185
	SSI	5.1501	0.0288	5.1415	5.1586
	FSDD	5.1643	0.0347	5.1549	5.1737
7 (H3)	NExT-ERA	6.3400	0.0436	6.3231	6.3569
	SSI	6.3783	0.0720	6.3268	6.4298
	FSDD	6.3362	0.0490	6.3229	6.3494
8 (V3)	NExT-ERA	6.9335	0.0510	6.9261	6.9409
	SSI	6.9285	0.0482	6.9201	6.9369
	FSDD	6.9729	0.0270	6.9656	6.9802

5.5.2. Damping ratio

Central tendency, dispersion and confidence bounds for the identified damping ratios using NExT-ERA, SSI and FSDD are presented in Table 5.2. It can be observed from Table 5.2 that

Table 5.2. Mean, standard deviation and confidence bounds of the identified damping ratios

Mode No. (Mode type)	Identification Technique	Mean	Standard deviation	95% Confidence bounds	
				Lower	Upper
1 (H1)	NExT-ERA	0.0356	0.0164	0.0316	0.0396
	SSI	0.0307	0.0107	0.0282	0.0331
	FSDD	0.0243	0.0084	0.0220	0.0266
2 (V1)	NExT-ERA	0.0156	0.0074	0.0148	0.0165
	SSI	0.0241	0.0161	0.0217	0.0264
	FSDD	0.0130	0.0046	0.0116	0.0144
3 (H2)	NExT-ERA	0.0178	0.0047	0.0104	0.0253
	SSI	0.0306	0.0124	0.0240	0.0372
	FSDD	0.0111	0.0043	0.0097	0.0125
4 (T1)	NExT-ERA	0.0084	0.0038	0.0076	0.0091
	SSI	0.0069	0.0024	0.0064	0.0073
	FSDD	0.0068	0.0017	0.0063	0.0073
5 (V2)	NExT-ERA	0.0173	0.0069	0.0162	0.0184
	SSI	0.0220	0.0160	0.0194	0.0246
	FSDD	0.0058	0.0019	0.0052	0.0063
6 (T2)	NExT-ERA	0.0064	0.0003	0.0059	0.0070
	SSI	0.0137	0.0040	0.0125	0.0149
	FSDD	0.0041	0.0014	0.0036	0.0045
7 (H3)	NExT-ERA	0.0144	0.0062	0.0120	0.0168
	SSI	0.0341	0.0112	0.0262	0.0421
	FSDD	0.0040	0.0010	0.0037	0.0044
8 (V3)	NExT-ERA	0.0081	0.0059	0.0072	0.0090
	SSI	0.0094	0.0060	0.0083	0.0104
	FSDD	0.0038	0.0016	0.0033	0.0044

damping ratios identified using these three techniques show lesser agreement to each other in comparison with the case of natural frequency. It may be noticed that FSDD has estimated the damping ratios as comparative lower than those estimated with NExT-ERA or SSI. However, trend of damping ratios from lower to higher modes, identified using each of the techniques, shares similarity to some extent. On the other hand, the identified damping ratios have shown higher dispersion as compared to the case of natural frequency.

5.5.3. Mode shape

Mode shapes identified from different data-sets for a particular mode are averaged to find out the central tendency of mode shape i.e. mean mode shape for that mode. Mean mode shapes are evaluated using all three employed techniques and are shown in the Figs. 5.8–5.15. It may be mentioned that during the identification of a mode from different data-sets, close similarity in the mode shape is always maintained since a particular mode identified from various data-sets should have similar signatures in terms of mode shape. Hence dispersion analysis for the mode-shape may be disregarded unlike natural frequency and damping ratio. It can be clearly obsrerved from the Figs. 5.8–5.15 that mean mode shapes as identified using three techniques for different modes are in good aggrement. Further, similiarities between mean mode shapes are quantified using MAC and presented in the Table 5.3.

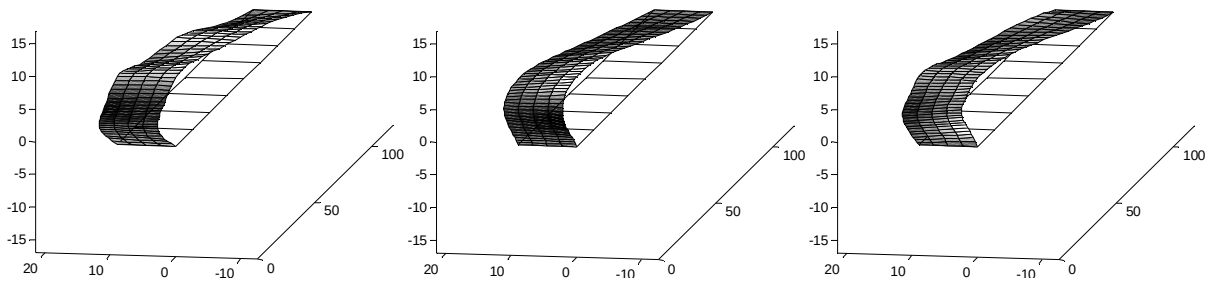

(a) (b) (c)

Fig. 5.8. 1st mode (H1) identified employing (a) NExT-ERA (b) SSI and (c) FSDD

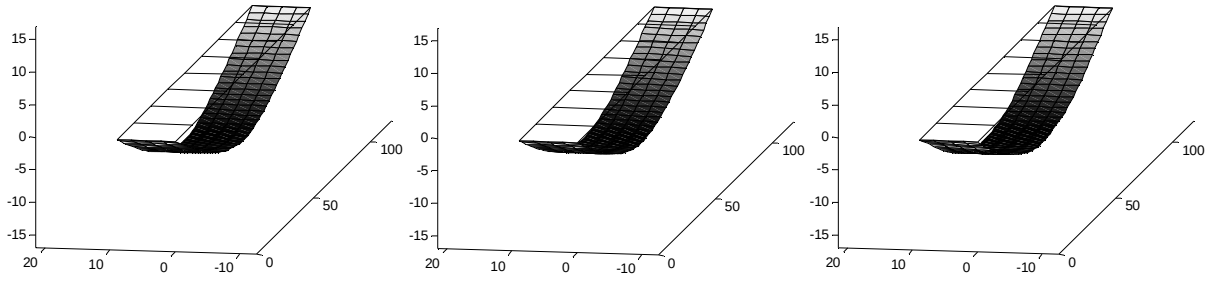

(a) (b) (c)

Fig. 5.9. 2nd mode (V1) identified employing (a) NExT-ERA (b) SSI and (c) FSDD

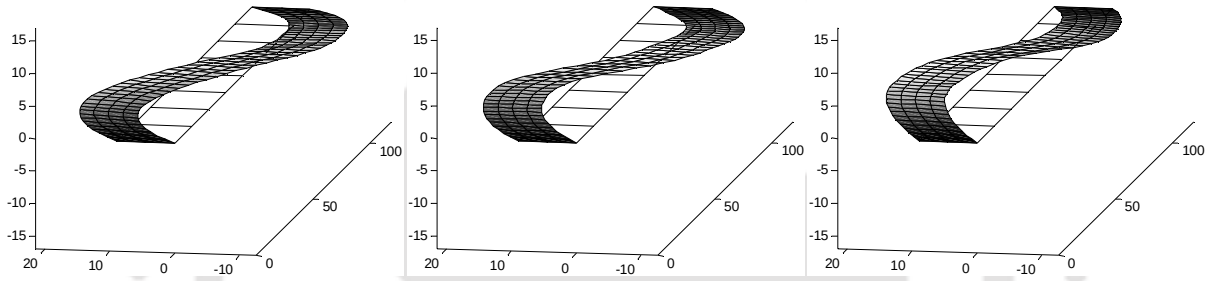

(a) (b) (c)

Fig. 5.10. 3rd mode (H2) identified employing (a) NExT-ERA (b) SSI and (c) FSDD

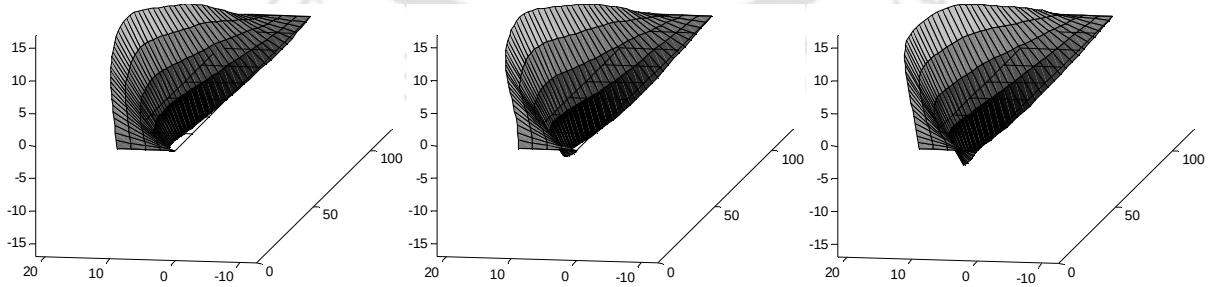

(a) (b) (c)

Fig. 5.11. 4th mode (T1) identified employing (a) NExT-ERA (b) SSI and (c) FSDD

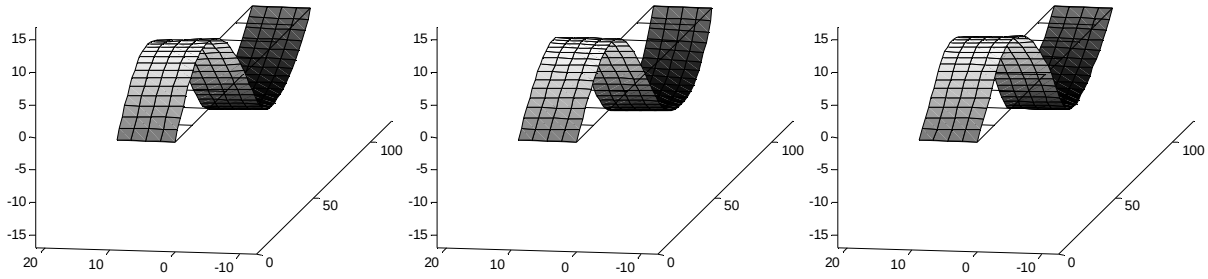

(a) (b) (c)

Fig. 5.12. 5th mode (V2) identified employing (a) NExT-ERA (b) SSI and (c) FSDD

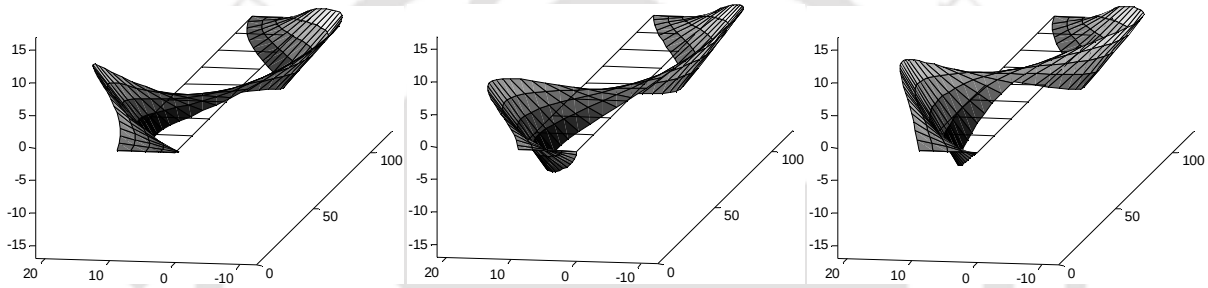

(a) (b) (c)

Fig. 5.13. 6th mode (T2) identified employing (a) NExT-ERA (b) SSI and (c) FSDD

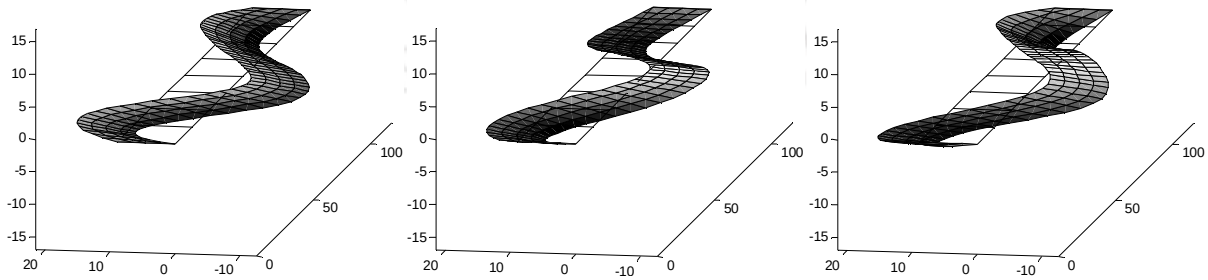

(a) (b) (c)

Fig. 5.14. 7th mode (H3) identified employing (a) NExT-ERA (b) SSI and (c) FSDD

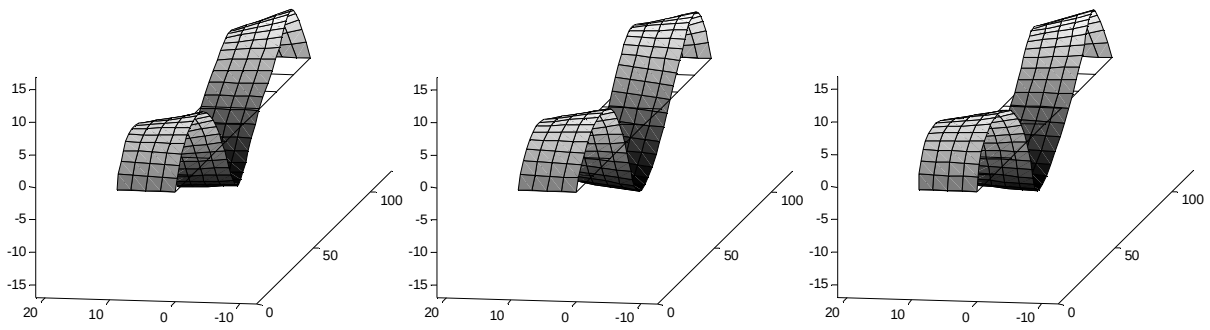

(a) (b) (c)

Fig. 5.15. 8th mode (V3) identified employing (a) NExT-ERA (b) SSI and (c) FSDD

Table 5.3. MAC values between identified mean mode shapes using three techniques

Mode No.	MAC (NExT-ERA and SSI)	MAC (NExT-ERA and FSDD)	MAC (SSI and FSDD)
1	0.9833	0.9826	0.9915
2	0.9986	0.9992	0.9994
3	0.9726	0.6623	0.7341
4	0.9912	0.9779	0.9944
5	0.9964	0.9952	0.9925
6	0.9308	0.9238	0.9088
7	0.8880	0.9380	0.9103
8	0.9871	0.9930	0.9934

5.6. CONCLUDING REMARKS

Although the present work involves a case study on OMA like many other published case studies, there are some noteworthy uniqueness of this work like: (a) Credibility of modal identification considering various unfavourable issues involved in OMA has been enhanced by combining two approaches like application of multiple identification techniques and statistical analysis of modal parameters based on multiple data-sets (b) Stabilization diagram

is employed for estimation of suitable size of Hankel matrix leading to better modal identification (c) No existing study is found in literature, where OMA on a bridge structure like the Saraighat Bridge was performed. Three prominent techniques, based on both the time and frequency domain, have been employed for identification of the modal parameters of the Saraighat Bridge using a statistical approach. Ambient vibration data in the form of acceleration response is used for the modal identification. Following conclusions are made based on the observations of the identified modal parameters of the Saraighat Bridge.

(a) Identification of modal parameters in the form of central tendency ensures higher confidences against the effect of measurement noise as well as deviations of real ambient vibration from theoretical assumption of white-noise induced vibration.

(b) Major horizontal, vertical and torsional modes have been identified for the Saraighat Bridge.

(c) Central tendencies of mode shapes identified using three techniques are found to be in good agreement.

(d) On the other hand, central tendencies of natural frequencies identified using three techniques are found to be in good agreement as well. Moreover the 95% confidence bounds for the natural frequencies are observed to be in narrow range.

(e) Higher variations, however, are observed for the central tendencies of damping ratios identified using three techniques. Damping ratios identified using FSDD are found to be lower in comparisons to those identified using NExT-ERA and SSI.

(f) Natural frequencies and mode shapes (considered modal parameters in model updating) are identified generally with good agreement based on three employed techniques. Thus, these parameters identified by any of these three techniques may be considered for the FE model updating exercise. However, SSI based parameters are considered for the updating in view of key features of SSI like: sophisticated mathematical formulation, less likely influence from spectral leakage.

Chapter 6

DIRECT UPDTING OF THE FE MODEL

6.1. INTRODUCTION

The topic of finite element (FE) model updating is considered presently as one of the most important applications associated to modal analysis. FE model updating deals with refining of an initial analytical model using the experimentally measured data from the corresponding actual structure. Model Updating generally requires considerable care in order to obtain reliable results. Both direct and iterative techniques are observed to be used for updating of FE models. However, direct updating techniques are usually known for their better performance in terms of updating the system matrices such that the updated modal parameters can closely match the experimentally identified modal parameters. However, direct updating techniques generally do not preserve structural connectivity and hence the corrections suggested may not be very physically meaningful. This disadvantage can be overcome by applying the iterative updating techniques. In view of this, iterative techniques are commonly attempted for damage detection in structural systems. Therefore, the direct updating techniques may be employed where the purposes of FE model updating is primarily for the design of efficient control systems instead of damage detection. Direct techniques may provide ease in handling multiple modes as well as higher efficiency, especially for complicated structures as compared to iterative techniques (Yang and Chen 2009). In the present study, the sole purpose of updating is to design a realistic passive control system based on a modal approach. Considering good reliability of the experimentally identified modal parameters, direct updating technique is adopted for the updating of FE model of the bridge. Two important techniques, with the ability of exact reproduction of experimental natural frequencies and mode shapes in the updated model, are employed in this exercise.

6.2. UPDATING TECHNIQUES

Two significant direct updating techniques are employed in this updating exercise as: (a) Berman and Nagy updating technique (Berman and Nagy 1983) and (b) matrix mixing updating (Friswell and Mottershead 1995). In this study, it has been taken care that the system matrices especially the mass matrix are updated with minimum changes. It may be mentioned that there are other techniques which only update the stiffness matrix without any changes in the original analytical mass matrix, namely, Baruch and Bar-Itzhack updating technique (Baruch and Bar-Itzhack 1978; Baruch 1978), a recently proposed technique – incomplete data handling method (IDHM) (Carvalh et al. 2007) etc. But those techniques have difficulties in reproduction of the mode shapes exactly and hence are considered in this updating study. Outlines of the two techniques considered in this study are briefly mentioned in the following sub-sections.

6.2.1. Berman and Nagy updating technique

Berman and Nagy (1983) technique uses the identified modal parameters in terms of natural frequencies and mode shapes for updating. Firstly, the mass matrix is updated ensuring the orthogonality of the measured modes. The updating of the mass matrix is considered by finding the updated mass matrix [M_U] that minimizes a cost function (as in Eq. (6.1)) in terms of the following norm when the experimentally identified mode shape matrix $[\Phi_E]$ and the analytical mass matrix [M_A] are given.

$$J_1 = \left\| [M_A]^{-1/2} \left([M_U] - [M_A] \right) [M_A]^{-1/2} \right\| \tag{6.1}$$

This minimization is subjected to the orthogonality constraint expressed as

$$[\Phi_E]^T [M_U] [\Phi_E] = [I] \tag{6.2}$$

The difference between the updated and the analytical mass matrices are minimized. The expression of the updated mass matrix is provided as

$$[M_U]=[M_A]+[M_A][\Phi_E]\left[\bar{M}_A\right]^{-1}\left([I]-\left[\bar{M}_A\right]\right)\left[\bar{M}_A\right]^{-1}[\Phi_E]^T[M_A] \tag{6.3}$$

where, the matrix $\left[\bar{M}_A\right]$ is defined as $\left[\bar{M}_A\right]=[\Phi_E]^T[M_A][\Phi_E]$. Subsequently, the updated stiffness matrix is obtained by minimizing a cost function in terms of the following norm.

$$J_2=\left\|[M_U]^{-1/2}\left([K_U]-[K_A]\right)[M_U]^{-1/2}\right\| \tag{6.4}$$

Two constraints are imposed on the updated stiffness matrix [K_U] such that: (a) [K_U] is able to reproduce the measured modal data and (b) at the same time, [K_U] is symmetric. These constraints are expressed by Eqs. (6.5) and (6.6) respectively.

$$[K_U][\Phi_E]=[M_U][\Phi_E][\Lambda_E] \tag{6.5}$$

$$[K_U]^T=[K_U] \tag{6.6}$$

where, $[\Lambda_E]$ represents the diagonal matrix where the diagonal elements are the measured natural frequencies in eigen-value format. The difference between the updated and the analytical stiffness matrices are minimized as in the case of mass matrix updating. The expression of the updated stiffness matrix is written as

$$\begin{aligned}[K_U]=[K_A]&-[K_A][\Phi_E][\Phi_E]^T[M_U]-[M_U][\Phi_E][\Phi_E]^T[K_A]\\&+[M_U][\Phi_E][\Phi_E]^T[K_A][\Phi_E][\Phi_E]^T[M_U]\\&+[M_U][\Phi_E][\Lambda_E][\Phi_E]^T[M_U]\end{aligned} \tag{6.7}$$

Details regarding these derivation can be found in literatures like Friswell and Mottershead (1995), Berman and Nagy (1983) etc. The measured mode shapes vectors need to be same as the size of analytical system matrices. Usually mode shapes are experimentally identified along much lesser DOF locations than the DOF locations available in the corresponding FE

model. In such cases measured mode shape vectors can be expanded or the analytical system matrices can be reduced to the size of a measured mode shape vector.

6.2.2. Matrix mixing updating technique

Berman and Nagy technique obtains the updated mass matrix with an objective of minimal changes with respect to the initial analytical mass matrix. However, still there exists interest to work with an alternative technique which may also perform well. It is known that mass and stiffness matrices can be exactly reconstructed using all the modal frequencies and all mode shapes, when (a) the mode shapes are mass normalized and (b) all DOFs are retained in the mode shapes. Reconstruction of mass and stiffness matrices are carried out as

$$[M]^{-1} = [\Phi][\Phi]^T = \sum_{i=1}^{n} \{\Phi_i\}\{\Phi_i\}^T \tag{6.8}$$

$$[K]^{-1} = [\Phi][\Lambda]^{-1}[\Phi]^T = \sum_{i=1}^{n} \frac{\{\Phi_i\}\{\Phi_i\}^T}{\omega_i^2} \tag{6.9}$$

where, $\{\Phi_i\}$ is the i^{th} mode shape, $[\Lambda]$ is the matrix of eigen values and ω_i is the i^{th} natural frequency. Usually the measured modal data is incomplete as measurements of responses are carried out generally at limited numbers of coordinates. Moreover the numbers of identified modes are quite fewer than the numbers of analytical DOFs. Such incompleteness in estimation of modal parameters gives raises various problems in estimating of mass and stiffness matrices. Some attempts were carried out to avoid such difficulties by different investigators (Ross 1971; Thoren 1972; Luk 1987). Matrix mixing technique (Caser 1987; Link et al. 1987) is considered as a development over the methods proposed by Ross (1971) and Thoren (1972). Matrix mixing technique demonstrates that if the estimated mode shapes are expanded to the size of analytical system matrices, then computational difficulties can be reduced. Generally, number of measured modes, *p*, is fewer than the number of modes based

on FE model. Matrix mixing technique uses the data from the FE model to compensate the gaps in measured data. Thus, updated mass and stiffness matrices can be computed as

$$\left[M_U\right]^{-1} = \sum_{i=1}^{p} \left\{\Phi_{Ei}\right\}\left\{\Phi_{Ei}\right\}^T + \sum_{i=p+1}^{n} \left\{\Phi_{Ai}\right\}\left\{\Phi_{Ai}\right\}^T \tag{6.10}$$

$$\left[K_U\right]^{-1} = \sum_{i=1}^{p} \frac{\left\{\Phi_{Ei}\right\}\left\{\Phi_{Ei}\right\}^T}{\omega_{Ei}^2} + \sum_{i=p+1}^{n} \frac{\left\{\Phi_{Ai}\right\}\left\{\Phi_{Ai}\right\}^T}{\omega_{Ai}^2} \tag{6.11}$$

where, $\left\{\Phi_{Ei}\right\}$ and $\left\{\Phi_{Ai}\right\}$ denotes experimental and analytical i^{th} mode shape vectors respectively, ω_{Ei} and ω_{Ai} represents corresponding experimental and analytical natural frequencies respectively. In many cases, number of experimentally identified modes is much less than the number of modes available from the FE model. In such cases, it is wiser to compute the summation terms associated to higher frequencies as in Eqs. (6.10) and (6.11) using the following equations.

$$\sum_{i=p+1}^{n} \left\{\Phi_{Ai}\right\}\left\{\Phi_{Ai}\right\}^T = \left[M_A\right]^{-1} - \sum_{i=1}^{p} \left\{\Phi_{Ai}\right\}\left\{\Phi_{Ai}\right\}^T \tag{6.12}$$

$$\sum_{i=p+1}^{n} \frac{\left\{\Phi_{Ai}\right\}\left\{\Phi_{Ai}\right\}^T}{\omega_{Ai}^2} = \left[K_A\right]^{-1} - \sum_{i=1}^{p} \frac{\left\{\Phi_{Ai}\right\}\left\{\Phi_{Ai}\right\}^T}{\omega_{Ai}^2} \tag{6.13}$$

6.2.3. Expansion of the experimental mode shapes

In the present study, both the Berman-Nagy technique and matrix mixing technique are implemented using the expanded mode shape vectors. The system equivalent reduction expansion process (SEREP) (O'Callahan et al. 1989), an extensively used technique in this regard, is applied for the expansion of the experimental mode shapes. SEREP uses the analytical mode shapes to produce the transformation matrix enabling the expansion process. The analytical mode shapes are partitioned into the master and slave coordinates as

$$\left[\Phi_A\right] = \begin{bmatrix} \left[\Phi_{Am}\right] \\ \left[\Phi_{As}\right] \end{bmatrix} \tag{6.14}$$

DOFs corresponding to the measured coordinates are considered as master category, while rest of the DOFs are considered as slave. Finally the transformation matrix is computed as

$$[T] = \begin{bmatrix} [\Phi_{Am}] \\ [\Phi_{As}] \end{bmatrix} [\Phi_{Am}]^{+} \tag{6.15}$$

where, $[\Phi_{Am}]^{+}$ is the pseudo inverse of $[\Phi_{Am}]$ and computed as

$$[\Phi_{Am}]^{+} = \left([\Phi_{Am}]^{T} [\Phi_{Am}] \right)^{-1} [\Phi_{Am}]^{T} \tag{6.16}$$

Experimental mode shapes then can be expanded to the size of FE model as

$$[\Phi_{Ef}] = [T][\Phi_{E}] \tag{6.17}$$

6.3. DIRECT UPDATING OF THE FE MODEL

The direct updating is considered in the present study with the sole aim of efficient design of passive vibration control system for the Saraighat Bridge. Implementation of direct updating of the FE model of this bridge structure is detailed in the following sub-sections.

6.3.1. Preliminary adjustment of the FE model

As mentioned in Chapter 3, high in-plane rigidity of concrete deck slabs along the road level has been considered using massless and diagonally-positioned link elements. Link elements, assigned with only axial stiffness, demostrate substantial influence on the modal parameters. A senstivity analysis is carried out for the natural frequencies for 1st transverse mode and 1st vertical mode of the bridge with respect to axial stiffness of those link elements. This senstivity analysis is presented in Fig. 6.1. Natural frequencies corresponding to the 1st tranverse mode show significant senstivity, where as natural frequencies corresponding to the 1st vertical mode vertical mode are quite insenstivite. A reasonable choice for the axial stiffness is made as 2900000 KN/m. Thus, the natural frequencies associated to the 1st

tranverse and 1st vertical modes become as 0.8973 and 1.8725 respectively. These frequencies are in good agreement with those identified experimentally.

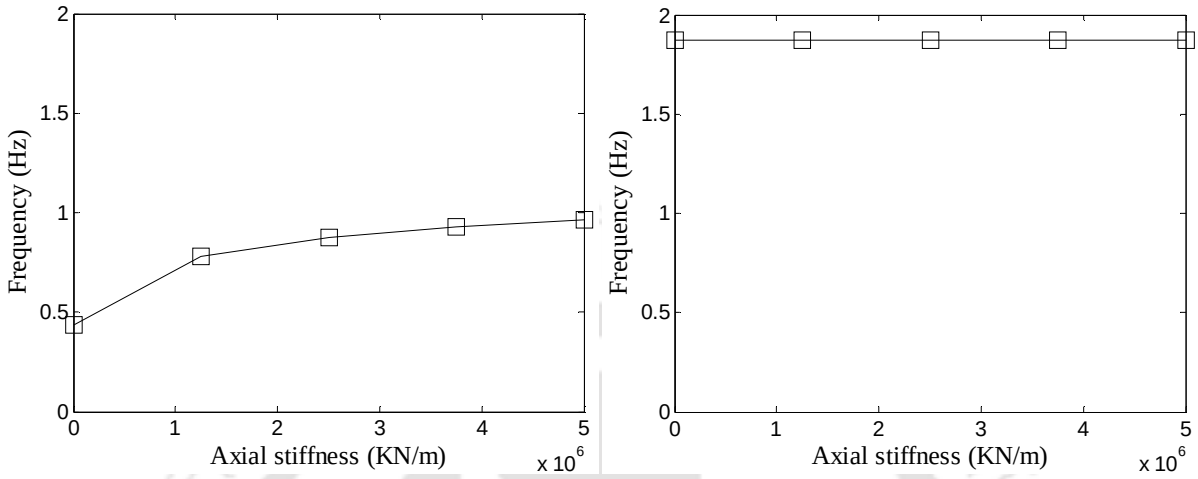

(a) (b)

Fig. 6.1. Sensitivity of natural frequency (Hz) with respect to the axial stiffness (KN/m) of link element for (a) 1st transverse mode and (b) 1st vertical mode

6.3.2. Selection of the analytical modes for updating

Analytical modes from the FE model are selected based on similarity in mode shapes with the experimentally identified shapes. Similarity is considered along the rail-level plane for 1st, 2nd, 3rd transverse as well as vertical modal displacement pattern and 1st, 2nd torsional displacement pattern. It has been possible to select distinct eight analytical modes having such transverse, vertical and torsional modal displacement pattern. The 1st, 2nd, 3rd transverse modes, 1st, 2nd, 3rd vertical modes, 1st, 2nd torsional modes are denoted as H1, H2, H3, V1, V2, V3, T1, T2 respectively. Analytical mode shapes are evaluted using the SAP2000 (V14.2.2) based FE model and are shown in Fig. 6.2. The position-vectors of the view-point associated to Fig. 6.2 are considered for transvers modes as [–1, 0, 0.05] and for vertical along with torsional modes as [0, –1, 0].

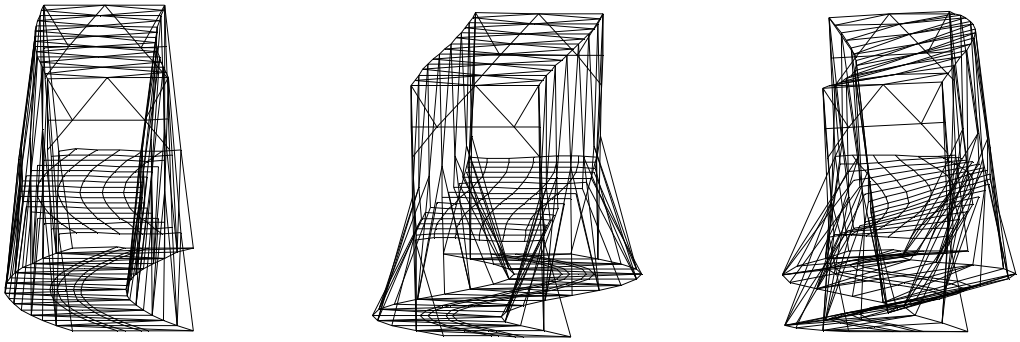

(a) (b) (c)

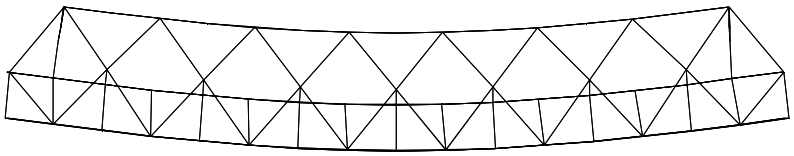

(d)

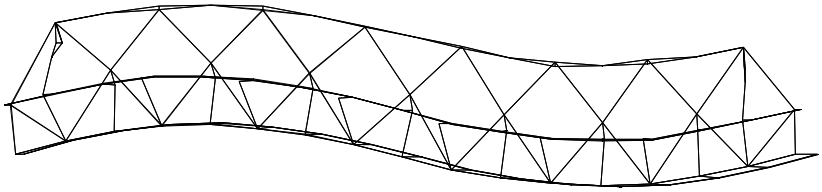

(e)

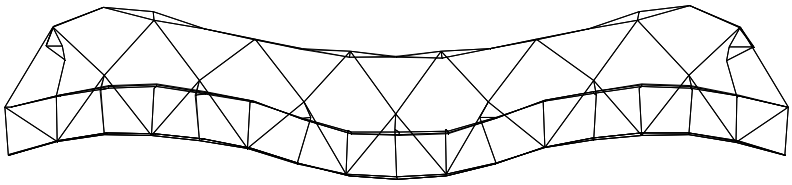

(f)

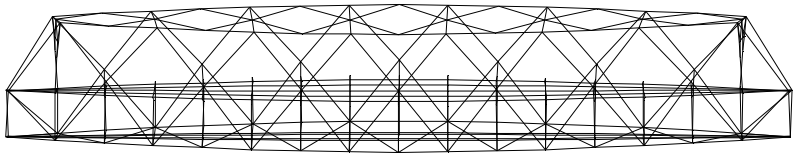

(g)

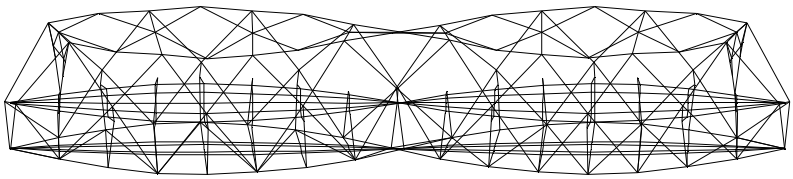

(h)

Fig. 6.2. Selected analytical mode shapes with modal displacemnet pattern as: (a) 1st transverse (b) 2nd transverse (c) 3rd transverse (d) 1st vertical (e) 2nd vertical (f) 3rd vertical (g) 1st torsional and (h) 2nd torsional

6.3.3. Observation on the expanded measured mode shapes

During implementation of FE model updating of this large bridge structure, it has been observed that a significant difference exists between the sizes of the analytical mode shape vector and the experiment mode shape vector. Analytical mode shape contains 854 numbers of DOFs where as the experimental mode shape has just 28 numbers of DOFs corresponding to the locations of sensors in the bridge. Transverse and vertical DOFs along seven locations distributed uniformly on both the sides of the rail-level deck, as presented in Chapter 4, are considered as measured DOFs in this updating exercise. At first, eight experimental mode shapes are expanded using the SEREP to the size of analytical mode shape. The expanded mode shapes are shown in Fig. 6.3. The position-vectors of the view-point associated to these figures are considered for transvers modes as [–1, 0, 0.05] and for vertical along with torsional modes as [0, –1, 0]. It is observed from Fig. 6.3 that expended mode shapes are in reasonably good agreement with the corresponding analytical mode shapes (Fig. 6.2). In terms of the quality of mode shape agreement, however the 3rd transverse mode is not found to be as good as the other modes.

Further observation on the correlation between the analytical and the experimental mode shapes has been carried out. In this connection, the expanded experimental mode

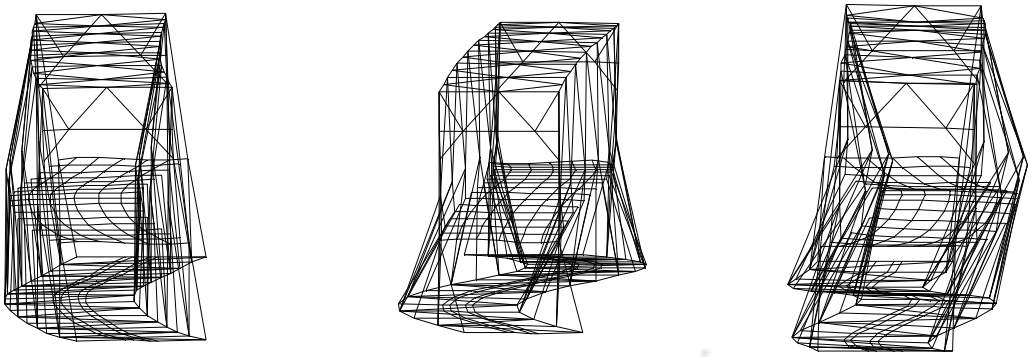

(a) (b) (c)

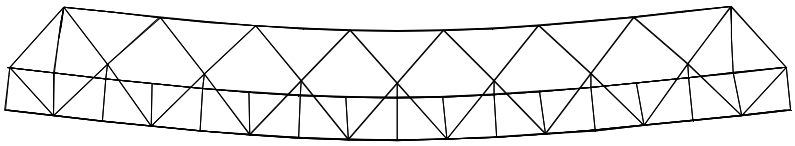

(d)

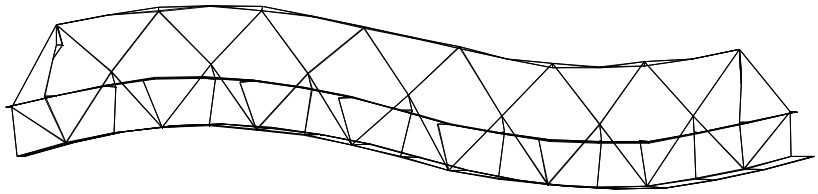

(e)

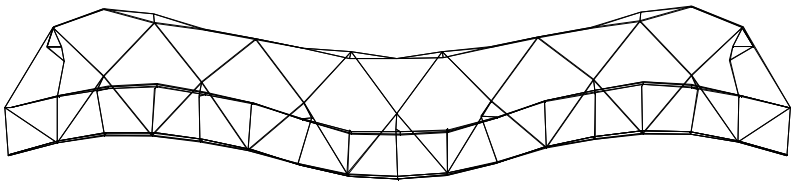

(f)

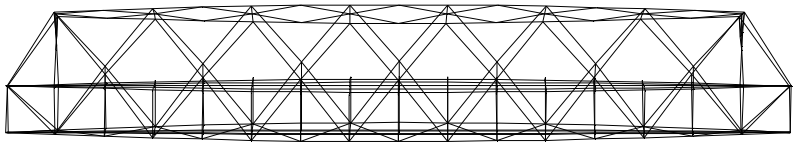

(g)

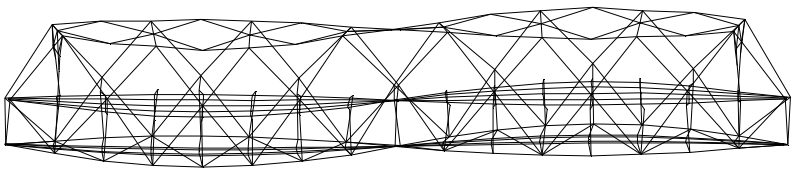

(h)

Fig. 6.3. Expanded form of the experimentally identified mode shapes associated to (a) 1st transverse (b) 2nd transverse (c) 3rd transverse (d) 1st vertical (e) 2nd vertical (f) 3rd vertical (g) 1st torsional and (h) 2nd torsional modes

shapes and the corresponding analytical mode shapes are compared. Two types of measures used here are: modal assurance criteria (MAC) and orthogonality based checks. The MAC based correlation between the experimental and analytical mode shapes are shown in Fig. 6.4. The orders of modes, as considered in Fig. 6.4, are: H1, H2, H3, V1, V2, V3, T1 and T2. Least value of MAC is observed for the mode H3 i.e. 3rd transverse. The global shape/form of the analytical and expanded-experimental mode shapes associated to H3 mode demonstrates reasonable agreement, although MAC value is quite low. The complex geometry of this bridge structure as well as differences in local modal behaviour might have affected the MAC to be low. MAC values associated to the torsional modes are also observed to be lesser possibly due to the same reason.

In regard to the orthogonality based checks, experimental mode shapes can be checked for orthogonality using the analytical mass matrix or stiffness matrix. Analytical mass matrix based check is usually considered and the same is considered here as well. Analytical mass matrix is normally derived from a FE model of the structure. Two such mass matrix based orthogonality checks are considered as follows:

(a) Traditional orthogonality check (OC) where the experimental mode shapes are used together with mass matrix to observe the orthogonality of experimental mode shapes.

(b) Pseudo orthogonality check (POC) (Avitabile et al. 1988) where the experimental modal vectors are used together with mass matrix and the analytical mode shape vectors to observe the orthogonality of experimental mode shapes.

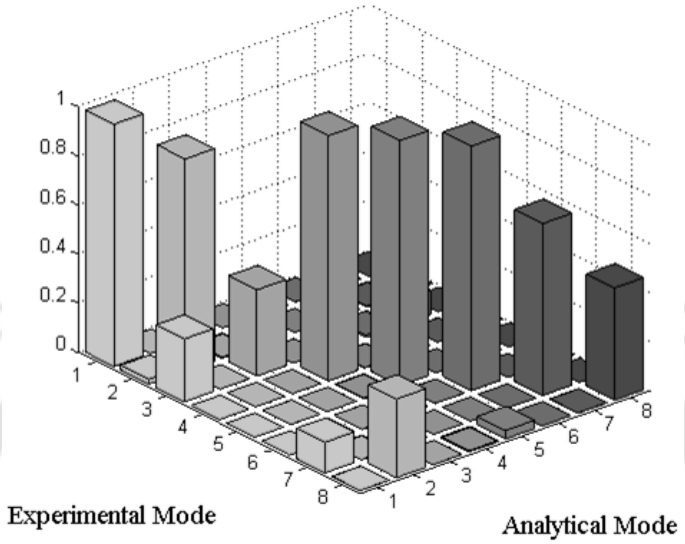

Fig. 6.4. MAC plot associated with eight experimental mode shapes in expanded form and the corresponding analytical mode shapes

The expression for the traditional orthogonality check and pseudo orthogonality check are provided in Eqs. (6.18) and (6.19) respectively.

$$[I_{OC}] = [\Phi_E]^T [M_A][\Phi_E] \tag{6.18}$$

$$[I_{POC}] = [\Phi_E]^T [M_A][\Phi_A] \tag{6.19}$$

To perform these orthogonality checks with compatible sizes of matrices, the mass matrix can be reduced to the size of experimentally identified modal model or the experimental mode shape vectors can be expanded to the size of analytical mass matrix. Usually, the experimental and analytical modal vectors are scaled in such a way that the diagonal terms of $[I_{OC}]$ and $[I_{POC}]$ become unity. The off-diagonal terms of these two matrices are expected to

be low according to the concept of orthogonality. In this present updating exercise, $[I_{OC}]$ and $[I_{POC}]$ are computed based on the expanded experimental mode shapes and displayed in Figs. 6.5(a) and 6.5(b) respectively. The off-diagonal terms are observed to be fairly low except

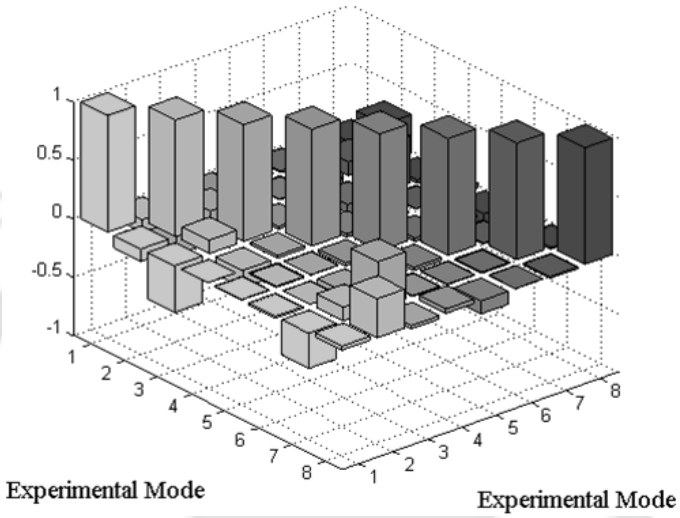

(a)

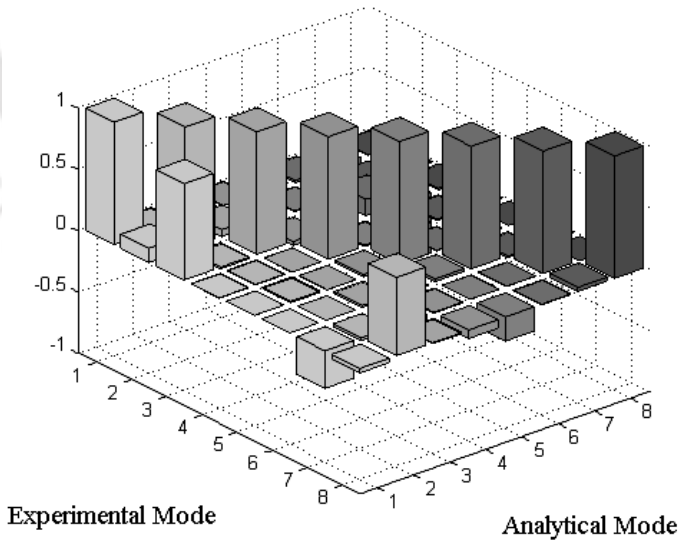

(b)

Fig. 6.5. Orthogonality based checks using (a) traditional orthogonality check (OC) and (b) pseudo orthogonality check (POC)

few exceptions. Therefore, the expanded measured mode shapes may be considered as fairly acceptable as per orthogonality criteria. It may be mentioned that the orders of modes, as considered in these plots, are: H1, H2, H3, V1, V2, V3, T1 and T2.

6.3.4. Implementation of matrix mixing technique

Matrix mixing updating carried out using the experimentally identified eight modes in terms of associated modal frequencies and mode shapes. The experimental mode shapes vectors are extended in Section 6.3.3 as per the requirement of the adopted updating techniques. Subsequently, these expanded mode shapes are studied in detail in terms of visual observation on similarity with their analytical counterparts, similarity quantification using MAC and orthogonality observation. The extended mode shape vectors are observed to be in reasonably good agreement with the analytical shapes based on these assessments. Thus, this updating exercise encompasses a good level of confidence. The expanded experimental shapes are scaled in such a way that the diagonals of $[I_{POC}]$ become unity and the analytical mode shapes are mass normalized. Such scaling of the measured mode shapes are done in order to minimize the changes in updated system matrices with respect to the initial analytical system matrices.

6.3.5. Implementation of Berman and Nagy technique

Berman and Nagy updating is performed using the expanded measured shapes. The measured mode shape (in expanded form) matrix $[\Phi_E]$, which is having 854 rows and eight columns, is appended to the rest of the analytical mode shapes to finally have the size of $[\Phi_E]$ as 854×854. Similarly, eigen-value matrix $[\Lambda_E]$ also becomes a matrix of size 854×854. Subsequently, the updated mass and stiffness matrices are computed. It may be mentioned

that the measured data in terms of natural frequencies and expanded mode shapes are exactly replicated without availability of any spurious mode.

6.4. RESULTS AND DISCUSSION

The evaluated updated mass and stiffness matrices and the associated modal parameters are discussed in details in the following sub-section.

6.4.1. Updated mass and stiffness matrices

The initial mass matrix, the updated mass matrices based on Berman-Nagy technique and matrix mixing technique are presented in the form of 3D plots in Figs. 6.6(a), 6.6(b) and 6.6(c) respectively. Clarity in Fig. 6.6 is poor to some extent due to large numbers of DOFs of the model. However, it still can be observed that changes in the updated mass matrix are not significant as compared to the original mass matrix. The original mass matrix is computed using lumped mass idealization and hence it is a diagonal matrix. For better understanding of changes in the updated mass matrix, the diagonal elements of the original mass matrix, Berman-Nagy technique based updated mass matrix and matrix mixing technique based updated mass matrix are presented in Figs. 6.7(a), 6.7(b) and 6.7(c) respectively. It is observed that changes in the diagonal elements of the updated mass matrices are insignificant in case of both the updating techniques. Finally, the updated stiffness matrices based on Berman-Nagy technique and matrix mixing technique along with the original stiffness matrix are plotted as in Figs. 6.8(b), 6.8(c) and 6.8(a) respectively. Changes in the updated stiffness matrices are also insignificant as compared to the original stiffness matrix for both the updating techniques. Changes in the updated mass matrix are observed to be quite insignificant based on the matrix mixing updating using the adopted procedure of scaling of expanded experimental mode shape vectors. Moreover, insignificant

changes in the updated stiffness matrix are observed due to lower differences among the experimental frequencies and associated analytical natural frequencies. Interestingly, both the updating techniques have evaluated the updated system matrices in quite similar fashion. Hence, updated system matrices based on any of this two updating techniques can be used for updating.

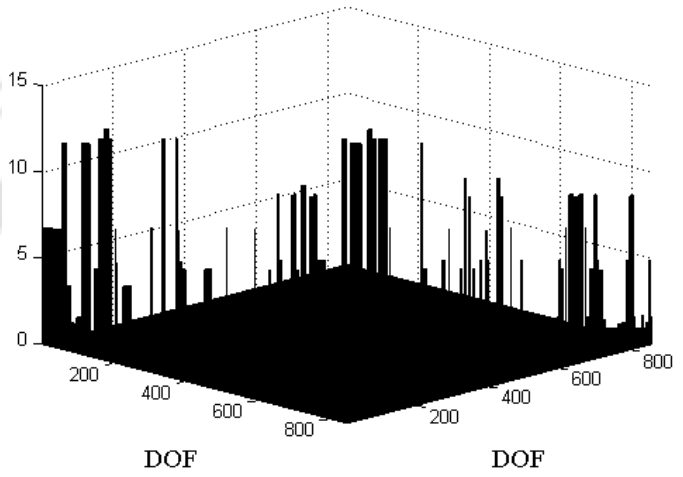

(a)

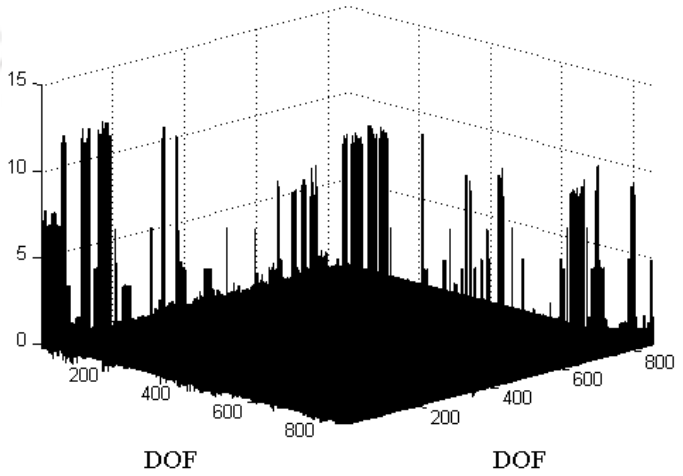

(b)

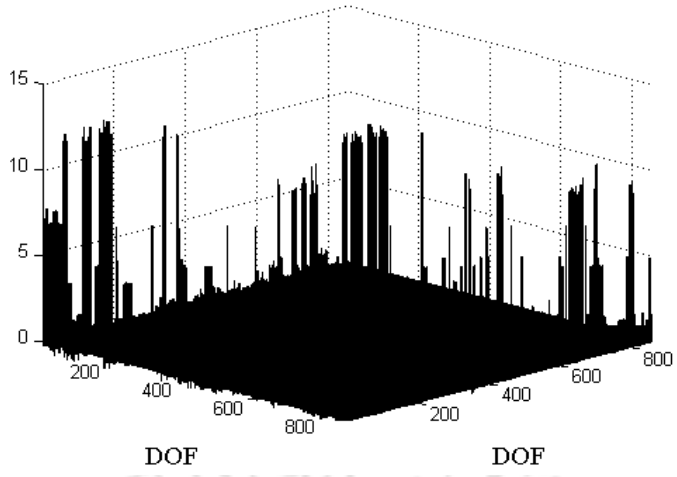

(c)

Fig. 6.6. Elements (metric ton) of (a) intial analytical mass matrix (b) Berman-Nagy method based updated mass matrix and (c) matrix mixing method based updated mass matrix

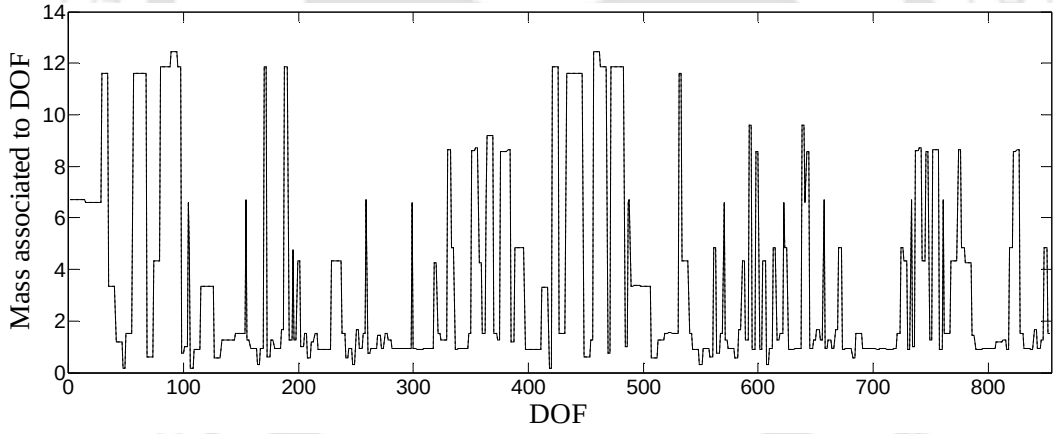

(a)

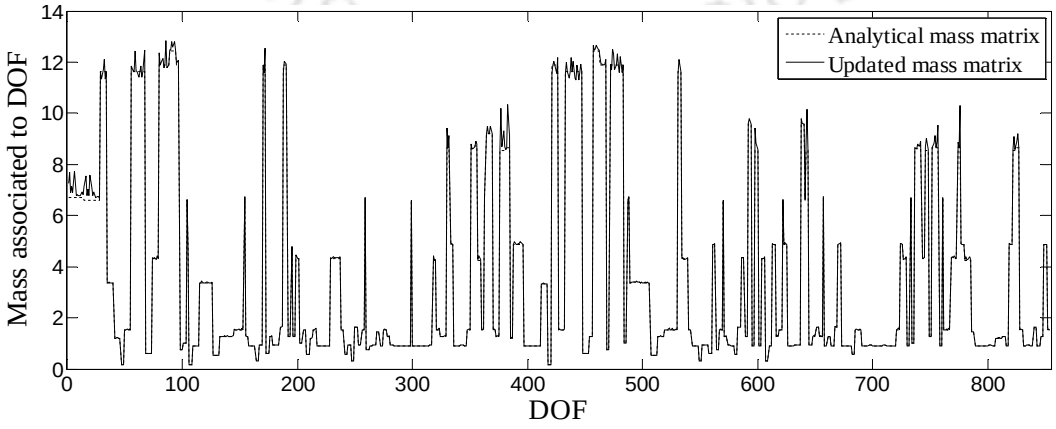

(b)

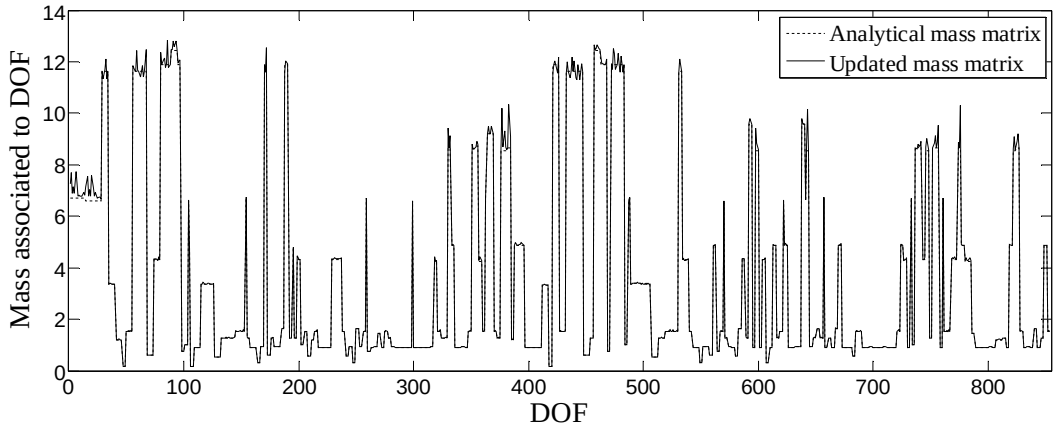

(c)

Fig. 6.7. Diagonal elements of (a) intial analytical mass matrix (b) Berman-Nagy technique based updated mass matrix and (c) matrix mixing technique based updated mass matrix

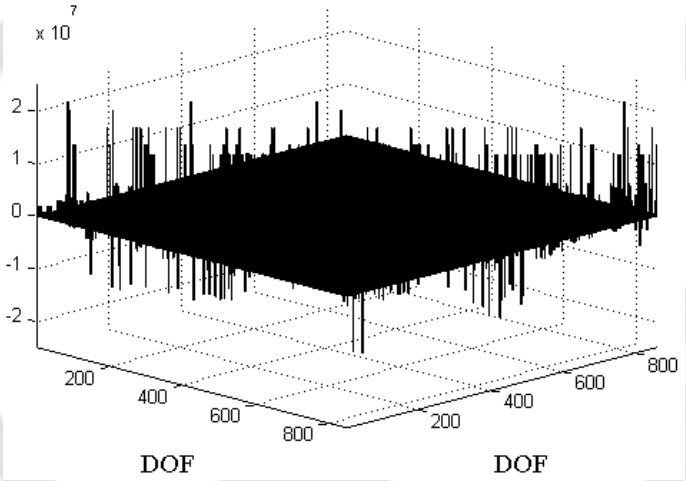

(a)

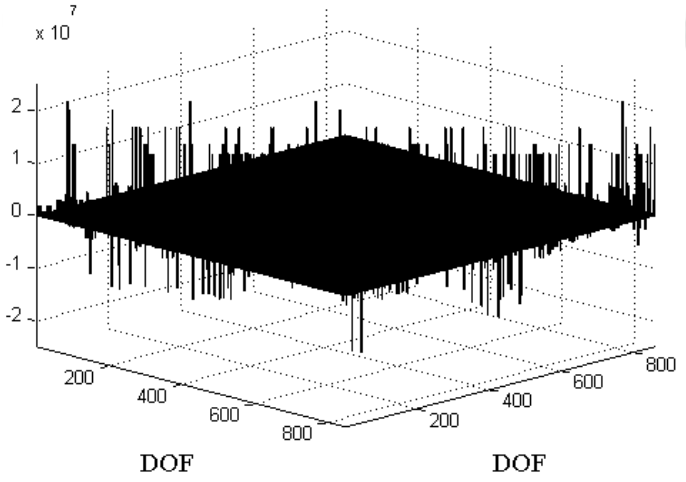

(b)

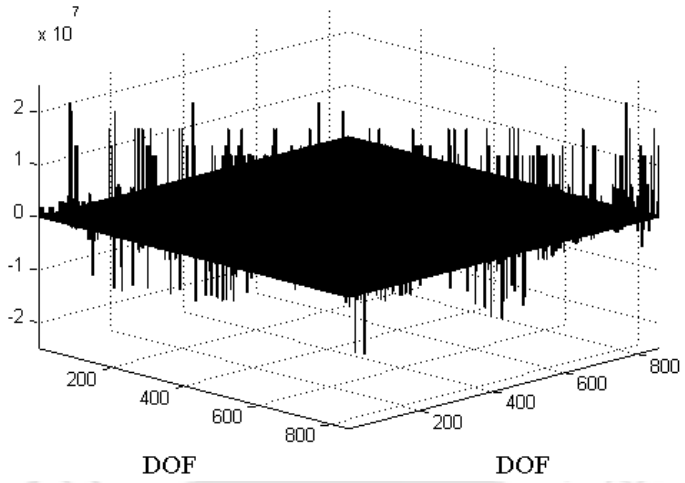

(c)

Fig. 6.8. Elements (KN/m) of (a) intial analytical stiffness matrix (b) Berman-Nagy technique based updated stiffness matrix and (c) matrix mixing technique based updated stiffness matrix

6.4.2. Updated modal parameters

In both the Berman-Nagy technique and the matrix mixing updating technique, the updated natural frequencies are observed to be in complete agreement with the measures frequencies as presented in Table 6.1. Further, mode shapes are also found to be in complete agreement with the measured ones. Therefore, mode shapes obtained based on the updated system matrices are same as corresponding expanded measured shapes (as in Fig. 6.3). The updated mode shape vectors in terms of measured DOFs are displayed in Fig. 6.9 proving a clearer comparison with the experimental mode shapes at rail-level deck (as shown in Figs. 5.8–5.15). It is clearly observed that similarities are very good. The MAC between these experimental and the updated mode shapes are evaluated and presented in Table 6.2.

Table 6.1. Natural frequencies associated to the updated modes

Mode no. in Experimental-order	Mode Type	Expermental frequency (Hz)	Updated frequency (Hz)	
			Berman-Nagy	Matrix mixing
1	1st transverse	0.9119	0.9119	0.9119
2	1st vertical	1.8624	1.8624	1.8624
3	2nd transverse	2.1550	2.1550	2.1550
4	1st torsional	2.9626	2.9626	2.9626
5	2nd vertical	4.3976	4.3976	4.3976
6	2nd torsional	5.1501	5.1501	5.1501
7	3rd transverse	6.3783	6.3783	6.3783
8	3rd vertical	6.9285	6.9285	6.9285

Table 6.2. MAC between the experimental and updated mode shapes

Mode no.	Mode Type	Notation	MAC
1	1st transverse	H1	0.9974
2	1st vertical	V1	0.9999
3	2nd transverse	H2	0.9941
4	1st torsional	T1	0.9928
5	2nd vertical	V2	0.9959
6	2nd torsional	T2	0.9223
7	3rd transverse	H3	0.9606
8	3rd vertical	V3	0.9832

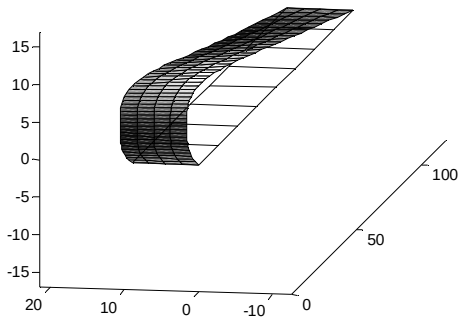

(a)

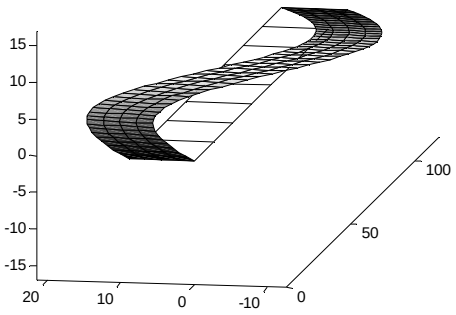

(b)

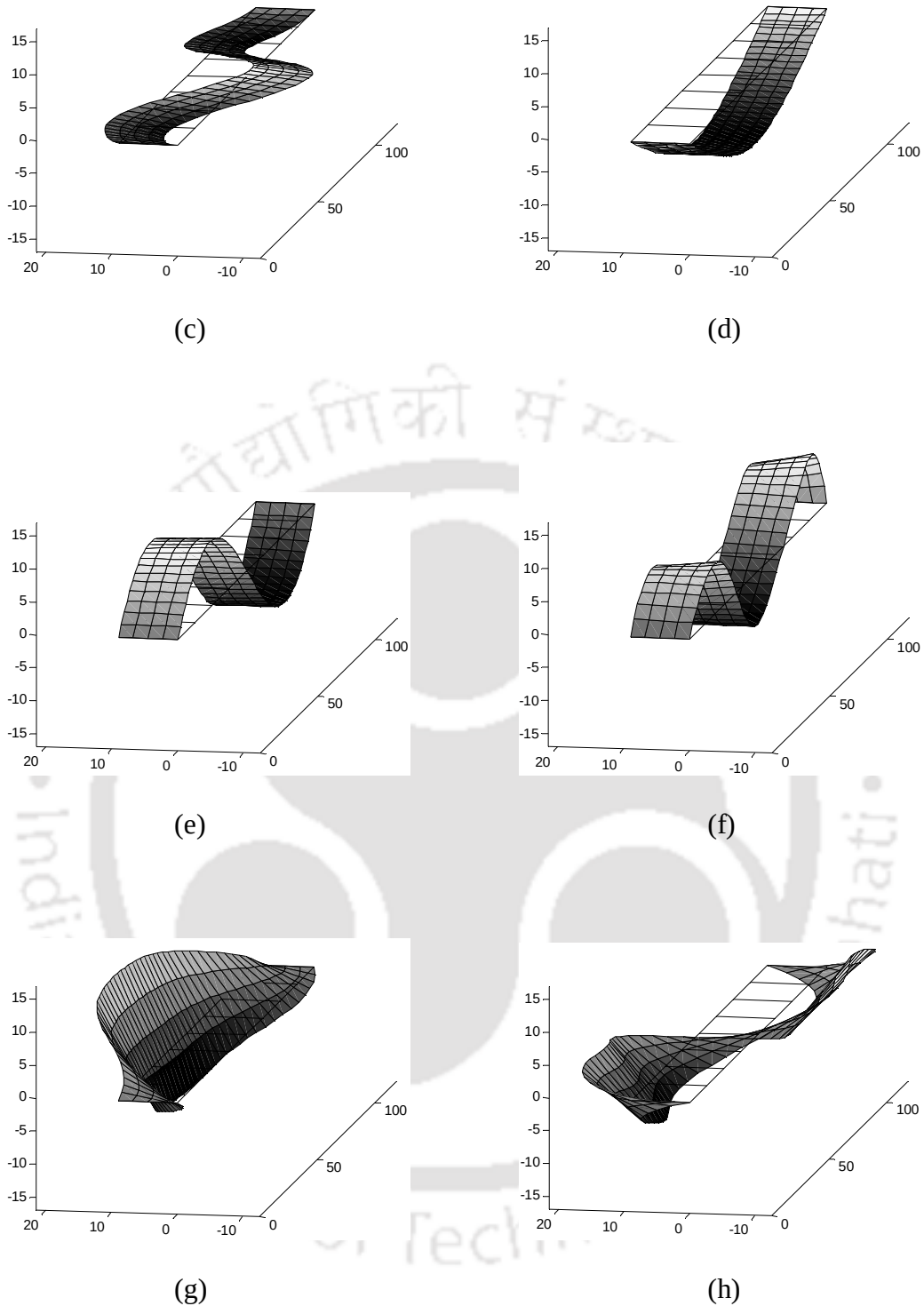

Fig. 6.9. Updated mode shapes corresponding to (a) 1st transverse (b) 2nd transverse (c) 3rd transverse (d) 1st vertical (e) 2nd vertical (f) 3rd vertical (g) 1st torsional and (h) 2nd torsional modes

6.5. CONCLUDING REMARKS

Direct updating techniques, with their inherent advantage of more accurate reproduction of experimental modal data in the updated model, have good potential for applicability in areas like deign of controller, prediction of dynamic response etc. In literature, however, applications of direct updating for large structural systems are not much observed. It is therefore a matter of great interest as well as challenge to undertake a direct updating exercise for this large steel structure. The present work performs direct model updating for this large steel structure employing two major direct updating techniques. Following concluding remarks are made based on the present study.

(a) Eight measured mode shapes at rail-deck level having 28 DOFs have been expanded to 854 DOFs. These expanded measured mode shapes associated to this complicated bridge structure have demonstrated good agreement.

(b) Both of the updating techniques have determined updated mass and stiffness matrices while exactly reproducing the measured natural frequencies and mode shapes (in expanded form).

(c) The updated mode shapes along the rail-deck level are in excellent agreement with those identified experimentally.

(d) In case of matrix mixing updating, the adopted scale has been able to update the system matrices with insignificant changes with respect to the initial analytical system matrices.

(e) Interestingly, changes in the updated system matrices are observed as insignificant in case of both the updating techniques. Thus, updated system matrices based on any of these techniques can be considered for further similar applications.

(f) With the updated system matrices having exact match of modal parameters to the corresponding measured parameters with quite insignificant changes in initial mass and stiffness properties, the updated system matrices can be applied with a good confidence for design of passive control system based on any modal approach.

Chapter 7

DESIGN OF TMD SYSTEM FOR THE SARAIGHAT BRIDGE

7.1. INTRODUCTION

Structural control has received considerable attention from researchers in the recent past for improving structural functionality as well as safety. In regard to passive vibration control of structural systems, the tuned mass damper (TMD) is considered as amongst the oldest passive vibration control devices in existence. Early applications of TMDs are observed towards mitigation of wind-induced vibrations. Though the TMD system is among the oldest structural vibration control devices, the TMD system is considered a useful choice as a passive vibration control device even today. In recent times, many practical applications of TMDs are observed for mitigation of vibration of structures subjected to wind-excitations as well as vehicle induced excitations. Besides such applications for non-seismic vibration, numerical and experimental studies have been carried out to study the effectiveness of TMDs for reduction of seismic responses as well. In addition to wide applications of TMDs to the building systems, TMD systems are also observed to be applied for bridge structures for passive vibration control. Important applications of TMD systems for bridge structures are found in case of train induced vibration control (Wang et al. 2003; Yau and Yang 2004a; Yau and Yang 2004b; Lin et al. 2005; Li et al. 2005). Wind induced vibration control of bridge structure such as Trans-Tokyo Bay Crossing Bridge is another useful application of TMDs (Fujino and Yoshida 2002). Many footbridges or pedestrian bridges are also observed to use TMDs for vibration control (Li et al. 2010; Daniel et al. 2011). Primarily, applications of TMD systems for bridge structures are observed for vibration control against non-seismic excitations. Steel truss bridges have often been constructed because of their advantages in terms of light weight, high strength and effectiveness in bridging short to medium spans.

Compared to concrete bridges, steel truss bridges are generally more flexible and experience relatively higher displacement responses under natural loading conditions. The Saraighat Bridge, a steel truss bridge having 118.72m span, experiences considerable vibration although vibration intensities are usually not found to create major difficulties. Although, vibration control measures are not urgently required from safety and serviceability demand on the bridge, the same would help in extending the fatigue life of the bridge. In view of the above, passive vibration controlling is aimed using the TMD system. Multiple TMD (MTMD) system, which is widely accepted to perform better than the single unit based TMD system, is considered in this study. A strategy using modal frequency response function (FRF) is proposed based on the traditional mode-wise control approach. Further, an approach for simultaneous control of horizontal and vertical modes is proposed in this study. Prominent modes, both in horizontal (transverse) and vertical directions are simultaneously targeted to be taken into account in design considerations of TMD system, while assigning equal importance for both the directions. Therefore, the designed TMD system is supposed to perform effectively against vehicle type loading as well as wind type loading, which is contrary to the traditional design where either transverse modes or the vertical modes are usually taken into account. Such design is also expected to perform reasonably well against seismic excitations, since the design is carried out following mode-wise approach.

7.2. DESIGN OF MTMD SYSTEM: A MODAL FRF BASED APPROACH

MTMD systems are considered in the design exercise due to its widely accepted high performance in vibration control. In case of designing of TMD device for a MDOF structural system, it is possible to design the TMD device separately targeting any mode in a similar way of designing TMD device for single degree of freedom (SDOF) structural system. Such individual mode-wise deign is feasible if the corresponding mode shape is normalized in an

appropriate way (Rana and Soong 1998). Finally, the MTMD systems individually designed for various target modes are attached to the primary structure in the respective design-locations to work as multi-modal control device as a whole. This approach is usually considered as a fundamental modal framework for TMD design. In this present study, a design strategy is proposed using modal FRF based on the modal framework for TMD design. Further a strategy is suggested for controlling both the horizontal (transverse) and vertical modes simultaneously. Details of this control-strategy are presented in the following sub-sections.

7.2.1. Modal FRF associated to a target mode

Equation of motion of the MDOF structural systems can be expressed as:

$$[M]\{\ddot{x}\}+[D]\{\dot{x}\}+[K]\{x\}=\{F\} \tag{7.1}$$

Definitions of the matrices [*M*], [*D*] and [*K***]** are as mentioned in Chapter 3, while {*F*} represents the force vector. With the assumption of proportional damping and using a transformation as $\{x\}=[\Phi]\{Q\}$, Eq. (7.1) can be transformed into *n* (system size) uncoupled equations in modal coordinates (Q_i). Such an uncoupled equation associated to the i^{th} mode can be mentioned as follows.

$$M_i\ddot{Q}_i+D_i\dot{Q}_i+K_iQ_i=\{\Phi_i\}^T\{F\} \tag{7.2}$$

where, M_i, D_i, K_i, Q_i and $\{\Phi_i\}$ represent the modal mass, modal damping coefficient, modal stiffness, modal coordinate and mode shape associated to the i^{th} mode. If $\{\Phi_i\}$, mode shape for i^{th} mode, is scaled or normalized such that the modal deformation along a DOF (suppose *j*) connected to the MTMD becomes unity (i.e. Φ_{ij} = 1), then it becomes feasible to individually design an MTMD device targeting the i^{th} mode of an MDOF structural system (Rana and Soong 1998). Similar scaling is maintained for a mode associated to both the

controlled and uncontrolled cases, which helps to compare modal coordinate of both the cases. It may be mentioned that in the present work only displacement control is considered. Acceleration for bridge structures having low to moderate level of vibration (in terms of displacement) is possibly not a matter of major concern. The displacement response based frequency response of a structural system can be expressed as the summation of all the modal frequency responses (Gawronski 2004). The state space matrices, required to form the i^{th} modal FRF matrix based on displacement response, are expressed as in Eqs. (7.3a–7.3d) and the relation for computation of modal FRF matrix is expressed as in Eq. (7.4).

$$[A_i]=\begin{bmatrix} 0 & 1 \\ -\omega_i^2 & -2\xi_i\omega_i \end{bmatrix} \tag{7.3a}$$

$$[B_i]=\begin{bmatrix} \{0\}^T \\ \frac{1}{M_i}\{\Phi_i\}^T \end{bmatrix} \tag{7.3b}$$

$$[C_i]=\begin{bmatrix} \{\Phi_i\} & \{0\} \end{bmatrix} \tag{7.3c}$$

$$[E_i]=[0] \tag{7.3d}$$

$$[G_i(\omega)]=[C_i]\left(i\omega[I]-[A_i]\right)^{-1}[B_i]+[E_i] \tag{7.4}$$

In Eq. (7.3) ω_i and ξ_i denote the circular modal frequency and modal damping ratio of i^{th} mode. In Eq. (7.4) $\sqrt{-1}$ is denoted as i while [I] represents identity matrix. It may be observed that the modal state space matrices [A_i] and [B_i] represent the 2nd order modal Eq. (7.2) and are associated to 1st order state-vector as $\begin{Bmatrix} Q_i & \dot{Q}_i \end{Bmatrix}^T$. The input and the output vectors {u} and {y} are now represented by Eqs. (7.5a) and (7.5b) respectively.

$$\{u\}=\{F\} \tag{7.5a}$$

$$\{y\}=\{\Phi_i\}Q_i \tag{7.5b}$$

Subsequently, the i^{th} mode is taken into account for control using MTMD device in a similar way of controlling a SDOF system using MTMD device. A schematic diagram of such modal control problem is shown in Fig. 7.1 for i^{th} mode. The quantities as $q_{i,l}$, $m_{i,l}$, $d_{i,l}$ and $k_{i,l}$ represent the displacement coordinate, mass, damping coefficient and stiffness of the l^{th} unit of the MTMD system. The equations of motion for this system as shown in Fig. 7.1 may be expressed as:

$$\begin{bmatrix} M_i & \{0\}^T \\ \{0\} & [m_{TMD}] \end{bmatrix} \begin{Bmatrix} \ddot{Q}_i \\ \{\ddot{q}_{TMD}\} \end{Bmatrix} + \begin{bmatrix} (D_i + D_{TMD}) & \{\bar{d}_{TMD}\}^T \\ \{\bar{d}_{TMD}\} & [d_{TMD}] \end{bmatrix} \begin{Bmatrix} \dot{Q}_i \\ \{\dot{q}_{TMD}\} \end{Bmatrix} + \begin{bmatrix} (K_i + K_{TMD}) & \{\bar{k}_{TMD}\}^T \\ \{\bar{k}_{TMD}\} & [k_{TMD}] \end{bmatrix} \begin{Bmatrix} Q_i \\ \{q_{TMD}\} \end{Bmatrix} = \begin{Bmatrix} \{\Phi_i\}^T \{F\} \\ \{0\} \end{Bmatrix} \tag{7.6}$$

where,

$$[m_{TMD}] = \text{diag}\left(m_{i,1},\ m_{i,2}\ \ldots\ m_{i,p}\right)$$

$$[d_{TMD}] = \text{diag}\left(d_{i,1},\ d_{i,2}\ \ldots\ d_{i,p}\right)$$

$$\{\bar{d}_{TMD}\} = \text{diag}\left\{-d_{i,1},\ -d_{i,2}\ \ldots\ -d_{i,p}\right\}$$

$$D_{TMD} = \sum_{r=1}^{p} d_{i,r}$$

$$[k_{TMD}] = \text{diag}\left(k_{i,1},\ k_{i,2}\ \ldots\ k_{i,p}\right)$$

$$\{\bar{k}_{TMD}\} = \text{diag}\left\{-k_{i,1},\ -k_{i,2}\ \ldots\ -k_{i,p}\right\}$$

$$K_{TMD} = \sum_{r=1}^{p} k_{i,r}$$

It is quite straightforward to form the state space matrices A and B associated to Eq. (7.6) as mentioned below.

$$\left[\bar{A}_i\right]=\left[\begin{array}{c|c} [0] & [I] \\ \hline -\begin{bmatrix} M_i & \{0\}^T \\ \{0\} & [m_{TMD}] \end{bmatrix}^{-1}\begin{bmatrix} (K_i+K_{TMD}) & \{\bar{k}_{TMD}\}^T \\ \{\bar{k}_{TMD}\} & [k_{TMD}] \end{bmatrix} & -\begin{bmatrix} M_i & \{0\}^T \\ \{0\} & [m_{TMD}] \end{bmatrix}^{-1}\begin{bmatrix} (D_i+D_{TMD}) & \{\bar{d}_{TMD}\}^T \\ \{\bar{d}_{TMD}\} & [d_{TMD}] \end{bmatrix} \end{array}\right] \tag{7.7a}$$

$$\left[\bar{B}_i\right]=\left[\begin{array}{c} [0] \\ \hline \begin{bmatrix} M_i & \{0\}^T \\ \{0\} & [m_{TMD}] \end{bmatrix}^{-1}\begin{bmatrix} \{\Phi_i\}^T \\ [0] \end{bmatrix} \end{array}\right] \tag{7.7b}$$

The input vector $\{u\}$ is $\{F\}$ and thus same as Eq. (7.5a). The state vector becomes $\left\{Q_i,\ q_{i,1},\ \ldots\ q_{i,p},\ \dot{Q}_i,\ \dot{q}_{i,1},\ \ldots\ \dot{q}_{i,p}\right\}$. The 1st state in this state-vector is Q_i and this helps to form the state space matrix $\left[\bar{C}_i\right]$ as shown in Eq. (7.7c) having similar output as per Eq. (7.5b).

$$\left[\bar{C}_i\right]=\left[\{\Phi_i\}\quad [0]\right] \tag{7.7c}$$

$$\left[\bar{E}_i\right]=[0] \tag{7.7d}$$

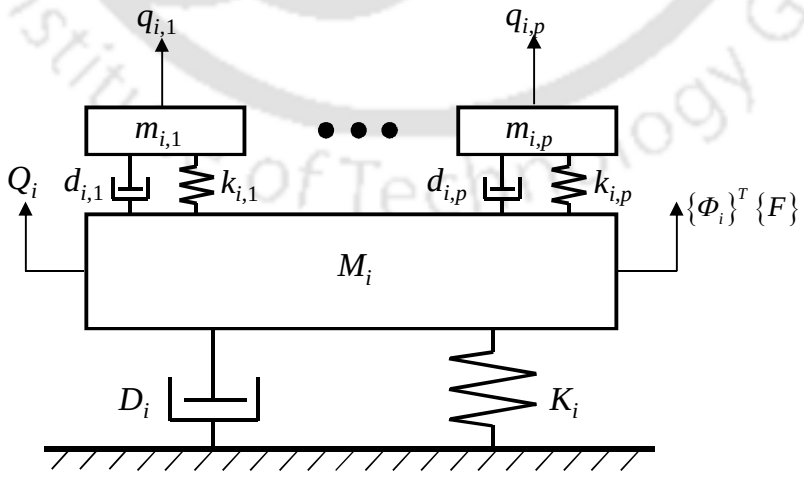

Fig. 7.1. Schematic diagram of the MTMD system associated to the i^{th} mode

It may be noticed that the input and output are similarly associated to the FRF matrices for both the cases of uncontrolled and controlled modal coordinate Q_i. It makes possible to compare the frequency response measures (magnitude along an input-output channel or spectral norm) for the uncontrolled and controlled cases associated to the modal coordinate Q_i. Modal coordinate Q_i for with and without TMD cases are denoted as $Q_{i\text{-WT}}$ and $Q_{i\text{-WOT}}$ respectively for sake of clarity, though $Q_{i\text{-WT}}$ and $Q_{i\text{-WOT}}$ actually represent the same quantity.

7.2.2. Design strategy of MTMD system targeting multiple modes

Both the uncontrolled and controlled systems as represented by Eqs. (7.3a–7.3d) and Eqs. (7.7a–7.7d) respectively are indeed MIMO systems. In the present study, the goal is to control a single mode according to the adopted mode-wise strategy. In case of single modal vibration for any mode, changes in modal deformation for all the DOFs will be proportionate. Therefore, minimization of frequency response associated to any input-output channel similarly minimizes the frequency responses of other input-output channels. Hence, a single input-output channel based frequency response can be minimized for controlling a particular mode. Suitable input-output channel can be considered along the DOF with maximum modal deformation having maximum level of frequency response (Gawronski 2004). Input-output channel associated to the DOF with maximum modal deformation also represents highest controllability and observability (Gawronski 2004). In this present work, a single input-output channel based FRF having maximum level of frequency response is considered for minimization with the objective of control.

The modal frequency response is quantified using H_∞ norm (Francis 1987; Doyle and Francis 1992; Zhou et al. 1995). H_∞ norm is found as a useful tool for both passive and active control. H_∞ norm for SISO systems is defined as the maximum magnitude of the frequency response of the system in entire frequency range and commonly expressed as

$$\| G \|_{\infty} = \max_{\omega} | G(\omega) | \tag{7.8}$$

For MIMO systems, H_∞ norm is defined as maximum gain i.e. worst-case gain in entire frequency range. The gain of the system is evaluated (Eq. (7.9)) as spectral norm of the FRF-matrix i.e. as induced norm of FRF-matrix using Euclidean vector-norm (||.||) and finally becomes equal to the largest singular value (Golub and Van Loan 1996) of the FRF matrix.

$$\beta(\omega) = \max \left\{ \frac{\| \{Y(\omega)\} \|}{\| \{U(\omega)\} \|} : \{U(\omega)\} \neq \{0\} \right\} = \max \left\{ \frac{\| [G(\omega)] \{U(\omega)\} \|}{\| \{U(\omega)\} \|} \right\} = \bar{\sigma}\left([G(\omega)] \right) \tag{7.9}$$

H_∞ norm for MIMO systems is usually expressed as

$$\| G \|_{\infty} = \sup_{\omega} \bar{\sigma}\left([G(\omega)] \right) \tag{7.10}$$

Computation of H_∞ norm for complete frequency range is commonly carried out based on the algorithm proposed by Bruinsma and Steinbuch (1990).

In many applications, it is observed that dominant modes in any single direction (e.g. vertical) are usually taken into account to be controlled using TMD devices. In this present work, a strategy is introduced to consider modes dominant in two leading directions (horizontal-transverse and vertical). This strategy uses the H_∞ norms of the FRF for multiple target modes where H_∞ norm of a target mode is computed for FRF (SISO type) along the input-output channel having maximum frequency response intensity. H_∞ norms for the uncontrolled and controlled cases associated to the r^{th} horizontally (transverse) dominant mode are denoted here as γ_r^{H} and $\bar{\gamma}_r^{\mathrm{H}}$ respectively. Similar representations for the r^{th} vertically dominant mode are considered as γ_r^{V} and $\bar{\gamma}_r^{\mathrm{V}}$. Two performance factors are considered representing the horizontal and vertical directions as pf_{H} and pf_{V} respectively. These factor are defined as

$$pf_{\mathrm{H}} = \frac{\max(\bar{\gamma}_1^{\mathrm{H}},\ \bar{\gamma}_2^{\mathrm{H}}\ ...)}{\max(\gamma_1^{\mathrm{H}},\ \gamma_2^{\mathrm{H}}\ ...)} \tag{7.11a}$$

$$pf_{\mathrm{V}} = \frac{\max(\bar{\gamma}_1^{\mathrm{V}},\ \bar{\gamma}_2^{\mathrm{V}}\ ...)}{\max(\gamma_1^{\mathrm{V}},\ \gamma_2^{\mathrm{V}}\ ...)} \tag{7.11b}$$

The denominators in Eqs. (7.11a) and (7.11b) are constants while the numerators are variable based on the TMD parameters. It is a minimization problem of the performance factors pf_{H} and pf_{V}. A simultaneous minimization of pf_{H} and pf_{V} are considered with minimizing a factor defined as:

$$pf = (c_{\mathrm{H}}.pf_{\mathrm{H}} + c_{\mathrm{V}}.pf_{\mathrm{V}}) \tag{7.12a}$$

where,

$$c_{\mathrm{H}} + c_{\mathrm{V}} = 1 \tag{7.12b}$$

where, c_{H} and c_{V} are considered as importance factor for the horizontal-transverse and vertical modes respectively.

7.2.3. Strategy for control of torsional mode

Torsional modes have dominant modal deformations in both the horizontal (transverse) and vertical directions. Hence, a torsional mode has significant frequency responses in both the directions. Unlike the pure horizontal or vertical modes where one MTMD system is assigned for one such mode, a torsional mode is controlled with two MTMD systems in this present study: (a) one MTMD system to control the horizontal modal component and (b) another MTMD system to control the vertical modal component. Two separate frequency response channels are considered for such a torsional mode to achieve the control in both the directions. In both the cases, the input channel for frequency response is considered as the DOF having maximum modal deformation as well as maximum controllability. On the other

hand, output channel for the transverse as well as vertical directions are considered as the transverse and vertical DOF respectively having maximum modal deformation.

7.2.4. Optimization framework

Various types of formulations for MTMD system are available in literature (Li 2002). In the present study, a model of MTMD system is considered where both stiffness values and damping ratios of all the individual units of MTMD are kept same. Keeping stiffness same for all the MTMD-units are generally considered to be beneficial in view of manufacturing. Stiffness value and the damping ratio for the j^{th} unit of MTMD associated to the i^{th} mode is denoted as k_i (= $k_{i,1}$ = $k_{i,2}$ … = $k_{i,p}$) and ξ_{Ti} ($= \xi_{Ti,1} = \xi_{Ti,2}$ ... $= \xi_{Ti,p}$) respectively. Total number of MTMD-units is taken here as p. The mass ratio of total mass of the MTMD system with respect to the i^{th} modal mass (M_i) is denoted as μ_i. Average frequency of the MTMD-units for the i^{th} mode is considered as $\omega_{Ti} = (1/p)\sum_{j=1}^{p} \omega_{i,j}$. Average frequency ω_{Ti} is related to natural frequency for the i^{th} mode (ω_{Si}) by a factor (f_i) as $f_i = \omega_{Ti} / \omega_{Si}$. Ratio of natural frequency of the j^{th} unit of MTMD ($\omega_{i,j}$) with respect to ω_{Si} is expressed as

$$r_{i,j} = f_i \left[1 + \left(j - \frac{p+1}{2} \right) \frac{\beta_i}{p-1} \right] \tag{7.13a}$$

where,

$$\beta_i = \frac{\omega_{i,p} - \omega_{i,1}}{\omega_{Ti}} \tag{7.13b}$$

Now, the natural frequency and mass ratio of the j^{th} unit of MTMD can be obtained as in Eqs. (7.14) and (7.15) respectively.

$$\omega_{i,j} = r_{i,j} \omega_{Si} \tag{7.14}$$

$$\mu_{i,j} = \frac{\mu_i}{r_{i,j}^2 \sum_{j=1}^{p} (1/r_{i,j}^2)} \tag{7.15}$$

It may be observed that the complete configuration of the MTMD system can be found out, if the MTMD parameters like μ_i, p, f_i, β_i and ξ_{Ti} are available along with a primary system parameter ω_{Si}. On the other hand, both the parameters μ_i and p are usually assumed. Optimization is thus carried out considering f_i, β_i and ξ_{Ti} as the optimization variables. The mass ratio μ_i for a mode is varied within a wide range to take into account diverge spectrum of assigned-mass to the MTMD system. Parameter p is kept same for all the MTMD systems associated to different target modes. Steps for obtaining optimal parameters of MTMD system are:

(a) For each of the possible values of μ_i associated to the i^{th} mode, optimal values of f_i, β_i and ξ_{Ti} are evaluated along with corresponding minimum norm values. This exercise is carried out for all the target modes.

(b) Individual collection of various possible mass ratios associated to a target mode is incorporated with other such collections of possible mass ratios associated to other target modes. The purpose is to find out feasible sets of mass ratio combination (MRC), where an MRC contains mass ratios with each one corresponding to each of the target modal mass. A feasible MRC is one where summation of masses represented by all its mass ratios becomes closely equal to the total assigned mass for the secondary system.

(c) Finally, the exercise is to select a particular MRC out of feasible combinations of MRCs based on objective function defined in Eq. (7.12a). The computational prerequisite for this exercise is already performed in step (a).

7.3. SELECTION OF TARGET MODES FOR THE SARAIGHAT BRIDGE

In practical problems associated to MTMD design for bridges (e.g. Fujino and Yoshida 2002; Yau and Yang 2004b), it is usually observed that first two modes are controlled. In the present study, first two modes each in horizontal (transverse) and vertical direction are considered in case of the Saraighat Bridge. Additionally, the 1st torsional mode is also considered. The torsional mode is controlled with two separately assigned MTMD systems tuned for horizontal as well as its vertical directions as mentioned in Section 7.2.3. The target-modal-cases corresponding to 1st horizontal, 2nd horizontal, 1st vertical, 2nd vertical, 1st torsional controlling horizontal component and 1st torsional controlling vertical component are denoted as H1, H2, V1, V2, T1(H) and T1(V) respectively. Locations of each of the MTMD systems are considered along the DOF corresponding to maximum modal deformation ensuring maximum observability. Locations of the MTMD system for these target-modal-cases are shown in Fig. 7.2. The mode-shapes are scaled as per criterion mentioned in Section 7.2.1 considering such selected MTMD system locations. Modal

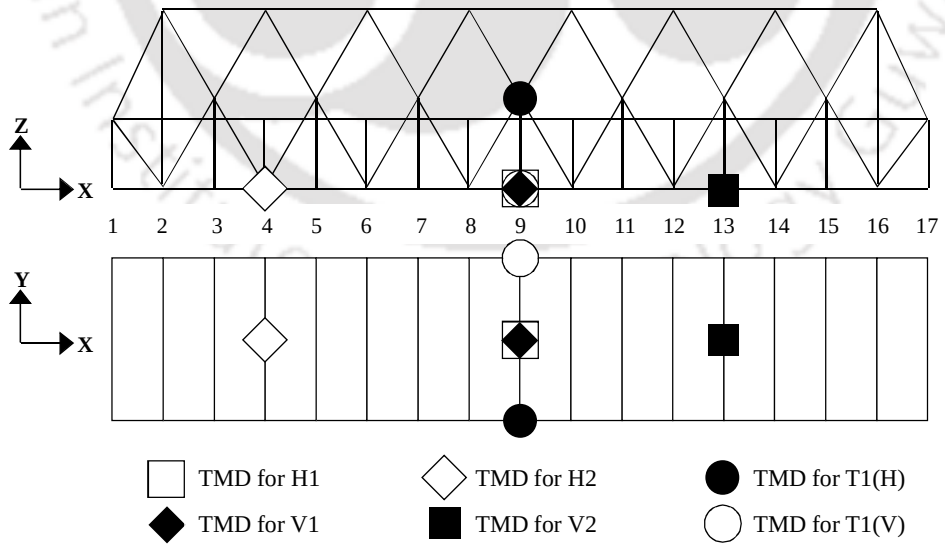

Fig. 7.2. Locations of the MTMD systems corresponding to the target-modal-cases: H1, H2, V1, V2, T1(H) and T1(V)

frequency response is considered in SISO form having single input channel (related to maximum modal deformation of modes associated with each of six modal-cases: H1, H2, V1, V2, T1(H) and T1(V)) and single output-channel (related to maximum modal deformation of modes associated with each of six modal-cases: H1, H2, V1, V2, T1(H) and T1(V)). Modal frequency responses for these target modal-cases are shown in Fig. 7.3. It may be observed for Fig. 7.3 that horizontal modes are more sensitive to displacement response. Target-modal-case T1(H) shows quite strong frequency response. On the other hand, 2nd vertical mode shows weaker frequency response.

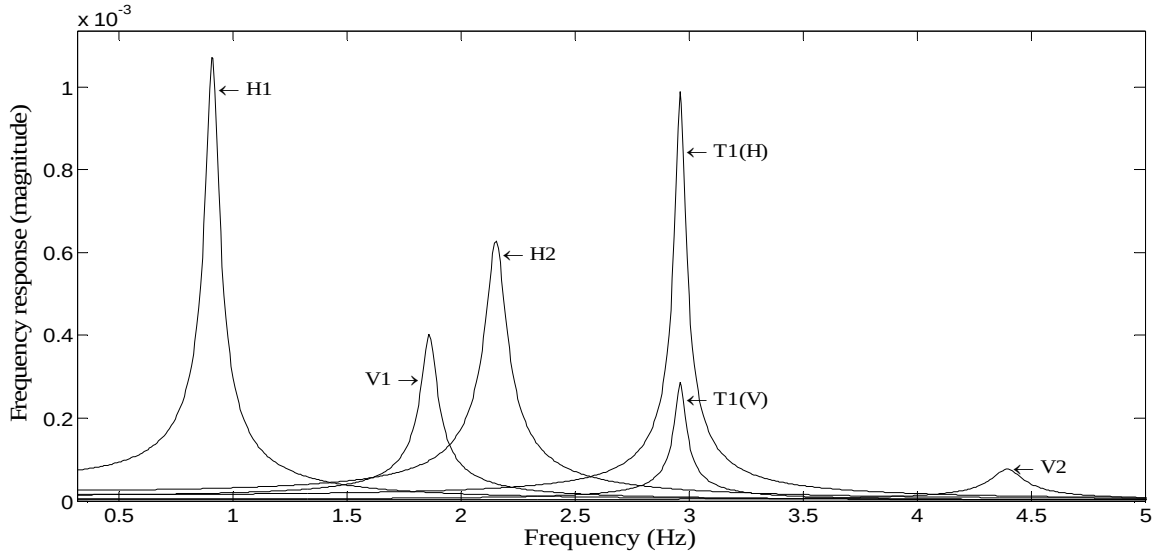

Fig. 7.3. Frequency response (magnitude) associated to the input-output channel having maximum frequency response for all the target-modal-cases

7.4. DESIGN OF MTMD SYSTEMS FOR THE SARAIGHAT BRIDGE

Six MTMD systems are assigned for the target-modal-cases H1, H2, V1, V2, T1(H) and T1(V). Based on the assigned locations of these MTMD systems, appropriate scaling of the corresponding mode-shapes are carried out and subsequently the corresponding modal masses are computed. Modal masses along with corresponding modal frequencies and modal

damping are presented in Table 7.1. It may be mentioned the considered modes are the updated modes based on direct updating technique as detailed in Chapter 6. In the computation of frequency response, damping ratio is required and the same for a mode is considered as equal to the average of experimentally identified damping ratios using three techniques as detailed in Chapter 5. Average value is taken as considerable dispersion is observed in the experimentally identified damping ratios.

Table 7.1. Modal masses, modal frequencies and modal damping ratios corresponding to the six target-modal-cases

Target-modal-cases	Modal mass (t)	Modal frequency (Hz)	Modal damping ratio
Mode (H1)	466.4475	0.9119	0.0302
Mode (V1)	519.2367	1.8624	0.0176
Mode (H2)	219.2702	2.1550	0.0198
Mode (V2)	569.6536	4.3976	0.0150
Mode (T1-H)	197.2645	2.9626	0.0074
Mode (T1-V)	2335.1670	2.9626	0.0074

7.4.1. MTMD design parameters

It is quite useful to examine MTMD parameters at the beginning of design. Observations are carried out for the 1st horizontal mode and 1st vertical mode. Four different numbers of MTMD-units are considered as 1, 4 12, 30 with a reasonable wide range of representation of MTMD-units numbers. The total mass assigned to the secondary system i.e. total mass of all the MTMD systems put together (m_{TMD}) is taken as 1% of total superstructure mass, which amounts to 10.123 metric ton (t). Wide range of possible mass ratio (μ_i) for a mode (i^{th}) is considered as mentioned in step (a) of Section 7.2.4. This range is considered in such a way that actual mass of the corresponding MTMD system varies in a range ($0.01m_{\mathrm{TMD}}$) to ($0.95m_{\mathrm{TMD}}$). For a given number of MTMD-units and given mass ratio, the optimal value of

the parameters f_i, β_i and ξ_{Ti} are evaluated to achieve minimum H_∞ norm value. Such optimal parameters β_i^{opt}, f_i^{opt} and ξ_{Ti}^{opt} along with the minimum norm values for 1st horizontal and 1st vertical modes are shown in Figs. 7.4–7.7. Plot of β_i^{opt} is avoided for the number of MTMD-units as one as in Fig. 7.4, since the parameter β_i becomes zero for the number of MTMD-units as one. This parameter shows an increasing trend with increasing mass ratio for any numbers of MTMD-units. The parameter f_i^{opt} appears less sensitive to mass ratio as well as numbers of MTMD-units and appears quite close to unity as shown in Fig. 7.5. The optimal damping ratio ξ_{Ti}^{opt} is found to increase with the increasing mass ratio as shown in Fig. 7.6. Moreover, ξ_{Ti}^{opt} is observed to get reduced with the increasing numbers of MTMD-units. Finally, Fig 7.7 demonstrates that higher minimization of norm can be achieved with higher mass ratios. Higher numbers of MTMD-units can also be helpful for higher minimization of norm, though increasing the numbers of MTMD-units may not increase the performance proportionally.

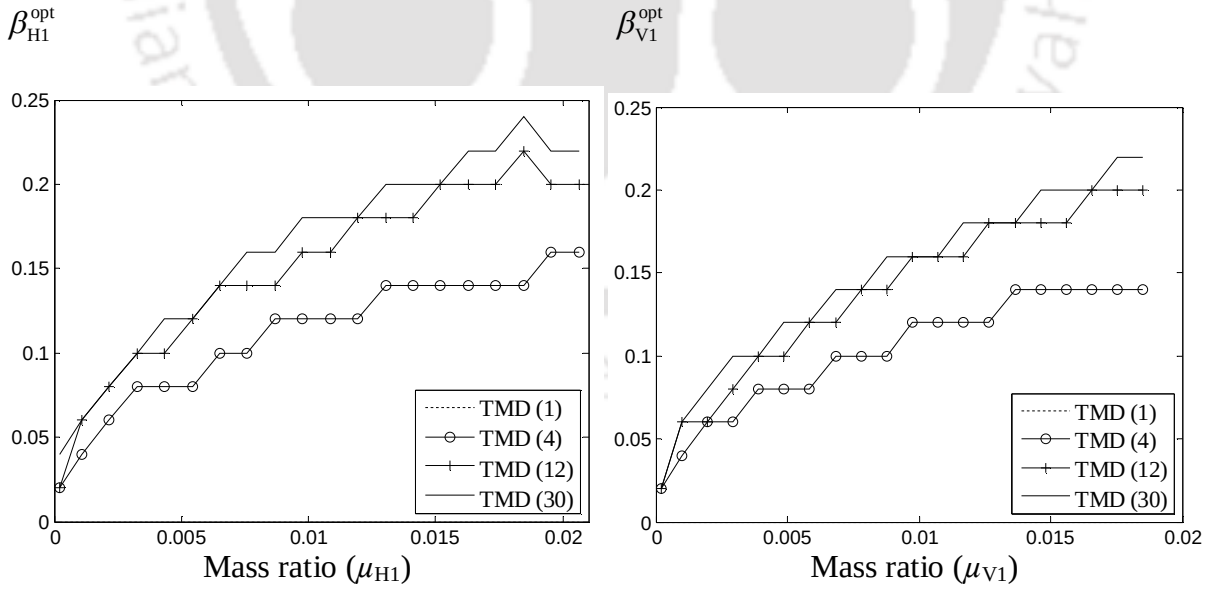

(a) (b)

Fig. 7.4. Optimal parameter β_i^{opt} with various mass ratio and numbers of MTMD-units corresponding to (a) 1st horizontal mode and (b) 1st vertical mode

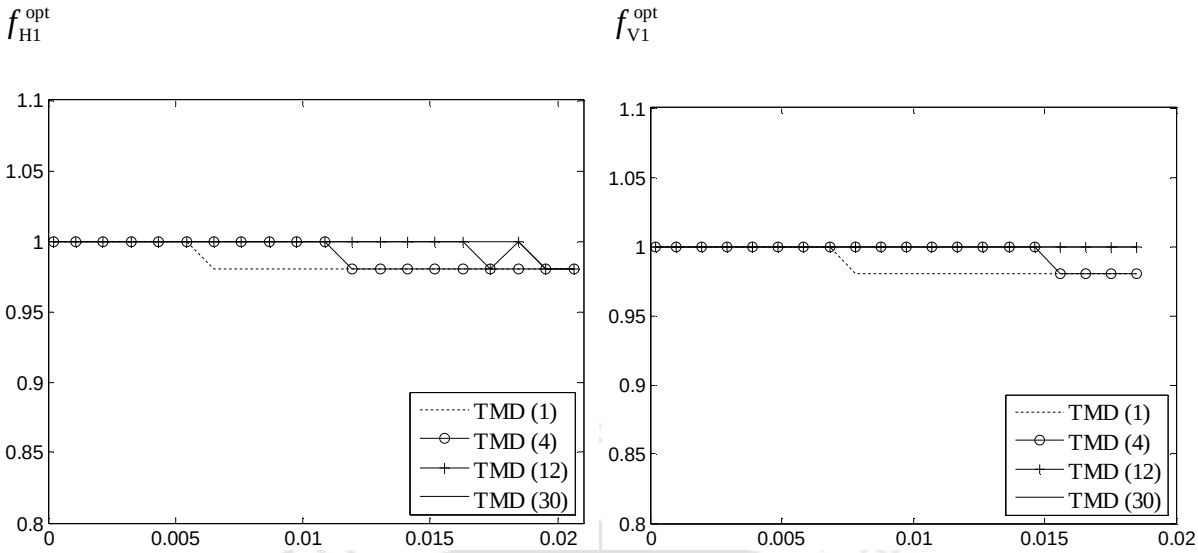

Fig. 7.5. Optimal parameter f_i^{opt} with various mass ratio and numbers of MTMD-units corresponding to (a) 1st horizontal mode and (b) 1st vertical mode

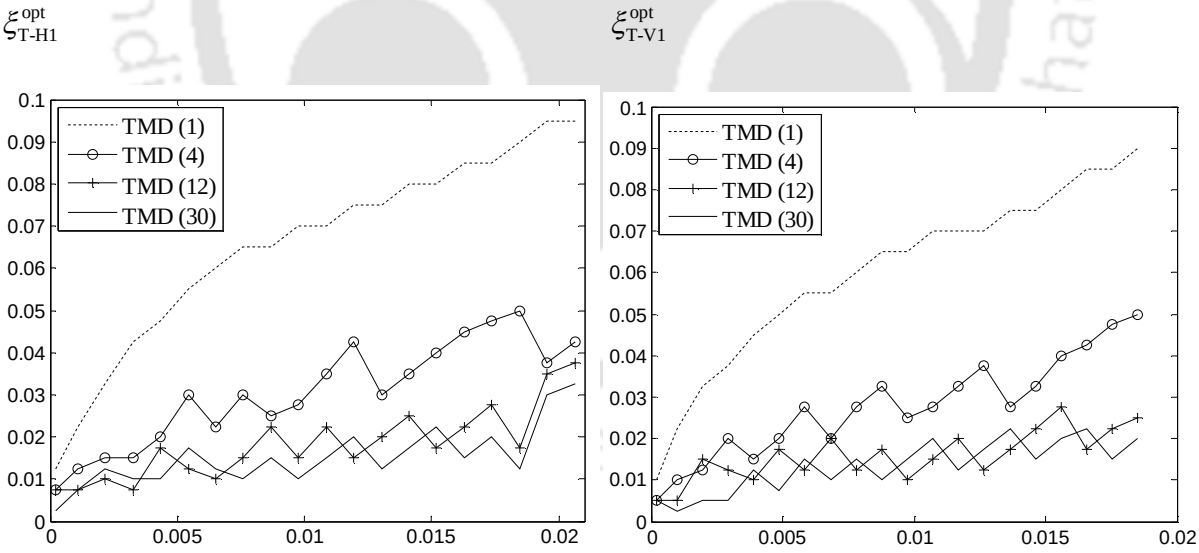

Fig. 7.6. Optimal parameter ξ_{Ti}^{opt} with various mass ratio and numbers of MTMD-units corresponding to (a) 1st horizontal mode and (b) 1st vertical mode

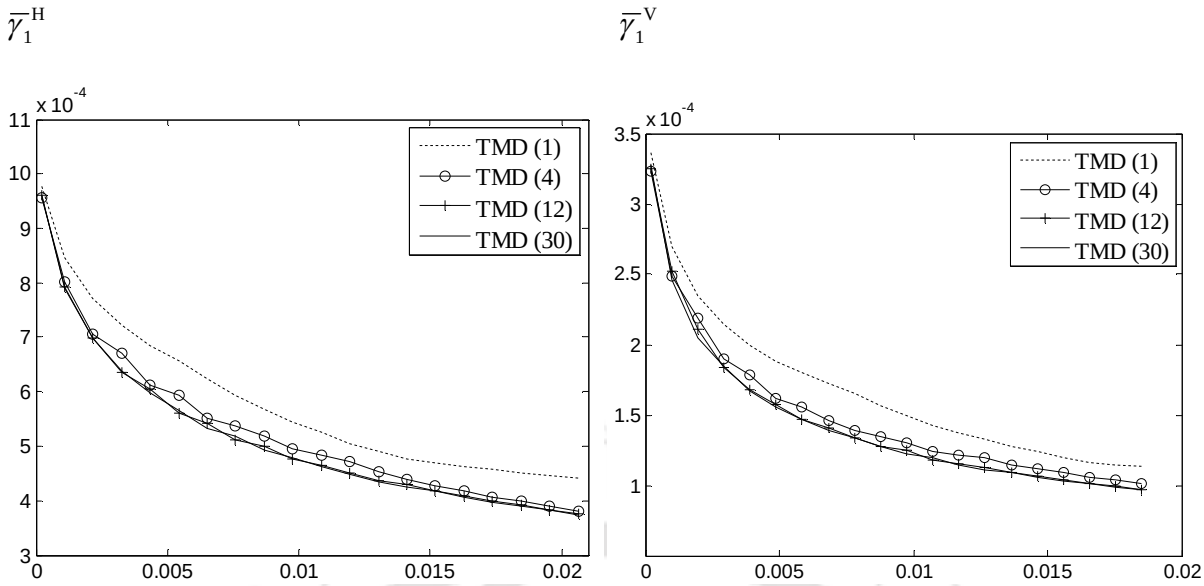

Fig. 7.7. Minimum values of norm with various mass ratio and numbers of MTMD-units corresponding to (a) 1st horizontal mode and (b) 1st vertical mode

7.4.2. MTMD stroke length

Stroke length is an important issue which becomes evident while actually designing the TMD system. Sadek et al. (1997) demonstrated that stroke length can be reduced by increasing the damping. An alternative study is performed in the present study by considering a SDOF primary system coupled with MTMD system, where stroke length issue is considered in a more general way using the value of H_∞ norm. Moreover the numbers of MTMD-units are also considered as a parameter here. To carry out this exercise three types of system (SISO type) are formed: (i) system (sys_{P}) considering input and output channels as the DOF of primary system, while primary system is not coupled with MTMD system (ii) system (sys_{C}) considering input and output channels as the DOF of primary system, while primary system is coupled with MTMD system (iii) system (sys_i) considering input and output channels as the DOF of primary system and the DOF of j^{th} MTDM-unit, while primary system is coupled

with MTMD system. Two quantities considered for observation are: (a) max($\|sys_1\|_\infty$, $\|sys_2\|_\infty$, … $\|sys_p\|_\infty$) and (b) ratio of $\|sys_C\|_\infty$ and $\|sys_P\|_\infty$. Modal mass, modal damping coefficient and modal stiffness corresponding to the 1st horizontal mode are considered as the primary system. Further, mass ratio of 5% and parameters β=0 and f=1 are reasonably considered. Two quantities, as mentioned in (a) and (b) above, are plotted in Fig. 7.8. It is clearly observed from Fig. 7.8(a) that stroke length is expected to decrease with the increasing damping ratio. However, just adhering with the objective of stroke length minimization may lead to compromise with the control performance as shown in Fig. 7.8(b). Interestingly, numbers of MTMD-units have almost no effect based on the assumed values of parameters as: β=0 and f=1. Although this observation may not be same for other values of β and f, however numbers of MTMD-units may be considered as lesser sensitive parameter

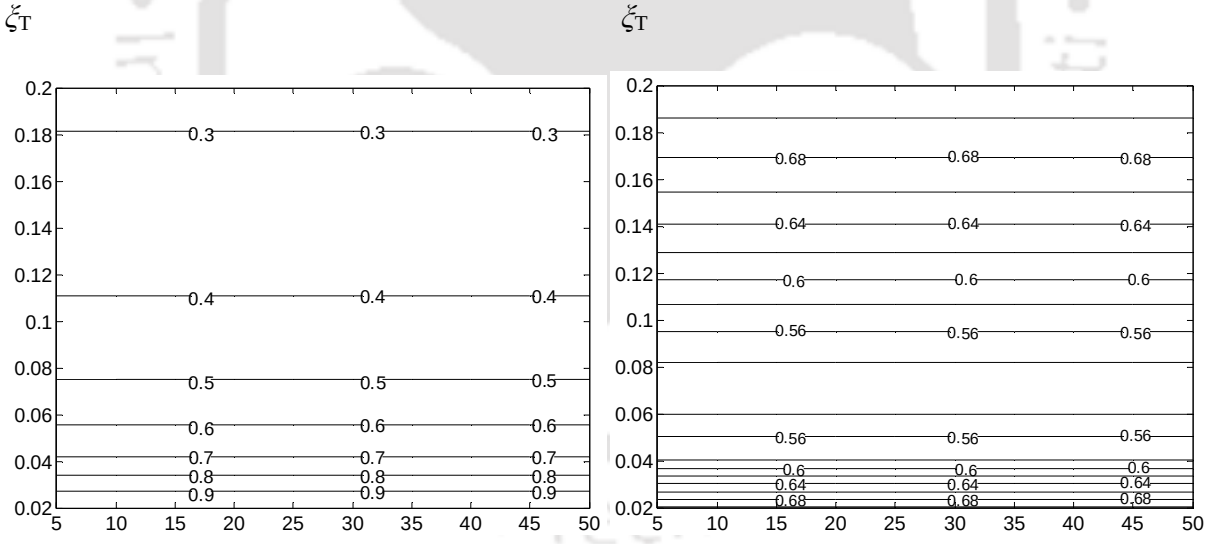

(a) (b)

Fig. 7.8. Observation on stroke length in terms of (a) max($\|sys_1\|_\infty$, $\|sys_2\|_\infty$, … $\|sys_p\|_\infty$) (normalized to unity using overall maximum value over the plot range); (b) ratio of $\|sys_C\|_\infty$ and $\|sys_P\|_\infty$

regarding the issue of stroke length. In the present work, lower demands of damping ratio is observed as shown in Fig. 7.6. Further detailed studies regarding stoke length will be appropriate while actually designing the MTMD system. Presently, a lower bound for damping ratio (ξ_{Ti}) is fixed as 0.02 from consideration of the issue of stroke length.

7.4.3. Evaluation of MTMD systems for multiple target modes

The computation regarding the optimal parameters of MTMD systems is carried out according to the steps mentioned in Section 7.2.4. The range of mass ratio is considered such that actual mass of the corresponding modal MTMD system varies in a range from ($0.01m_{TMD}$) to ($0.95m_{TMD}$). Optimization is carried out based on exhaustive search. Exhaustive search is considered as very basic and natural choice as global optimization tool, however computational cost becomes the primary disadvantage of this approach. The number of variables in the present optimization problem is just three and moreover the ranges of variables are not large as shown in Figs. 7.4–7.5. Hence exhaustive search may be considered as a reasonable choice as optimization tool in this problem, though there are scopes for applying further sophisticated techniques. Ranges of optimization variables are considered as (a) $0 \le \beta_i \le 0.4$ (b) $0.85 \le f_i \le 1.15$ (c) $0.02 \le \xi_{Ti} \le 0.20$. Optimal parameters are identified for four numbers of MTMD-units as 1, 4, 12 and 30. These optimal parameters are presented in Table 7.2. It may be mentioned that lower bound of β_i is a compulsory requirement while the lower bound of ξ_{Ti} is the stroke length requirement. Except these two lower bounds none of the optimal parameters have been close to the search-bounds as shown in Table 7.2. The optimal mass assigned to a MTMD system is represented as ratio ($\bar{\mu}_i^{opt}$) with respect to the total secondary system mass (m_{TMD}) instead of modal mass ratio for better understanding. Significant higher mass demand is observed for the 1st horizontal mode compared to other

target-modal-cases. Vertical-control of the torsional mode demands more mass for MTMD system in comparison to its horizontal-control though frequency response is stronger in

Table 7.2. Optimal parameters of the MTMD systems for various numbers of MTMD-units

MTMD parameters	Units no. of MTMD	Target-modal-cases					
		H1	V1	H2	V2	T1(H)	T1(V)
$\bar{\mu}_i^{\text{opt}}$	1	0.5889	0.2982	0.0100	0.0100	0.0248	0.0841
	4	0.5889	0.2537	0.0248	0.0100	0.0248	0.1137
	12	0.5889	0.2537	0.0248	0.0100	0.0248	0.1137
	30	0.5296	0.2982	0.0248	0.0100	0.0248	0.1285
β_i^{opt}	1	0.0000	0.0000	0.0000	0.0000	0.0000	0.0000
	4	0.1400	0.0800	0.0400	0.0000	0.0200	0.0000
	12	0.1800	0.1000	0.0400	0.0000	0.0400	0.0000
	30	0.1800	0.1200	0.0400	0.0000	0.0400	0.0000
f_i^{opt}	1	0.9800	1.0000	1.0000	1.0000	1.0000	1.0000
	4	0.9800	1.0000	1.0000	1.0000	1.0000	1.0000
	12	1.0000	1.0000	1.0000	1.0000	1.0000	1.0000
	30	1.0000	1.0000	1.0000	1.0000	1.0000	1.0000
$\xi_{\text{T}i}^{\text{opt}}$	1	0.0750	0.0550	0.0200	0.0200	0.0250	0.0200
	4	0.0300	0.0225	0.0200	0.0200	0.0200	0.0200
	12	0.0200	0.0200	0.0200	0.0200	0.0200	0.0200
	30	0.0200	0.0200	0.0200	0.0200	0.0200	0.0200

Table 7.3. Designed spring-stiffness of the MTMD units

	Units no. of MTMD	Target-modal-cases					
		H1	V1	H2	V2	T1(H)	T1(V)
Spring Stiffness (KN/m)	1	187.9570	413.3210	18.5600	77.2850	87.0520	294.9510
	4	46.6060	87.6910	11.5070	19.3210	21.7590	99.7260
	12	16.1530	29.2220	3.8370	6.4400	7.2510	33.2420
	30	5.8162	13.7244	1.5347	2.5762	2.9005	15.0293

horizontal direction. The V2 mode demands least mass as its frequency response is significantly lower. Stiffness values for the units (all the units in a MTMD system are designed with equal stiffness) of designed MTMD systems are presented in Table 7.3.

Finally, it is interesting to observe the behaviour of the modal coordinates (Q_i) in terms of frequency response to understand the control performance while the coupled MTMD systems are considered with optimal parameters. Such a modal frequency response is evaluated along similar input-output channel like its uncontrolled counterpart as mentioned in Section 7.3. Modal frequency responses for six target-modal-cases associated to various numbers of MTMD-units as considered are shown in Figs. 7.9(a–d). Figs. 7.9(a–d), in general, demonstrate an increasing reduction performance of frequency responses associated to all the modal cases with increasing number of MTMD-units. However, improvement in performance is not so significant while the numbers of MTMD-units are increased from 12 to 30. Minimum values of frequency response functions (for displacement) for all the target-modal-cases are presented in Table 7.4 corresponding to various numbers of MTMD-units as considered.

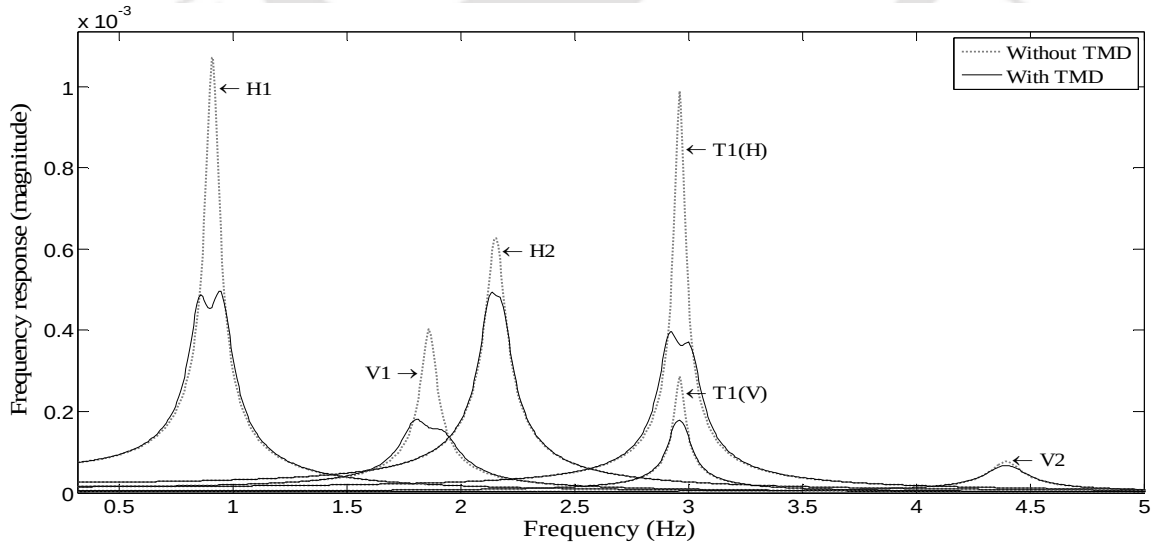

(a)

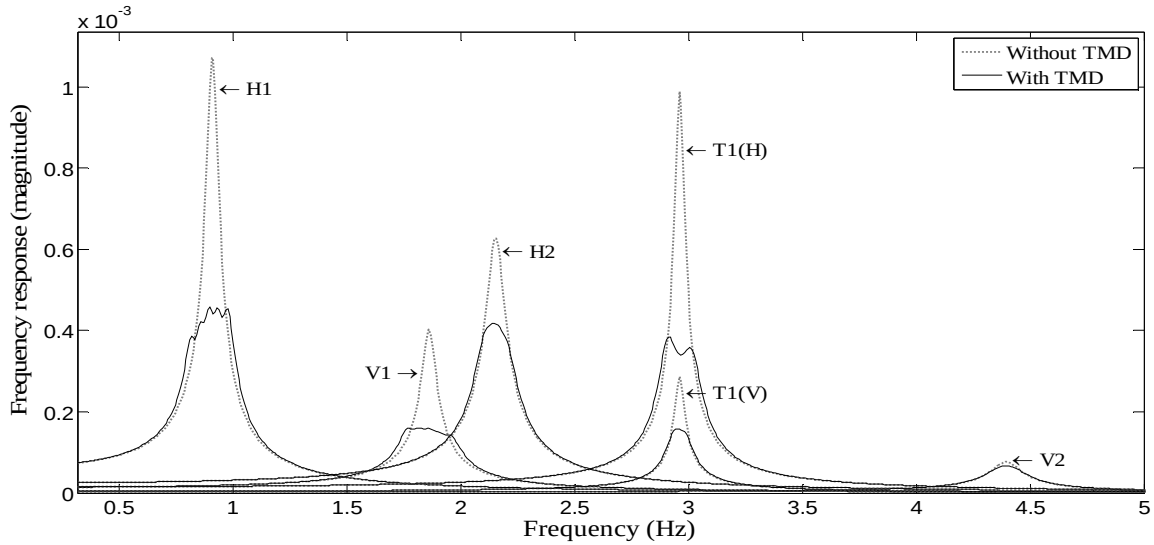

(b)

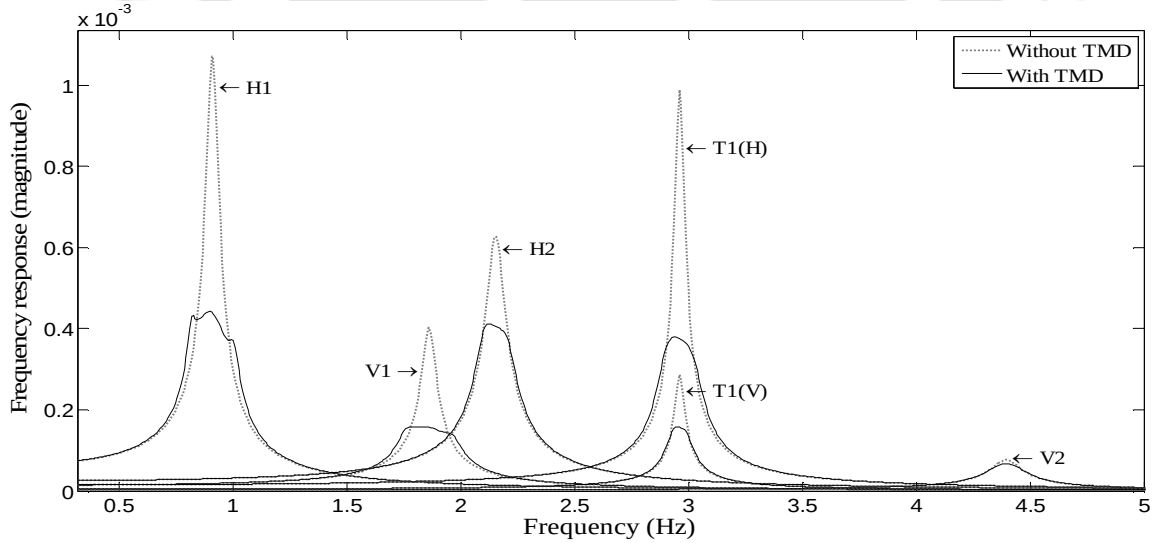

(c)

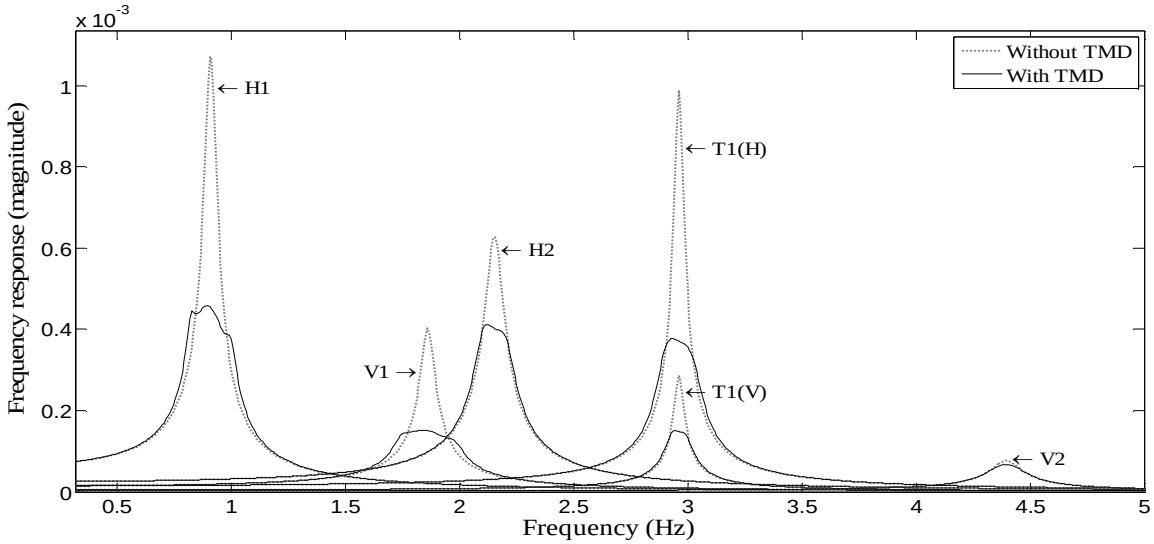

(d)

Fig. 7.9. Modal frequency responses for six modal cases associated to number of MTMD-units as (a) 1 (b) 4 (c) 12 and (d) 30

Table 7.4. Minimum norm values associated to optimal parameters of the MTMD systems

	Without TMD	**With TMD (*n*=1)**	**With TMD (*n*=4)**	**With TMD (*n*=12)**	**With TMD (*n*=30)**
Mode (H1)	0.001082	0.000493	0.000457	0.000443	0.000458
Mode (V1)	0.000403	0.00018	0.000161	0.000158	0.000152
Mode (H2)	0.000628	0.000492	0.000417	0.000412	0.000412
Mode (V2)	0.000077	0.000067	0.000067	0.000067	0.000067
Mode (T1-H)	0.000993	0.000396	0.000383	0.000379	0.000377
Mode (T1-V)	0.000289	0.000179	0.000157	0.000157	0.000151

7.5. NUMERICAL TIME HISTORY SIMULATION

Time history simulation is carried out for observation on control behaviour. Three types of loading are considered as: (a) vehicle loading (b) random excitation along all DOFs (c) base-excitation. In all the cases, noise (Gaussian white noise) is considered as excitation with

reasonably wide frequency spectrum. Moreover, in all the simulations noise is considered with duration of 50 sec with sampling time of 0.02 sec. A sample noise-excitation is plotted in Fig. 7.10(a) along with the frequency spectrum in terms of fft-amplitude as in Fig. 7.10(b).

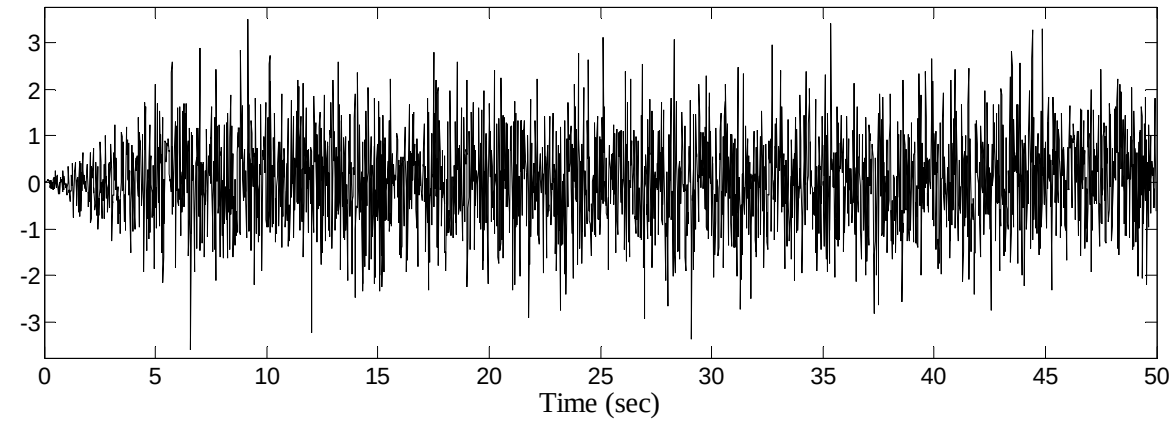

(a)

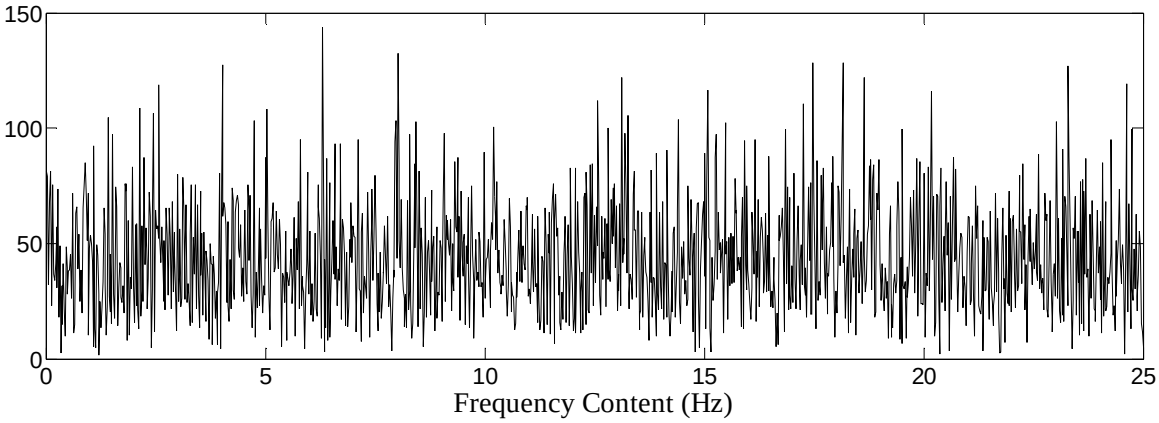

(b)

Fig. 7.10. (a) A typically considered noise-excitation signal; (b) corresponding frequency spectrum in terms of fft-amplitude

The vehicle loading is considered along both the road as well as rail level as shown in Fig. 7.11. Different white noise excitations are provided at different loading points. In case of loading type (b), superstructure is excited along all DOFs by randomly generated white noise.

In the final type of load simulation, base is excited along all the three directions using a white-noise signal. All these simulation exercises are carried out using optimal MTMD parameters having 12 numbers of MTMD-units, as this configuration shows better performance than the cases of 1 and 4 as well as shows almost similar performance with the case of 30. Performances vary with different runs of simulation using different sets of noise samples. A simulation run having reasonably good control performance is considered for observation on each of the loading case. Vibration control at the deck level (carrying traffics) is usually considered important. In case of this Saraighat Bridge, it is observed that the rail-level deck shows much higher modal deformations than the road-level deck. In view of this, vibration responses at the mid span along the rail level are considered for the time history plot for the demonstration of control performance. Such time history plots for vehicle loading, random excitation along all DOFs and base-excitation are shown in Figs. 7.12, 7.13 and 7.14 respectively. Both horizontal and vertical responses are considered except for the vehicle loading case. Responses are shown as normalized with respect to the maximum response of the uncontrolled response. Reasonably good control performances are observed in all these simulations. Control performances are quantified in terms of maximum control as well as root mean square (RMS) value and presented in Table 7.5. Such control performances using the total secondary system mass as 1% of the super structure mass may be considered as reasonably satisfactory.

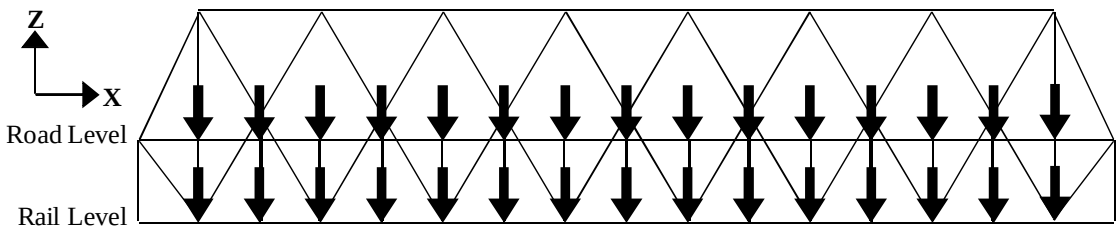

Fig. 7.11. Locations of vehicle loading along both rail and road level

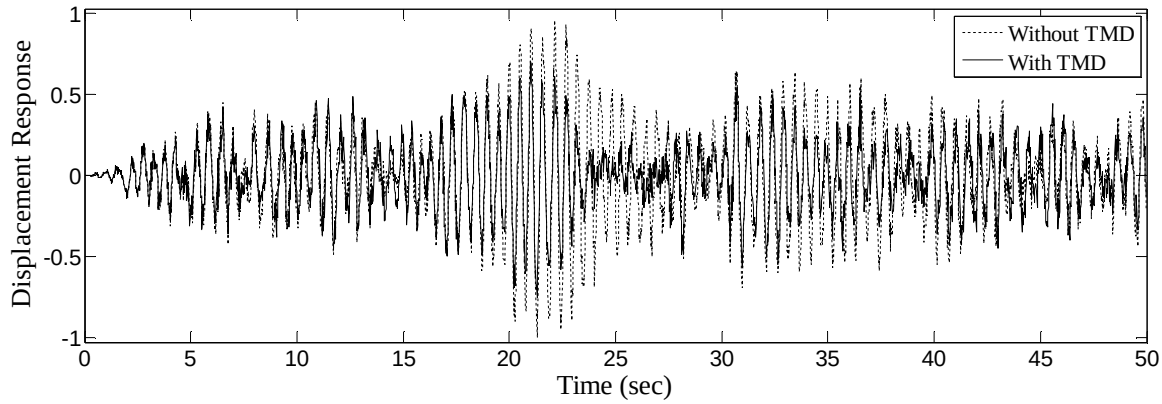

Fig. 7.12. Time history plot demonstrating control performance along vertical direction subjected to vehicle loading

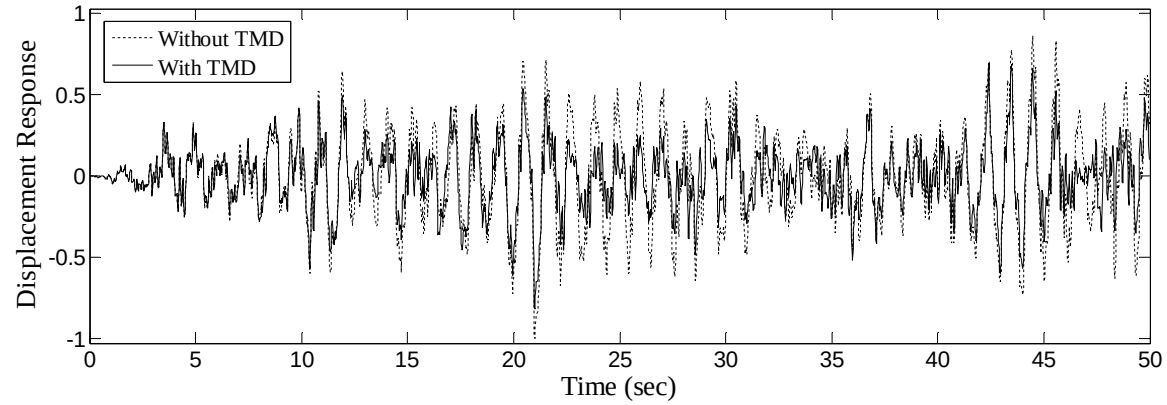

(a)

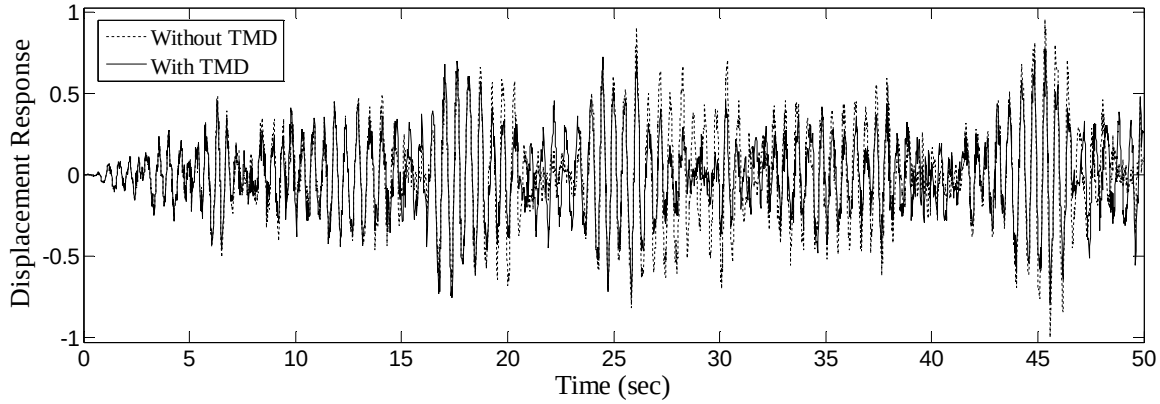

(b)

Fig. 7.13. Time history plot demonstrating control performance along (a) horizontal and (b) vertical directions subjected to random excitation along all DOFs

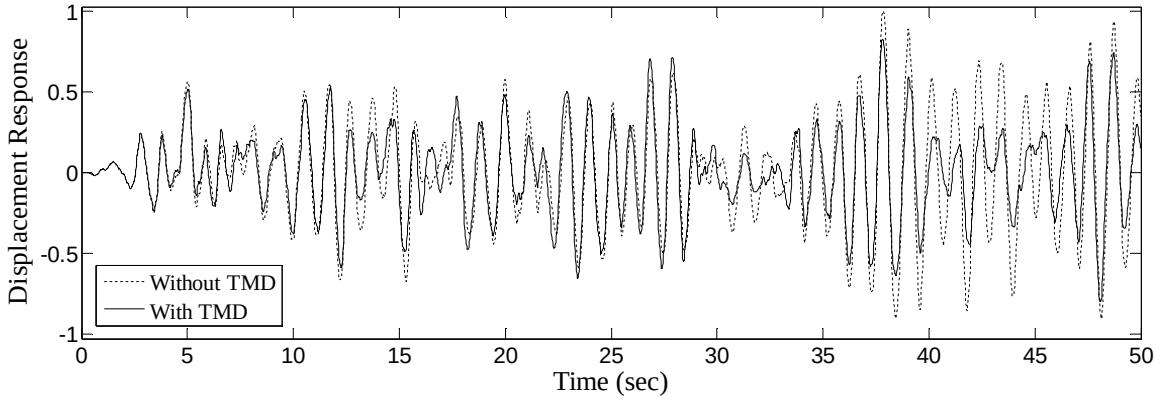

(a)

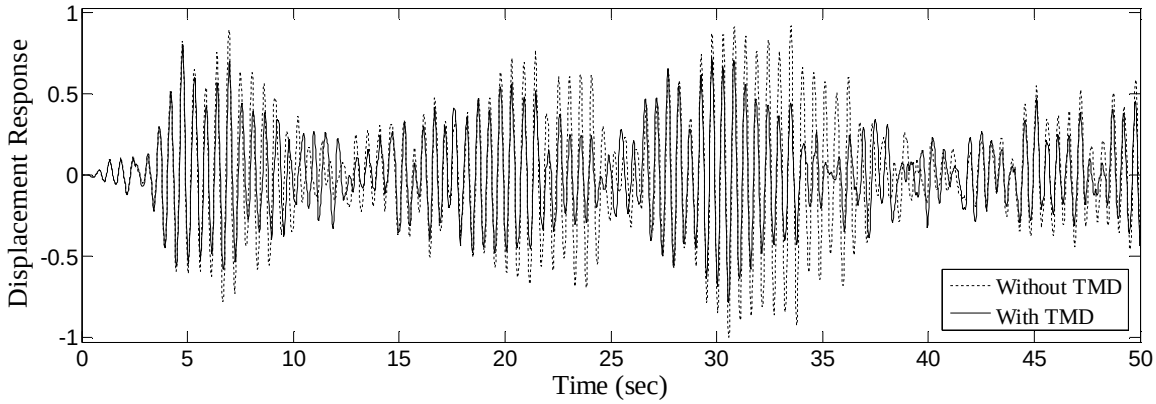

(b)

Fig. 7.14. Time history plot demonstrating control performance along (a) horizontal and (b) vertical directions subjected to base-excitation

Table 7.5. Control performances in time history for various loading cases

Excitation cases	Response direction	Control performance	
		Max (%)	RMS (%)
Random vehicle loading	Vertical	24.47	27.76
Random superstructure loading	Horizontal	18.39	29.94
	Vertical	21.66	14.89
Random base-excitation	Horizontal	17.78	20.83
	Vertical	19.67	26.46

7.6. CONCLUDING REMARKS

A strategy using modal frequency response function (FRF) is proposed based on the traditional mode-wise control approach. Further, an approach for simultaneous control of horizontal, vertical and torsional modes is presented in this study. Design of TMD devices for the Saraighat Bridge are carried out based on such approach of simultaneous control of dominant horizontal, vertical and torsional modes. Therefore, the designed TMD system is supposed to perform effectively against loading of general type. Prominent modes of the Saraighat Bridges as 1^{st} horizontal, 1^{st} vertical, 2^{nd} horizontal, 2^{nd} vertical and 1^{st} torsional modes are simultaneously considered in the design of MTMD system. Following concluding remarks are drawn from this study:

(a) Designed MTMD systems assigned with 1% of the total superstructure-mass has been quite effective to reduce the peak frequency responses.

(b) Equal weightage has been provided for both the cases of horizontal (transverse) and vertical modes based on the proposed strategy. Such consideration of weightage is duly reflected in the control performances in both the directions.

(c) The designed MTMD system has demonstrated good control performance against different types of loading i.e. vehicle type loading as well as random superstructure loading.

(d) Design of the MTMD systems is carried out for non-base excitation type loading. However, such deign is observed to perform well in case of seismic loading as well, since design of the MTMD systems is carried out in a mode-wise manner.

Chapter 8

SUMMARY AND CONCLUSIONS

8.1. SUMMARY

The present study is an effort involving both analytical and experimental studies associated with the domains of structural lifespan management like SHM and structural vibration control (passive). A very important existing large truss bridge structure, named as Saraighat Bridge which is situated in northeast region of India has been considered as the sample structure in the present study. Health monitoring aspect associated to the present study can be considered as vibration based non-continuous health monitoring. In this health monitoring strategy, modal parameters identified before and after the occurrence of damages are taken into account for damage diagnosis. The health monitoring aspect of the present study however has been kept limited only to modal parameter identification as field data has been collected over a relatively small period of time. In-stead, additional studies have been carried out for the analytical design of passive vibration control system for the Bridge using updated FE model. However, the identified modal parameters would be useful as benchmark for comparison during the next phase of modal identification. The Saraighat Bridge is in service for more than fifty years as a lifeline structure for the north-east India and moreover situated in the highest seismic zone of India. Therefore, the present study considering such a large bridge structure is quite useful. Although the experimental and vibration control aspects of this study are associated with the Saraighat Bridge, works/developments related to the analytical aspect of this study are indeed general in nature.

Modal parameters of the Saraighat Bridge are identified by carrying out OMA or output-only system identification. Optimal placement of sensors, another area of research associated to the wide area of SHM, is studied in details. A modal approach is considered for

sensor placement evaluation where modal participation at individual degree of freedom (DOF) is evaluated separately for the target modes. Subsequently suitable locations are identified using these participation profiles. Modal contribution in output energy (MCOE) is proposed as modal measure to evaluate modal participation and the same has been applied in this modal approach framework for sensor placement evaluation. MCOE technique is found to be in very good agreement with other major techniques for optimal sensor placement. Regarding sensor placement in Saraighat Bridge, it is observed that the rail-level deck is suitable for placing the accelerometers. Ambient acceleration responses recorded using suitably placed accelerometers are utilized by OMA techniques to identify modal parameters like natural frequencies, mode shapes and damping ratios. Two approaches are considered for enhanced precision against various unfavourable conditions involved in OMA like measurement noise, deviations of real ambient vibration from theoretical assumption of white-noise induced vibration. These approaches are: (a) employing multiple techniques both in time and frequency domain for comparison of identified modal parameters from different techniques and (b) identifying modal parameters in terms of central tendency and dispersion based on multiple data sets.

After the identification of modal parameters, FE model updating is carried out for an initial FE model of the Saraighat Bridge to obtain an updated model having modal parameters with closer agreement with the experimentally identified modal parameters. In the updating of FE model, both direct and iterative techniques are observed to be used. In the present study, the sole purpose of updating is to design a more efficient passive control system based on a modal approach in-stead of any damage detection study. Hence, direct updating is considered for the Saraighat Bridge, where the adopted direct updating techniques reproduce modal parameters, which are same as the experimentally identified modal parameters. Two important techniques, with the ability of exact reproduction of experimental natural

frequencies and mode shapes in the updated model are employed, namely, Berman and Nagy updating technique and matrix mixing updating technique. Eight experimentally evaluated mode shapes at rail-deck level having 28 DOFs have been expanded to 854 DOFs matching the size of analytical matrices. These expanded measured mode shapes associated to this complicated bridge structure have demonstrated good agreement with their analytical counterparts. Both of the updating techniques have determined updated mass and stiffness matrices while exactly retaining the measured natural frequencies and mode shapes (in expanded form). The updated mode shapes along the rail-deck level are in excellent agreement with those identified experimentally. After performing FE model updating, the final phase of the study is carried out regarding design of passive vibration control system for the Saraighat Bridge using the updated FE model. Tuned mass damper (TMD) system is used as the passive vibration control device since it is known as one of the oldest passive vibration control devices. The TMD systems are efficient and have found wide applications for vibration control. Multiple TMD (MTMD) system, widely accepted to perform better than single unit based TMD system, is considered. A strategy using modal frequency response function (FRF) is proposed based on the traditional mode-wise control approach. Further, an approach for simultaneous control of horizontal and vertical modes is proposed in this study. Prominent modes both in horizontal (transverse) and vertical directions are simultaneously targeted in design considerations of TMD system by assigning equal weightage for both the directions. Therefore, the designed TMD system is supposed to perform effectively against vehicle type loading as well as wind type loading, contrary to the traditional design, where either transverse or vertical modes are usually taken into account. Such design is also expected to perform reasonably well against seismic excitations, since the design is carried out based on mode-wise approach. Predominant modes of the Saraighat Bridges as 1st horizontal, 1st vertical, 2nd horizontal, 2nd vertical and 1st torsional modes are

simultaneously considered in the design of MTMD system based on the proposed strategy, where MTMD systems have been assigned mass as 1% of the total superstructure mass.

8.2. MAJOR FINDINGS

Major findings ascribed to the present study may be summarized as follows:

(a) A modal measure having simple physical understanding is proposed and referred as MCOE. Modal participations of any mode along individual DOF evaluated using MCOE and based on the assumption of low damping as well as well separated modes demonstrate exact analytical agreement with modal participations evaluated using popularly used EI method. Such comparisons of modal participations as carried out numerically for the sample large bridge structure demonstrate very good agreement with EI method, good agreement with MHSV as well as system norms and reasonable agreement with MKE method. MCOE based technique adopts flexible approach for sensor location identification for multiple target modes. Thus, the proposed technique may be viewed as an effective methodology with better physical understanding for optimal placement of sensors in OMA.

(b) The proposed modal measure MCOE has no limitation for computational difficulty while considering acceleration response unlike other modal measures e.g. H_2, H_∞, Hankel norms. MCOE considers the free vibration response instead of forced vibration response without contribution from direct feed through matrix [*E*].

(c) MCOE only considers output unlike other existing modal measures e.g. system norms which considers both the input and output. Thus MCOE is more suitable modal measure for sensor placement based modal approach in OMA, since precise identification of input-locations is difficult in OMA.

(d) In the present study, it has been possible to identify the major horizontal, vertical and torsional modes for such a large and fairly complicated truss bridge structure like Saraighat Bridge. Further, identification in the form of central tendency employing multiple techniques has ensured higher confidences (on those identified modal parameter of Saraighat Bridge) against the effect of measurement noise as well as deviations of real ambient vibration from theoretical assumption of white-noise induced vibration.

(e) Central tendencies of mode shapes as well as natural frequencies identified using three techniques are found to be in good agreement. Moreover, 95% confidence bounds for the natural frequencies are observed to be in narrow range. Higher variations, however, are observed for damping ratios identified using three techniques.

(f) The adopted direct updating techniques (Berman and Nagy updating technique; matrix mixing updating technique) have performed the updating fairly well for a large bridge structure like Saraighat Bridge. Updated mass and stiffness matrices are evaluated with quite insignificant changes over the initial analytical matrices and at the same time exact matching is maintained between the updated modal parameters and the experimental modal parameters.

(g) Designed MTMD systems with assigned mass of 1% of the total superstructure mass have been quite effective to reduce the peak frequency responses. It has been possible to reduce the peak frequency responses in both the vertical and transverse directions simultaneously. Therefore, the designed MTMD systems are observed to be effective for general types of loadings which may be active along vertical or transverse or along both the directions. Studies through numerical simulations have demonstrated good level of control performance.

8.3. SCOPE OF FUTURE WORKS

Following additional works may be considered as the scope of future works:

(a) SHM activities for the Saraighat Bridge, a lifeline structure of the North-Eastern part of India, has been initiated in the present study in terms of vibration based non-continuous health monitoring approach. Continuous health monitoring of this lifeline bridge structure remains as major scope of future work.

(b) Working towards suitable damage detection framework for such a large truss bridge structure taking into account the identified modal parameters before and after occurrences of major event (if any) remains as an interesting scope of future work.

(c) FE model updating for this large bridge structure with more physically meaningful updating techniques like Bayesian updating technique etc.

(d) Design of actual MTMD system for the Saraighat Bridge based on the analytical design guidelines carried out in the present study and use of same for vibration control of the bridge at site.

REFERENCES

Abé M., Fujino Y., Dynamic characterization of multiple tuned mass dampers and some design formulas, *Earthquake Engineering and Structural Dynamics* 23 (8) (1994) 813–835.

Abé M., Igusa T., Tuned mass dampers for structures with closely spaced natural frequencies, *Earthquake Engineering and Structural Dynamics* 24 (2) (1995) 247–261.

Altunişik A., Bayraktar A., Sevim B., Özdemir H., Experimental and analytical system identification of Eynel arch type steel highway bridge, *Journal of Constructional Steel Research* 67 (12) (2011a) 1912–1921.

Altunişik A., Bayraktar A., Sevim B., Output-Only System Identification of Post-tensioned Segmental Concrete Highway Bridges, *Journal of Bridge Engineering* 16 (2) (2011b) 259–266.

Alvin K.F., Robertson A.N., Reich G.W., Park K.C., Structural system identification: from reality to models, *Computers and Structures* 81 (2003) 1149–1176.

Andry A.N., Shapiro E.Y., Chung J.C., Eigenstructure assignment for linear systems, *IEEE Transactions on Aerospace and Electronic Systems* AES-19 (5) (1983) 711–729.

Asami T., Nishihara O., Baz A.M., Analytical solutions to H_∞ and H_2 optimization of dynamic vibration absorbers attached to damped linear systems. *Journal of Vibration and Acoustics* 124 (2002) 284–295.

Au S.K., Fast Bayesian ambient modal identification in the frequency domain, Part I: Posterior most probable value, *Mechanical Systems and Signal Processing* 26 (2012a) 60–75.

Au S.K., Fast Bayesian ambient modal identification in the frequency domain, Part II: Posterior uncertainty, *Mechanical Systems and Signal Processing* 26 (2012b) 76–90.

Au S.K., Zhang F.L., Ni Y.C., Bayesian operational modal analysis: Theory, computation, practice, *Computers and Structures* 126 (2013) 3–14.

Avitabile P., O'Callahan J., Milani J., Model Correlation and Orthogonality Criteria, *Proceedings of the Sixth International Modal Analysis Conference*, Orlando, Florida, February 1988.

Bai Y., Keller T., Modal parameter identification for a GFRP pedestrian bridge, *Composite Structures* 82 (2008) 90–100.

Balageas D., Introduction to structural health monitoring. in: Balageas D., Fritzen C.P., Güemes A. (Eds.), *Structural Health Monitoring*, ISTE Ltd, USA, 2006, pp.13–40.

Baruch M., Bar-Itzhack I.Y., Optimal weighted Orthogonalization of measured modes, *AIAA Journal* 16 (4) (1978) 346–351.

Baruch M., Optimization procedure to correct stiffness and flexibility matrices using vibration data, *AIAA Journal* 16 (11) (1978) 1208–1210.

Baruch M., Methods of Reference Basis for Identification of Linear Dynamic Structures, *Proceedings of the 23rd Structures, Structural Dynamics and Material Conference*, New Orleans, Louisiana, May 1982, pp. 557–563.

Baruch M., Methods of Reference Basis for Identification of Linear Dynamic Structures, *AIAA Journal* 22 (4) (1984) 561–564.

Baruch M., Bar-Itzhack I.Y., Optimal weighted orthogonalization of measured modes, *AIAA Journal* 16 (4) (1998) 346–351.

Benedettini F., Gentile C., Operational modal testing and FE model tuning of a cable-stayed bridge, *Engineering Structures* 33 (6) (2011) 2063–2073.

Berman A., Nagy E.G., Improvement of large analytical model using test data, *AIAA Journal* 21 (8) (1983) 1168–1173.

Bishop R.E.D., Gladwell G.M.L., An investigation into the theory of resonance testing, *Philosophical Transactions of the Royal Society of London* 255 (1055) (1963) 241–280.

Bonisoli E., Delprete C., Rosso C., Proposal of a modal-geometrical-based master nodes selection criterion in modal analysis, *Mechanical Systems and Signal Processing* 23 (3) (2009) 606–620.

Brincker R., Zhang L.M., Anderson P., Modal identification of output-only systems using frequency domain decomposition, *Smart Materials and Structures* 10 (3) (2001) 441–445.

Brownjohn J.M.W., Pavic A., Experimental methods for estimating modal mass in footbridges using human-induced dynamic excitation, *Engineering Structures* 29 (11) (2007) 2833–2843.

Bruinsma N.A., Steinbuch M., A fast algorithm to compute the H_∞ norm of a transfer function matrix. *Systems and Control Letters* 14 (4) (1990) 287–293.

Bucher I., Braun S., The structural modification inverse problem: an exact solution, *Mechanical Systems and Signal Processing* 7 (1993) 217–238.

Caesar B., Update and identification of dynamic mathematical models, *Proceedings of the Fourth International Modal Analysis Conference*, Los Angeles, 1986, pp. 394–401.

Caesar B., Updating system matrices using modal test data, *Proceedings of the Fifth International Modal Analysis Conference*, London, England, April 1987, pp. 453–459.

Caetano E., Cunha Á., Magalhães F., Moutinho Carlos., Studies for controlling human-induced vibration of the Pedro e Inês footbridge, Portugal. Part 1: Assessment of dynamic behaviour, *Engineering Structures* 32 (4) (2010a) 1069–1081.

Caetano E., Cunha Á., Moutinho C., Magalhães F., Studies for controlling human-induced vibration of the Pedro e Inês footbridge, Portugal. Part 2: Implementation of tuned mass dampers, *Engineering Structures* 32 (4) (2010b) 1082–1091.

Carvalho J., Datta B.N., Gupta A., Lagadapati M., A direct method for model updating with incomplete measured data and without spurious modes, *Mechanical Systems and Signal Processing* 21 (7) (2007) 2715–2731.

Chang C.C., Gu M., Tang K.H., Tuned Mass Dampers for Dual-Mode Buffeting Control of Bridges, *Journal of Bridge Engineering* 8 (4) (2003) 237–240

Chen C.T., *Applied System Theory and Design*, Harcourt Brace College Publishers, USA, 1984.

Chen S.R., Cai C.S., Coupled vibration control with tuned mass damper for long-span bridges, *Journal of Sound and Vibration* 278 (1–2) (2004) 449–459.

Chen S.R., Wu J., Performance enhancement of bridge infrastructure systems: Long-span bridge, moving trucks and wind with tuned mass dampers, *Engineering Structures* 30 (11) (2008) 3316–3324.

Chen X., Kareem A., Efficacy of Tuned Mass Dampers for Bridge Flutter Control, *Journal of Structural Engineering* 129 (10) (2003) 1291–1300.

Cheng F.Y., *Matrix Analysis of Structural Dynamics: Applications and Earthquake Engineering*, CRC Press, 2000.

Cherng A.P., Optimal sensor placement for modal parameter identification using signal subspace correlation techniques, *Mechanical Systems and Signal Processing* 17 (2003) 361–378.

Cheung Y.L., Wong W.O., H-infinity optimization of a variant design of the dynamic vibration absorber – Revisited and new results. *Journal of Sound and Vibration* 330 (16) (2011) 3901–3912.

Conte J., He X., Moaveni B., Masri S., Caffrey J., Wahbeh M., Tasbihgoo F., Whang D., Elgamal A., Dynamic Testing of Alfred Zampa Memorial Bridge, *Journal of Structural Engineering* 134 (6) (2008) 1006–1015.

Cross E.J., Koo K.Y., Brownjohn J.M.W., Worden K., Long-term monitoring and data analysis of the Tamar Bridge, *Mechanical Systems and Signal Processing* 35 (1–2) (2013) 16–34.

CSI (Computer and Structures Inc.) Analysis Reference Manual, 2010.

Daniel Y., Lavan O., Levy R., Multiple-Tuned Mass Dampers for Multimodal Control of Pedestrian Bridges, *Journal of Structural Engineering* 138 (9) (2012) 1173–1178.

Das A.K., Dey S.S., Effects of tuned mass dampers on random response of bridges, *Computers and Structures* 43 (4) (1992) 745–750.

Datta B.N., Elhay S., Ram Y.M., Sarkissian D.R., Partial eigenstructure assignment for the quadratic pencil, *Journal of Sound and Vibration* 230 (1) (2000) 101–110.

Datta B.N., Finite element model updating, eigenstructure assignment and eigenvalue embedding techniques for vibrating systems, *Mechanical Systems and Signal Processing* 16 (1) (2001) 83–96 (special issue on Vibration Control).

Dayou J., Fixed-points theory for global vibration control using vibration neutralizer, *Journal of Sound and Vibration* 292 (3–5) (2006) 765–776.

Debnath N., Dutta A., Deb S.K., Placement of sensors in operational modal analysis for truss bridges, *Mechanical Systems and Signal Processing* 31 (2012) 196–216.

Den Hartog J.P., *Mechanical Vibrations*, McGraw-Hill, New York, 1956.

Dowell E.H., Kubota Y., Asymptotic modal analysis and statistical energy analysis of dynamical systems, *Journal of Applied Mechanics* 52 (1985) 949–957.

Doyle J.C., Francis B.A., Tannenbaum A., *Feedback Control Theory*, Macmillan Publications Co., New York, 1992.

Ewins D.J., *Modal Testing: Theory, Practice and Application*, second edition, Research Studies Press Ltd, England, 2000a.

Ewins D.J., Adjustment or updating of models, *Sadhana* 25 (3) (2000b) 235–245.

Flynn E.B., Todd M.D., A Bayesian approach to optimal sensor placement for structural health monitoring with application to active sensing, *Mechanical Systems and Signal Processing* 24 (4) (2010) 891–903.

Francis B.A., *A course in H_∞ control theory*, *Lecture Notes in Control and Information Sciences*, Vol. 88, Springer-Verlag, Berlin, 1987.

Friswell M., Mottershead J.E., *Finite Element Model Updating in Structural Dynamics*, Kluwer Academic Publishers, Dordrecht, 1995.

Friswell M.I., Inman D.J., Pilkey D.F., The direct updating of damping and stiffness matrices, *AIAA Journal* 36 (3) (1998) 491–493.

Fujino Y., Abé M., Design formulas for tuned mass dampers based on a perturbation technique, *Earthquake Engineering and Structural Dynamics* 22 (10) (1993) 833–854.

Fujino Y., Yoshida Y., Wind-induced vibration and control of Trans-Tokyo Bay Crossing Bridge, *Journal of Structural Engineering* 128 (8) (2002) 1012–1025.

Gandhi M.V., Thompson B.S., *Smart Materials and Structures*, Chapman and Hall, Chennai, India, 1992.

Gawronski W., Lim K.B., Balanced actuator and sensor placement for flexible structures, *International Journal of Control* 65 (1) (1996) 131–145.

Gawronski W., Almost-Balanced Structural Dynamics, *Journal of Sound and Vibration* 202 (5) (1997) 669–687.

Gawronski W., *Advanced Structural Dynamics and Active Control of Structures*, Springer-Verlag, New York, 2004.

Golub G.H., Van Loan C.F., *Matrix Computations*, The Johns Hopkins University Press, Baltimore, 1996.

Gu M., Xiang H., Optimization of TMD for suppressing buffeting response of long-span bridges, *Journal of Wind Engineering and Industrial Aerodynamics* 42 (1–3) (1992) 1383–1392.

Gu M., Xiang H.F., Chen A.R., A practical method of passive TMD for suppressing wind-induced vertical buffeting of long-span cable-stayed bridges and its application, *Journal of Wind Engineering and Industrial Aerodynamics* 51 (2) (1994) 203–213.

Gu M., Chen S.R., Chang C.C., Parametric study on multiple tuned mass dampers for buffeting control of Yangpu Bridge, *Journal of Wind Engineering and Industrial Aerodynamics* 89 (11–12) (2001) 987–1000.

Guyan R J., Reduction of stiffness and mass matrices, *AIAA Journal* 3 (2) (1965) 380.

Hac A., Liu L., Sensor and actuator location in motion control of flexible structures, *Journal of Sound and Vibration* 167 (2) (1993) 239–261.

Hadi M.N.S., Arfiadi Y., Optimum Design of Absorber for MDOF Structures, *Journal of Structural Engineering* 124 (11) (1998) 1272–1280

Halevi Y., Bucher I., Model updating via weighted reference basis with connectivity constraints, *Journal of Sound and Vibration* 265 (3) (2003) 561–581.

He X., Roeck G.D., System identification of mechanical structures by a high-order multivariate autoregressive model, *Computers and Structures* 64 (1997) 341–351.

He X., Moaveni B., Conte J.P., Elgamal A., Comparative study of system identification techniques applied to New Carquinez Bridge, *Proceedings of the 3rd International Conference on Bridge Maintenance, Safety and Management*, Portugal, July 2006.

He X., Moaveni B., Conte J., Elgamal A., Masri S., System Identification of Alfred Zampa Memorial Bridge Using Dynamic Field Test Data, *Journal of Structural Engineering* 135 (1) (2009) 54–66.

Heo G., Wang M.L., Satpathi D., Optimal transducer placement for health monitoring of long span bridge, *Soil Dynamics and Earthquake Engineering* 16 (7–8) (1997) 495–502.

Hermans L., Van der A.H., Guiliaume P., A frequency-domain maximum likelihood approach for the extraction of modal parameters from output-only data, *Proceedings of the ISMA*, 1998, pp. 367–376.

Ho B.L., Kalman R.E., *Effective construction of linear state-variable models from input/output functions*, Regelungstechnik 14 (1966) 545–548.

Hu W.H., Caetano E, Cunha Á. Structural health monitoring of a stress-ribbon footbridge, *Engineering Structures* (doi: 10.1016/j.engstruct.2012.06.051).

Huang C.S., Structural identification from ambient vibration measurement using the multivariable AR model, *Journal of Sound and Vibration* 241 (3) (2001) 337–359.

Ibrahim S.R., Milkulcik E.C., The experimental determination of vibration parameters from time response, *Shock and Vibration Bulletin* 46 (5) (1976) 187–196.

Ibrahim S.R., Random decrement technique for modal identification of structures, *Journal of Spacecraft and Rockets* 14 (11) (1977) 696–700.

Ibrahim S.R., Milkulcik E.C., A method for the direct identification of vibration parameters from the response, *Shock and Vibration Bulletin* 47 (4) (1977) 183–198.

Igusa T., Xu K., Vibration Control Using Multiple Tuned Mass Dampers, *Journal of Sound and Vibration* 175 (4) (1994) 491–503.

Jacquelin E., Adhikari S., Friswell M.I., A second-moment approach for direct probabilistic model updating in structural dynamics, *Mechanical Systems and Signal Processing* 29 (2012) 262–283.

James G.H., Carne T.G., Lauffer J.P., The natural excitation technique (NExT) for modal parameter extraction from operating structures, *International Journal of Analytical and Experimental Modal Analysis* 10 (4) (1995) 260–277.

Jangid R.S., Dynamic characteristics of structures with multiple tuned mass dampers, *Structural Engineering and Mechanics* 3 (1995) 497–509.

Jangid R.S., Datta T.K., Performance of multiple tuned mass dampers for torsionally coupled systems, *Earthquake Engineering and Structural Dynamics* 26 (3) (1997) 307–317.

Jensen H., Setareh M., Peek R., TMDs for Vibration Control of Systems with Uncertain Properties, *Journal of Structural Engineering* 118 (12) (1992) 3285–3296

Jo B.W., Tae G.H., Lee D.W., Structural vibration of tuned mass damper-installed three-span steel box bridge, *International Journal of Pressure Vessels and Piping* 78 (10) (2001) 667–675.

Juang J.N., Pappa R.S., An eigensystem realization algorithm for modal parameter identification and model reduction, *Journal of Guidance Control and Dynamics* 8 (5) (1985) 620–627.

Juang J.N., Pappa R.S., Effects of noise on modal parameters identified by the eigensystem realization algorithm, *Journal of Guidance Control and Dynamics* 9 (3) (1986) 294–303.

Juang J.N., Suzuki H., An eigensystem realization algorithm in frequency domain for modal parameter identification, *Journal of Vibration, Acoustics, Stress, and Reliability in Design* 110 (1988) 24–29.

Kabe A.M., Stiffness matrix adjustment using modal data, *AIAA Journal* 23 (9) (1985) 1431–1436.

Kammer D.C., Optimum approximation for residual stiffness in linear system identification, *AIAA Journal* 26 (1) (1988) 104–112.

Kammer D.C., Sensor Placement for On-Orbit Modal Identification and Correlation of Large Space Structures, *Proceedings of the American Control Conference*, San Diego, CA, May 1990, pp. 2984 – 2990.

Kenigsbuch R., Halevi Y., Model updating in structural dynamics: a generalised reference basis approach, *Mechanical Systems and Signal Processing* 12 (1) (1998) 75–90.

Kirkegaard P.H., Brincker R., On the optimal locations of sensors for parametric identification of linear structural systems, *Mechanical System and Signal Processing* 8 (6) (1994) 639–647.

Kirkegaard P.H., Anderson P., Brincker R., Identification of civil engineering structures using multivariate ARMAV and RARMAV models, *Proceedings of the International Conference on Identification in Engineering Systems*, Swansea, 1996, pp. 678–688.

Kuo Y.C., Lin W.W., Xu S.F., New Methods for Finite Element Model Updating Problems, *AIAA Journal* 44 (6) (2006) 1310–1316.

Kwon H.C., Kim M.C., Lee I.W., Vibration control of bridges under moving loads, *Computers and Structures* 66 (4) (1998) 473–480.

Kwon S.D., Park K.S., Suppression of bridge flutter using tuned mass dampers based on robust performance design, *Journal of Wind Engineering and Industrial Aerodynamics* 92 (11) (2004) 919–934.

Larose G.L., Larsen A., Svensson E., Modelling of tuned mass dampers for wind-tunnel tests on a full-bridge aeroelastic model, *Journal of Wind Engineering and Industrial Aerodynamics* 54–55 (1995) 427–437.

Larsena A., Svensson E., Andersen H., Design aspects of tuned mass dampers for the Great Belt East Bridge approach spans, *Journal of Wind Engineering and Industrial Aerodynamics* 54–55 (1995) 413–426.

Li C., Optimum multiple tuned mass dampers for structures under the ground acceleration based on DDMF and ADMF, *Earthquake Engineering and Structural Dynamics* 31 (4) (2002) 897–919.

Li Z.N., Tang J., Li Q.S., Optimal sensor locations for structural vibration measurements, *Applied Acoustics* 65 (2004) 807–818.

Li J., Su M., Fan L., Vibration Control of Railway Bridges under High-Speed Trains Using Multiple Tuned Mass Dampers, *Journal of Bridge Engineering* 10 (3) (2005) 312–320.

Li D.S., Li H.N., Fritzen C.P., The connection between effective independence and modal kinetic energy methods for sensor placement, *Journal of Sound and Vibration* 305 (4–5) (2007) 945–955.

Li D.S., Fritzen C.P., Li H.N., Extended MinMAC algorithm and comparison of sensor placement methods, *Proceedings of the IMAC-XXVI*, Florida, USA, 2008, Paper No.78.

Li D.S., Li H.N., Fritzen C.P., A note on fast computation of effective independence through QR downdating for sensor placement, *Mechanical Systems and Signal Processing* 23 (4) (2009) 1160–1168.

Li Q., Fan J., Nie J., Li Q., Chen Y., Crowd-induced random vibration of footbridge and vibration control using multiple tuned mass dampers, *Journal of Sound and Vibration* 329 (19) (2010) 4068–4092.

Lin Y.Y., Cheng C.M., Lee C.H., A tuned mass damper for suppressing the coupled flexural and torsional buffeting response of long-span bridges, *Engineering Structures* 22 (9) (2000) 1195–1204.

Lin C.C., Wang J.F., Chen B.L., Train-Induced Vibration Control of High-Speed Railway Bridges Equipped with Multiple Tuned Mass Dampers, *Journal of Bridge Engineering* 10 (4) (2005) 398–414.

Link M., Weiland M., Barragan J.M., Direct physical matrix identification as compared to phase resonance testing - An assessment based on practical application, *Proceedings of the Fifth International Modal Analysis Conference*, London, 1987, pp. 804–811.

Liu W., Gao W.C., Sun Y., Xu M.J., Optimal sensor placement for spatial lattice structure based on genetic algorithms, *Journal of Sound and Vibration* 317 (1–2) (2008) 175–189.

Ljung L., *System Identification: Theory for the User*, second edition, Prentice Hall PTR, NJ, 1999.

Loh C.H., Wu T.S., Identification of Fei-Tsui arch dam from both ambient and seismic response data, *Soil Dynamics and Earthquake Engineering* 15 (1996) 465–483.

Luk Y., Identification of physical mass, stiffness and damping matrices using pseudo-inverse, *Proceedings of the Fifth International Modal Analysis Conference*, London, 1987, pp. 679–685.

Luu M., Zabel V., Könke C., An optimization method of multi-resonant response of high-speed train bridges using TMDs, *Finite Elements in Analysis and Design* 53 (2012) 13–23.

Lynch J.P., Wang Y., Loh K., Yi J.H., Yun C.B., Wireless Structural Monitoring of the Geumdang Bridge using Resolution Enhancing Signal Conditioning, *Proceedings of the 24th International Modal Analysis Conference (IMAC XXIV)*, St. Louis, 2006.

Magalhães F., Cunha Á., Caetano E., Online automatic identification of the modal parameters of a long span arch bridge, *Mechanical Systems and Signal Processing* 23 (2) (2009) 316–329.

Maia N.M.M., Silva J.M.M., He J., Lieven N.A.J, Lin R.M., Skingle G.W., To W.M., Urgueira A.P.V., Modal analysis identification methods, in: Maia N.M.M, Silva J.M.M. (Eds.), *Theoretical and Experimental Modal Analysis*, Research Studies, England, 1998, pp. 185–264.

Maia N.M.M., Silva J.M.M. (Eds.), *Theoretical and Experimental Modal Analysis*, Research Studies Press Ltd, England , 1998.

Mao X., Dai H., Finite element model updating with positive definiteness and no spill-over, *Mechanical Systems and Signal Processing* 28 (2012) 387–398.

Meo M., Zumpano G., On the optimal sensor placement techniques for a bridge structure, *Engineering Structures* 27 (10) (2005) 1488–1497.

Minas C., Inman D.J., Correcting Finite Element Models with Measured Modal Results Using Eigenstructure Assignment Methods, *Proceedings of the Sixth International Modal Analysis Conference*, Orlando, Florida, 1988, pp. 583–587.

Minas C., Inman D.J., Matching Finite Element Models to Modal Data, *Journal of Vibration and Acoustics* 112 (1) (1990) 84–92.

Moore B., Principal component analysis in linear systems: Controllability, observability, and model reduction, *IEEE Transactions on Automatic Control* 26 (1) (1981) 17–32.

Mottershead J.E., Friswell M.I., Model updating in structural dynamics: a survey, *Journal of Sound and Vibration* 167 (2) (1993) 347–375.

Nestorovic T., Trajkov M., Optimal actuator and sensor placement based on balanced reduced models, *Mechanical Systems and Signal Processing* 36 (2) (2013) 271–289.

Nishihara O., Asami T., Closed-form solutions to the exact optimizations of dynamic vibration absorbers (minimizations of the maximum amplitude magnification factors). *Journal of Vibration and Acoustics* 124 (2002) 576–582.

O'Callahan J., Avitabile P., Riemer R., System equivalent reduction expansion process (SEREP), *Proceedings of the 7th IMAC*, 1989, pp.29–37.

Obinata G., Anderson D.O., *Model Reduction for control system design*, Springer-Verlag, London, 2001.

Ormondroyd J., Den Hartog J.P., The theory of the dynamic vibration absorber, *Transactions of ASME, Applied Mechanics* 50 (7) (1928) 9–22.

Ozer M.B., Royston T.J., Extending DenHartog's vibration absorber technique to multidegree-of-freedoms systems, *ASME Journal of Vibration and Acoustics* 127 (2005) 341–350.

Pakzad S., Fenves G., Statistical Analysis of Vibration Modes of a Suspension Bridge Using Spatially Dense Wireless Sensor Network, *Journal of Structural Engineering* 135 (7) (2009) 863–872.

Pandit S.M., *Modal and Spectrum Analysis: Data Dependent Systems in State Space*, first edition, John Wiley, New York, 1991.

Papadimitriou C., Katafygiotis L.S., Au S.K., Effects of structural uncertainties on TMD design: A reliability-based approach, *Journal of Structural Control* 4 (1) (1997) 65–88.

Papadimitriou C., Optimal sensor placement for parametric identification of structural systems, *Journal of Sound and Vibration* 278 (2004) 923–947.

Papadopoulos M., Garcia E., Sensor placement methodologies for dynamic testing, *AIAA Journal* 36 (1998) 256–263.

Patil A., Jung S., Lee S., Kwon S.D., Mitigation of vortex-induced vibrations in bridges under conflicting objectives, *Journal of Wind Engineering and Industrial Aerodynamics* 99 (12) (2011) 1243–1252.

Peeters B., De Roeck G., Reference-based stochastic subspace identification for output only modal analysis, *Mechanical System and Signal Processing* 13 (6) (1999) 855–878.

Peeters B., Van der A.H., Guillaume P., Leuridan J., The polyMAX frequency-domain method: a new standard for modal parameter estimation, *Shock and Vibration* 11 (2004) 395–409.

Peeters B., De Roeck G., Reference-based combined deterministic-stochastic subspace identification for experimental and operational modal analysis, *Mechanical System and Signal Processing* 22 (3) (2008) 617–637.

Pickrel C.R., A practical approach to modal pretest design, *Mechanical Systems and Signal Processing* 13 (1999) 271–295.

Pourzeynali S., Datta T.K., Control of flutter of suspension bridge deck using TMD, *International Journal of Wind and Structure* 5 (5) (2002) 407–422.

Qin Q., Li H.B., Qian L.Z., Modal Identification of Tsing Ma Bridge by Using Improved Eigensystem Realization Algorithm, *Journal of Sound and Vibration* 247 (2001) 325–341.

Rana R., Soong T.T., Parametric study and simplified design of tuned mass dampers, *Engineering Structures* 20 (3) (1998) 193–204.

Randall S.E., Halsted D.M., Taylor D.L., Optimum vibration absorbers for linear damped systems, *ASME Journal of Mechanical Design* 103 (4) (1981) 908–913.

Ren W.X., Zatar W., Harik I.E., Ambient vibration-basedseismic evaluation of a continuous girder bridge, *Engineering Structures* 26 (2004) 631–640.

Reynier M., Abou-Kandil H., Sensors location for updating problems, *Mechanical Systems and Signal Processing* 13 (2) (1999) 297–314.

Richardson M.H., Formenti D.L., Global curve fitting of frequency response measurements using the rational fraction polynomial method, *Proceedings of the Third International Modal Analysis Conference*, 1985, pp. 390–397.

Richardson M.H., Global frequency & damping estimates from frequency response measurements, *Proceedings of the Fourth International Modal Analysis Conference*, 1986, pp. 465–470.

Ross R., Synthesis of stiffness and mass matrices from experimental vibration modes, *SAE Technical Paper* 710787, 1971.

Sadek F., Mohraz B., Taylor A.W., Chung R.M., A method of estimating the parameters of tuned mass dampers for seismic applications, *Earthquake Engineering and Structural Dynamics* 26 (6) (1997) 617–635.

Scanlan R.H., Gade R.H., Motion of suspended bridge spans under gusty wind, *Journal of Structural Division ASCE* 103 (1977) 1867–1883.

Shama A.A., Mander J.B., Chen S.S., Aref A.J., Ambient vibration and seismic evaluation of a cantilever truss bridge, *Engineering Structures* 23 (2001) 1281–1292.

Shi W., Shan J., Lu X., Modal identification of Shanghai World Financial Center both from free and ambient vibration response, *Engineering Structures* 36 (2012) 14–26.

Shih C., Tsuei Y., Allemang R., Brown D.L., Complex mode indication function and its applications to spatial domain parameter estimation, *Mechanical System and Signal Processing* 2 (4) (1988) 367–377.

Siringoringo D.M., Fujino Y., System identification of suspension bridge from ambient vibration response, *Engineering Structures* 30 (2) (2008) 462–477.

Skudrzyk E., *Simple and Complex Vibratory Systems*, Pennsylvania State University Press, 1968.

Sladek J.R., Klingner R.E., Effect of Tuned-Mass Dampers on Seismic Response, *Journal of Structural Engineering* 109 (8) (1983) 2004–2009.

Smail M., Thomas M., Lakis A.A., Assessment of optimal ARMA model orders for modal analysis, *Mechanical Systems and Signal Processing* 13 (5) (1999a) 803–819.

Smail M., Thomas M., Lakis A.A., ARMA models for modal analysis: effect of modal orders and sampling frequency, *Mechanical Systems and Signal Processing* 13 (6) (1999b) 925–941.

Smith S.W., Beattie C.A., Secant-method adjustment for structural models, *AIAA Journal* 29 (1) (1991) 119–126.

Soom A., Lee M., Optimal design of linear and nonlinear vibration absorbers for damped systems, *ASME Journal of Vibration and Acoustics* 105 (1) (1983) 112–119.

Srinathkumar S., Eigenvalue/eigenvector assignment using output feedback, *IEEE Transactions on Automatic Control* 23 (1) (1978) 79 – 81.

Stephan C., Sensor placement for modal identification, *Mechanical Systems and Signal Processing* 27 (2012) 461–470.

Thompson A.G., Optimum tuning and damping of a dynamic vibration absorber applied to a force excited and damped primary system. *Journal of Sound and Vibration* 77 (3) (1981) 403–415.

Thoren A.R., Derivation of mass and stiffness matrices form dynamic test data, *AIAA conference paper* 72346, 1972.

Tsai H.C., Lin G.C., Optimum tuned-mass dampers for minimizing steady-state response of support-excited and damped systems, *Earthquake Engineering and Structural Dynamics* 22 (11) (1993) 957–973.

Ubertini F., Gentile C., Materazzi A.L., Automated modal identification in operational conditions and its application to bridges, *Engineering Structures* 46 (2013) 264–278.

Udwadia F.E., Methodology for optimal sensor locations for parameter identification in dynamic systems, *ASCE Journal of Engineering Mechanics* 120 (2) (1994) 368–390.

Van Overschee P., De Moor B., *Subspace Identification for Linear Systems: Theory Implementation Applications*, Kluwer Academic Publishers, Dordrecht (Netherlands), 1996.

Vold H., Kundrat J., Rocklin G.T., Russel R., A multi-input modal estimation algorithm for mini-computers, *SAE Technical Paper*, No.820194 (1982) 828–841.

Waldraff W., Dochain D., Bourrel S., Magnus A., On the use of observability measures for sensor location in tubular reactor, *Journal of process control* 8 (5–6) (1998) 497–505.

Wang J.F., Lin C.C., Chen B.L., Vibration suppression for high-speed railway bridges using tuned mass dampers, *International Journal of Solids and Structures* 40 (2) (2003) 465–491.

Wei F.S., Structural dynamic model modification using vibration test data, *Proceedings of the Seventh International Modal Analysis Conference*, Las Vegas, 1989, pp. 562–567.

Wei F.S., Analytical dynamic model improvement using vibration test data, *AIAA Journal* 28 (1) (1990a) 175–177.

Wei F.S., Mass and stiffness interaction effects in analytical model modification, *AIAA Journal* 28 (9) (1990b) 1686–1688.

Weng J., Loh C., Lynch J., Lu K., Lin P., Wang Y., Output-only modal identification of a cable-stayed bridge using wireless monitoring systems, *Engineering structures* 30 (2008) 1820–1830.

Wiesner K.B., Tuned Mass Dampers to Reduce Building Wind Motion, *ASCE Convention and Exposition*, Boston, April, 1979.

Wilson J.A., Guhe S.Y., Observability matrix condition number in design of measurement strategies, *Computer Aided Chemical Engineering* 20 (2005) 397–402.

Xing C., Wang H., Li A., Xu Y., Study on Wind-Induced Vibration Control of a Long-Span Cable-Stayed Bridge Using TMD-Type Counterweight, *Journal of Bridge Engineering* (doi: 10.1061/(ASCE)BE.1943-5592.0000500).

Xu K., Igusa T., Dynamic characteristics of multiple substructures with closely spaced frequencies, *Earthquake Engineering and Structural Dynamics* 21 (12) (1992) 1059–1070.

Yamaguchi H., Harnpornchai N., Fundamental characteristics of Multiple Tuned Mass Dampers for suppressing harmonically forced oscillations, *Earthquake Engineering and Structural Dynamics* 22 (1) (1993) 51–62.

Yang Y.B., Chen Y.J., Direct versus iterative model updating methods for mass and stiffness matrices, *International Journal of Structural Stability and Dynamics* 10 (2) (2010) 165–186.

Yao L., Sethares W.A., Kammer D.C., Sensor placement for on-orbit modal identification of large space structure via a genetic algorithm, *Proceedings of the IEEE International Conference on Systems Engineering*, Kobe, September 1992, pp. 332–335.

Yau J.D., Yang Y.B., Vibration reduction for cable-stayed bridges travelled by high-speed trains, *Finite Elements in Analysis and Design* 40 (3) (2004a) 341–359.

Yau J.D., Yang Y.B., A wideband MTMD system for reducing the dynamic response of continuous truss bridges to moving train loads, *Engineering Structures* 26 (12) (2004b) 1795–1807.

Yuan Q., Proximal-point method for finite element model updating problem, *Mechanical Systems and Signal Processing* 34 (1–2) (2013) 47–56.

Yuen K.V., Katafygiotis L.S., Papadimitriou C., Mickleborough N.C., Optimal sensor placement methodology for identification with unmeasured excitation, *Journal of Dynamic Systems, Measurement, and Control* 123 (4) (2001) 677–686.

Yuen K.V., Katafygiotis L.S., Bayesian fast Fourier transform approach for modal updating using ambient data, *Advances in Structural Engineering* 6 (2) (2003) 81–95.

Zhang L., Wang T., Tamura Y., A frequency-spatial domain decomposition (FSDD) technique for operational modal analysis, *Proceedings of the First International Operational Modal Analysis Conference*, 2005, pp. 551–561.

Zhang L., Wang T., Tamura Y., A frequency–spatial domain decomposition (FSDD) method for operational modal analysis, *Mechanical Systems and Signal Processing* 24 (2010) 1227–1239.

Zhou K., Doyle J.C., Glover K., *Robust and Optimal Control*, New York, Prentice-Hall,1995.

Zimmerman D.C., Windengren M., Correcting finite element models using a symmetric eigenstructure assignment technique, *AIAA Journal* 28 (9) (1990) 1670–1676.

APPENDIX-A

ANALYTICAL DERIVATIONS FOR MODAL CONTRIBUTION IN OUTPUT ENERGY

In the proposed strategy, participation of a mode along chosen set of DOF is measured in the form of uncoupled contribution of that mode in the output energy associated to those DOF, when the system is released from any initial condition. Specifying the initial condition in terms of any of the two response parameters like displacement, velocity and acceleration is sufficient. In the state space representation, displacement and velocity are considered for specifying initial conditions. Here, the closed form solution of observability grammian is carried out with Lyapunov equation as in Eq. (4.17b). The modal state vector is considered as in Eq. (4.5) for the present derivation. The uncoupled pure contribution of a modal state in the output energy can be considered as the corresponding diagonal element of the observability grammian matrix. According to this modal state vector, the uncoupled contribution of r^{th} mode in output energy can be evaluated with the addition of $(2r–1)^{th}$ and $(2r)^{th}$ diagonal elements of observability grammian. For displacement and velocity measurement state space matrices $[C]$ are mentioned in the Eqs. (A-4.1) and (A-4.2) respectively,

$$[C] = [\{\phi_1\} \quad \{0\} \quad \{\phi_2\} \quad \{0\} \quad \dots \quad \{\phi_n\} \quad \{0\}] \tag{A-4.1}$$

$$[C] = [\{0\} \quad \{\phi_1\} \quad \{0\} \quad \{\phi_2\} \quad \dots \quad \{0\} \quad \{\phi_n\}] \tag{A-4.2}$$

However, for acceleration measurement $[C]$ is first formed as per the state vector

$$\{z\} = \{q_1 \; q_2 \dots q_n \; \dot{q}_1 \; \dot{q}_2 \dots \; \dot{q}_n\}^T \tag{A-4.3}$$

Hence, $[C]$ can be written as

$[C] = [[C_q] \quad [C_v]]$

Or, $[C] = -[\Phi]\left[[M_m]^{-1}[K_m] \quad [M_m]^{-1}[D_m]\right]$

Or, $[C] = -[\Phi][[\Omega]^2 \quad 2[\Xi][\Omega]]$

Or, $[C] = -[\Phi][[\Omega] \quad 2[\Xi]]\begin{bmatrix}[\Omega] & [0]\\ [0] & [\Omega]\end{bmatrix}$

While damping is low as$[\Xi] << [\Omega]$, $[[\Omega] \quad 2[\Xi]]$ is approximated as $[[\Omega] \quad [0]]$ and $[C]$ can be approximately written as

$$[C] \approx -[\Phi][[\Omega]^2 \quad [0]] \tag{A-4.4}$$

Now $[C]$ matrix according to the state vector as in Eq. (4.5) can be written as,

$$[C] \approx \left[-\omega_1^2\{\phi_1\} \quad \{0\} \quad -\omega_2^2\{\phi_2\} \quad \{0\} \quad \dots \quad -\omega_n^2\{\phi_n\} \quad \{0\}\right] \tag{A-4.5}$$

When any subset of total DOF is considered for output, the state space matrix $[C]$ is presented for displacement, velocity and acceleration respectively as

$[C] = \left[\{\psi_1\} \quad \{0\} \quad \{\psi_2\} \quad \{0\} \quad \dots \quad \{\psi_n\} \quad \{0\}\right]$

$[C] = \left[\{0\} \quad \{\psi_1\} \quad \{0\} \quad \{\psi_2\} \quad \dots \quad \{0\} \quad \{\psi_n\}\right]$

$[C] \approx \left[-\omega_1^2\{\psi_1\} \quad \{0\} \quad -\omega_2^2\{\psi_2\} \quad \{0\} \quad \dots \quad -\omega_n^2\{\psi_n\} \quad \{0\}\right]$

where, $\{\psi\}$ is subset of full mode shape vector $\{\phi\}$ and retains the elements of $\{\phi\}$ corresponding to the retained DOF for output.

The derivation is carried out using the 2×2 sub-blocks of the related matrices in Eq. (4.17b). The 2×2 sub-blocks are demonstrated with an arbitrary matrix $[Z]$ as

$$[Z] = \begin{bmatrix} Z_{11} & Z_{12} & \cdots & Z_{1n} \\ Z_{21} & Z_{22} & \cdots & Z_{2n} \\ \vdots & \vdots & \ddots & \vdots \\ Z_{n1} & Z_{n2} & \cdots & Z_{nn} \end{bmatrix}$$

where, Z_{pq} represents the p,q^{th} sub-block. Diagonal block structure of $[A]$ and $[A]^T$ makes the solution easier since it is observed from the Lyapunov equation that,

(a) The p,q^{th} block of matrix $[A]^T[W_o]$ can be evaluated as the product of p^{th} modal block of $[A]^T$ and the p,q^{th} block of $[W_o]$.

(b) The p,q^{th} block of matrix $[W_o]$ $[A]$ can be evaluated as the product of p,q^{th} block of $[W_o]$ and q^{th} modal block of $[A]$.

Then the addition of p,q^{th} block of matrices $[A]^T[W_o]$, $[W_o]$ $[A]$ and $[C]^T[C]$ equals to zero according to the Lyapunov equation. This 2×2 matrix equation is represented as

$$\begin{bmatrix} 0 & -\omega_p^2 \\ 1 & -2\xi_p\omega_p \end{bmatrix}\begin{bmatrix} w_{11} & w_{12} \\ w_{21} & w_{22} \end{bmatrix}+\begin{bmatrix} w_{11} & w_{12} \\ w_{21} & w_{22} \end{bmatrix}\begin{bmatrix} 0 & 1 \\ -\omega_q^2 & -2\xi_q\omega_q \end{bmatrix}+\begin{bmatrix} c_{11} & c_{12} \\ c_{21} & c_{22} \end{bmatrix}=\begin{bmatrix} 0 & 0 \\ 0 & 0 \end{bmatrix} \tag{A-4.6}$$

Further, this matrix equation produces four numbers of linear equations as,

$$\begin{bmatrix} 0 & -\omega_q^2 & -\omega_p^2 & 0 \\ 1 & -2\xi_q\omega_q & 0 & -\omega_p^2 \\ 1 & 0 & -2\xi_p\omega_p & -\omega_q^2 \\ 0 & 1 & 1 & -2\xi_p\omega_p-2\xi_q\omega_q \end{bmatrix}\begin{Bmatrix} w_{11} \\ w_{12} \\ w_{21} \\ w_{22} \end{Bmatrix}=\begin{Bmatrix} -c_{11} \\ -c_{12} \\ -c_{21} \\ -c_{22} \end{Bmatrix} \tag{A-4.7}$$

Eq. (A-4.7) can provide the general solution of any p^{th},q^{th} block of the observability grammian. The elements of the p,q^{th} block of matrix $[C]^T[C]$ depends on the response measurement type. Thus,

(a) For displacement measurement, $\begin{bmatrix} c_{11} & c_{12} \\ c_{21} & c_{22} \end{bmatrix}=\begin{bmatrix} \{\psi_p\}^T\{\psi_q\} & 0 \\ 0 & 0 \end{bmatrix}$

(b) For velocity measurement, $\begin{bmatrix} c_{11} & c_{12} \\ c_{21} & c_{22} \end{bmatrix}=\begin{bmatrix} 0 & 0 \\ 0 & \{\psi_p\}^T\{\psi_q\} \end{bmatrix}$

(c) For acceleration measurement, $\begin{bmatrix} c_{11} & c_{12} \\ c_{21} & c_{22} \end{bmatrix}=\begin{bmatrix} \omega_p^2\omega_q^2\{\psi_p\}^T\{\psi_q\} & 0 \\ 0 & 0 \end{bmatrix}$

The solution of this Eq. (A-4.7) is carried with Cramer's rule. First the derivation for displacement is considered. With few algebraic operations the solution becomes as

$$w_{11}=\{\psi_p\}^T\{\psi_q\}\frac{(8\xi_p^2\xi_q\omega_p^2\omega_q+8\xi_p\xi_q^2\omega_p\omega_q^2+2\xi_p\omega_p^3+2\xi_q\omega_q^3)}{d_{pq}}$$

$$w_{12}=\{\psi_p\}^T\{\psi_q\}\frac{(4\xi_p^2\omega_p^2+4\xi_p\xi_q\omega_p\omega_q-\omega_p^2+\omega_q^2)}{d_{pq}}$$

$$w_{21}=\{\psi_p\}^T\{\psi_q\}\frac{(4\xi_p\xi_q\omega_p\omega_q+4\xi_q^2\omega_q^2+\omega_p^2-\omega_q^2)}{d_{pq}}$$

$$w_{22} = \{\psi_p\}^T\{\psi_q\}\frac{(2\xi_p\omega_p + 2\xi_q\omega_q)}{d_{pq}}$$

where, $d_{pq} = 4\omega_p\omega_q(\xi_p\omega_p + \xi_q\omega_q)(\xi_p\omega_q + \xi_q\omega_p) + (\omega_p^2 - \omega_q^2)^2$. With $p = q$ i.e. with a diagonal block corresponding to the p^{th} mode, $d_{pp} = 16\xi_p^2\omega_p^4$ and the diagonal pair for modal displacement and velocity states for p^{th} mode becomes

$$\left[\frac{\{\psi_p\}^T\{\psi_p\}(1 + 4\xi_p^2)}{4\xi_p\omega_p}, \frac{\{\psi_p\}^T\{\psi_p\}}{4\xi_p\omega_p^3}\right]$$

Here, with $\xi << 1$ the component $4\xi_p^2$ has negligible contribution. Hence, diagonal elements are found proportional to $(1/\xi)$. For the off-diagonal blocks, while the damping ratios are small and natural frequencies are well-separated, d_{pq} can be approximated as $d_{pq} \approx (\omega_p^2 - \omega_q^2)^2$. The other elements except the diagonal elements are observed to be either independent of ξ or proportional to ξ. So, the observability grammian $[W_o]$ tends to diagonal form as $\xi \rightarrow 0$. Now, the uncoupled contribution of the p^{th} mode in the output energy for displacement measurement can be considered with the addition of p^{th} modal displacement state and p^{th} modal velocity sate as

$$e_p = \{\psi_p\}^T\{\psi_p\}\left(\frac{\omega_p^2 + 4\xi_p^2\omega_p^2 + 1}{4\xi_p\omega_p^3}\right) \quad \text{(A-4.8)}$$

With similar algebraic operations, closed form solution can be derived for velocity and acceleration measurement. Uncoupled contribution of the p^{th} mode in the output energy for velocity and acceleration measurement are found as in Eqs. (A-4.9) and (A-4.10) respectively. Also the diagonal dominancy of grammian are ensured similarly while $\xi \rightarrow 0$.

$$e_p = \{\psi_p\}^T\{\psi_p\}\left(\frac{\omega_p^2 + 1}{4\xi_p\omega_p}\right) \quad \text{(A-4.9)}$$

$$e_p = \{\psi_p\}^T\{\psi_p\}\left(\frac{\omega_p^3 + 4\xi_p^2\omega_p^3 + \omega_p}{4\xi_p}\right) \quad \text{(A-4.10)}$$

From the Eqs. (A-4.8), (A-4.9) and (A-4.10) for displacement, velocity and acceleration measurement respectively, it is clear that uncoupled contribution of p^{th} mode along chosen set of DOF is similar with $\{\psi_p\}^T\{\psi_p\}$ which is just scaled with some p^{th} modal constants as $\left(\frac{\omega_p^2 + 4\xi_p^2\omega_p^2 + 1}{4\xi_p\omega_p^3}\right)$, $\left(\frac{\omega_p^2 + 1}{4\xi_p\omega_p}\right)$ and $\left(\frac{\omega_p^3 + 4\xi_p^2\omega_p^3 + \omega_p}{4\xi_p}\right)$. Hence, participation of a mode is similar whether displacement, velocity or acceleration is measured.

Publications from this thesis-work

(A) Journals:

1. Debnath N., Dutta A., Deb S.K., Placement of sensors in operational modal analysis for truss bridges, *Mechanical Systems and Signal Processing* 31 (2012) 196–216.
2. Debnath N., Deb S.K., Dutta A., Frequency band wise passive control of linear time invariant structural systems with H_∞ optimization, *Journal of Sound and Vibration* 332 (23) (2013) 6044 - 6062.
3. Debnath N., Dutta A., Deb S.K., Operational Modal Analysis of a Large Truss Bridge. (*Under review*).
4. Multi-modal passive vibration control of an existing large truss bridge using tuned mass damper system. (*Under review*).
5. Finite element model updating of an existing large truss bridge: A case study (*Under review*).

(B) Conferences:

1. Debnath N, Dutta A, Deb S K. Placement of sensors in operational modal analysis for large structural systems, *7th international workshop of Asian-Pacific Network of Centres for Research in Smart Structures Technology* (ANCRiSST), Bangalore, July 2012.
2. Debnath N, Deb S K, Dutta A. System identification of the Saraighat Bridge using ambient vibration data: a case study, *Proceedings of the 15th World Conference on Earthquake Engineering*, Lisbon, Portugal, September 2012.